CHAPTER ONE

1.0 INTRODUCTION

1.1 Neurodegenerative disease and its prevalence

Neurodegenerative disease is a word applied to a diversity of conditions ascending from a prolonged collapse and deterioration of the nervous system, especially the nerve cells in the brain which are electrically excitable cells responsible for the transmission of signals via connections known as synapses (Houghton and Howes, 2005). In the year 1906 a Bavarian neuropsychiatrist known as Alois Alzheimer described Alzheimer's disease for the first time (Hostettmann *et al*., 2006). Alzheimer's disease is a neurons deteriorating condition which is described by progressive loss of structure and function of neurons ultimately leading to cognitive decline and deterioration of virtually all intellectual functions (Ferreira *et al*., 2006). It is due to the cholinergic neurons distributed in the specific region of brain such as hippocampal and cortical areas.

Alzheimer's disease happens to be the most common form of dementia that affects millions of people globally (Singhal *et al*., 2012). One in every three (3) seconds is down with a new case of dementia around the globe. As said by World Alzheimer report 2018, it is projected that Fifty (50) million people worldwide are living with dementia. These numbers will almost double every 20 years, reaching Eighty two (82) million in 2030 and One hundred and fifty two (152) million in 2050 (Figure 1.1). It's estimated that 58% of all people with dementia live in countries currently classified by the World Bank as low or middle income countries. The percentage of people with dementia living in these same countries is estimated to increase to 63% in 2030 and 68% in 2050. The projected numbers of people living with dementia in each world region in 2015 are as follows; The Americas (9.4 million), Africa (4.0 million), Asia (22.9 million) and Europe (10.5 million) (ADI, 2015). Alzheimer's disease is the 4^{th} leading cause of death especially in the elderly population over the age of 65 years (Abou-Donia *et al*., 2014).

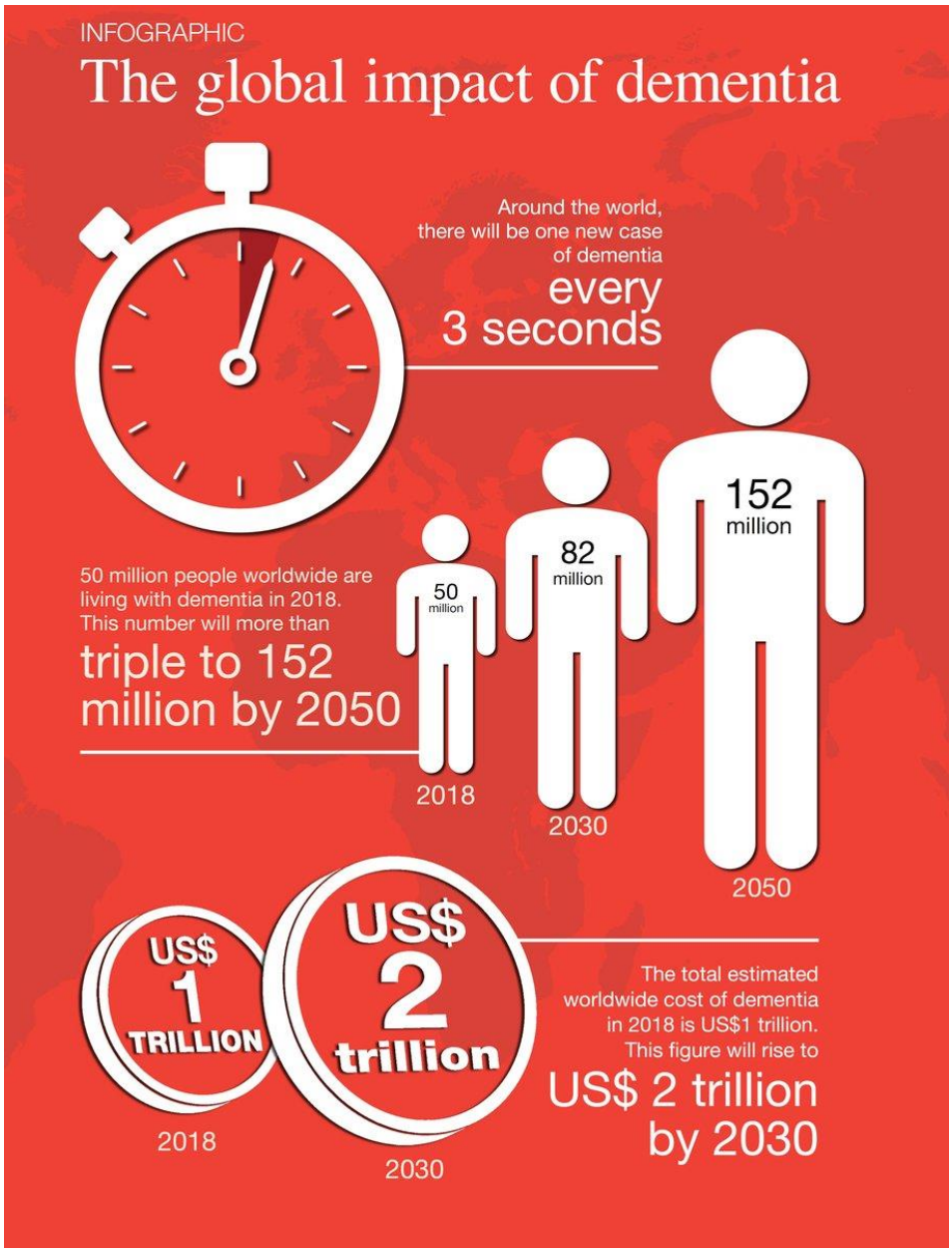

Figure 1.1: Source: World Alzheimer Report 2018

1.2 Alzheimer's disease pathology and tactics to improve cholinergic function

The neuropathological hallmark identified with Alzheimer's disease are neurofibrillary tangles, β-amyloid plaques, inflammatory processes and disruption of important neurotransmitters which are responsible for communication and integration in the nervous system (Bossy-Wetzel *et al*., 2004). The chief clinical feature of this disease is the impairment of memory, short term memory and cognitive disability. The common symptoms associated with Alzheimer's disease are, memory loss, poor judgment or inability to make daily plans, challenges in solving glitches, trouble in implementation of accustomed tasks, deepened misperception with time and place, losing items, struggle in understanding visual images, new difficulties with words in writing or speaking, radical changes in attitude and personality. As the condition progresses additional cognitive abilities are impaired such as ability to calculate visuospatial skills and idiomotor apraxia. In the advance stage, a motor weakness increase that leads to muscular contractions which produces immobility such as pneumonia, pulmonary embolism and death (Hostettmann *et al*., 2006). No treatments are available to cure Alzheimer's disease but to manage and prevent and stop progression. Two classes of mediators approved are inhibitors of cholinesterase and N-methyl-D aspartase receptor antagonist. New entities for Alzheimer's disease in pipeline therapy are β-secretory stimulator, γ-seretase inhibitor, α-secretase stimulator, immunotherapy and TAU inhibitors (Rachel *et al*., 2011).

The pathophysiology of Alzheimer's disease is multifaceted and involves numerous biochemical pathways. Acetylcholine which plays an imperative role in learning and memory processes was the first neurotransmitter defect discovered in Alzheimer's disease condition. In the central nervous system, acetylcholine stimulation of the nicotinic receptors appears to be linked with intellectual function. Usually, acetylcholine is stowed in the nerve terminals, in structures called vesicles and is released from the nerve endings when the nerve terminal is depolarized, thereby entering the synapse and binding to the receptor (Houghton *et al*., 2006). However, in Alzheimer's disease patients, there is a radical decrease in the production of acetylcholine which has a very short half-life due to the availability of the enzymes acetylcholinesterase and butyrylcholinesterase which catalyzes the breakdown of acetylcholine and of some other choline esters that function as neurotransmitters in the brain by hydrolysing the ester bond in the ACh molecule (Orhan *et al.*, 2004).

There are considerable financial, social and emotional and huge economic burdens associated with caring for patients living with dementia worldwide (Akhondzadeh and Noroozian, 2002). Tactics to improve cholinergic function in Alzheimer's disease have included stimulation of cholinergic receptors or increasing the half-life of acetylcholine released into the neuronal synaptic cleft by use of agents which restore the level of acetylcholine through inhibition of both acetylcholinesterase and butyrylcholinesterase (Loizzo *et al*., 2009). Lately, Hodges (2006) proved that the inhibition of acetylcholinesterase holds a key role not only to boost cholinergic transmission in the brain but also to decrease the aggregation of β-amyloid plaques and the formation of the neurofibrillary tangles in Alzheimer's disease. Consequently, acetylcholinesterase and butyrylcholinesterase inhibitors are been considered as effective or have become noteworthy alternatives in treatment of Alzheimer's disease by prolonging or increasing acetylcholine availability in the brain (Orhan *et al*., 2004). Surprisingly, anticholinesterase drugs that exist such as galanthamine, donepezil, tacrine, physostigmine for the treatment of Alzheimer's disease are reported to have numerous dangerous effects such as low bioavailability, narrow therapeutic window, hepatotoxicity, short duration of biological action (Sancheti *et al*., 2009).

Also, an enzyme known as prolyl endopeptidase (PEP, also called prolyl oligopeptidase (POP)) has also been connected in the pathology of Alzheimer's disease via cleavage of important neuropeptide (Shinoda *et al*. 1997). Walter *et al*. (1971) first identified the activity of Prolyl endopeptidase in the human uterus, where it was found to cleave oxytocin. Prolyl oligopeptidase is an 80-kDa serine protease belonging to the family S9 of the serine carboxypeptidase clan (Rawlings and Barrett 1994). The closest phylogenetic relatives to prolyl oligopeptidase are dipeptidyl peptidase IV (DPPIV; EC 3.4.14.5), acylaminoacyl peptidase (EC 3.4.19.1), and oligopeptidase B (EC 3.4.21.83) (Venäläinen *et al*., 2004). The Prolyl oligopeptidase family has antique origins, and it is broadly distributed in organisms ranging from bacterial and archaeal species to humans; only fungi do not seem to possess a prolyl oligopeptidase enzyme (Venäläinen *et al*., 2004). Nevertheless, homologs of the S9A peptidase family are present in some fungi species (MEROPS peptidase database; Rawlings *et al*., 2008). In humans and rats, prolyl oligopeptidase enzyme activities have been found in most tissues, with the uppermost enzyme activity generally discovered in brains (Kato *et al*.,

1980b, Irazusta *et al*., 2002). Prolyl endopeptidase (PEP) is a serine protease which is known to play a role in degradation of proline containing neııropeptides shorter than thirty (30) amino acids involved in the processes of learning and memory (Wallen *et al*., 2002, Irazusta *et al*., 2001). Formation of beta-amyloid and neurofibrillary tangles in the brain due to genetic or other factors and marked reduction of certain brain neuropeptide levels are constant findings in patients with Alzheimer's disease, together with the decline of cholinergic neurons (Toide *et al*., 1998, Yoshida *et al*., 1996). PEP inhibitors are expected to exert their beneficial effects by increasing the brain levels of those neuropeptides which may improve and restore cognitive functions and protect vulnerable nerves against damage and cell death. Therefore, potent, selective and permanent inhibitors of PEP could serve as probes to evaluate the genuine involvement of this enzyme in Alzheiıner's pathology (Barelli *et al*., 1999, Orhan, 2002, Maes *et al*., 1998).

1.3 Molecular docking is an important tool in drug design and discovery

Molecular docking is an important tool in drug design and discovery process and is rapidly gaining attention (Kitchen *et al*., 2004). Docking is a method that helps to predict or anticipate the favored orientation of drug candidates (ligands) against macromolecular targets (protein) to make a stable complex. The process of a new drug discovery is a very difficult task. The field of computer aided drug design and discovery is an area that has gained popularity and has seen several successes in the last few years especially towards discovery of new drug leads (Lengauer and Rarey, 1996). The docking and molecular dynamics, the binding mechanism of three FDA-approved Alzheimer drugs: donepezil, galantamine and rivastigmine have been reported. Free-energy scores show strong affinity of the inhibitors for the enzyme binding pocket. Three independent molecular dynamics simulation runs indicated general stability of donepezil, galantamine and rivastigmine in their respective enzyme binding pocket as well as the tendency to form hydrogen bonds with the water molecules. The binding of rivastigmine in the *Torpedo california* AChE binding pocket is interesting as it eventually undergoes carbamylation and breaks apart according to the X-ray structure of the complex (Ali *et al*., 2018). The estimated free energy of binding (ΔG) for the target molecule, AChE with donepezil (Aricept), rivastigmine (Exelon), galantamine (Reminyl) and tacrine (Cognex) were found to be 3.58, -5.61, -7.86 and -6.95 kcal/mol, respectively in a study conducted by (Jagmohan *et al*., 2011). Authors concluded

that galantamine have the better binding affinity with AChE than the other drug molecules due to higher number of intermolecular interaction.

1.4 Reactive oxygen species and Alzheimer's disease

Reactive oxygen species are continuously produced in all living cells and is a part of normal cellular functions. Nevertheless, surplus of free radicals originating from endogenous or exogenous sources are accountable for aging and causing diverse diseases of human. Free radicals cause oxidative damage to diverse macromolecules that are imperative such as lipids, proteins and nucleic acids and therefore, are involved in the initiation phase of some degenerative diseases. Also, strong experimental proofs have shown that reactive oxygen species (ROS) are linked with the pathogenesis of Alzheimer's disease (Zhu *et al*., 2014). Largely, the physiological role of molecules with antioxidant potentials is to mitigate the oxidation chain reactions by eradicating free-radical intermediates which is critical for maintaining optimal health (Liu *et al*., 2010). Therefore, the use of compounds with antioxidant potentials has been explored in an effort to reduce the development and neuronal collapse of Alzheimer's disease (Howes *et al*., 2003).

1.5 Medicinal plants as a good source of clinical drugs

Medicinal plants have been good sources of clinical drugs in general for many years (Silverman and Holladay, 2014). Many drugs in clinical practice today are either directly from medicinal plants or have their basic template from compounds derived from plants such as digitoxin (cardiotonic drug) isolated from *Digitalis purpurea* (foxglove), vinblastine (anti-cancer drug) isolated from *Vinca rosea* (Madagascar periwinkle), aspirin (pain killer drug) isolated from *Salix* spp (willow bark), quinine (anti-malaria drug) isolated from *Cinchona officinalis* (Briskin, 2000). Huge quantities of medicinal plants have been expolred in medicine for prophylactic or therapeutic purposes. The therapeutic potentials of medicinal plants are ascribed to the existence of secondary metabolites or bioactive components such as glycosides, coumarins, flavonoids and alkaloids in them (Daniel, 2006). In traditional practices, numerous medicinal plants in nature have contributed significantly in providing drugs for the treatment of CNS conditions as well as to improve memory and intellectual functions (Elufioye *et al*., 2013). These include Rivastigmine which was

synthesized from the lead compound physostigmine derived from *Physostigma venenosum* approved in 2000 by US-FDA (Lopez *et al*., 2002), galanthamine, an alkaloid isolated from *Galanthus nivalis* was permitted in 2001 by the US-FDA for use in the treatment of Alzheimer's disease (Ingkaninan *et al*., 2003). Also, huperzine A an alkaloid isolated from *Huperzia serrata* is sold as a food supplement used for memory enhancement and to treat symptoms of AD in China (Marston *et al*., 2002).

Phyllanthus muellerianus (Kuntze) Excell is widely used in the treatment of jaundice, constipation, intestinal troubles, urethral discharge, severe dysentery, stomach ache (Katsayal and Lamal, 2009). Poultices of the leaves of *Phyllanthus muellerianus* are applied as wound dressing (Agyare *et al*., 2011) and various extracts of the leaf are used to treat veneral diseases and toothache (Arbonnier, 2004). Ethanolic extract of *P. muellerianus* stem bark demonstrated strong antibacterial activity against some selected bacteria depending on the concentration (Katsayal and Lamal, 2009). Also, the essential oil from *Phyllanthus muellerianus* displayed potent antibacterial activity against *Streptococcus mutans, Clostridium sporogenes* and *S. pyogenes* (Brusotti *et al*., 2012).

Tinospora cordifolia has been found also useful in management of countless diseases such as diabetes (Nagaraja, 2007), Immunomodulatory activity through animal and human studies (Nair, 2004), amelioration of cyclophosphamide induced toxicity (Mathew, 1997). *Tinospora cordifolia* was found to create modulation of chemotaxis, interlukin-1 and tumor necrosis factor in mouse macrophages (Dhuley, 1997) and has also been reported to have valuable effects in treatment of cerebral ischemia (Gupta, 2010). Evidence indicates that *Tinospora cordifolia* has antistress action. The important implications involve an antidepressant effect, improvement in cognition, concentration and memory, and improvement in cerebral ischemia. *Tinospora cordifolia* has been considered a *rasayana* or a substance useful as a rejuvenator or restorative, and is hence classed as an adaptogen. This action has been correlated with its antioxidant properties that protect against stress (Kennedy, 2009, Palpu, 2008).

A leaf decoction of *Cola hispida* is used to ameliorate stomach trouble and cough. The sap from fresh leaves is dripped into the ear for treatment of inflammation of the outer ear tract. The root grind to powder mixed with palm oil is rubbed for treatment of skin infections and also to kill lice (Burkill, 2000). It is also used to treat cutaneous and subcutaneous parasitic

infection. Ethnomedicinally, the root is used to treat genital stimulants/depressants while the leaf is used to treat pulmonary troubles.

Since Alzheimer's disease has become a massive economic burden and there are no effective drugs for its management so the use of medicinal plants or phytochemicals from natural sources could be new treatment strategies in the management of this disease and also as effective inhibitors of acetylcholinesterase and prolyl endopeptidase. In the present study, the enzymatic inhibitory activities and antioxidant properties of plant crude extracts, various fractions and compounds isolated from *P. muellerianus, Tinospora cordifolia* and *Cola hispida* were scientifically evaluated to ascertain their usefulness in traditional medicine practices in the treatment of neurodegenerative diseases.

1.6 Justification of research

Currently, there are no effective drugs for the management of Alzheimer's disease which necessitated the search for new potent neurotherapeutic agents. New treatment strategies based on the use of medicinal plants or its metabolites have been the panacea in developing new drugs. In traditional medical practices, many medicinal plants have been used to treat intellectual maladies which include neurodegenerative diseases and diverse neuropharmacological disarrays (Mukherjee *et al*., 2007a). Also, existing anticholinesterase drugs such as galanthamine, donepezil, tacrine, physostigmine and heptylphysostigmine in the treatment of Alzheimer's have been reported to have limitations such as low bioavailability, narrow therapeutic window, hepatotoxicity, short duration of biological action (Sancheti *et al*., 2009).

1.7 Research hypothesis

Acetylcholine (ACh) is an important neurotransmitter used by cholinergic neurons, which has been involved in critical physiological processes, such as attention, learning, memory, stress response, wakefulness and sleep and sensory information (Sarter and Bruno, 1997, Haam and Yakel, 2017). Cholinergic neurons damage was considered to be a critical pathological change that correlated with cognitive impairment in AD. Thus, cholinergic hypothesis was firstly tested with cholinesterase inhibitors in AD treatment. Inhibiting cholinesterase is a symptomatic relief treatment with marginal benefits. It is currently the

most available clinical treatment which gives desperate AD patients a glimmer of hope. Also, prolyl oligopeptidase (PEP) is a ubiquitous post-proline cleaving enzyme that is highly expressed in brain. Current knowledge about the biochemical features of PEP and the pharmacological action of its specific inhibitors has indicated that POP participates in several aspects of the central nervous system (CNS), including learning, memory and mood. Furthermore, a role has been suggested for PEP in pathological processes such as eating and mood disorders, hypertension and cell-cycle disturbances, in addition to its proposed connection with the neurodegenerative processes which occur in Alzheimer's, diseases. Today, several PEP inhibitors have already been evaluated in preclinical trials as potential drugs for the treatment of natural memory deficits that occur with aging or the pathological memory loss characteristic of Alzheimer's disease. Thus, modulating the activity of proline-specific proteases may be a relevant therapeutic approach (Lawandi *et al*., 2010).

Oxidative stress is considered to play an important role in the pathogenesis of AD. The human brain utilizes more oxygen than other tissues and undergoes mitochondrial respiration, which increases the potential for ROS exposure. In fact, AD is highly associated with cellular oxidative stress, including augmentation of protein oxidation, protein nitration, glycoloxidation and lipid peroxidation as well as accumulation of amyloid β (Aβ) which can induce oxidative stress (Butterfield and Lauderback , 2002, Butterfield *et al*., 2002). Thus, the treatment with anti-oxidant compounds would provide protection against oxidative stress and Aβ toxicity.

1.8 Aims and objectives

1.8.1 Aim of study

The present study is therefore aimed at isolating and identifying bioactive molecules from selected Nigerian medicinal plants with memory enhancing potential that may be useful in the management of Alzheimer’s disease.

1.8.2 Research objectives

- To carryout qualitative phytochemical screening on plant materials
- To carry out anti-oxidant activities of crude extracts and partitioned fractions *in vitro*.
- To evaluate the acetylcholinesterase inhibitory activities of plant crude extracts and partitioned fractions *in vitro*.
- To isolate, structurally elucidate and identify bioactive molecules in AD management.
- To evaluate the acetylcholinesterase and prolyl endopeptidase inhibition potential of isolated compounds *in vitro.*
- To carry out molecular docking study of active compounds on the active site of enzyme (AChE and PEP).

CHAPTER TWO

2.0 LITERATURE REVIEW

2.1 Alzheimer's disease

Dementia is an acquired impairment of intellectual and memory functioning caused by disease of the brain (Figure 2.1). The term is not used in reference to individuals with mental retardation who have not acquired an adult level of intellectual development. Diagnosis of dementia initiates with the clinical recognition of a progressive degeneration in memory as well as defects in other mental abilities such as abstract thinking, judgement, personality, language, praxis, and visuospatial skills. The deficits must be of ample magnitude to interfere significantly with work or social activities (American Psychiatric Association, 1994 (DSM-IV)). Dementia may have onset which is known as pre-senile dementia (before the age of 65 years) or senile dementia (after the age of 65 years). It is inappropriate to use the terms dementia, senile dementia, or presenile dementia as a final diagnosis in the individual patient, as they are simply symptomatic classifications similar to the terms headache or seizure disorders. It is now recognised that the disease can affect people of any adult age, although it is more common in the older age groups. The most common form of dementia is Alzheimer's disease (Friedland and Wilcock, 2000).

Alois Alzheimer (1907) reported an incident of presenile dementia in a fifty one year old woman known as Auguste D. The author demonstrated the neurofibrillary tangles and neuritic plaques in the brain which today are the diagnostic markers of the disease that now carries his name. Neuritic plaques are microscopic foci of extra cellular amyloid aggregation and associated axonal and dendritic injury, found in large numbers in the limbic and associated cortices (Dickson, 1997). Such plaques contain extracellular deposits of amyloid β-protein that occur as star-shaped masses of amyloid fibrils. Much of the fibrillar Aβ found in the neuritic plaques is the species ending at amino acid 42 (Aβ42), a hydrophobic form that is particular prone to aggregation. The neurofibrillary tangles are intracellular aggregation of abnormal fibres comprising of paired filaments composed of

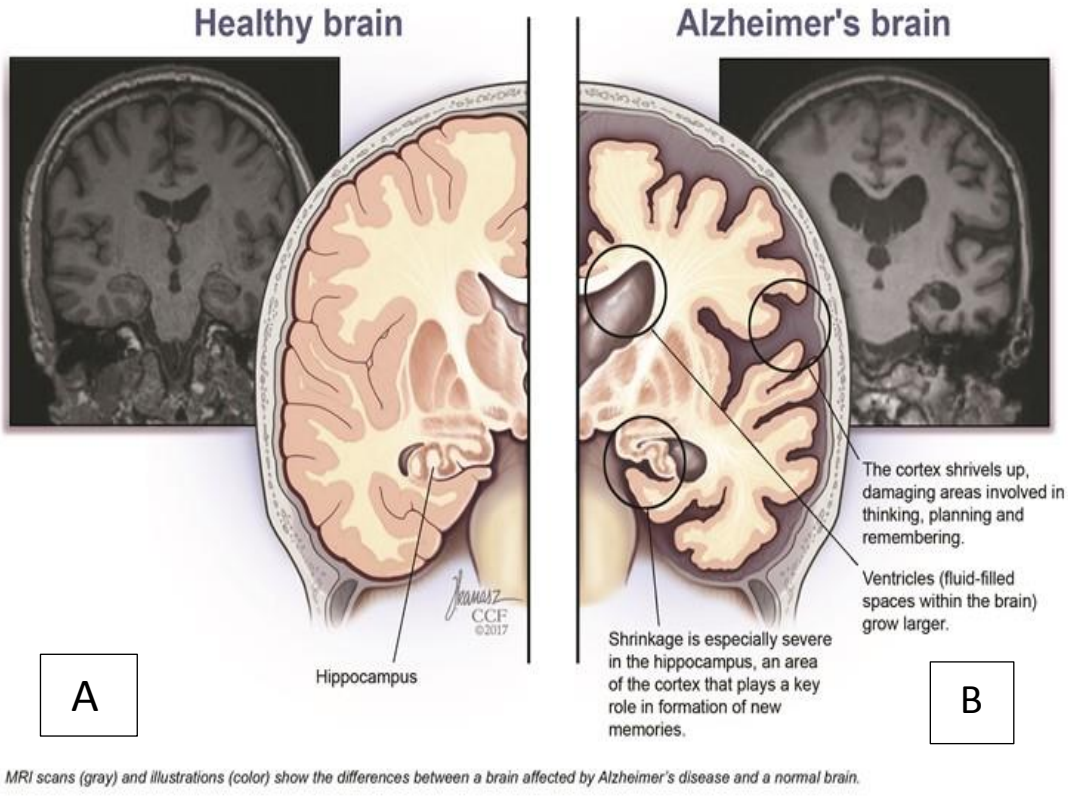

Figure 2.1: Healthy human brain (A) vs demented human brains (B)

Source: Cleveland Clinic Lou Ruvo Center for Brain Health

hyperphosphorylated tau proteins and contain no Aβ deposits and neuritic plaques (Selkoe, 2001).

2.2 Symptoms

The most common initial symptom is a gradually worsening ability to remember new information. This memory decline occurs because the first neurons to malfunction and die are usually neurons in brain regions involved in forming new memories. The rate at which symptoms of AD advance from mild to severe differs from person to person. The common symptoms associated with Alzheimer's are as follows:

i) Memory loss
ii) Misplacing items
iii) Unfounded emotions
iv) Confusion with time and location
v) Withdrawal from social activities
vi) Difficulty completing familiar tasks
vii) Difficulty solving problems
viii) Poor judgement
ix) Difficulty with words
x) Trouble with images and spaces

2.3 Risk factors for Alzheimer's disease

2.3.1 Age

As age progresses, individuals have higher risk of developing AD. Most patients develop Alzheimer disease after the age of 65 years old. The risk of developing Alzheimer disease reaches 50% for individuals beyond age 85. Since more and more people live longer, this disease has become a serious concern worldwide (Vinutha *et al*., 2007).

2.3.2 Genetics of AD

Mutations in the APP and presenilin genes lead to the production of protein Aβ42 (β-amyloid 1-42) that amasses into amyloid plaques and cause death of neurones by enhancing

the production of protein Aβ42 (Selkoe, 1999). The inheritances of the e4 allele of the alipoprotein (APOE) have been identified as a genetic risk factor (Mahley *et al*., 2006). Risk genes increase one's possibility of having the disease but do not ascertain it will occur. Individual carrying a mutation in the APOE e4 allele have a three to fifteen times increase risk of developing Alzheimer disease (Alzheimer Europe, 2004).

2.3.3 Family History

The tendency for individuals who have first-degree relative with Alzheimer's to develop the disease is higher than those who do not have (Loy *et al*., 2014). Those who have more than one first-degree relative with Alzheimer's are at even higher risk (Lautenschlager *et al*., 1996).

2.3.4 Cardiovascular Disease Risk Factors

The health of the brain is closely linked to the overall health of the heart and blood vessels. The brain is supplied with the oxygen and nutrient-rich blood it needs to function normally. Many factors such as smoking, obesity and diabetes that elevate the menace of cardiovascular disease are also linked with a higher risk of dementia (Gudala *et al*., 2013).

2.3.5 Traumatic Brain Injury

Traumatic brain injury (TBI) is the interference of normal brain function caused by a blow or jolt to the head or penetration of the human skull by a foreign object. Individuals who have experienced recurrent head injuries are at higher risk of cognitive impairment and neurodegenerative disease than individuals who have not experienced head injury (Smith *et al*., 2013).

2.4 Cholinergic systems of normal brain

Neuroanatomical identification of cholinergic neurons occurs through the immunohistochemical demonstration of ChAT, the enzyme which synthesises the neurotransmitter acetylcholine (ACh). A neuron is said to be cholinergic when it synthesizes ACh for the purpose of neurotransmission. Non-cholinergic or cholinoceptive neurons in the brain, which are ChAT-negative, include the glutamatergic, gabaergic, dopaminergic, histaminergic, serotonergic, and noradrenergic neurons (Mesulam, 2000), as well as many neuropeptides. Based on anatomic location, four groups of cholinergic neurons (Chl-Ch4) have been described in the human basal forebrain. These neurons are located around the medial septum, the vertical and horizontal limbs of the diagonal band of Broca, and the nucleus basalis of Meynert (Nagai *et al*., 1983). Among these four groups Ch4 is the most extensive (Geula *et al*., 1993). The human Ch4 can be subdivided further into another six sectors (Mesulam and Geula, 1988). The Chl and Ch2 neurons may provide the major cholinergic innervation of the hippocampus. The Ch-33 of the olfactory bulb and the Ch4 of the entire cortical mantle and amygdale.

Cholinergic cell groups are found in the upper brainstem, the pedunculopontine nucleus (Ch5), the laterodorsal tegmental nucleus (Ch6), the medial nucleus of the habenula (Ch7), the parabigeminal nucleus (Ch8) (Mesulam *et al*., 1989). The neurons Ch5 and Ch6 provide the major cholinergic innervation of the thalamus (Hallanger *et al*., 1987). The Ch5-Ch6 can also provide an additional, but minor source of cholinergic innervation of the interpenduncular nucleus and the Ch8 neurons project mostly to the superior colliculus but also to the thalamus (Hall *et al*., 1989). The Ch neurons of the striatum have almost entirely local connections with a lesser cholinergic input from Chl-Ch4 (Geula and Mesulam, 1999). Geula and Mesulam (1996) reported that the highest density of cholinergic fibers (axons) is found within core limbic areas such as the hippocampus and amygdala. Paralimbic cortical areas show the next highest density of cholinergic fibers, whereas the primary visual cortex contains the lowest. The cortical structures within the temporal lobe show a high density of cholinergic fibers, while within the occipital lobe lesser (Figure 2.2).

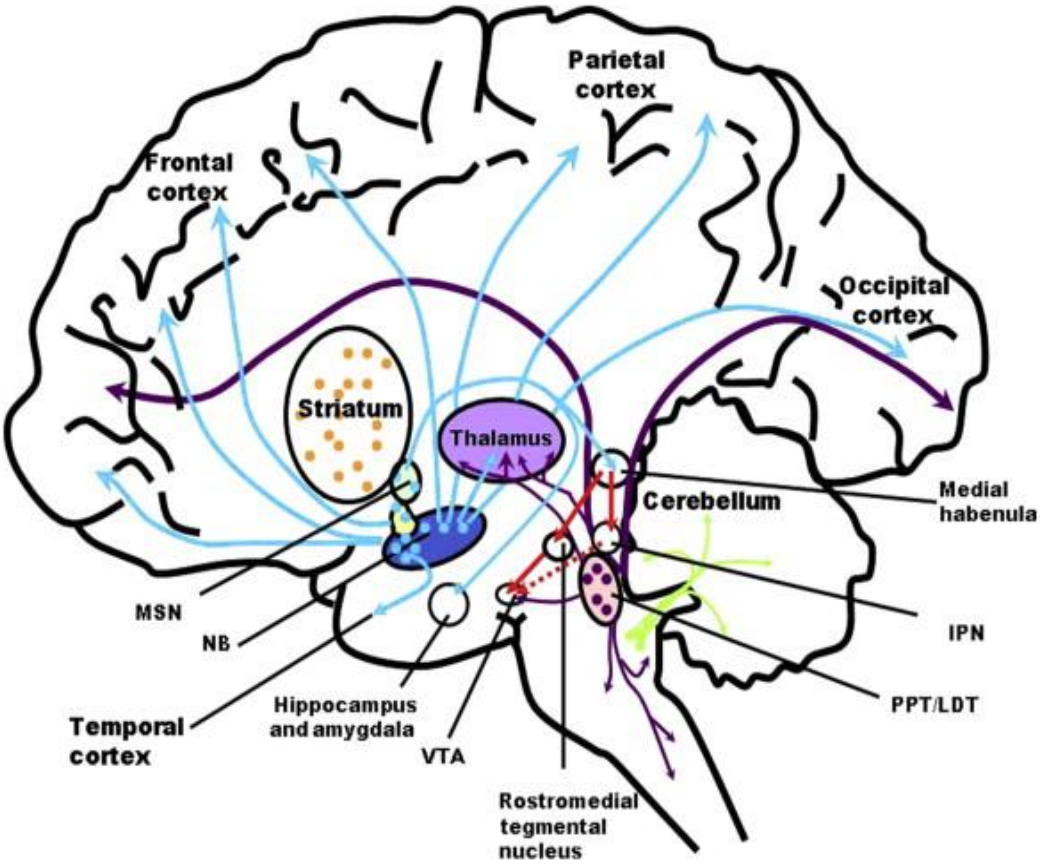

Figure 2.2: Human brain cholinergic systems
Source: ScienceDirect.com

2.4.1 Cholinesterases

Acetylcholine is found throughout the nervous system being indispensable for cerebral blood flow control, cerebral cortical development and chiefly for learning and memory processes (Schliebs and Arendt, 2001). Cholinesterase enzymes hydrolyse acetylcholine thereby reducing its half-life. So, cholinesterase inhibition encourages increase half-life of acetylcholine and subsequently extends its activity. Presently, there are two main cholinesterase (Acetylcholinesterase and butyrylcholinesterase) known (Fukami and Yokoi, 2012).

2.4.2 Acetylcholinesterase

All cholinergic neurons of the human basal forebrain and brainstem contain the cholinergic enzymes ChAT and acetylcholinesterase (Mesulam *et al*., 1989). Acetylcholinesterase may also occur in non-cholinergic neurons. The latter is synthesized in the perikaryon and then transported to dendrites, axons and further into the cell membranes. AChE is encoded by a gene on chromosome 3 and belongs to the Type B carboxylesterase gene family (Ballard, 2001). Analysis of the three dimensional structure of AChE and homologous lipase (Cygler *et al*., 1993) indicates that these enzymes have a common fold termed the a/β hydrolase fold (Ollis *et al*., 1992), in which a central ß-sheet is surrounded by loops and helices. Solution of the 3D structure provided that the cholinesterase (ChEs) contain a catalytic triad, albeit with a glutamate in place of the aspartate found in the serine proteases. The active site is situated in a deep cleft, being located almost 20 Å from the surface of the catalytic subunit, at the bottom of a long and narrow cavity. This cavity was named the active-site gorge or, since over 60% of its surface is lined by the rings of conserved aromatic residues, the aromatic gorge (Sussman *et al*., 1991).

Acetylcholinesterase comprises 90% of the total cholinesterases in the temporal cortex of normal brain (Perry *et al*., 1978 a). In adult human brain AChE is mainly present as the membrane-bound globular tetramer G4 form, and the more soluble monomer Gl form, with minor contributions of dimeric G2 and other asymmetric forms. In the cortex and hippocampus however, the G1 form represents approximately from 30% to 40% of total AChE (Attack *et al*., 1986). Studies (Ogane *et al*., 1992a) on brain fractions suggest that 60-90% of the G4 form is intracellular and membrane located while 90% of the GI form is

intracellular and cytoplasmic. The major role of the AChE is to terminate the action of ACh through catalytic hydrolysis (Volkova *et al*., 1976). Rapid hydrolysis of acetylcholine by AChE is vital for cholinergic neurotransmission, the main feature involved in cognition.

This importance is underlined by the large value of catalytic constants Kcat/Km ≈, $109M^{-1}.s^{-1}$ (Nolte *et al*., 1980), which ranks as one of the highest catalytic efficiencies known (Fersht, 1985) despite the fact that the substrate has to reach the active site at the bottom of a narrow, 20 Å deep gorge (Sussman *et al*., 1991) by diffusion. Zhou *et al*. (1998) showed that such enzyme specificity is achieved by dynamic configuration of the five aromatic rings of tyrosine (Tyr) amino acids Tyr_{121} and $_{334}$ and phenylalanine (Phe) amino acids ($Phe_{290\ 330}$ and $_{331}$), serving as the gate, where it can rapidly switch between the open and closed states (Figure 2.3). One of these open states may correspond with the ACh entering state allowing the entrance of the substrate with high efficiency.

Moreover, binding between the acetyl moiety of acetylcholine and catalytic binding site involves an interaction with three key amino acid residues. These amino acids are involved in a charge relay system within the gorge, which for acetylcholinesterase is centred on a serine (Ser_{200}) residue and involves histidine (His_{447}) and glutamine ($G1u_{334}$). In this region of the gorge two large amino acids Phe_{295} and Phe_{297} may restrict a passage to the active site for larger substrates (Greig *et al*., 2001).

The neurotransmitter ACh is synthesised in presynaptic cholinergic neurons by choline acetyltransferase (CAT). The process entails transfer of an acetyl group from acetyl-coenzyme A to choline. Until needed, the ACh molecules are stored in discrete vesicles at the ends of the presynaptic neurons. Arrival of a nerve impulse triggers the release of Ca^{2+} ions, which activate actin microfilaments that in turn pull the storage vesicles into position for ACh release. In a single event the vesicles empty their contents into the synaptic cleft. Most of these molecules bind to cholinergic receptors on adjacent postsynaptic neurons. Any that remain unbound are rapidly hydrolysed by AChE. The choline released in the process is reused in synthesising new ACh. The inhibition of acetylcholinesterase and butyrylcholinesterase increase the amount of ACh available for neurotransmission (Figure 2.4).

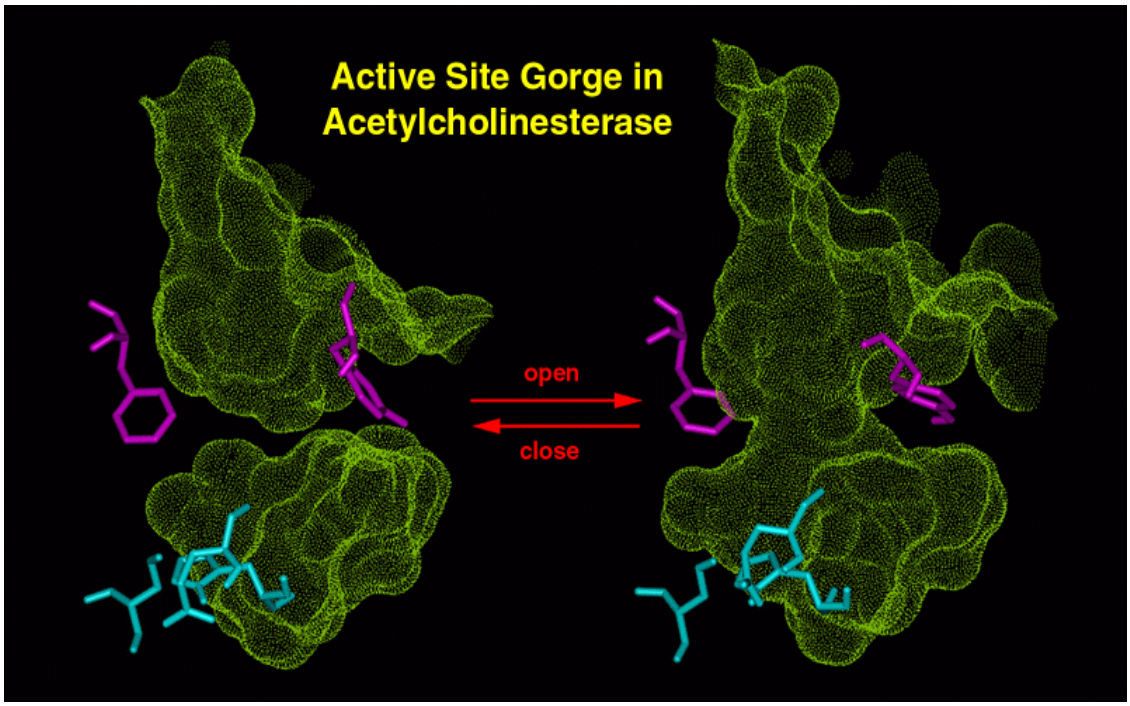

Figure 2.3: Open and close state of acetylcholinesterase with Tyr and Phe residues
Source: McCammon Group-UCSD, 2003

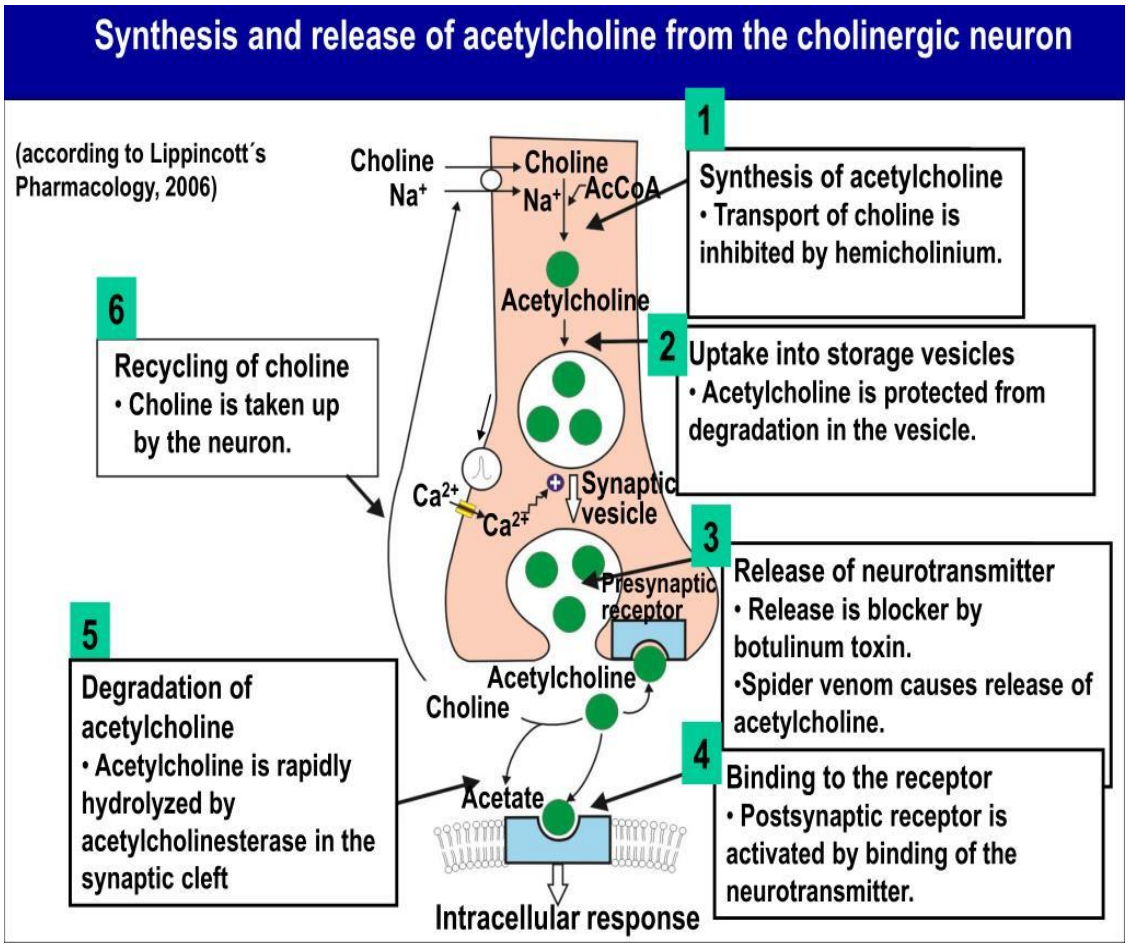

Figure 2.4: Cholinergic neurotransmission.

Source: Lippincott's Pharmacology, 2006

2.4.3 Butyrylcholinesterase

Butyrylcholinesterase is encoded by a gene on chromosome 3 and as AChE belongs to the Type B carboxylesterase gene family (Gnatt *et al*., 1991). AChE and BuChE share 65% amino acid homology despite being encoded by different genes (Soreq and Zaku, 1993). The human cerebral neurocortex also contains BuChE-rich neurons (Darvesh *et al*., 1998). The number of these neurons is approximately two orders of magnitude less than the number of AChE-rich neurons (Mesulam, 2000). In the normal brain BuChE, primary located in glial cells, accounts for 20% of ChE activity, while AChE accounts for the remaining 80% (Greig *et al*., 2001). Most cortical BuChErich neurons are non-pyramidal, lie predominantly in deeper cortical layers, including layer 6 and in the immediately adjacent juxtacortical region (Mesulam *et al*., 1995). Limbic structures such as amygdala, hippocampus, and entorhinal cortex contain a slightly higher density of BuChE-rich neurons. In the hippocampal complex, BuChE-rich neurons are located mostly within a white-matter layer. There are no BuChE-rich axons in the cerebral cortex.

Ekholm and Konschin (1999) summarised structural differences between BuChE and AChE. In BuChE a similar channel, an aromatic gorge, as in AChE leading to the active site was found, although it was not as narrow as in AChE and it did not contain as many aromatic amino acids. Moreover, Phe_{295} and Phe_{297} in comparison with AChE are replaced with two smaller amino acids-valine and leucine-creating additional space for entering large substrates. The space of the active centre in BuChE is greater than in AChE. An intra-atomic distance analysis of the active site indicates that two hydrogen bonds easily form in AChE but only one in BuChE. The active site in BuChE is therefore less rigid than in AChE, allowing the substrate move more freely. BuChE, like AChE, also occurs in asymmetric and globular forms where they exist as amphiphilic and hydrophilic species in different brain regions. Six major molecular forms are recognised, three globular (G_1, G_2 and G_4) and three asymmetric (A_4, A_8 and A_{12}), the latter being associated with a triple-strand collagen like tail (Mesulam, 2000). G_4 form is the most abundant form of ChEs in the healthy human brain and is central to breakdown of ACh. In contrast, G_1 form present in smaller amounts in the healthy human brain and plays a relatively minor role in ACh degradation (Arendt *et al*., 1992).

2.5 Prolyl oligopeptidase

Prolyl oligopeptidase was discovered in the human uterus as an oxytocin-degrading enzyme (Walter *et al*., 1971). A similar enzyme was found in *Chryseobacterium meningosepticum* (Yoshimoto *et al*., 1980). Since the enzyme showed a high specificity for proline residues, and hydrolyzed the peptide bond on their carboxyl side, it was originally named post-proline cleaving enzyme. During the period 1978-1983, several enzymes hydrolyzing the Pro-Xaa bonds of biologically active peptides (thyrotropin-releasing hormone, bradykinin, substance P, neurotensin, angiotensin II and luteinizing hormone - releasing hormone, α-melanocyte-stimulating hormone and dynorphin were described. They were referred to as post-proline endopeptidase, TRH deamidase and brain kinase B or endooligopeptidase B. However, all of them were finally found to be identical to the post-proline cleaving enzyme. The name post-proline endopeptidase was recommended by IUBMB in 1978, and then changed to prolyl endopeptidase in the supplement to Enzyme Nomenclature in 1981.

Although prolyl oligopeptidase was recognized as a serine peptidase as early as 1977 (Yoshimoto *et al*., 1977), it is commonly found to be activated by thiol compounds, and for a time the thiol-dependent activity was recognized by a separate EC number, EC 3.4.22.18. On the basis of the oligopeptidase nature of the reaction catalyzed, and the amino acid sequence homology with other oligopeptidases, the name prolyl oligopeptidase (POP) was proposed (Barrett and Rawlings, 1992). The wide distribution of POP as well as its high activity and specificity towards biologically active peptides suggest that the enzyme participates in the regulation of these substances. Accordingly, there has been significant research interest in the enzyme, and there are indications of roles in memory and other neurological processes (Li *et al*., 1996, Toide *et al*., 1997).

2.6. Molecular Docking

Molecular docking is one of the most frequently used methods in structural based drug design (SBDD) because of its ability to predict, with a substantial degree of accuracy, the conformation of small-molecule ligands within the appropriate target binding site (Meng *et al*., 2011). Following the development of the first algorithms in the 1980s, molecular docking became an essential tool in drug discovery (López-Vallejo and Caulfield, 2011). For example, investigations involving crucial molecular events, including ligand binding

modes and the corresponding intermolecular interactions that stabilize the ligand-receptor complex, can be conveniently performed. Furthermore, molecular docking algorithms execute quantitative predictions of binding energetics, providing rankings of docked compounds based on the binding affinity of ligand-receptor complexes (Huang and Zou, 2010). Molecular docking programs perform these tasks through a cyclical process, in which the ligand conformation is evaluated by specific scoring functions. This process is carried out recursively until converging to a solution of minimum energy (Yuriev *et al*., 2011).

2.7 Licensed anticholinesterase drugs

2.7.1 Tacrine (Cognes ®)

The first marketed acetylcholinesterase inhibitor approved by FDA in 1993 was Tacrine (I) (Figure 2.3) (Thal, 1999). Harel *et al*. (1993) demonstrated that the three-ring structure of tacrine is stacked against the indole tryptophan (Trp_{84}) at the aromatic gorge and that the N-methylacridinium forms a charge-transfer complex with a tryptophan in the active site of AChE. They also reported that in tacrine/AChE complex, the only residue undergoing significant conformational change is phenylalanine (Phe_{330}). Tacrine thus binds between the rings of Phe_{330} and Trp_{84}.

Acetylcholinesterase is inhibited preferentially by tacrine especially in the hippocampus and cortex areas of the brain (Enz *et al*., 1993). Moreover, Zhao and Tang (2002) reported that tacrine also preferentially inhibits the Gl human form of AChE of hippocampal, striatum and cortical origins, exhibiting significant differences in Ki values between G4 and G1 forms. The Gl form is predominant in the brain of people living with AD. Tacrine is a non-competitive type of inhibitor not only with the enzyme but also the G1 and G4 forms. In addition, Pacheco *et al*. (1995) showed that tacrine readily inhibits both AChE and BuChE in a mixed, noncompetitive way. Giacobini (2000) also summarised evidence confirming that tacrine is a non-selective inhibitor of cholinesterases.

Increased binding of [^{11}C]-nicotine has been observed in the temporal cortex of AD patients treated with tacrine, 80 mg/day for 3 months (Nordberg, 2000). He also suggested that the restoration of cortical nicotinic receptors, following tacrine treatment, may be due to a stimulatory effect of the inhibitor on these receptors via an allosteric site which is separately located from ACh binding site. Nevertheless, Prince *et al*. (2002) reported on an *in vitro*

study of tacrine on nAChRs expressed in human adult cells. They found that the mean channel open time decreased with increasing tacrine concentration in a voltage-dependent manner, suggesting that tacrine acts as an open channel blocker.

2.7.2 Donepezil (Aricept®)

In 1996 donepezil (Figure 2.3) received FDA approval for marketing (Nightingale, 1997). Donepezil (II) (E2020) is a drug with both high affinity and a high degree of selectivity for acetylcholinesterase, as opposed to butyrylcholinesterase (Snape *et al*., 1999), with the BuChE/AChE ratio of inhibition is around 1000 (Giacobini, 2000). The high affinity and selectivity results from a fact that Phe_{330} and Trp_{279} residues are preserved in acetylcholinesterase but absent in butyrylcholinesterase.

Zhao and Tang (2002) reported that E2020 is more selective for G1 human form of AChE in striatum and hippocampus than G_4 form. In contrast, in cortex both forms were inhibited to similar degree, namely Ki values for G_1 and G_4 forms were $3.5\pm1.2x10^{-9}$ M and $4.0\pm1.5 \times 10^{-9}$ M, respectively. In addition, E2020, as tacrine, shows non-competitive type of inhibition not only with the enzyme but it's both forms, indicating that it is down to the inhibitor to determine the nature of inhibition, not the molecular form of the enzyme or its tissue source.

Donepezil readily penetrates the blood brain barrier (BBB) in rats (Kosasa *et al*., 2000) and has non-competitive, reversible type of inhibition of AChE. Donepezil, like tacrine, is antagonist to M1 receptor with binding activity at nicotinic sites in both the prefrontal cortex and hippocampus of aged rats (Barnes *et al*., 2000). Moreover, Takada *et al*. (2003) showed that the drug safeguards cortical neurons against glutamate neurotoxicity via α4β2- and α7-nAChRs and also protects apoptotic neuronal death.

2.7.3 Rivastigmine (Exelon ®)

Rivastigmine (III) (Figure 2.3) belongs to the carbamate class of acetylcholinesterase inhibitors and was approved by the FDA in 2000 and was shown to have kinetic and structural studies on interaction of ChEs with rivastigmine (Bar-On *et al*., 2002). They found that the carbamvl moiety of the inhibitor is covalently linked to the active site serine (Ser_{200}) with the leaving group. (-)-S-3-[1-(dimethylamino) ethyl] phenol (NAP), being retained in the "anionic" site without causing any conformational changes.

Reaction with rivastigmine resulted in disruption of the catalytic triad not only within Torpedo califoi"nica AChE (TcAChE) but also recombinant human ACNE. Bar-On *et al*. (2002) suggested that this is due to NAP (a competitive inhibitor of AChE) causing a disturbance of His440 away from its catalytic triad. Alternatively, the disturbance of His440 may occur by NAP orienting the transition state such that the V-ethylmethyl group crowds the histidine. Rivastigmine preferentially inhibits the G_1 form of human brain acetylcholinesterase in cortex, hippocampus and striatum (Zhao and Tang, 2002). The G_4 form was also inhibited in these brain areas but to a lesser degree. The level of G_1 form in AD does not decline in the cerebral cortex and it found to be present in plaques and tangles (Greig *et al*., 2001).

2.7.4 Galanthamine (Reminyl ®)

Galanthamine (IV) (Figure 2.3) is a naturally occurring alkaloid in plant species of *Galanthus* and *Narcissus* (Hanks, 2002). The drug was approved in February, 2001 by FDA for the treatment of Alzheimer's diseasse (Alzheimer Research Forum). Greenblatt *et al*. (1999) reported that the inhibitor binds at the base of the active site gorge of TcAChE, interacting with both the choline-binding site (Trp_{84}) and the acyl-binding pocket (Phe_{288}, Phe_{290}). The tertiary amine group of galanthamine does not interact closely with Trp_{84}; rather, the double bond of its cyclohexene ring stacks against the indole ring. The tertiary amine appears to make a non-conventional hydrogen bond, via its N-methyl group, to Asp72, near the top of the gorge. The hydroxyl group of the inhibitor makes a strong hydrogen bond (2.7 Å) with $G1u_{199}$. The binding of galanthamine to TcAChE is tight due the rigid chemical structure of the inhibitor.

2.7.5 Unlicensed plant derived drugs

The inhibitor of acetylcholinesterase huperzine A (V) (Figure 2.3) is naturally occurring sesquiterpene alkaloid in species of *Huperzia serrata* (Liu *et al*., 1986). Huperzine A is a non-competitive, slow reversible inhibitor of acetylcholinesterase (Liu *et al*., 1986). It inhibits mammalian AChE more than BuChE with a BuChE/AChE ratio of 908 (Giacobini, 2000). It also inhibits the G4 form of human AChE more than the GI form in cortex with Ki values of $7.0\pm3.5 \times 10^{-9}$ M and $3.5\pm1.5 \times 10^{-7}$M respectively, whereas in hippocampus and striatum this selectivity is less apparent (Zhao and Tang, 2002).

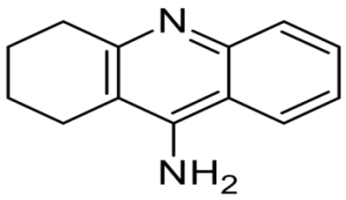

Tacrine ($C_{13}H_{14}N_2$) (I)

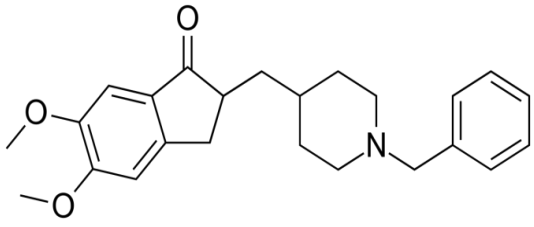

Donepezil ($C_{24}H_{29}N0_3$) (II)

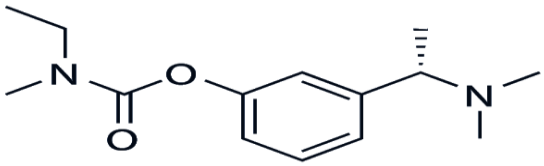

Rivastigmine ($C_{14}H_{22}N_20_2$) (III)

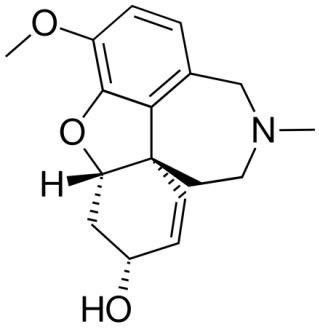

(-)-Galanthamine ($C_{17}H_{21}NO_3$) (IV)

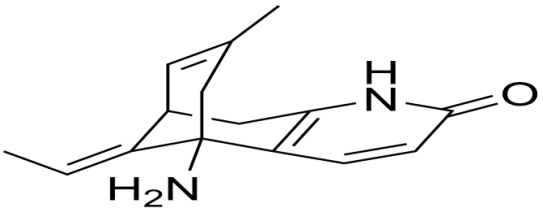

Huperzine-A (V)

Figure 2.5: Licensed and unlicensed drugs for treatment of Alzheimer's

2.8 Natural compounds with cholinesterase inhibitory activity

2.8.1 Alkaloids

Alkaloids are perhaps the major group of bioactive principles with cholinesterase inhibitory activity at lower dose. Two synthetic analogues neostigmine and pyridostigmine were developed from physostigmine (VI) (*Physostigma venenosum*). Neostigmine (VII) and pyridostigmine (VIII) are hydrophilic compounds used in peripheral cholinergic deficiencies such as in myasthenia gravis. Cymserine (IX) is another physostigmine analogue an active reversible and selective human BuChE inhibitor (Zhu *et al*., 2000) (Figure 2.6). Berberine (X), an isoquinoline alkaloid isolated from the dried rhizome of Chinese *Rhizoma coptidis* has promising cholinesterase inhibitory potentials with mostly hydrophobic interactions with the enzyme (Ji *et al*., 2012).

The possible interactions among geissospermine (XI) (indole-indoline alkaloid) isolated from *Geissospermum vellosii* Allem. and AChE of the Pacific electric ray were studied by molecular docking; hydrogen bonds, hydrophobic interactions and p-p stacking are involved (Figure 2.6) (Araujo *et al.,* 2011). Infractopicrin (XII) an indole alkaloid (Figure 2.6) isolated from *Cortinarius infractus* binds preferentially to the oxyanion hole of the AChE enzyme by p-p interactions with the aromatic residues (Geissler *et al*., 2010). Juliflorine (XIII) (Figure 2.6) a piperidine alkaloid isolated from the leaves of *Prosopis juliflora*, noncompetitively inhibits both acetylcholinesterase and butyrylcholinesterase with IC_{50} value of 0.42 µM and 0.12 µM, respectively (Choudhary *et al*., 2005).

Houghton *et al*. (2004) reported the cholinesterase inhibitory properties of alkaloids from Two Nigerian *Crinum* species. *Crinum jagus, Crinum glaucum* Haemanthamine (XIV) and Hamayne (XV).Two other *Crinum* alkaloids are Crinamine (XVI) and Lycorine (XVII) isolated from the same species (Figure 2.7). The most active alkaloids isolated were hamayne (IC_{50} 250 microM) and lycorine (IC_{50} 450 microM) whilst other alkaloids were comparatively inactive with haemanthamane giving 3% inhibition and crinamine giving 4.4% inhibition at 50 mg ml(-1) (174 microM).

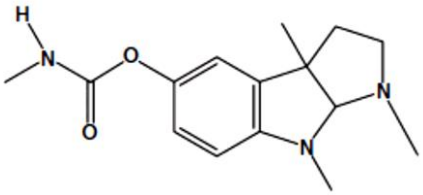

Physostigmine (VI)

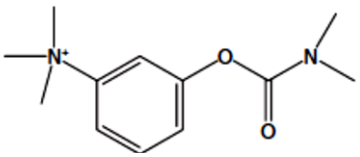

Neostigmine (VII)

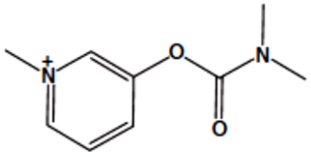

Pyridostigmine (VIII)

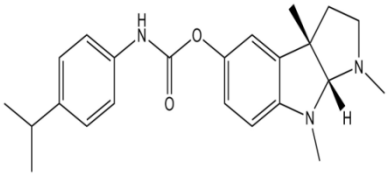

Cymserine (IX)

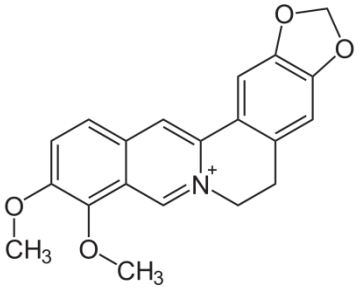

Berberine (X)

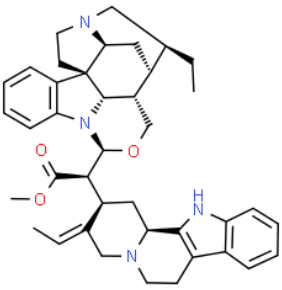

Geissospermine (XI)

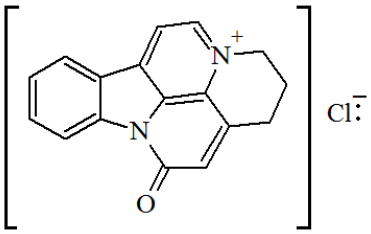

Infractopicrin (XII)

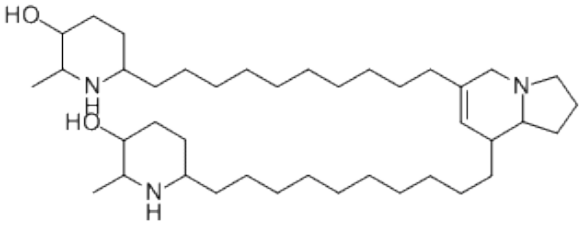

Juliflorine (XIII)

Figure 2.6: Chemical structure of alkaloids with cholinesterase inhibitory activities.

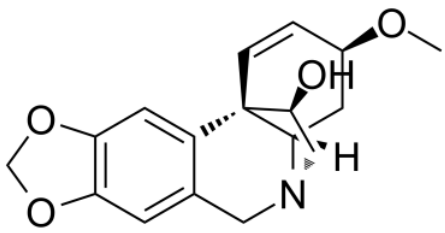

Haemanthamine (XIV)

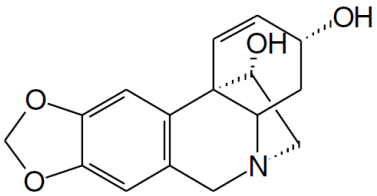

Hamayne (XV)

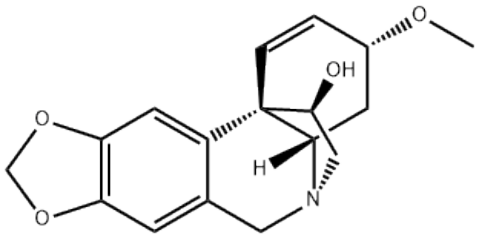

Crinamine (XVI)

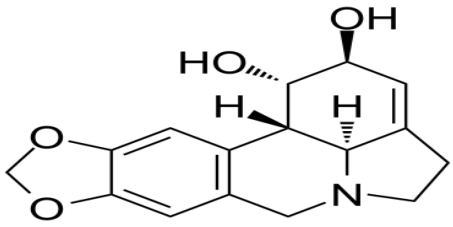

Lycorine (XVII)

Figure 2.7: Chemical structure of four crinum alkaloids with cholinesterase inhibitory activities.

2.8.2 Coumarins

Methoxsalen (XVIII) (xanthotoxin) (Figure 2.8), a furanocoumarin isolated from *Poncirus trifoliate* demonstrated a potent inhibition of acetylcholinesterase. The anti-AChE activity of methoxsalen was confirmed by the inhibition of mouse brain enzyme and amelioration of drug-induced behavioural impairment in an AD-like mouse model (Kim *et al*., 2011). Also, decursinol (XIX) (Figure 2.8), a pyranocoumarin isolated from *Angelica gigas* showed good activity against acetylcholinesterase (Kang *et al*., 2001).

2.8.3 Flavonoids

Isoflavones or flavones possess high AChE activity compared to other class of flavonoids. Pomiferin (Figure 2.9) a prenylated isoflavone isolated from *Maclura pominifera* was found to possess high acetylcholinesterase inhibitory activity with IC_{50} value of 96 µM (Uriarte-Pueyo and Calvo, 2011). Also, scopolamine-induced amnesia in mice was ameliorated by naringenin (Figure 2.9) a flavanone isolated from *Citrus junos* (Heo *et al*., 2004).

2.8.4 Quinones

Thespesia populnea (L.) Sol. ex Correa is a plant reported to enhance memory and reduce brain ChE activity in mice (Vasudevan *et al*., 2006). It was hypothesized that mansonones (naphthoquinones) were responsible for this activity. Mansonone E (XXII) (Figure 2.10) was the tested naphthoquinone with highest activity towards AChE and BuChE (IC_{50} of 23.5 µm and 62.4 µm, respectively) (Changwong *et al*., 2012).

2.8.5 Stilbenes

Gnetol (XXIII), a stilbene isolated from *Ficus foveolata* has proven to have potent BuChE inhibitory activity via a reversible and competitive mechanism (Sermboonpaisarn and Sawasdee, 2012). Kobophenol A (XIV) (Figure 2.11), a tetramer of resveratrol showed lower acetylcholinesterase inhibitory potential with IC_{50} value of 115.8 mM probably due to steric hindrance (Sung *et al*., 2002).

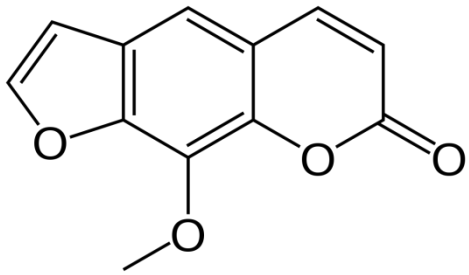

Methoxsalen (XVIII)

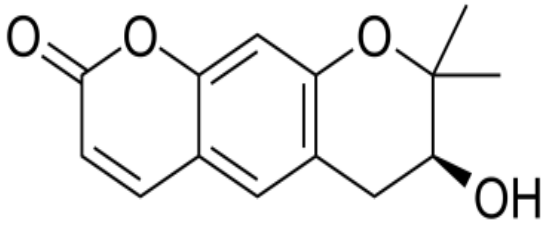

Decursinol (XIX)

Figure 2.8**:** Chemical structure of two coumarins with cholinesterase inhibitory activities.

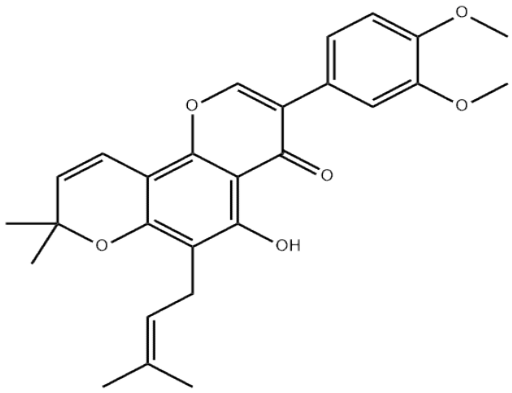

Pomiferin (XX)

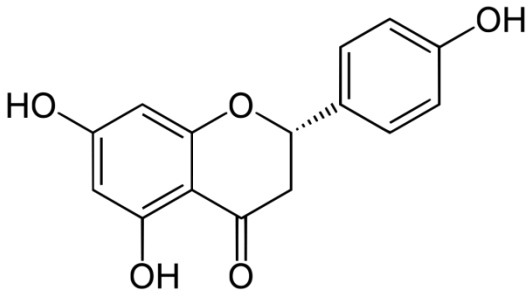

Naringenin (XXI)

Figure 2.9: Chemical structure of two flavonoids with memory enhancing activities

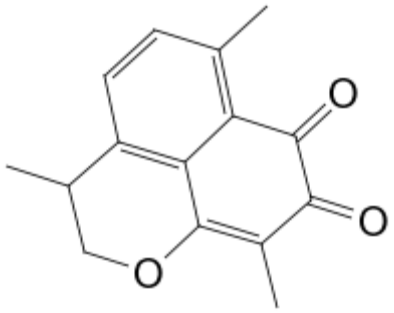

Mansonone E (XXII)

Figure 2.10: Chemical structure of Mansonone E, a quinone with cholinesterase inhibitory activities

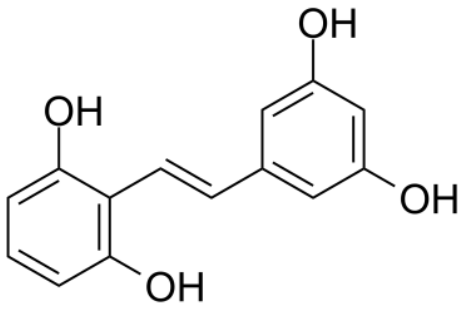

Gnetol (XXIII)

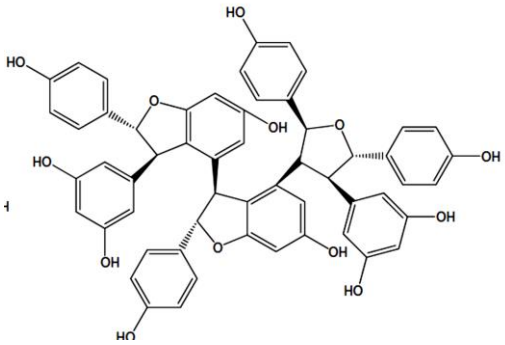

Kobophenol A (XXIV)

Figure 2.11: Chemical structure of two stilbenes with acetylcholinesterase inhibitory activities.

2.8.6 Terpenic compounds

Perry *et al*. (2000) reported that 1,8-cineole (XXV) (Figure 2.12) a volatile oil (monoterpene) from *Salvia lavandulaefolia* is the main constituents proven to be potent against mammalian acetylcholinesterase than against AChE from the electric eel (Picollo *et al.*, 2008).

Also, two diterpenoids, dihydrotanshinone (XXVI) and cryptotanshinone (XXVII) (Figure 2.12) isolated from *Salvia miltiorrhiza* Bunge root which are proven to inhibit AChE in a noncompetitive manner. In addition, attending to their lipophilicity, dihydrotanshinone and cryptotanshinone have the potential to penetrate the blood–brain barrier (Ren *et al*., 2004).

Further more, sclareol (XXVIII), (Figure 2.12) a diterpenoid isolated from *Salvia chrysophylla* is testified to show potent acetylcholinesterase and butyrylcholinesterase inhibitory activity (Çulhaogˇlu *et al*., 2013). Labdane-type diterpenoids leoheteronin A (XXIX) and leopersin G (XXX) are hopeful acetylcholinesterase inhibitors (Hung *et al*., 2011).

Taraxerol (XXXI), leucisterol (XXXII), ursolic acid (XXXIII) (Figure 2.12) are amongst the steroids and triterpenes that possess cholinesterase inhibitory action. Ursolic and oleanolic acids are reported to be selective against AChE as described by Yilmaz *et al*. (2012).

2.8.7 Xanthones

Xanthones are in general, weak ChE inhibitors, however, prenylated xanthone (Allanxanthone A (XXXIV)) showed good acetylcholinesterase and butyrylcholinesterase inhibitory activity (Lenta *et al*., 2007). Triptexanthoside C (XXXV) (Figure 2.12) isolated from *Gentianella amarella* (L.) Borner was proven to inhibit AChE due to the presence of methoxy group at C3 (Urbain *et al*., 2008) and bellidifolin (XXXVI) (Figure 2.13) isolated from *Gentiana campestris* (Gentianaceae) were reported to exhibit significant inhibition of AChE (Urbain *et al*., 2004).

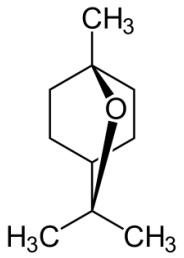

1,8-cineole (XXV)

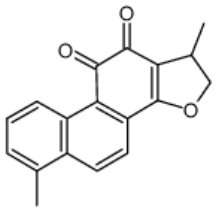

Dihydrotanshinone (XXVI)

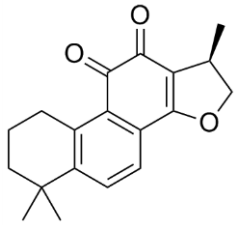

Cryptotanshinone (XXVII)

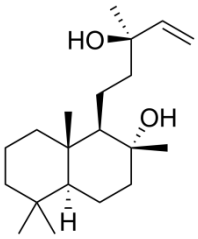

Sclareol (XXVIII)

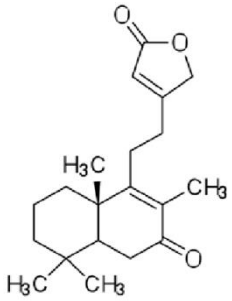

Leoheteronin A (XXIX)

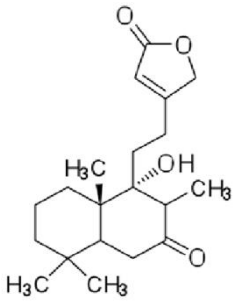

Leopersin G (XXX)

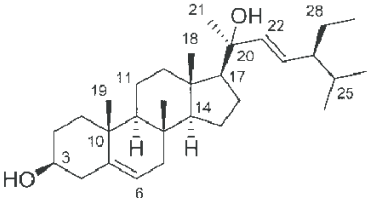

Taraxerol (XXXI)

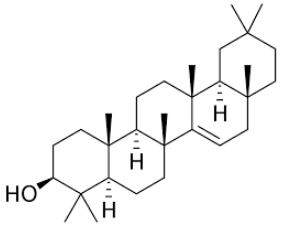

Leucisterol (XXXII)

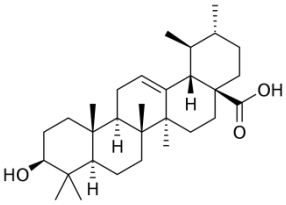

Ursolic acid (XXXIII)

Figure 2.12: Chemical structure of terpenic compounds with cholinesterase inhibitory activities.

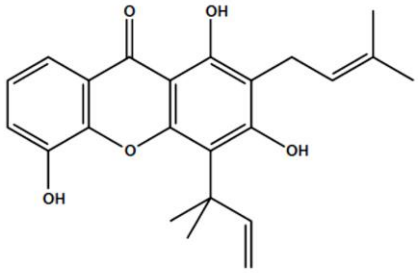

Allanxanthone A (XXXIV)

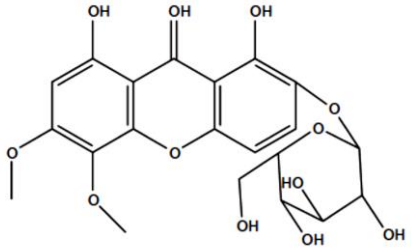

Triptexanthoside C (XXXV)

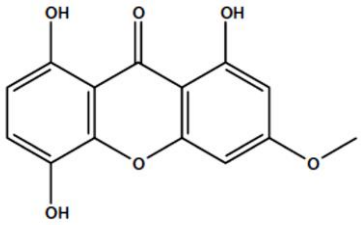

Bellidifolin (XXXVI)

Figure 2.13: Chemical structure of xanthones with cholinesterase inhibitory activities.

2.8.8 Lignans

The secondary metabolite from the fruit of *Schizandra chinensis* (Schisandraceae) having both aromatic methylenedioxy and hydroxyl groups on their cyclooctadiene ring such as gomisin C (XXXVII), gomisin D (XXXVIII), gomisin G (XXXIX), schisandrol B (XL) and gomisin A (XLI) (Figure 2.14) completely inhibited AChE in a concentration-dependent way (Ingkaninan *et al*., 2006).

2.8.9 Sesquiterpene, meroterpenoids, ceramides

A sesquiterpene known as Zerumbone (XLII) (Figure 2.15) isolated from *Zingiber zerumbet* (Zingiberaceae) was reported to have inhibition effect against acetylcholinesterase using thin layer bioautography assay method. Zerumbone has an enzymolytic effect towards acetylcholinesterase (Bustamam *et al*., 2008). Similarly, Territrem B (XLIII) (Figure 2.15) a bioactive compound isolated from the fungus *Aspergillus* terreus (Zhao *et al*., 2000), Arisugacins (XLIV) a meroterpenoid from *Penicillium* species (Otoguro *et al*., 1997) along with tanacetamides (XLV) a ceramide isolated from whole plants of *Tanacetum artemisioides* (Asteraceae) (Ahmad *et al*., 2004) were reported to have good acetylcholinesterase inhibitory activities.

2.9 Research plant

2.9.1 Description of *Phyllanthus muellerianus* (Kuntze) Exell (Euphorbiaceae)

Phyllanthus muellerianus (Kuntze) Exell (Euphorbiaceae) (Figure 2.16) is a climbing shrub or small tree up to 12 m tall, branches spreading or pendulous, main branches stout, angular, reddish tinged, branchlets 15–20 cm long with several short axillary shoots; branch basis transformed into a pair of spines. It has fleshy fruit that are copious panicles of small red, shining berries that eventually turn black. It can be found in riverine forest and wooded grassland (Agyare *et al*., 2011). Common names in Nigeria includes: EDO igbehen = thorns of a fish, IGBO *(Idumuje)* Anya nnụ̀nụ̀ = bird's eye, YORUBA (arunjeran).

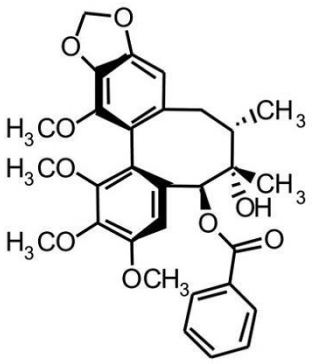

Gomisin C (XXXVII)

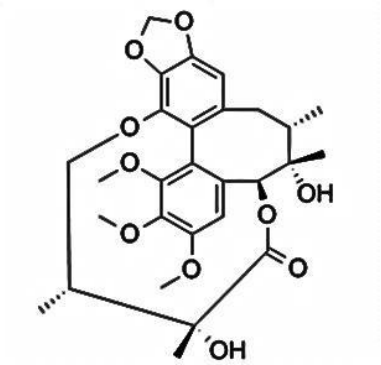

Gomisin D (XXXVIII)

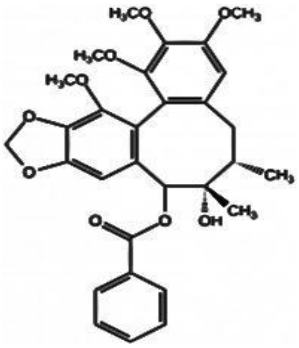

Gomisin G (XXXIX)

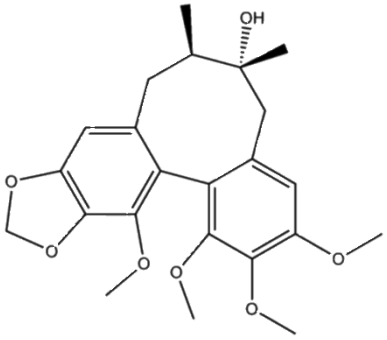

Schisandrol B (XL)

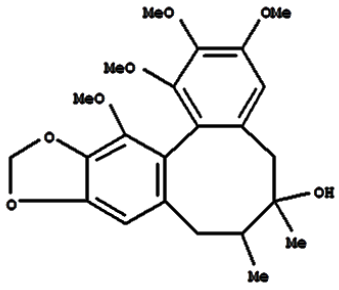

Gomisin A (XLI)

Figure 2.14: Structure of five lignans with cholinesterase inhibitory activities.

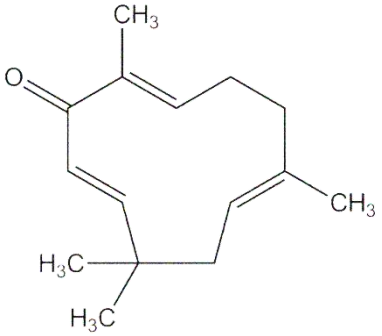

Zerumbone (XLII)

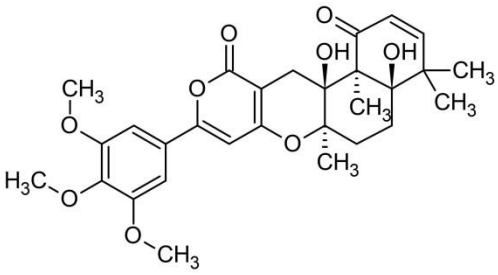

Territrem B (XLIII)

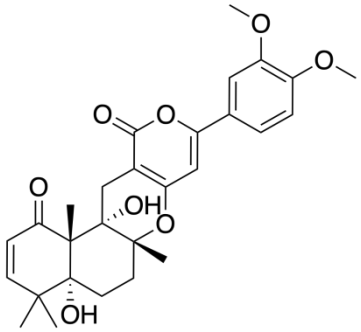

Arisugacins (XLIV)

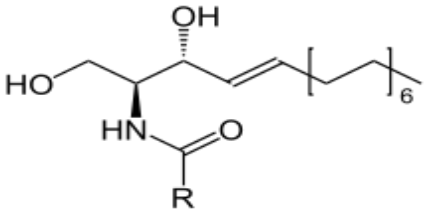

Tanacetamides (XLV)

Figure 2.15: Chemical structure of Sesquiterpene, meroterpenoids, ceramides with cholinesterase inhibitory activities.

Figure 2.16: *Phyllantus muellerianus* (Kuntz) Excell (Euphorbiaceae)

2.9.2 Medicinal Uses of *Phyllanthus muellerianus*

Phyllanthus muellerianus is widely used in the treatment of intestinal problems. The young shoots is prepared in form of a tea (infusion) and taken to treat severe dysentery. Decoction of the leaf is taken to treat constipation in Sierra Leone. Powdered roasted roots with palm oil are taken to treat stomach problems and as an anti-emetic in Congo while in Tanzania, roots of *Phyllanthus muellerianus* are pounded in water and the liquid is drunk to treat diarrhoea.

Leaf sap or sap from the thick hollow stem is applied as eye drops to treat pain in the eyes or eye infections in the West African region. Decoction of the bark is known to treat sore throat, cough, pneumonia and enlarged glands. Crushed leafy twigs are rubbed on the body to treat paralysis. Decoction of the root bark is taken as an alterative and to treat fever In Nigeria (Fowler, 2006). A twig and decoction of the root is taken to treat jaundice and urethral discharges (Siram *et al*., 2004). In Central African Republic the fresh root bark is crushed and macerated in water or palm wine and the liquid drunk as an aphrodisiac. In Gabon roasted powdered twigs are eaten with plant ash to treat dysmenorrhoea. In DR Congo dried bark powder is sniffed to treat colds and sinusitis (an inflammation of the tissue lining the sinuses). A root bark decoction is applied to swellings and is drunk to treat gonorrhoea. Stem ash is applied to scarifications to treat rheumatism and intercostal pain. In Tanzania, a root decoction is taken to treat hard abscesses. Powdered dried roots, stem bark and pounded leaves are sprinkled on wounds as a dressing (Doughari and Sunday 2008, Agyare *et al*., 2009). Maceration of the leaves and roots in Cameroon is used to wash the body to treat rash with fever in children. A leaf decoction is taken to treat anaemia and also used as a mouthwash to treat toothache In DR Congo. A leaf extract is used as a bath and a vapour bath to treat venereal diseases (Dalziel, 1937).

2.9.3 Compounds previously isolated from *Phyllanthus muellerianus*

Compounds isolated from *Phyllanthus muellerianus* includes 3-Friedelanone (XLVI), β-Sitosterol (XLVII), Bis(2-ethyloctyl)phthalate (XLVIII), caffeic acid (XLIX), corilagin (L), astragalin (LI), isoquercitrin (LII), quercitrin (LIII), 3,5-dicaffeoylquinic acid (LIV), caffeoylmalic acid (LV), chlorogenic acid (LVI), gallic acid (LVII), methyl gallate (LVIII) and geraniin (LIX) (Figure 2.17) (Saleem *et al*., 2009, Agyare *et al*., 2011, Ndjonka *et al*., 2012).

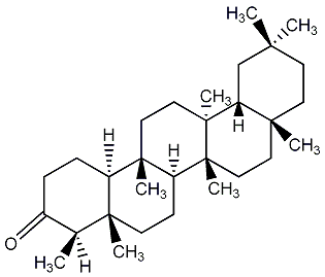

3-Friedelanone (XLVI)

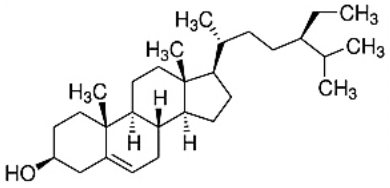

β-Sitosterol (XLVII)

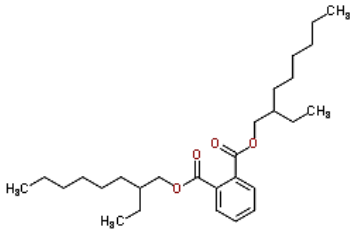

Bis(2-ethyloctyl)phthalate (XLVIII)

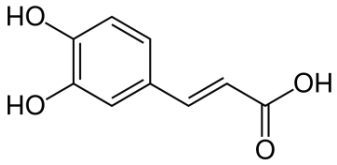

Caffeic acid (XLIX)

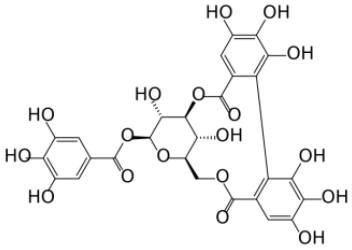

Corilagin (L)

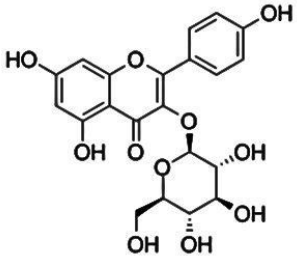

Astragalin (LI)

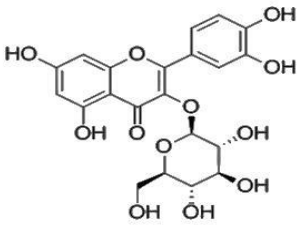

Isoquercitrin (LII)

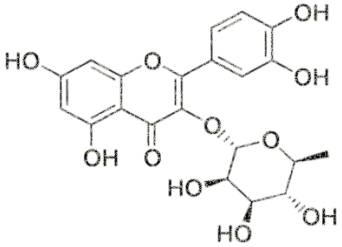

Quercitrin (LIII)

Figure 2.17: Compounds isolated from *Phyllanthus muellerianus*

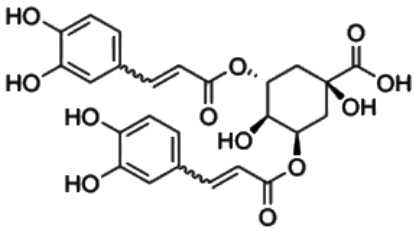

3,5-Dicaffeoylquinic acid (LIV)

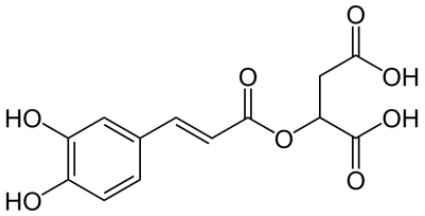

Caffeoylmalic acid (LV)

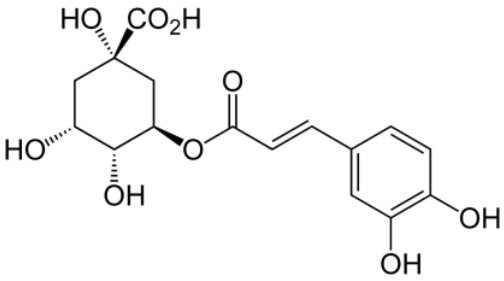

Chlorogenic acid (LVI)

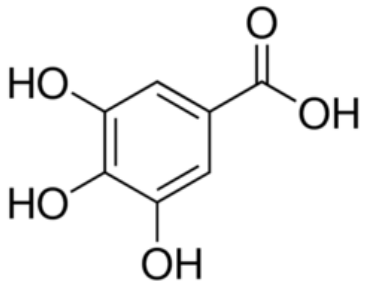

Gallic acid (LVII)

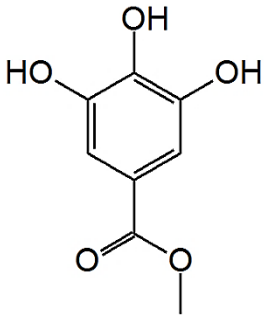

Methyl gallate (LVIII)

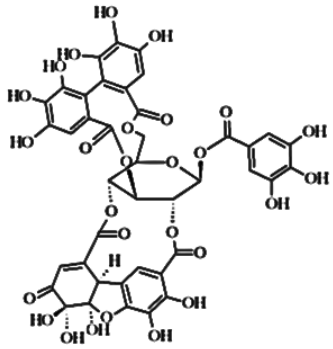

Geraniin (LIX)

Figure 2.17: Compounds isolated from *Phyllanthus muellerianus* (contd.)

2.10 Description of *Tinospora cordifolia* (Willd.) Miers ex Hook. F. and Thoms

Tinospora cordifolia (heart leaved moonseed) (Figure 2.18) is a large deciduous, extensively spreading climbing shrub with a number of coiling branches. Stem of this plant is rather succulent with long, filiform, fleshy and climbing in nature. Aerial roots arise from the branches. The bark is creamy white to grey in colour and deeply left spirally (Khosa and Prasad, 1971). Leaves of this plant are simple, alternate, pulvinate, heart shaped, twisted partially and half way round. Lamina is ovate, 10-20 cm long, 7 nerved and deeply cordate at the base and membranous. Flowers are unisexual, recemes, greenish yellow in colour, appears when plant is leaf less. Male flowers are clustered and female flowers exist in solitary inflorescence (Kirtikar and Basu, 1975). Their fruit are orange-red in colour, fleshy, aggregate of 1-3 and ovoid, smooth, drupelets on thick stalk with a sub terminal style scars (Nadkarni and Nadkarni, 1976).

2.10.1 Constituents of *Tinospora cordifolia*

Compounds isolated from *Phyllanthus muellerianus* includes berberine (LX) a major alkaloid in the stem, choline (LXI), furanolactone (LXII), magnoflorine (LXIII), tinocordifolin (LXIV), isocolumbin (LXV), cordioside (LXVI), ecdysterone (LXVII), palmatosides (LXVIII), Tetrahydropalmetine (LXIX), Syringin (LXX), Tetrahydrofuran (LXXI), Jatrorrhizine (LXXII) and Tembetarine (LXXIII) (Figure 2.19) (Upadhaya *et al*., 2010, De-Oliveria *et al*., 2012).

2.10.2 Pharmacological importance of *Tinospora cordifolia*

2.10.2.1 Anti-inflammatory potential

The aqueous extract of *Tinospora cordifolia* proved significant anti-inflammatory effect on cotton pellet granuloma and formalin induced arthritis models (Jana *et al*., 1999).

2.10.2.2 Cardio-protective

The cardioprotective activity of a herbal formulation "Caps HT2" which contains methanol extract of *Tinospora cordifolia* has been proven to show hypolipidaemic activity *in vivo* (Mary *et al*., 2003).

2.10.2.3 Stress and depression

Antidepressant-like effect of Gulvel was significantly reversed on tail suppression test by pretreatment of swiss young albino mice with prazosin (an alpha-1 adrenoceptor antagonist), sulpiride (a selective dopamine D2-receptor antagonist), p-chlorophenylalanine (PCPA – a serotonin synthesis inhibitor) and baclofen (GABA-B agonist). The extract also reduced the mouse whole brain monoamine oxidase (MAO-A and MAO-B) activities resulting in increased levels of brain monoamines (Dhingra, 2008).

2.10.2.4 Cognition

Tinospora cordifolia has found a place in traditional herbal medicine as a neuropsychopharmacological agent for enhancing memory and improving learning. Effect of a polyherbal formulation containing *Tinospora cordifolia* on aluminium induced cognitive deficits and cognition in aged wistar rats was studied in a one-trial stepthrough passive avoidance task. *Tinospora cordifolia* containing formulation was found to significantly prolong the shortened latency of step-through induced by aluminium administration. It also significantly improved retention of learning in aged rats (Dua, 2009).

2.11 Description of *Cola hispida* Brenan & Keay (Malvaceae)

A shrub or tree up to 40 ft. high can be found in a forest. Their leaves are up to 30 cm long and 24 cm broad. Flowers greenish-yellow inside with brown pubescence outside, inside varying to reddish-pink. It has a fruit that looks like a billy goat testicles clustered together. It is orange in colour when riped containg seeds in white coat typical of the Cola genus (Figure 2.20). The common names in Nigeria are; EDO ẹvbóhā ẹ́bítan, IGBO *(Asaba)* oji-ogodo (KO&S), YORUBA *(Kabba)* ikpa obukọ = billy goat's testicles (Boston) (Burkill, 1985).

2.11.1 Medicinal Uses of *Cola hispida*

A leaf decoction of *Cola hispida* is used to ease cough and stomach trouble and the sap from fresh leaves is dripped into the ear for inflammation of the outer ear tract. The powdered root mixed with palm oil is applied to the skin for skin infection and to kill body lice. Is also used to treat cutaneous, subcutaneous parasitic infection, the root is used to treat genital stimulants/depressants and the leaf is also used to treat pulmonary troubles (Burkill, 2000).

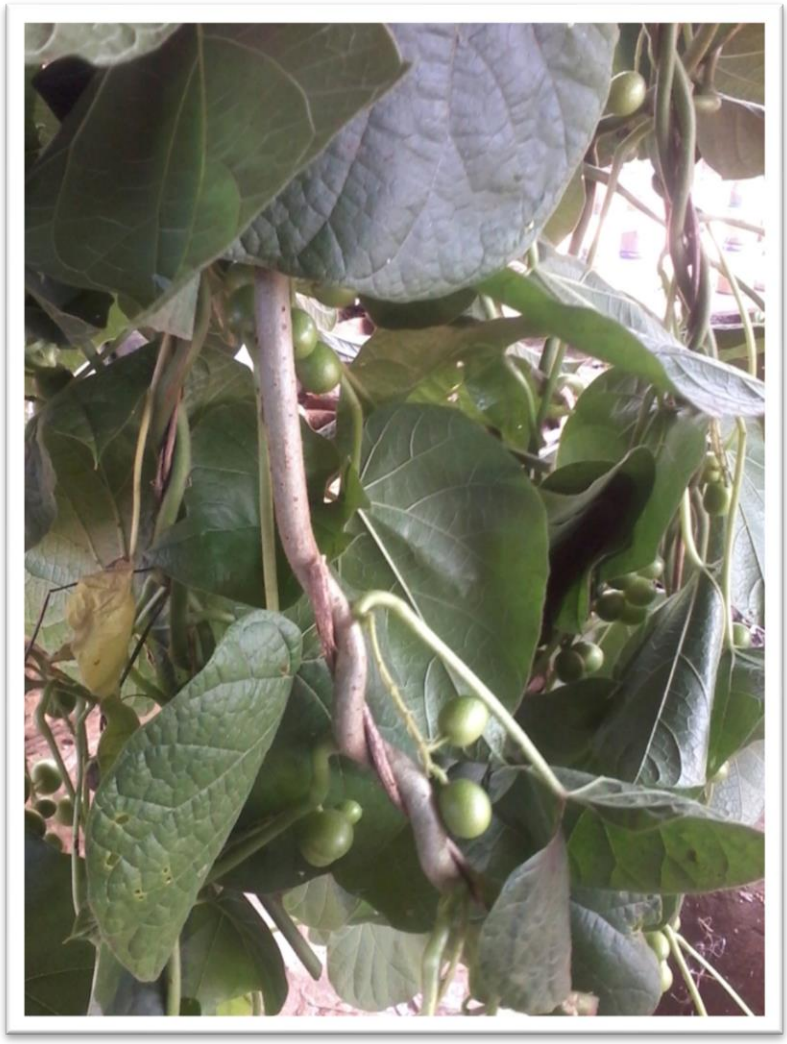

Figure 2.18: *Tinospora cordifolia* (Willd.) Miers ex Hook. F. & Thoms (Menispermaceae)

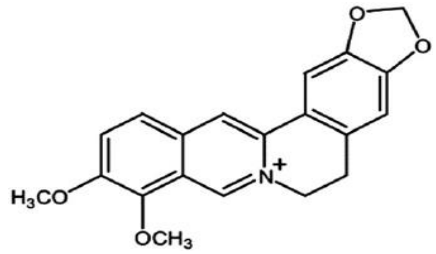

Berberine (LX)

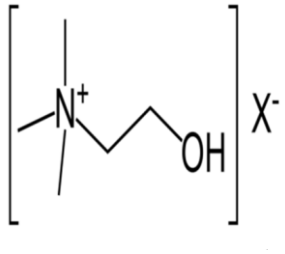

Choline (LXI)

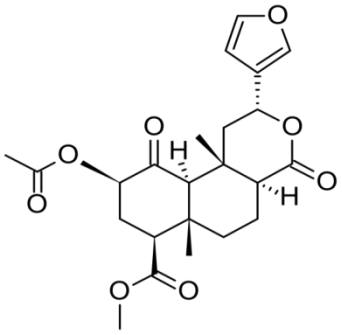

Furanolactone (LXII)

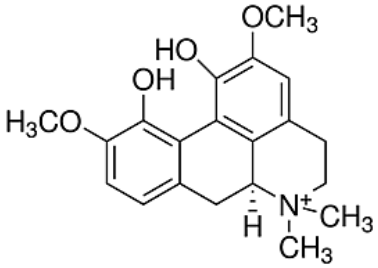

Magnoflorine (LXIII)

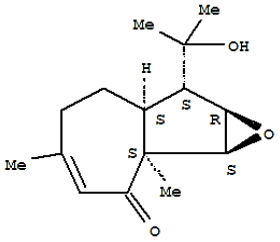

Tinocordifolin (LXIV)

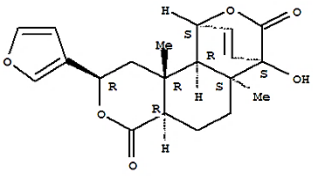

Isocolumbin (LXV)

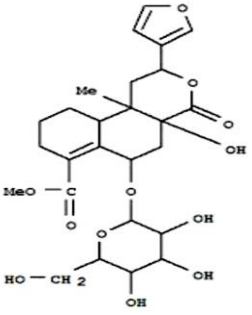

Cordioside (LXVI)

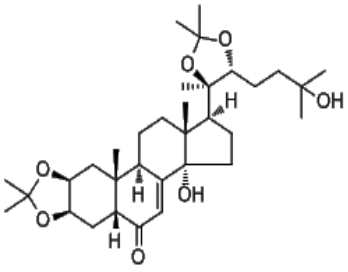

Ecdysterone (LXVII)

Figure 2.19: The chemical structures of chemical compounds reported in *Tinospora cordifolia*

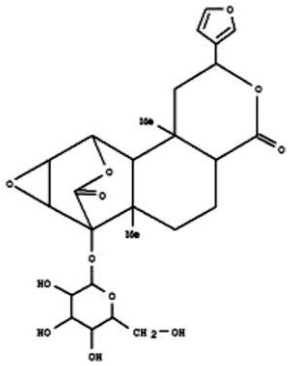

Palmatosides (LXVIII)

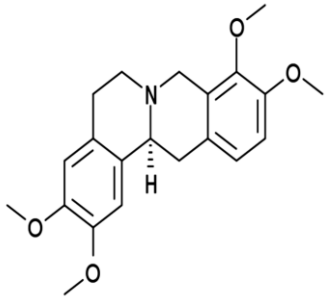

Tetrahydropalmetine (LXIX)

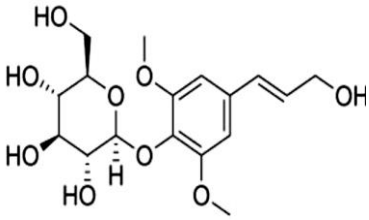

Syringin (LXX)

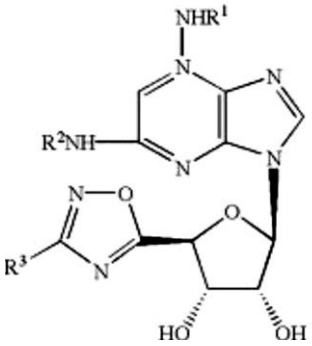

Tetrahydrofuran (LXXI)

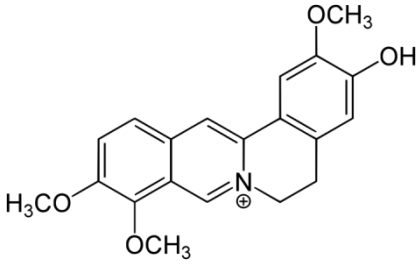

Jatrorrhizine (LXXII)

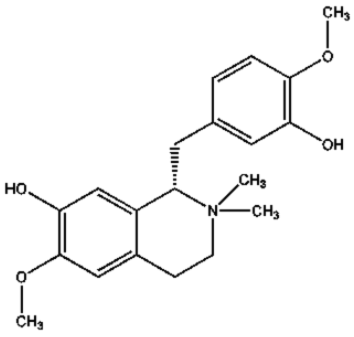

Tembetarine (LXXIII)

Figure 2.19: The chemical structures of chemical compounds reported in *Tinospora cordifolia* (contd.)

Figure 2.20: *Cola hispida* Brenan & Keay (Malvaceae)

CHAPTER THREE

MATERIALS AND METHODS

3.1 Materials

3.1.1 Solvents

The solvents used are as follows: n-hexane, dichloromethane, ethyl acetate, acetone, chloroform and methanol where of analytical grade purchased from Sigma Co. UK.

3.1.2 Reagents

The reagent used are 5,5-Dithio-bis(2-nitrobenzoic) acid, acetylthiocholine iodide, acetylcholinesterase, eserine, β-naphthyl acetate, fast blue B salt were obtained from Sigma Aldrich, sodium phosphate buffer salts, Buffer components were of highest purity, Prolyl endopeptidase (EC 3.4.21.26), Z-Gly-Pro-pNA, bacitracin, purified water from a TKA ROS 300 system was used to prepare buffers and standard solutions, 1,1-diphenyl-2-picrylhydrazyl (DPPH), 2, 4, 6-tri-(2-pyridyl)-1, 3, 5-triazine, 300 mmol/L acetate buffer of pH 3.6, 20 mmol/L $FeCl_3.6H_2O$, 2 mM $FeCl_2 \cdot 4H_2O$, 5 mM ferrozine, acetic anhydride, glacial acetic acid, 2.0% $FeCl_3$, 10% ferric chloride, 10% ammonia solution, benzene, vitamin C, ascorbic acid, sodium carbonate, potassium acetate, sodium phosphate, ammonium molybdate, potassium ferricyanide, trichloroacetic acid (TCA), sodium hydroxide, concentrated sulphuric acid, dragendorffs reagent, hydrochloric acid, column silica gel where purchased from Bristol scientific (Sigma Aldrich).

3.1.3 Instruments

Infrared (Bruker Vector 22, USA), Melting point (BUCHI M-560, England), Thermo Scientific UV-Visible Spectrophotometer (Evolution 300, England), EI-MS (JEOL MS route, JEOL 600H1, USA), FAB +ve/-ve (JEOL-600H-2, USA), HR-ESI-MS (BRUKER MAXIS II, USA), LR-ESI-MS (BRUKER AMAZON SPEED, USA), MALDI-TOF-MS (ULTRAFLEX TOF/TOF MASS SPECTROMETER, Japan), Bruker D8 venture fitted with

Cu Kα radiation source (λ = 1.54178 Å) and CCD detector (PHOTON 100 diffractometer, USA), GC-MS Triple Quad (Agilent Technologies 7890A, USA), ^{1}H-NMR and ^{13}C-NMR (Broad band (BB) and Distortionless enhancement by polarization transfer (DEPT) 90^{o}, 135^{o}) experiments (Bruker Avance Neo 300, 400, 500 and 600, 800 Cryoprobe MHz, USA).

3.2 Selection, collection and authentication of research plants

3.2.1. Preliminary study to determine choice of research plants

The present study began with a preliminary investigation on the acetylcholinesterase inhibitory potentials of ten (10) selected Nigerian medicinal plants namely; *Tinospora cordifolia*, *Stephania dinklagei*, *Phyllanthus amarus*, *Cleome rutidosperma*, *Spilanthes filicaulis*, *Strophanthus hispidus*, *Gongronema latifolium*, *Cola hispida*, *Phyllanthus muellerianus* and *Hedranthera barteri* reported as memory enhancer in literature from ethnobotanical survey conducted in some parts of Southwest Nigeria.

3.2.2. Research plant collection and authentication

The plant *Phyllanthus muellerianus* (Kuntze) Exell (Euphorbiaceae) leaf, *Tinospora cordifolia* (Willd.) Miers ex Hook. F. & Thoms (Menispermaceae) stem were obtained from Nsukka Local Government Area and Obollo-afor of Enugu State, respectively in the month of November/December 2016 and *Cola hispida* Brenan & Keay (Malvaceae) seed was obtained from Okura-Ofante, Dekina Local Government Area of Kogi State in the month of March/April 2017. Plant was authenticated at Forestry Herbarium Ibadan (FHI) by Mr. Adeyemo, A. and Chukwuma C. Emmanuel where voucher specimen was deposited as *Phyllanthus muellerianus* (FHI 111339), *Tinospora cordifolia* (FHI 112287) and *Cola hispida* (FHI 111321).

3.3 Preparation of plant extracts

The plants were air dried for three weeks and pulverized. Powdered samples (7 Kg of *Phyllanthus muellerianus* leaf, 9 Kg of *Tinospora cordifolia* stem and 11 Kg of *Cola hispida* seed) were macerated with 100% methanol for 72 hours. The filterate was concentrated *in vacuo* at 50^{o}C. The dried concentrated extract was stored in a refrigerator at 4°C until required. The methanolic crude extract was suspended in water and partitioned successively

with n-hexane, dichloromethane, ethylacetate and aqueous methanol using a separating funnel.

The percentage yield was calculated as: Yield (%) = $[(W_e/ W_m] * 100$
Where: W_e = weight of extract, W_m = weight of plant material

3.4. Qualitative phytochemical screening

The crude extracts were screened for the presence or absence of secondary metabolites using standard procedures (Sofowora, 1993, Trease, 1996).

I. Test for alkaloids: Extract was dissolved individually in dilute hydrochloric acid and the solution was clarified by filtration.

a. Dragendorffs test: Filtrate was treated with Dragondroffs reagent (solution of Potassium Bismuth Iodide).

II. Test for phenols

a. Ferric chloride test: The filtered solution of extract was treated with three drops of freshly prepared 1% ferric chloride and potassium ferrocyanide.

III. Test for flavonoids

a. Alkaline reagent test: The extract was treated with few drops of sodium hydroxide solution.

IV. Test for anthroquinones

a. Free anthroquinones test: (Borntrager's test). The extract of the plant material (equivalent to 100 mg) was shaken vigorously with 10 mL of benzene, filtered, and 5 mL of 10% ammonia solution added to the filtrate.

V. Test for phytosterols

a. Salkowski's test: The extract was dissolved in 2 mL chloroform in a test tube. Concentrated sulphuric acid was carefully added on the wall of the test tube to form a lower layer.

VI. Test for tannins

a. Ferric chloride test. The extract was dissolved in distilled water. The solution was clarified by filtration. 10% ferric chloride solution was added to the clear filtrate.

VII. Test for saponins

a. Froth test: Extract was diluted with distilled water to 20 mL and this was shaken in a graduated cylinder for 15 minutes.

VIII. Test for carbohydrate

a. Molisch's test: Few drops of molisch's reagent were added to each of the portion dissolved in distilled water; this was then followed by addition of 1 ml of conc. H_2SO_4 by the side of the test tube. The mixture was then allowed to stand for two minutes and then diluted with 5 ml of distilled water.

IX. Test for glycoside

Keller-kiliani test: A solution of glacial acetic acid (4.0 mL) with 1 drop of 2.0% $FeCl_3$ mixture was mixed with the 10 mL aqueous plant extract and 1 mL H_2SO_4 concentrated.

X. Test for terpenoids: A little of each portion was dissolved in ethanol. To it 1 mL of acetic anhydride was added followed by the addition of concentrated H_2SO_4.

3.5 Determination of anticholinesterase activity

Acetylcholinesterase inhibitions were determined spectrophotometrically using acetylthiocholine iodide (ATChI) as substrate by the modified method of Ellman *et al*., 1961. In a 96-well plates was added 240 µL of buffer (50 mM Tris-HCl, pH 8.0), 20 µL of varying concentrations of the test samples (5 - 0.15625 mg/mL), 20 µL of acetylcholinesterase enzyme (rat brain) preparation (0.28 U/mL) the reaction mixture was then incubated for 30 min at 37^{o}C, after which 20 µL of 10 mM DTNB was added. The reaction was then initiated by the addition of 20 µL of 25 mM ATChI. The rate of hydrolysis of ATChI was determined spectrophotometrically by measuring the change in the

absorbance per minute (ΔA/min) at 412 nm over a period of 4 min at 30 s interval. A solution of buffer was used as negative control. All assays were carried out in triplicate. Eserine ((-) physostigmine) was used as positive control.

The percentage inhibition (%I) of test sample was obtained using the formula:

$I\ (\%) = [(V_o - V_i)/ V_o] * 100$

Where: I (%) = Percentage inhibition

V_i = enzyme activity in the presence of test sample

V_o = enzyme activity in the absence of test sample

3.6 Evaluation of AChE inhibitory activity using a new micro-well plate AChE inhibition assay (NA-FB)

The experiment was organized as a common spectrophotometric test using 96-microwell plates. In each well of a 96-well plate, 10 µL plant extract, 50 µL (0.25 mg/mL) of β-naphthyl acetate dissolved in methanol and 200 µL of AChE solution (3.33 U/mL) were added. The mixture was incubated at 4^oC for 40 min. Later, 10 µL (2.5 mg/mL) fast blue B dissolved in water were added to the mixture and the absorbance was measured at 600 nm. To overcome the error in absorbance reading as a result of the plant extract color, the absorbance readings before incubation were subtracted from the absorbance after the addition of the dye. The percentage of inhibition for each test solution was calculated as

Inhibition (%) = 1- (*As*/*Ac*) X 100

Where *As* is the absorbance of the sample extracts and *Ac* is the absorbance of the blank.

The concentrations of test samples that inhibited hydrolysis of the substrate by 50% (IC_{50}) were determined by monitoring the inhibitory effect of extracts with increasing concentrations in the assays.

3.7 Prolyl endopeptidase inhibition assay

Prolyl endopeptidase (EC 3.4.21.26) inhibitory assay was measured by the method of Yoshimoto *et. al*. (1978) with slight modifications. Using 96-well plates, 200 µL of total reaction volume containing 20 µL of PEP enzyme (0.02 U/well), 140 µL phosphate buffer (50 µM at pH 7.0) and 20 µL test compound (1mM in methanol, final concentration of methanol was 10% v/v) were incubated at 30℃. Z-Gly-Pro-pNA 20 µL (0.4 µM in 40% 1,4 dioxane) as a substrate was added after 10 minutes of incubation. Reaction mixtures were allowed for 30 min catalysis and the change in absorbance (OD) at 410 nm was measured by using Multiskan GO (Thermo Fisher Scientific Oy Ratastie 2, P.O. Box 100 FI-01621 FINLAND). The concentrations of tested compound that inhibited the hydrolysis of substrate (Z-Gly-Pro-pNA) by 50% (IC_{50}) were determined by monitoring the effect of increasing concentrations of these compounds in the assay on the inhibition values. The IC_{50} values were then calculated using the EZ-Fit enzyme kinetics program (Perella Scientific Inc., Amherst, USA). Bacitracin was used as a standard at 1 mM.

3.8 Molecular docking studies

3.8.1 Acetylcholinesterase

In order to predict the binding mode and mechanism of interaction of putative acetylcholinesterase inhibitors (Colovic *et al*., 2013), molecular docking studies were carried out with the available Protein Data Bank (PDB) ID:10CE (acetylcholinesterase (E.C. 3.1.1.7) of the enzyme from *Tetronarce californica* (Pacific electric ray) complexed with an inhibitor physostigmine analogue 8-(cis-2,6-dimethylmorpholino)octylcarbamoyleseroline (MF268) (Bartolucci *et al*., 1999). The builder module in MOE 2015 was used to draw the compounds. All the compounds were energy minimized, followed by the addition of partial charges as per Merck Molecular Force Field (MMFF94). The compounds were docked using MOE 2015.010 after initial protein preparation. The default rigid docking protocol in MOE Suite was utilized for docking. The resulting poses of the compounds were visually inspected to comprehend protein ligand interactions. The interactions were analyzed with the

help of PLIP web server (https://projects.biotec.tu-dresden.de/plip-web/plip). All the visuals were recorded using MOE 2015 Suite.

3.8.2 Prolyl endopeptidase

In order to predict the binding mode of putative inhibitors of proline endopeptidase (PEP), molecular docking studies were carried out with the available PDB of the enzyme. The reported assay demonstrated the IC_{50} of the three compounds Oxoglaucine, Corydine and Stigmasterol with a *Flavobacterium* prolyl endopeptidase (Heins *et al*., 1988). Due to unavailability of the crystal structure of Flavobacterium PEP, we chose the most reliable (with highest similarity) Swiss model PDB. The selected PDB was modelled using PDB ID :3IVM (Li *et al*., 2010a). The PDB ID: 3IVM was complexed with an inhibitor N-benzyloxycarbonyl-L-prolyl-L-prolinal. Thus, this PDB was chosen to further carry out the redocking experiments. The builder module in MOE 2015 was used to draw the compounds. All the compounds were energy minimized, following the addition of partial charges as per Merck Molecular Force Field (MMFF94). The three compounds were docked using MOE 2015.010 after initial protein preparation. The default rigid docking protocol in MOE Suite was utilized for docking. The resulting poses of the compounds were visually inspected to comprehend protein ligand interactions. The interactions were analyzed with the help of Protein Ligand Interaction Profiler (PLIP) web server (https://projects.biotec.tu-dresden.de/plip-web/plip). All the visuals were recorded using Chimera (Pettersen *et al*., 2004).

3.9 Metal (Fe^{2+}) chelation assay

The ferrous ion-chelating (FIC) assay was carried out according to the method of Singh and Rajini, (2004) with some modifications. Solutions of 2 mM $FeCl_2 \cdot 4H_2O$ and 5 mM ferrozine were diluted 20 times in distilled water. Briefly, an aliquot (1 mL) of different concentrations of extract (5-0.15625 mg/mL) was mixed with 1mL $FeCl_2 \cdot 4H_2O$. After 5 min incubation at 25^{o}C, the reaction was initiated by the addition of ferrozine (1 mL). The mixture was shaken vigorously and after a further 10 min incubation period of 25^{o}C, the absorbance of the solution was measured at 562 nm using UV spectrophotometer. Vitamin C

was used as positive control. The percentage inhibition of ferrozine–Fe^{+2} complex formations was calculated by using the formula:

Chelating effect % = $[(A_{control}-A_{sample})/A_{control}] \times 100$

Where $A_{control}$ = absorbance of control sample (the control contains $FeCl_2$ and ferrozine, complex formation molecules) and A_{sample} = absorbance of a tested samples.

The extract concentration providing 50% inhibition (IC_{50}) was calculated was obtained by interpolation from linear regression analysis.

3.10 Radical scavenging activity using DPPH

The radical scavenging ability of the extracts was determined using the stable radical DPPH (2,2-diphenyl-1-picrylhydrazyl hydrate) as described by Brand-Williams *et al.*, (1995). To 1 mL of different concentrations (5 - 0.15625 mg/mL) of the plant extracts or standard (vitamin C) in a test tube was added 1 mL of 0.3 mM DPPH in methanol. The mixture was mixed and incubated in the dark for 30 mins after which the absorbance was read at 517 nm against a DPPH control containing only 1 mL methanol in place of the extract.

The percent of inhibition was calculated in following way:

I% = $[(A_{blank}-A_{sample})/A_{blank}] \times 100$

Where A_{blank} is the absorbance of the control reaction (containing all reagents except the test samples), and A_{sample} is the absorbance of the test samples. Sample concentration providing 50% inhibition (IC_{50}) was calculated from the graph plotting inhibition percentage against extract concentration.

3.11 Determination of total antioxidant capacity

To 0.1 mL of the plant extracts or standard solutions of ascorbic acid (0.1 – 0.01mg/mL) was added 1mL of the reagent solution which consisted of 0.6 M sulphuric acid, 28 mM sodium phosphate and 4 mM ammonium molybdate. The tubes containing the reacting mixture were incubated in a water bath at 95^{o}C for 90 mins. The mixture was then allowed to stand and cool to room temperature and the absorbance measured at 695 nm against a blank which consisted of the reacting mixture containing distilled water in place of the extract using a spectrophotometer (Camspec M107 UV-VIS spectrophotometer). Ascorbic

acid equivalents were calculated using standard graph of ascorbic acid. The experiment was conducted in triplicates and values are expressed as ascorbic acid equivalent in mg per g of extract (Prieto *et al.,* 1999).

3.12 Ferric reducing antioxidant power assay (FRAP)

A 300 mmol/L acetate buffer of pH 3.6, 10 mmol/L 2, 4, 6-tri-(2-pyridyl)-1, 3, 5-triazine and 20 mmol/L $FeCl_3.6H_2O$ were mixed together in the ratio of 10:1:1, respectively to give the working FRAP reagent. A 50 µL aliquot of the plant extracts at 0.1mg/mL and 50 µL of standard solutions of ascorbic acid (0.1-0.01 mg/mL) was added to 1mL of FRAP reagent. Absorbance measurement was taken at 593 nm exactly 10 minutes after mixing against reagent blank containing 50 µL of distilled water.

All measurements were taken at room temperature with samples protected from direct sunlight. The reducing power was expressed as equivalent concentration (EC) which is defined as the concentration of antioxidant that gave a ferric reducing ability equivalent to that of the ascorbic acid standard. Increase in absorbance is commented as indicative of increased reducing power (Benzie and Strain, 1999).

3.13 Gas Chromatography Mass Spectroscopy (GC-MS)

Analysis of the hexane fractions was carried out by injecting 2 µL on Gas Chromatography Mass Spectroscopy Triple Quad (GC-MS TQQQ) (Agilent Technologies 7890A) fitted with ZEBRON -ZB-5 capillary column 360 °C:30 m x 250 µm x 0.25 µm. Initial column temperature was 50^{o}C, pressure: 9.05 psi, flow: 1.129 mL/min, average velocity: 38.724 cm/sec, hold up time: 1.2912 min, run time: 77.714. Automatic injection in split mode was adopted using PAL Sampler injection source (10ul syringe, cycle: MACRO GC_Liq4-V2), oven equilibration time: 0.5 min, max temperature: 360 degrees C, oven program: 50°C for 2 min, then 7 °C/min to 180 °C for 20 min, then 7 °C/min to 300 °C for 20 min. Thermal Aux 2 (MSD Transfer Line) heater: 260 °C. Helium was used as carrier gas. The chromatogram obtained from the GC was then analysed in the mass spectroscopy (MS) to get the mass of all the fractions. The identification of components was accomplished searching plant compound library (NIST Mass Spectrometry Data Center).

3.14 Purification of extract

3.14.1 Column chromatography (CC)

Glass columns of different lengths and widths, held in vertical position with the aid of retort stand were used for column chromatography. Fractions in grams of plant extracts were chromatographed using column chromatography (CC) on a column silica gel (Sigma Aldrich, 60-200 mesh size) as adsorbent material. Concentration gradients of solvents were used in order of increasing polarity. The eluates were collected into separate clean vials, concentrated *in vacuo* at 50^{o}C and were allowed to dry under a stream of cold air.

3.14.2 Preparative Thin Layer Chromatography (PTLC)

The preparative TLC plates, 20 cm X 20 cm coated with Silica gel G of 0.50 mm thickness was activated in an oven at 100^{o}C for 1 hour. Fractions were dissolved in methanol and applied in band on the plates. The plates were runned in solvent system and the bands were visualized under ultraviolet light (254 nm and 365 nm, Allen 425 UV lamp) and scraped off carefully. The components were collected into separate beakers and the adsorbent powder eluted with 20 mL acetone. Methanol was used for a final rinse to recover any polar components. Each component was collected into a separate vial and concentrated under a stream of cold air to dryness.

3.14.3 TLC analysis and pooling of fractions

The various fractions were collected and were monitored using precoated thin layer chromatography (TLC) plates (silica gel on aluminium F_{254}) using diverse solvent systems as eluent. The chromatograms were visualized under visible and ultraviolet light at 254 nm and 366 nm using Allen 425 UV lamp. Plates were also sprayed with 20% sulphuric acid reagent and heated with a heat gun within 1 to 2 min to allow visualization for compounds that are not UV active. Eluates having similar TLC profiles were pooled together and were allowed to air dry and the yields calculated.

3.14.4 Visualisation of compound

Majority of colourless compounds were viewed under illumination with UV light in a UV viewing cabinet with a long wavelength (366 nm) and short wavelength (254 nm) light sources. Also, spraying reagents like 20% sulphuric acid in water and ceric sulphate was used to detect spots on TLC plates.

3.14.5 TLC analysis of isolated compound

Thin layer chromatography (TLC) of the isolated compounds was done in several different solvents. R_f values of each spot was calculated using the formula:

Retardation factor (R_f) = Distance traveled by the solute / Distance traveled by the solvent.

3.15 Spectroscopic analysis of compound

Structural elucidation of compounds was achieved via the use of spectroscopy analysis. The mass of the isolated compounds were determined using Electron Impact Mass spectrometry (EI-MS) performed on JEOL MS route and JEOL 600H1, Fast atom bombardment performed on JEOL-600H-2 on the positive and negative mode (FAB-+ve/-ve mode) and Electrospray ionization mass spectrometry on the low and high resolution (ESI-MS-LR/HR) performed on BRUKER MAXIS II and LR-ESI-MS performed on BRUKER AMAZON SPEED, respectively. Proton Nuclear Magnetic Resonance (^{1}H-NMR), 1D and 2D NMR and ^{13}C-NMR were recorded on Bruker Avance Neo 300, 400, 500 and 600, 800 Cryoprobe MHz. Chemical shifts were calculated in δ (ppm) and coupling constants (*J*) in Hertz (Hz). Polarization transfer experiments (DEPT) were carried out with the last polarization pulse angle θ 90^0, 135^0 to determine the multiplicity of each carbon. ^{1}H-^{1}H COSY (Correlated spectroscopy) was used to determine which signals arise from neighnoring protons (usually up to four bonds). The heteronuclear single quantum coherence (HSQC) experiment was used to provide correlations between a carbon and its attached protons (^{1}H-^{13}C). The HMBC (Heteronuclear Multiple Bond Correlation) experiment gives correlations between carbons and protons that are separated by two, three, and, sometimes in conjugated systems, four bonds. Fourier transform infrared spectroscopy (FT-IR) was used to determine the functional group of compounds and was recorded on Bruker Vector 22 and Ultra violet spectroscopy (UV) was used to determine the wavelength of compounds on Thermo Scientific UV-Visible Spectrophotometer (Evolution 300). Melting point range was also determined to ascertain purity using BUCHI (M-560).

3.16 Isolation of compounds from *Phyllanthus muellerianus* leaf

3.16.1 Purification of dichloromethane and ethyl acetate fraction using column chromatography

Air dried and powdered leaves of *Phyllanthus muellerianus* (7 Kg) was macerated in 100% methanol for a period of 72 hours, concentrated *in vacuo* at 50^{o}C to yield 500.9 g. The dried concentrated extract was stored in a refrigerator at 4°C until required. The methanolic crude extract (250 g) was suspended in water (3:1) and partitioned successively with n-hexane (18.3 g), dichloromethane (23.9 g), ethyl acetate (102.5 g) and aqueous methanol (93.7 g) using a separating funnel. A slurry of the dichloromethane fraction (10 g) of *Phyllanthus muellerianus* (DPM) was chromatographed using column chromatography on 150 g coloumn silica gel (60-200 mesh size) as adsorbent material using gradient elution from n-hexane (100%, each 2000 mL), n-hexane:ethyl acetate (95:5 to 25:75, each 2000 mL), ethyl acetate (100%, each 2000 mL) and ethyl acetate: methanol (450:50 to 250:250, each 2000 mL). The obtained fractions were pooled based on their TLC profile to give sub-fractions. The TLC plates were visualised using UV lamp (254 nm and 366 nm) and spray with 20% sulphuric acid, then heated with a spray gun to visualize spots.

20 g of ethyl acetate fraction (EPM) was chromatographed using coloumn chromatography on 150 g column silica gel (60-200 mesh size) using gradient elution from n-hexane (100%), n-hexane:ethyl acetate (95:5 to 25:75, each 2000 mL), ethyl acetate (100%, each 2000 mL), ethyl acetate: methanol (95:5 to 1:3, each 2000 mL) and methanol (100%, each 2000 mL). The obtained fractions were pooled based on their TLC profile to give sub-fractions. The TLC plates were visualised using UV lamp (254 nm and 366 nm) and spray with 20% sulphuric acid, then heated with a spray gun to visualize spots. Sub fractions were evaporated to dryness and stored in the refrigerator prior to use.

3.17 Isolation of compounds from *Tinospora cordifolia* stem

3.17.1 Purification of dichloromethane fraction (DTC) using column chromatography

A slurry of 24 g of dichloromethane fraction (DTC-F) of *Tinospora cordifolia* was chromatographed using column chromatography on 150 g column silica gel (60-200 mesh size) on a 3 cm diameter and 80 cm long column using gradient elution of solvent system

starting with n-hexane (100%, each 2000 mL), n-hexane: ethyl acetate (95:5 to 20:80, each 2000 mL), ethyl acetate (100%, each 2000 mL) and ethyl acetate: methanol (490:10 to 50:450, each 2000 mL) and methanol (100%, each 2000 mL). The obtained fractions were pooled based on their TLC profile to give sub-fractions. The TLC plates were visualised using UV lamp (254 nm and 366 nm) and spray with 20% sulphuric acid, then heated with a spray gun to visualize spots. All sub fractions were evaporated to dryness and stored in the refrigerator prior to use.

3.17.2 Purification of ethyl acetate fraction using column chromatography

A slurry of the ethyl acetate fraction (30 g) of *Tinospora cordifolia* (ETC) was chromatographed using column chromatography on 600 g column silica gel (60-200 mesh size) on a 6cm diameter and 75 cm long column using gradient elution of mobile phase starting with n-hexane (100%, each 2000 mL), n-hexane: dichloromethane (9:1 to 1:9, each 2000 mL), dichloromethane (100%, each 2000 mL) and dichloromethane: methanol (98:2 to 1:3, each 2000 mL). The obtained fractions were pooled based on their TLC profile to give sub-fractions. The TLC plates were visualised using UV lamp (254 nm and 366 nm). Sub fraction EA-11 was subjected to PTLC to further purify using the solvent system ethyl acetate: acetone (3.5:1.5) and visualized using UV lamp (254 nm and 366 nm). The yellow bands were neatly scrapped, dissolved in acetone and filtered with Whatman filter paper which was allowed to dry to yield compound.

3.17.3 Purification of sub fraction 25 (EA-25) of ethyl acetate fraction using column chromatography

A slurry of nine (9) grams of sub fraction 25 (EA-25) of *Tinospora cordifolia* was chromatographed using coloumn chromatography on 150 g coloumn silica gel (60-200 mesh size) on a 3 cm diameter and 80 cm long column using the solvent systems n-hexane: ethyl acetate (95:5 to 5:95, each 2000 mL) and ethyl acetate (100%, each 2000 mL). The obtained fractions were pooled based on their TLC profile to give sub-fractions. The TLC plates were visualised using UV lamp (254 nm and 366 nm) and spray with 20% sulphuric acid, then heated with a spray gun to visualize spots. Sub fraction ETC-SF-9 was subjected to preparative thin layer chromatography (PTLC) on a 20 cm X 20 cm precoated plate of 0.5 mm thickness in a solvent system (ethyl acetate: methanol (8.5:1.5)) to further purify the

compounds. The deep blue band visualized under 254 nm was neatly scraped and dissolved in methanol for 20 minute and filtered with Whatman filter paper. Sub fraction ETC-SF-19 was further purified using Recycling Preparative HPLC (LC-908W-C60), column ODS-H80, flow rate 4 mL, IR=50, UV = 254 nm, sensitivity = 0.1, mobile phase methanol: water (95:5).

3.17.4 Purification of sub fraction 26 (EA-26) of ethyl acetate fraction using column chromatography

A slurry of two (2) grams of sub fraction 26 (EA-26) was chromatographed using coloumn chromatography on 60 g column silica gel (60-200 mesh size) on a 3 cm diameter and 80 cm long coloumn using the solvent systems n-hexane (100%, each 2000 mL), n-hexane: dichloromethane (1:1 to 1:3, each 2000 mL) and ethyl acetate (100%, each 2000 mL) and ethyl acetate: methanol (97:3 to 3:1, each 2000 mL). The obtained fractions were pooled based on their TLC profile to give sub-fractions. The TLC plates were visualised using UV lamp (254 nm and 366 nm) and spray with 20% sulphuric acid, then heated with a spray gun to visualize spots. All sub fractions were evaporated to dryness and stored in the refrigerator prior to use.

3.17.5 Purification of aqueous methanol fraction (MTC-F) using column chromatography

A slurry of nineteen (19) grams of aqueous methanol fraction (MTC-F) of *Tinospora cordifolia* was chromatographed using column chromatography on 150 g column silica gel (60-200 mesh size) on a 3 cm diameter and 80 cm long coloumn using the solvent systems n-hexane (100%, each 2000 mL), n-hexane: ethyl acetate (450:50 to 150:350, each 2000 mL) and ethyl acetate (100%, each 2000 mL) and ethyl acetate: methanol (490:10 to 150:350, each 2000 mL) and methanol (100%, 2000 mL). The obtained fractions were pooled based on their TLC profile to give sub-fractions. The TLC plates were visualised using UV lamp (254 nm and 366 nm) and spray with 20% sulphuric acid, then heated with a spray gun to visualize spots. All sub fractions were evaporated to dryness and stored in the refrigerator prior to use.

3.18 Isolation of compounds from *Cola hispida* seed

Purification of dichloromethane fraction (DCH-F) using Column chromatography

A slurry of the dichloromethane fraction (30 g) of *Cola hispida* (DCH) was chromatographed using column chromatography on 150 g column silica gel (60-200 mesh size) as adsorbent material using gradient elution of mobile phase starting with n-hexane (100%, each 2000 mL), n-hexane:ethyl acetate (95:5 to 15:85, each 2000 mL), ethyl acetate (100%, each 2000 mL) and ethyl acetate: methanol (98:20 to 350:150, each 2000 mL). The obtained fractions were pooled based on their TLC profile to give sub-fractions. The TLC plates were visualised using UV lamp (254 nm and 366 nm) and spray with 20% sulphuric acid, then heated with a spray gun to visualize spots. All sub fractions were evaporated to dryness and stored in the refrigerator prior to use.

3.18.1 Purification of ethyl acetate fraction using column chromatography

A slurry of the ethyl acetate fraction (70 g) of *Cola hispida* (ECH) was chromatographed using column chromatography on 600 g column silica gel (60-200 mesh size) as adsorbent material using gradient elution of mobile phase starting with n-hexane (100%, each 2000 mL), n-hexane: dichloromethane (9:1 to 1:9, each 2000 mL), dichloromethane (100%, each 2000 mL) and dichloromethane: methanol (99:1 to 1:3, each 2000 mL). The obtained fractions were pooled based on their TLC profile to give sub-fractions. The TLC plates were visualised using UV lamp (254 nm and 366 nm) and spray with 20% sulphuric acid, then heated with a spray gun to visualize spots. All sub fractions were evaporated to dryness and stored in the refrigerator prior to use.

3.19 Statistical analyses

The statistical analysis was carried out using Graphpad prism 7. All data was expressed as mean ± S.D. and of triplicate parallel measurements. Statistical analyses were performed using One-way ANOVA followed by Dunnett's Multiple Comparisons test at $\alpha_{0.05}$. Differences between means at 5% level ($P \leq 0.05$) were considered significant. Standard curves were generated and calculation of the 50% inhibitory concentration (IC_{50}) values was done using Microsoft Excel.

CHAPTER FOUR

4.0 RESULT

4.1 Preliminary acetylcholinesterase inhibitory activities of the ten selected medicinal plant extracts

Three of the ten plants namely *Phyllanthus muellerianus* leaves (Euphorbiaceae), *Tinospora cordifolia* stem (Menispermaceae) and *Cola hispida* seed (Malvaceae) demonstrated good acetylcholinesterase (hAChE) inhibitory activity *in vitro*. The smaller the IC_{50} value, the higher the enzyme inhibitory activity. *Phyllanthus muellerianus* leaves showed the highest acetylcholinesterase (hAChE) inhibitory activity with IC_{50} value of 3.70 $\pm$ 0.70 μg/mL as compared to standard drug Galanthamine (IC_{50} of 0.758 $\pm$ 0.057 μg/mL) followed by *Cola hispida* (IC_{50} value of 26.9 $\pm$ 7.8 μg/mL) and *Tinospora cordifolia* (IC_{50} value of 52.5 $\pm$ 0.6 μg/mL) at 200 μg/mL (Table 4.1).

4.2 The Percentage yield of crude extracts and fractions

Methanolic extracts obtained from the seed of *Cola hispida* extract gave the highest percentage yield (11.58%), followed by *Phyllanthus muellerianus* (7.15%) and *Tinospora cordifolia* with the lowest yield (3.25%) (Table 4.2). Ethyl acetate fractions of *Phyllanthus muellerianus* (41%) and *Tinospora cordifolia* (54%) gave the highest yield in the partitioned fractions while aqueous methanol fraction of *Cola hispida* gave (65.4%) (Table 4.2.1).

4.3 Qualitative phytochemical Screening

Phyllanthus muellerianus and *Tinospora cordifolia* contains all the phytochemicals tested showing various degree of abundance while tanins, phenol and steroid were not detected in *Cola hispida* extract (Table 4.3).

Table 4.1 Preliminary acetylcholinesterase inhibitory activities of methanol extracts of selected Nigerian medicinal plants at 200 µg/mL

Plants	Parts of plant	% inhibition hAChE	IC_{50} hAChE (µg/mL)
Tinospora cordifolia	stem	80.0 ± 0.7	52.5 ± 0.6
Stephania dinklagei	stem	68.1 ± 1.5	76.8 ± 0.2
Phyllanthus amarus	whole plant	73.6 ± 2.9	49.7 ± 7.8
Cleome rutidosperma	whole plant	na	nd
Spilanthes filicaulis	whole plant	29.6 ± 0.6	nd
Strophanthus hispidus	root	56.0 ± 1.7	150 ± 19
Gongronema latifolium	stem	12.9 ± 4.0	nd
Cola hispida	seed	88.0 ± 4.4	26.9 ± 7.8
Phyllanthus muellerianus	leaf	84.4 ± 1.7	3.70 ± 0.70
Hedranthera barteri	root	47.5 ± 1.4	nd
Galanthamine (standard)		-	0.758 ± 0.057

na: not active, **nd:** not determined

Table 4.2: Percentage yield of methanolic extracts of *Phyllanthus muellerianus*, *Tinospora cordifolia* and *Cola hispida*

Plant materials	Weight of plant material used (g)	Weight of Extract (g)	Percentage yield (%)
Phyllanthus muellerianus leaf	7000	500.9	7.15
Tinospora cordifolia stem	9000	293.1	3.25
Cola hispida seed	11,000	1274.1	11.58

Table 4.2.1: Percentage yield of partitioned fractions of methanolic extract of *Phyllanthus muellerianus*, *Tinospora cordifolia* and *Cola hispida*

Plant materials	Solvent(s)	Weight of methanolic extract used (g)	Weight of Extract (g)	Percentage yield (%)
***Phyllanthus muellerianus* leaf**	n-hexane		18.3	7.32
	Dichloromethane		23.9	9.56
	Ethyl acetate	250	102.5	41.0
	Aqueous methanol		93.7	37.48
***Tinospora cordifolia* stem**	n-hexane		4.6	2.70
	Dichloromethane		5.4	3.17
	Ethyl acetate	170	91.8	54.0
	Aqueous methanol		61.8	36.35
***Cola hispida* seed**	n-hexane		6.7	1.42
	Dichloromethane		6.2	1.31
	Ethyl acetate	470	132.7	28.2
	Aqueous methanol		307.6	65.4

Table 4.3: Preliminary phytochemical screening of methanolic extracts of *Phyllanthus muellerianus, Tinospora cordifolia* and *Cola hispida*

Chemical tests	*Phyllanthus muellerianus* leaf	*Tinospora cordifolia* stem	*Cola hispida* seed
Alkaloids	++	+++	+
Tannins	+	++	_
Flavonoids	+	++	++
Anthraquinones	+	+	+
Saponins	+	+	+
Phenols	++	++	_
Carbohydrate	+	+	+
Glycoside	+	++	+
Steroid	++	++	_
Terpenoids	+	++	+

Key: (+) = present, (-) = absent, (++) = moderately present, (+++) = highly present**.**

4.4 Anti-cholinesterase inhibitory activities of plant crude extracts and fractions of *Phyllanthus muellerianus* leaf, *Tinospora cordifolia* stem and *Cola hispida* seed

Ethyl acetate fraction of *Phyllanthus muellerianus* (IC_{50} = 0.742±0.12 mg/mL) and *Cola hispida* (IC_{50} = 0.656±0.24 mg/mL) gave promising AChE inhibitory activity compared to Tinospora cordifolia (IC_{50} = 1.457±0.47 mg/mL) and eserine (IC_{50} = 0.007±0.00 mg/mL) using ATCI and DTNB (Figure 4.1-4.3) while ethyl acetate fraction of *Phyllanthus muellerianus* leaves showed the highest acetylcholinesterase inhibitory activity with IC_{50} value of 0.258±0.10 mg/mL as compared to standard drug eserine (IC_{50} of 0.014±0.00 mg/mL) followed by ethyl acetate fraction of *Tinospora cordifolia* stem (IC_{50} value of 1.604±0.04 mg/mL) and *Cola hispida* (IC_{50} = 2.220±0.02 mg/mL) using NA-FB (Figure 4.4-4.6).

4.5 Anti-oxidant activities of plant crude extracts and fractions of *Phyllanthus muellerianus* leaf, *Tinospora cordifolia* stem and *Cola hispida* seed.

4.5.1 Metal chelating activity

The dichloromethane and ethyl acetate fraction of *Tinospora cordifolia* stem at 5-0.15625 mg/mL concentration showed good metal chelating activity by inhibition of ferrozine–Fe^{+2} complex formations with IC_{50} of 0.199±0.08 mg/mL and 0.273±0.12 mg/mL, respectively as compared to the ethyl acetate fractions of *Phyllanthus muellerianus* leaf and *Cola hispida* seed with IC_{50} values of 1.538±0.13 mg/mL and 0.624±0.05 mg/mL, respectively when compared to the standard vitamin C (IC_{50} = 0.019±0.00 mg/mL) (Figure 4.7-4.9).

4.5.2 DPPH radical scavenging activity

In DPPH (1,1-diphenyl-2-picrylhydrazyl) radical scavenging assay, at 5-0.15625 mg/mL concentration, ethyl acetate fraction of *Tinospora cordifolia* stem has the highest radical scavenging activity (IC_{50} = 0.419±0.03 mg/mL) followed by ethyl acetate fraction of *Phyllanthus muellerianus* ((IC_{50} = 1.005±1.07 mg/mL) and *Cola hispida* (IC_{50} = 1.427±0.64 mg/mL) when compared to vitamin C (IC_{50} = 0.008±0.00 mg/mL) (Figure 4.10-4.12).

4.5.3 Total antioxidant capacity

The total antioxidant capacity was higher in dichloromethane fraction of *Phyllanthus muellerianus* leaf with value of 217.52±16.01 mg/g followed by aqueous methanol fraction of *Cola hispida* with value of 108.70±21.2 mg/g and dichloromethane fraction of *Tinospora cordifolia* which has a value of 69.71±10.0 mg/g ascorbic acid equivalent/g of extract (R^2=0.9748) (Figure 4.13, Figure 4.13.1-4.15).

4.54 Ferric reducing antioxidant power

The reducing activity of ferrous ion was higher in ethyl acetate fraction of *Phyllanthus muellerianus* leaf with value of 36.19±3.33 mg/g followed by dichloromethane fraction of *Tinospora cordifolia* with value of 28.61±3.63 mg/g and ethyl acetate fraction of *Cola hispida* with value of 14.81±2.71 mg/g ascorbic acid equivalent/g of extract at 0.1-0.01 mg/mL concentration (R^2=0.9968) (Figure 4.16, Figure 4.16.1-4.18).

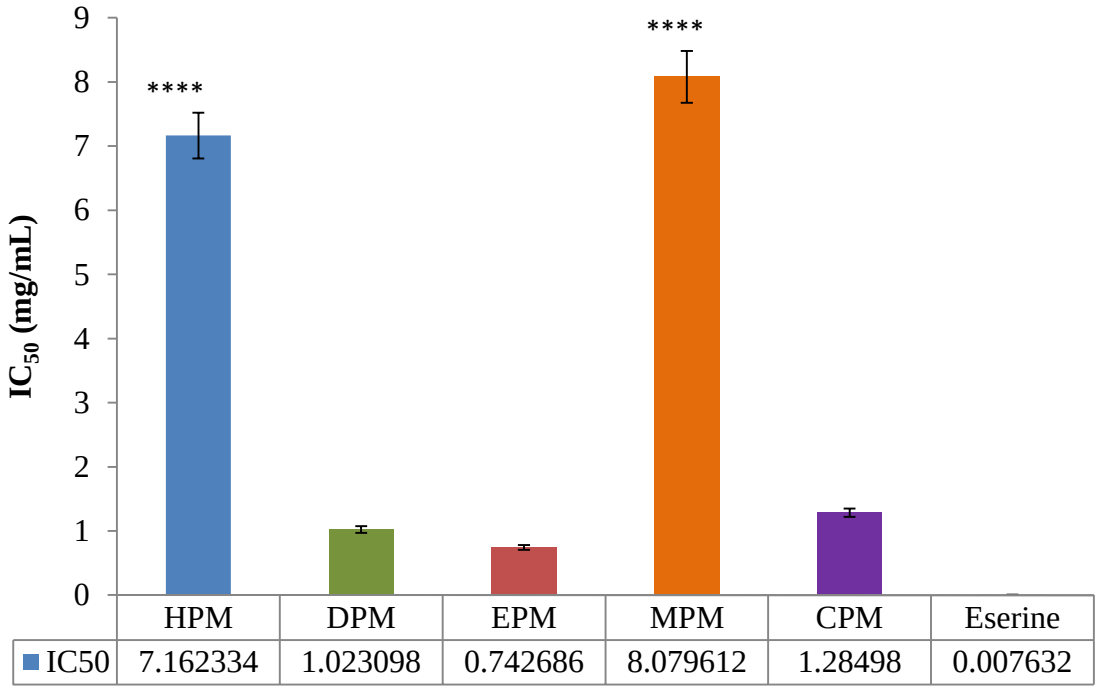

Figure 4.1: *In vitro* acetylcholinesterase inhibitory activity of crude extracts and fractions of *Phyllanthus muellerianus* at 5-0.15625 mg/mL using ATCI and DTNB (IC_{50}±SD (mg/mL)

Values are presented as mean ± standard deviation (n=3). Where HPM (hexane fraction), DPM (dichloromethane fraction), EPM (ethyl acetate fraction), MPM (aqueous methanol fraction), CPM (crude)

Comparison of each extract with standard (Eserine) was done and level of significant difference represented with *, **, *** and ****. Extracts with no asterisks are not significantly (NS) different from the standard

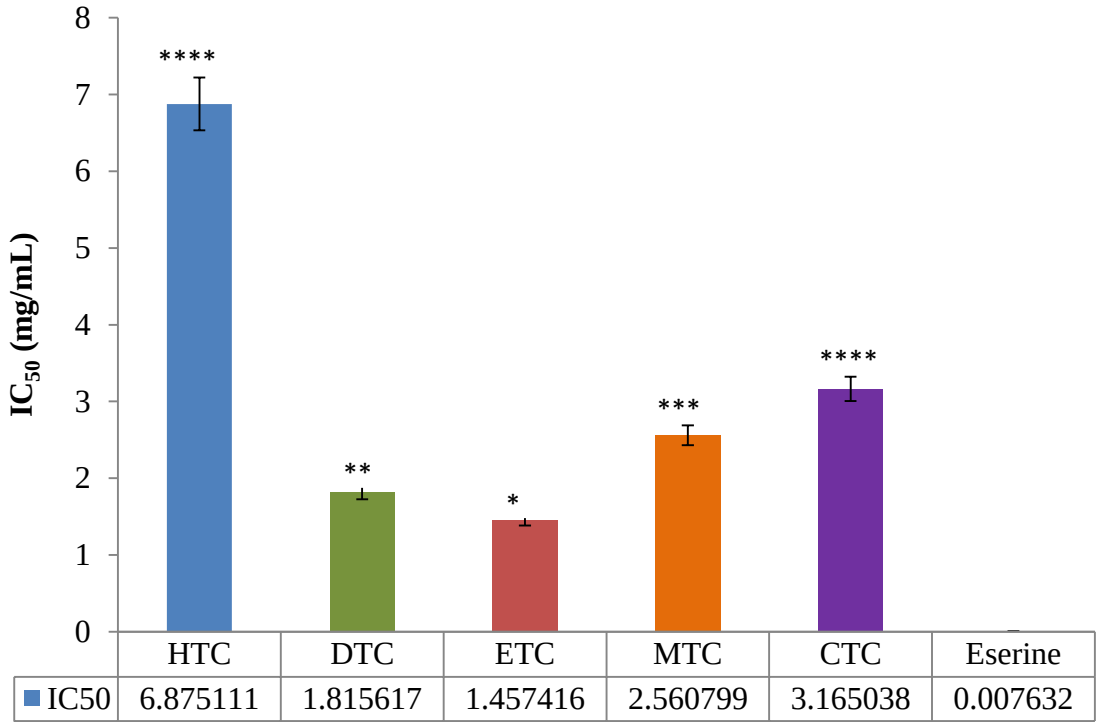

Figure 4.2: *In vitro* acetylcholinesterase inhibitory activity of crude extracts and fractions of *Tinospora cordifolia* at 5-0.15625 mg/mL using ATCI and DTNB (IC_{50}±SD (mg/mL)

Values are presented as mean ± standard deviation (n=3). Where HTC (hexane fraction), DTC (dichloromethane fraction), ETC (ethyl acetate fraction), MTC (aqueous methanol fraction), CTC (crude)

Comparison of each extract with standard (Eserine) was done and level of significant difference represented with *, **, *** and ****. Extracts with no asterisks are not significantly (NS) different from the standard

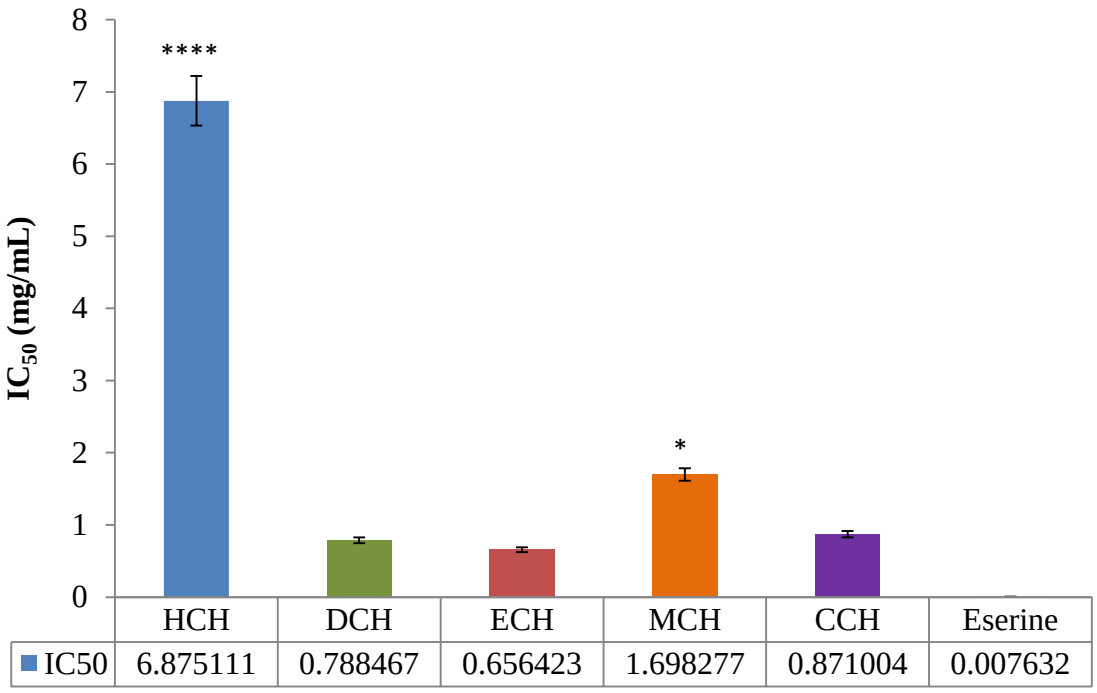

Figure 4.3: *In vitro* acetylcholinesterase inhibitory activity of crude extract and fractions of *Cola hispida* at 5-0.15625 mg/mL using ATCI and DTNB (IC_{50}±SD (mg/mL)

Values are presented as mean ± standard deviation (n=3). Where HCH (hexane fraction), DCH (dichloromethane fraction), ECH (ethyl acetate fraction), MCH (aqueous methanol fraction), CCH (crude)

Comparison of each extract with standard (Eserine) was done and level of significant difference represented with *, **, *** and ****. Extracts with no asterisks are not significantly (NS) different from the standard

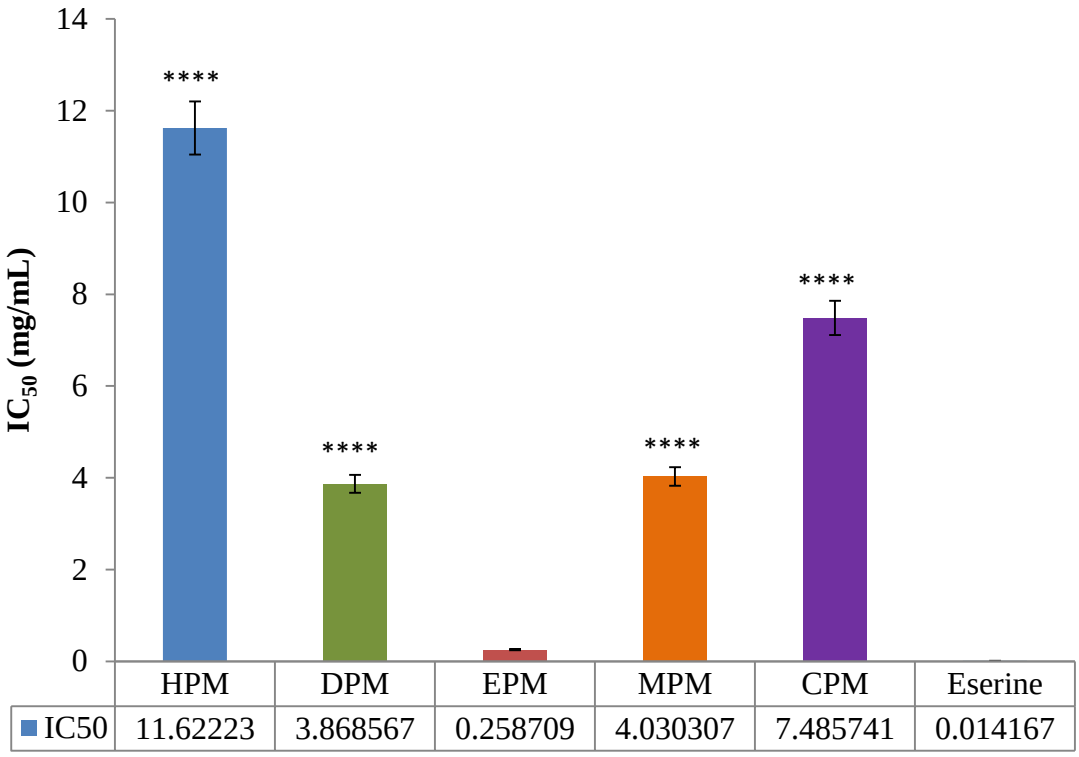

Figure 4.4: Evaluation of AChE Inhibitory Activity of crude extract and fractions of *Phyllanthus muellerianus* at 5-0.15625 mg/mL using NA-FB (IC_{50}±SD (mg/mL)

Values are presented as mean ± standard deviation (n=3). Where HPM (hexane fraction), DPM (dichloromethane fraction), EPM (ethyl acetate fraction), MPM (aqueous methanol fraction), CPM (crude)

Comparison of each extract with standard (Eserine) was done and level of significant difference represented with *, **, *** and ****. Extracts with no asterisks are not significantly (NS) different from the standard

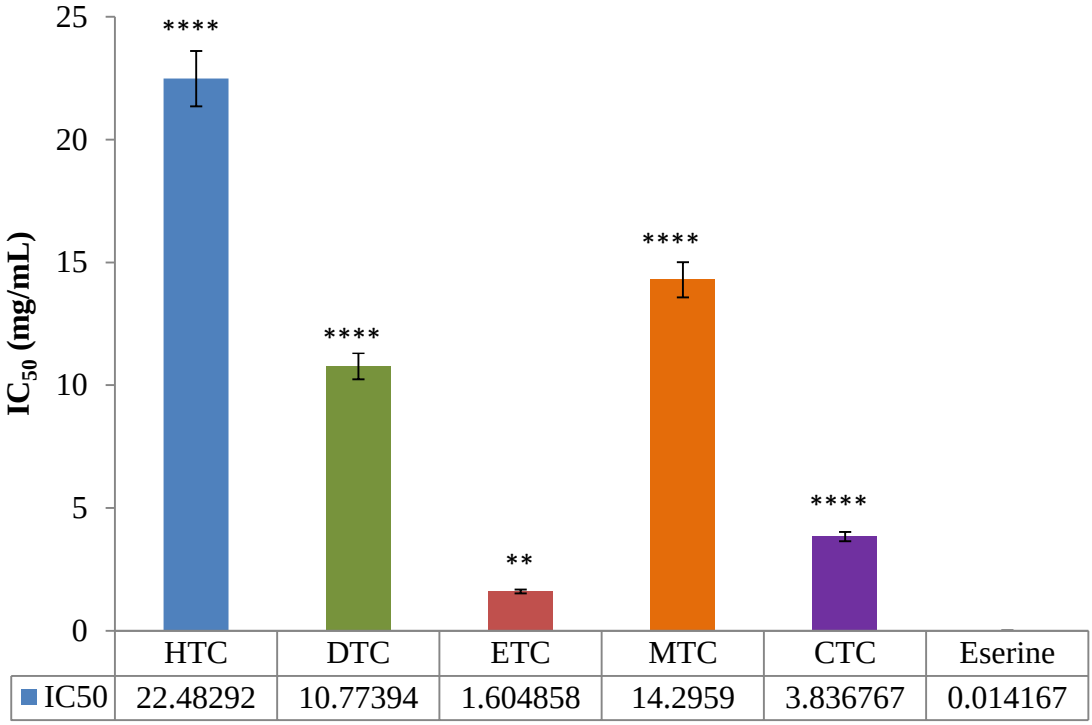

Figure 4.5: Evaluation of AChE Inhibitory Activity of crude extract and fractions of *Tinospora cordifolia* at 5-0.15625 mg/mL using NA-FB (IC_{50}±SD (mg/mL)

Values are presented as mean ± standard deviation (n=3). Where HTC (hexane fraction), DTC (dichloromethane fraction), ETC (ethyl acetate fraction), MTC (aqueous methanol fraction), CTC (crude)

Comparison of each extract with standard (Eserine) was done and level of significant difference represented with *, **, *** and ****. Extracts with no asterisks are not significantly (NS) different from the standard

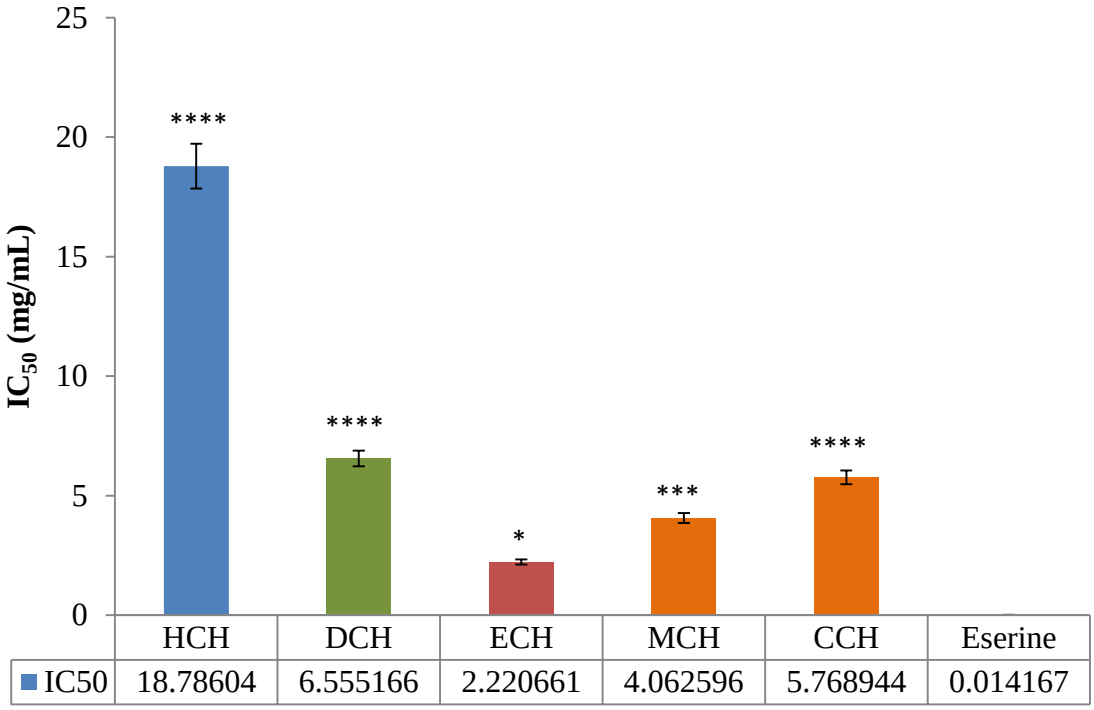

Figure 4.6: Evaluation of AChE Inhibitory Activity of crude extract and fractions of *Cola hispida* at 5-0.15625 mg/mL using NA-FB (IC_{50}±SD (mg/mL)

Values are presented as mean ± standard deviation (n=3). Where HCH (hexane fraction), DCH (dichloromethane fraction), ECH (ethyl acetate fraction), MCH (aqueous methanol fraction), CCH (crude)

Comparison of each extract with standard (Eserine) was done and level of significant difference represented with *, **, *** and ****. Extracts with no asterisks are not significantly (NS) different from the standard

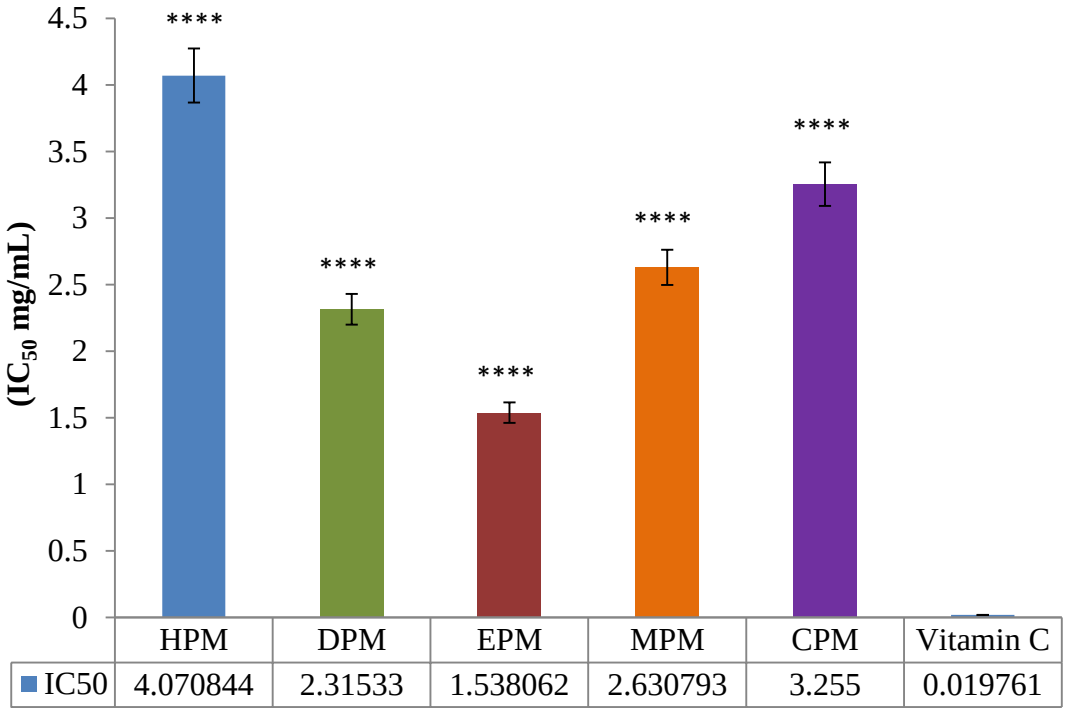

Figure 4.7: Metal chelating activity of crude and fractions of *Phyllanthus muellerianus* at 5-0.15625 mg/mL (IC_{50}±SD (mg/mL)

Values are presented as mean ± standard deviation (n=3). Where HPM (hexane fraction), DPM (dichloromethane fraction), EPM (ethyl acetate fraction), MPM (aqueous methanol fraction), CPM (crude)

Comparison of each extract with standard (Vitamin C) was done and level of significant difference represented with *, **, *** and ****. Extracts with no asterisks are not significantly (NS) different from the standard

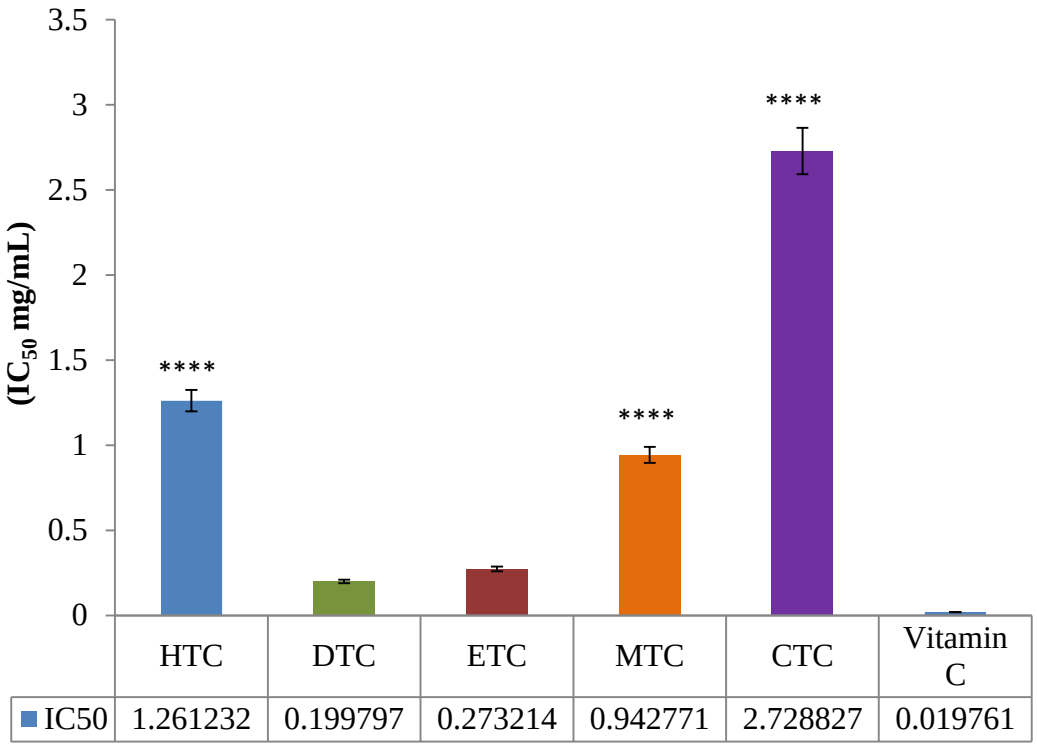

Figure 4.8: Metal chelating activity of crude and fractions of *Tinospora cordifolia* at 5-0.15625 mg/mL (IC_{50}±SD (mg/mL)

Values are presented as mean ± standard deviation (n=3). Where HTC (hexane fraction), DTC (dichloromethane fraction), ETC (ethyl acetate fraction), MTC (aqueous methanol fraction), CTC (crude)

Comparison of each extract with standard (Vitamin C) was done and level of significant difference represented with *, **, *** and ****. Extracts with no asterisks are not significantly (NS) different from the standard

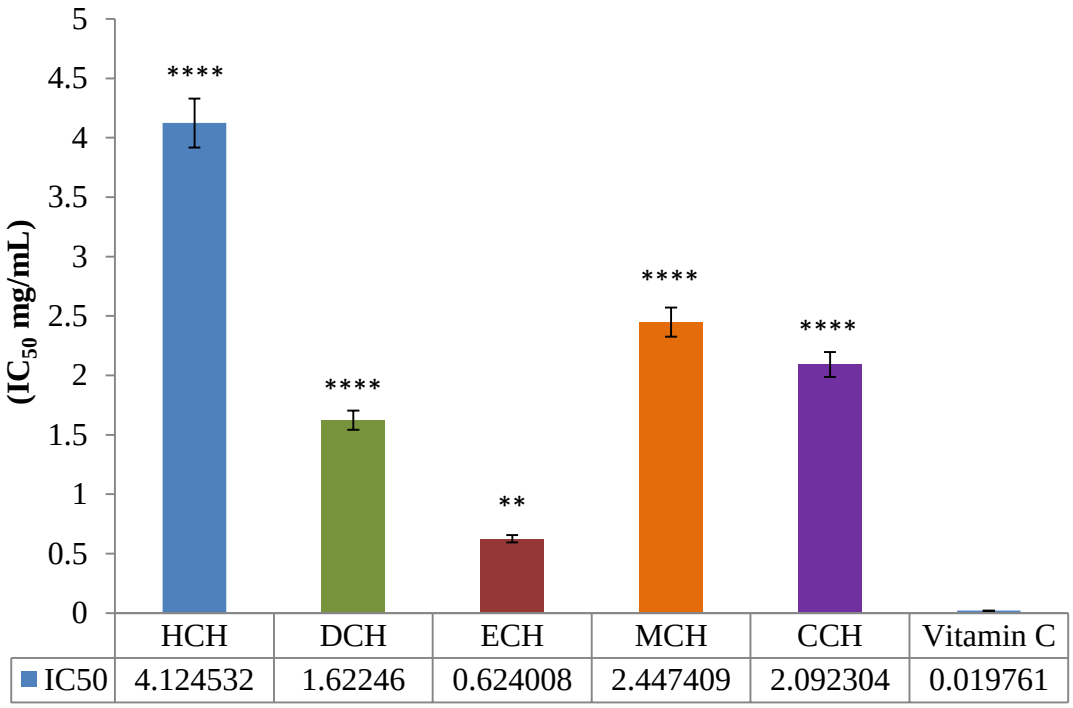

Figure 4.9: Metal chelating activity of crude and fractions of *Cola hispida* at 5-0.15625 mg/mL (IC_{50}±SD (mg/mL)

Values are presented as mean ± standard deviation (n=3). Where HCH (hexane fraction), DCH (dichloromethane fraction), ECH (ethyl acetate fraction), MCH (aqueous methanol fraction), CCH (crude)

Comparison of each extract with standard (Vitamin C) was done and level of significant difference represented with *, **, *** and ****. Extracts with no asterisks are not significantly (NS) different from the standard

.

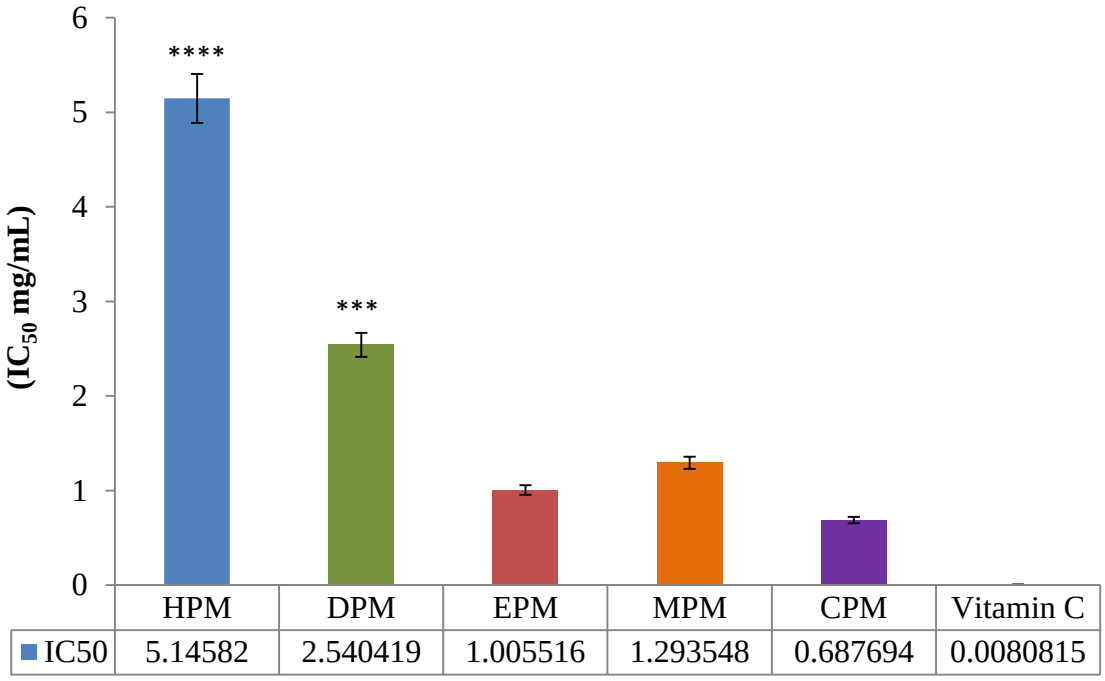

Figure 4.10: DPPH radical scavenging activity (RSA) of *Phyllanthus muellerianus* leaf crude extract and fractions at 5-0.15625 mg/mL (IC_{50}±SD (mg/mL)

Values are presented as mean ± standard deviation (n=3). Where HPM (hexane fraction), DPM (dichloromethane fraction), EPM (ethyl acetate fraction), MPM (aqueous methanol fraction), CPM (crude)

Comparison of each extract with standard (Vitamin C) was done and level of significant difference represented with *, **, *** and ****. Extracts with no asterisks are not significantly (NS) different from the standard

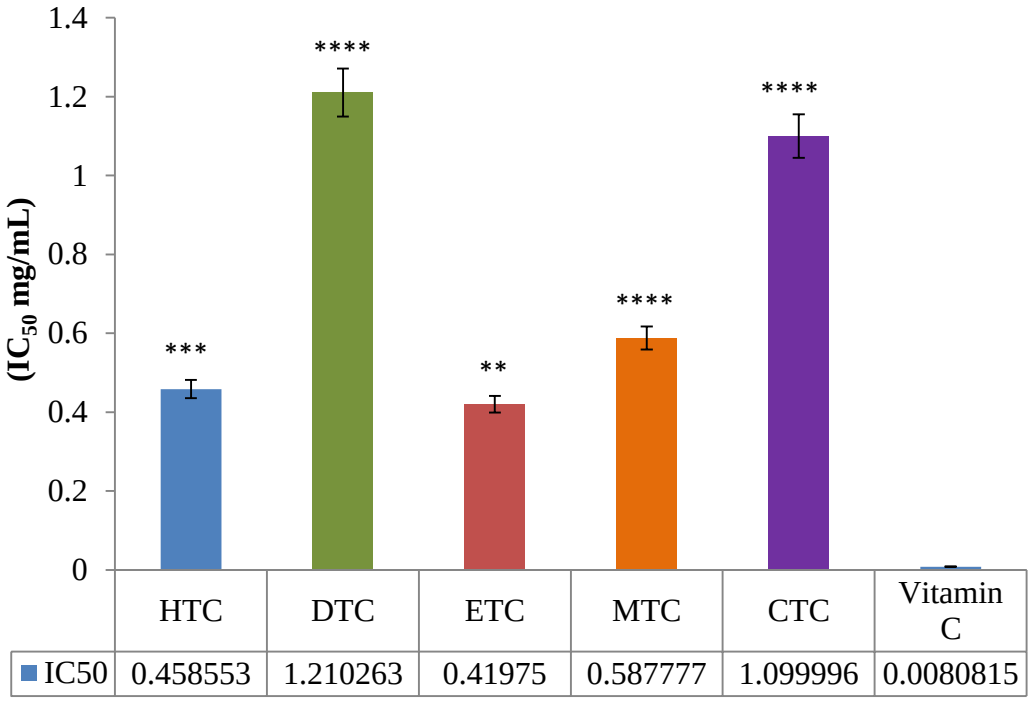

Figure 4.11: DPPH radical scavenging activity (RSA) of *Tinospora cordifolia* stem crude extract and fractions at 5-0.15625 mg/mL (IC_{50}±SD (mg/mL)

Values are presented as mean ± standard deviation (n=3). Where HTC (hexane fraction), DTC (dichloromethane fraction), ETC (ethyl acetate fraction), MTC (aqueous methanol fraction), CTC (crude)

Comparison of each extract with standard (Vitamin C) was done and level of significant difference represented with *, **, *** and ****. Extracts with no asterisks are not significantly (NS) different from the standard

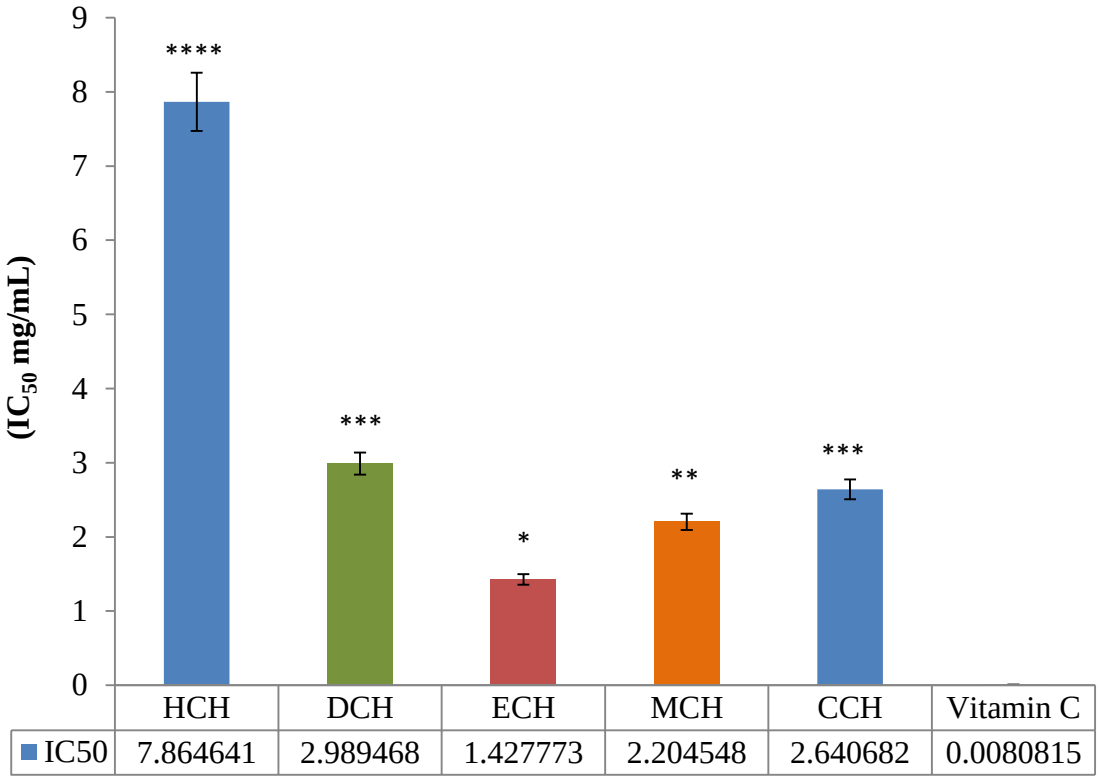

Figure 4.12: DPPH radical scavenging activity (RSA) of *Cola hispida* seed crude extract and fractions at 5-0.15625 mg/mL (IC_{50}±SD (mg/mL)

Values are presented as mean ± standard deviation (n=3). Where HCH (hexane fraction), DCH (dichloromethane fraction), ECH (ethyl acetate fraction), MCH (aqueous methanol fraction), CCH (crude)

Comparison of each extract with standard (Vitamin C) was done and level of significant difference represented with *, **, *** and ****. Extracts with no asterisks are not significantly (NS) different from the standard

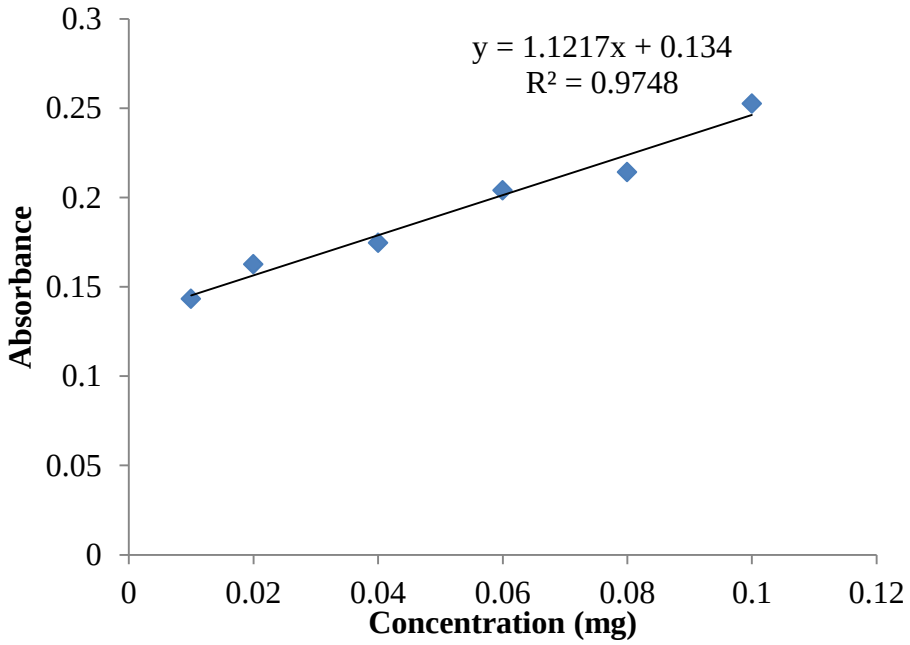

Figure 4.13: Calibration curve of ascorbic acid for total antioxidant capacity. Each point represents the mean of three experiments.

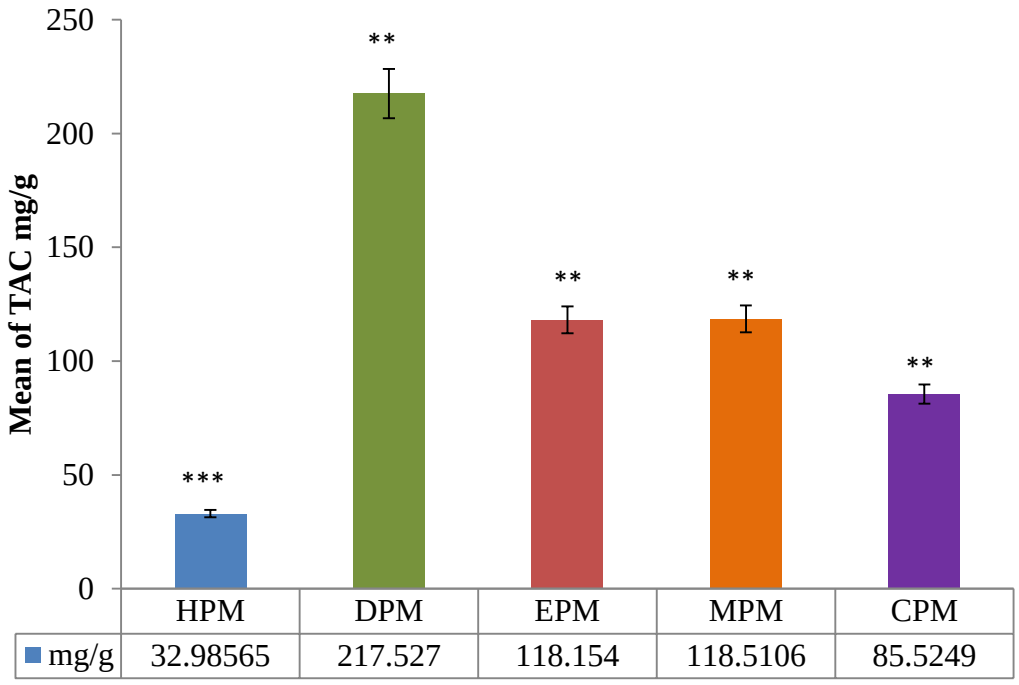

Figure 4.13.1: Total antioxidant capacity of *Phyllanthus muellerianus* leaf crude extract and fractions at 0.1- 0.01 mg/mL

Values are presented as mean ± standard deviation (n=3). Total antioxidant capacity is expressed as mg of AA equivalent per gm of extract. Where HPM (hexane fraction), DPM (dichloromethane fraction), EPM (ethyl acetate fraction), MPM (aqueous methanol fraction), CPM (crude)

Comparison of each extract with standard (Ascorbic acid) was done and level of significant difference represented with *, **, *** and ****. Extracts with no asterisks are not significantly (NS) different from the standard

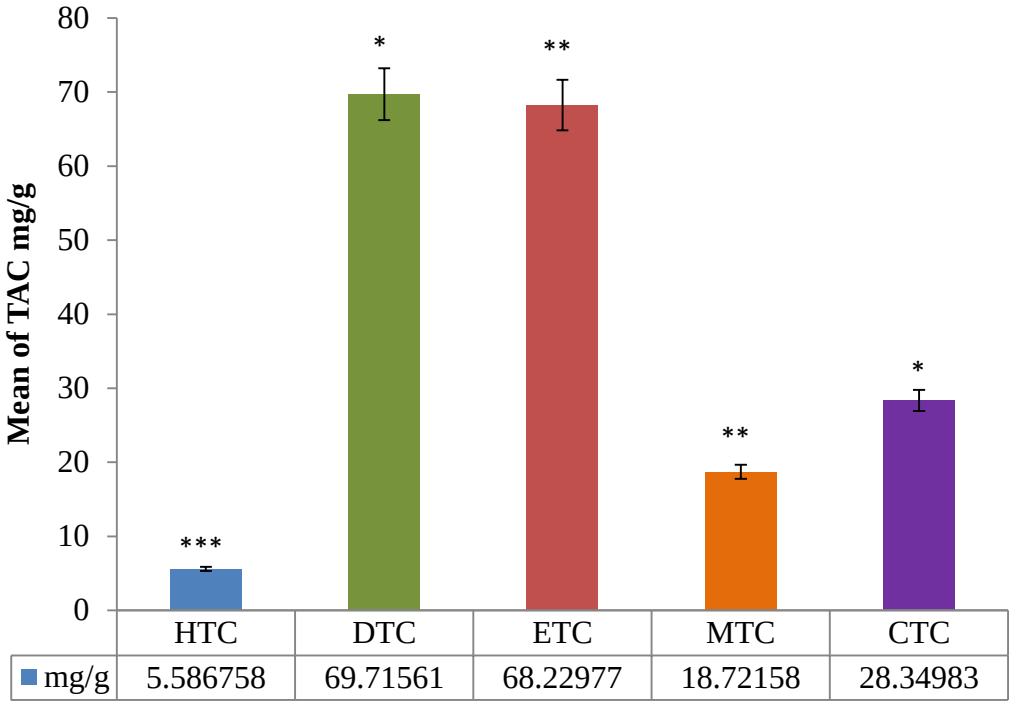

Figure 4.14: Total antioxidant capacity of *Tinospora cordifolia* stems crude extract and fractions at 0.1- 0.01 mg/mL

Values are presented as mean ± standard deviation (n=3). Total antioxidant capacity is expressed as mg of AA equivalent per gm of extract. Where HTC (hexane fraction), DTC (dichloromethane fraction), ETC (ethyl acetate fraction), MTC (aqueous methanol fraction), CTC (crude)

Comparison of each extract with standard (Ascorbic acid) was done and level of significant difference represented with *, **, *** and ****. Extracts with no asterisks are not significantly (NS) different from the standard

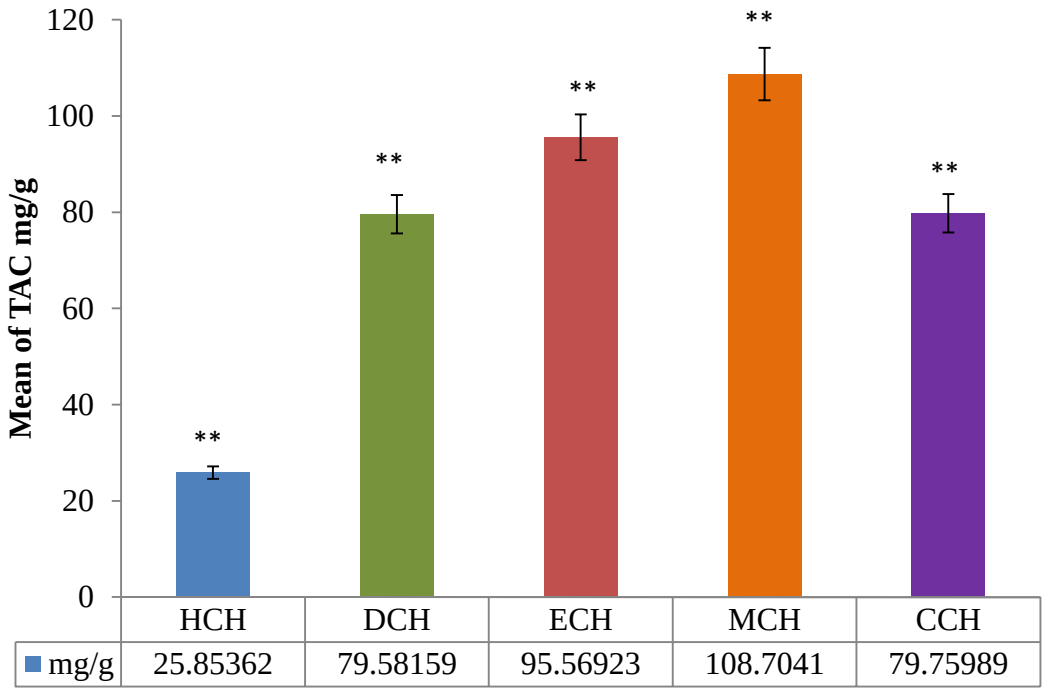

Figure 4.15: Total antioxidant capacity of *Cola hispida* seed crude extract and fractions at 0.1- 0.01 mg/mL

Values are presented as mean ± standard deviation (n=3). Total antioxidant capacity is expressed as mg of AA equivalent per gm of extract. Where HCH (hexane fraction), DCH (dichloromethane fraction), ECH (ethyl acetate fraction), MCH (aqueous methanol fraction), CCH (crude)

Comparison of each extract with standard (Ascorbic acid) was done and level of significant difference represented with *, **, *** and ****. Extracts with no asterisks are not significantly (NS) different from the standard

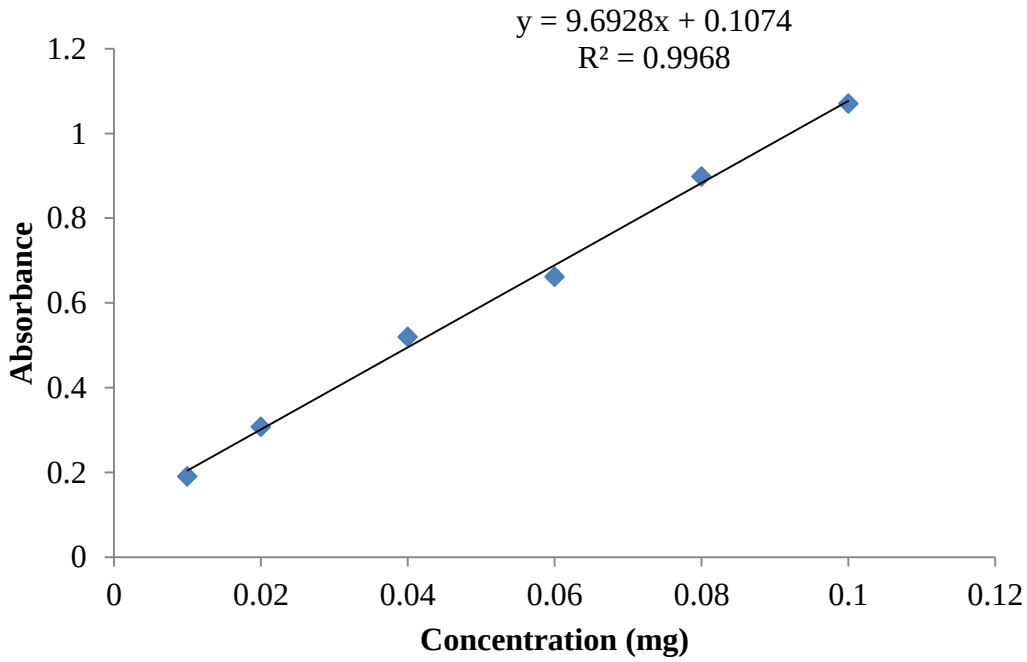

Figure 4.16: Calibration curve of ascorbic acid for ferric reducing antioxidant power. Each point represents the mean of three experiments

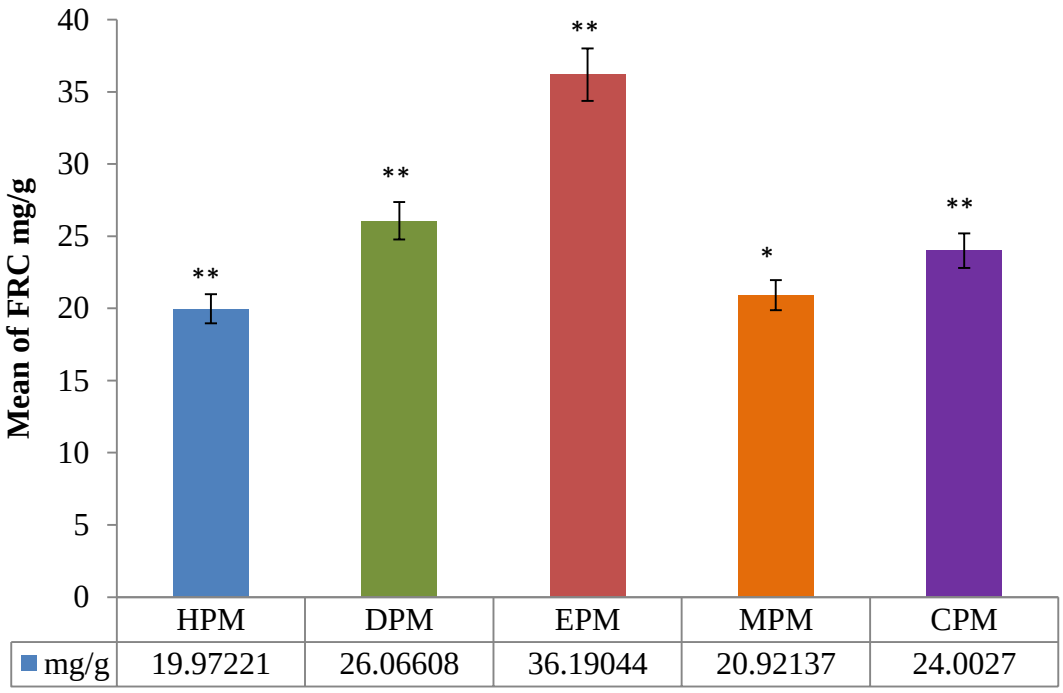

Figure 4.16.1: Ferric reducing antioxidant power assay (FRAP) of *Phyllanthus muellerianus* leaf crude extract and fractions at 0.1- 0.01 mg/mL

Values are presented as mean ± standard deviation (n=3). Ferric reducing capacity is expressed as mg of AA equivalent per gm of extract. Where HPM (hexane fraction), DPM (dichloromethane fraction), EPM (ethyl acetate fraction), MPM (aqueous methanol fraction), CPM (crude)

Comparison of each extract with standard (Ascorbic acid) was done and level of significant difference represented with *, **, *** and ****. Extracts with no asterisks are not significantly (NS) different from the standard

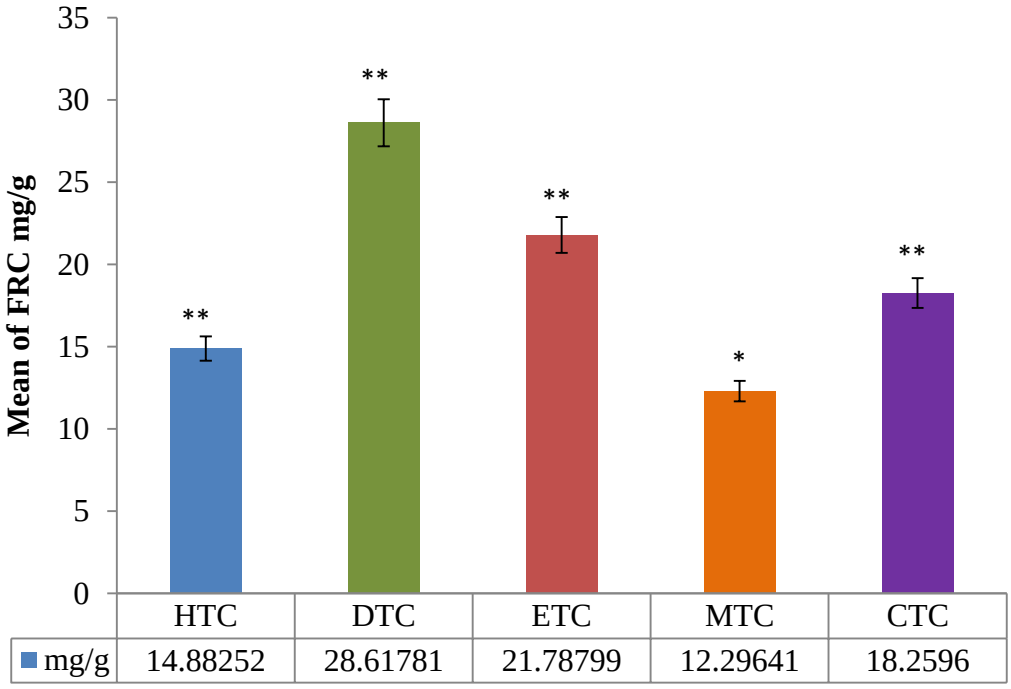

Figure 4.17: Ferric reducing antioxidant power assay (FRAP) of *Tinospora cordifolia* stem crude extract and fractions at 0.1- 0.01 mg/mL

Values are presented as mean ± standard deviation (n=3). Ferric reducing capacity is expressed as mg of AA equivalent per gm of extract. Where HTC (hexane fraction), DTC (dichloromethane fraction), ETC (ethyl acetate fraction), MTC (aqueous methanol fraction), CTC (crude)

Comparison of each extract with standard (Ascorbic acid) was done and level of significant difference represented with *, **, *** and ****. Extracts with no asterisks are not significantly (NS) different from the standard

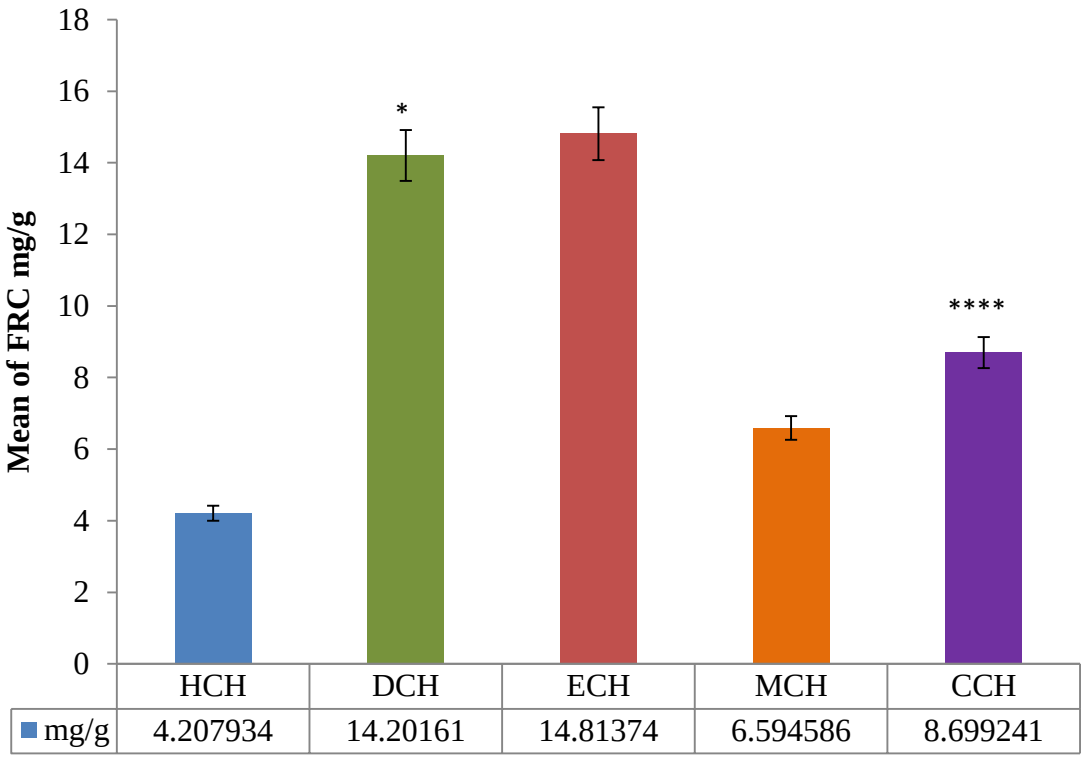

Figure 4.18: Ferric reducing antioxidant power assay (FRAP) of *Cola hispida* seed crude extract and fractions at 0.1- 0.01 mg/mL

Values are presented as mean ± standard deviation (n=3). Ferric reducing capacity is expressed as mg of AA equivalent per gm of extract. Where HCH (hexane fraction), DCH (dichloromethane fraction), ECH (ethyl acetate fraction), MCH (aqueous methanol fraction), CCH (crude)

Comparison of each extract with standard (Ascorbic acid) was done and level of significant difference represented with *, **, *** and ****. Extracts with no asterisks are not significantly (NS) different from the standard

4.6 Phytochemistry

4.6.1. GC-MS analysis of n-hexane fraction of *Phyllanthus muellerianus*

The GC-MS of *Phyllanthus muellerianus* leaf n-hexane fraction revealed eight (8) major compounds which are 3,7,11,15-Tetramethyl-2-hexadecen-1-ol (RT 35.76; 33.95%), Hexadecanoic acid, trimethylsilyl ester (RT 47.39;52.62%), Octadecanoic acid (RT 50.07;22.51%), Heptacosane (RT 60.52; 33.69%), 6,9,12-Octadecatrienoic acid, phenylmethyl ester, (Z,Z,Z)- (RT 48.80;4.26%), 9,12,15-Octadecatrienoic acid, (Z,Z,Z)- (RT 49.62;100%), Phenol, 2,2'-methylenebis[6-(1,1-dimethylethyl)-4-methyl- (RT 54.64;14.06%), Octadecanal, 2-bromo-(RT 55.96;15.67%) (Figure 4.19, Table 4.4).

4.6.2. GC-MS analysis of n-hexane fraction of *Tinospora cordifolia*

The GC-MS of *Tinospora cordifolia* stem n-hexane fraction reavealed eight (8) major compounds which are n-Hexadecanoic acid (RT 44.30;49.79%), Hexadecanoic acid, trimethylsilyl ester (RT 47.42;16.58%), 9,12-Octadecadienoic acid (Z,Z)- (RT 49.55;100%), Octadecanoic acid (RT 50.11;5.89%), Octadecanal, 2-bromo-(RT 54.63;3.14%), Hexadecanoic acid, 3-[(trimethylsilyl) oxy]propyl ester (RT 55.28;1.61%), Stigmastan-3,5-diene (RT 65.19;8.76%), β-Sitosterol (RT 71.16;14.37%) (Figure 4.20, Table 4.5).

4.6.3. GC-MS analysis of n-hexane fraction of *cola hispida*

The GC-MS of *Cola hispida* seed n-hexane fraction shows the presence of six (6) major compounds which are Hexadecanoic acid, methyl ester (RT 42.49; 35.54%), Hexadecanoic acid, trimethylsilyl ester (RT 47.42;97.32%), 9,12,15-Octadecatrienoic acid, methyl ester, (Z,Z,Z)- (RT 48.81;30.94%), Methyl 8,9-methylene-heptadec-8-enoate (RT 48.53;7.28%), Heptadecanoic acid, 16-methyl-, methyl ester (RT 49.38; 4.74%), Methyl 9,10-methylene-octadec-9-enoate (RT 50.73;21.82%) (Figure 4.21, Table 4.6).

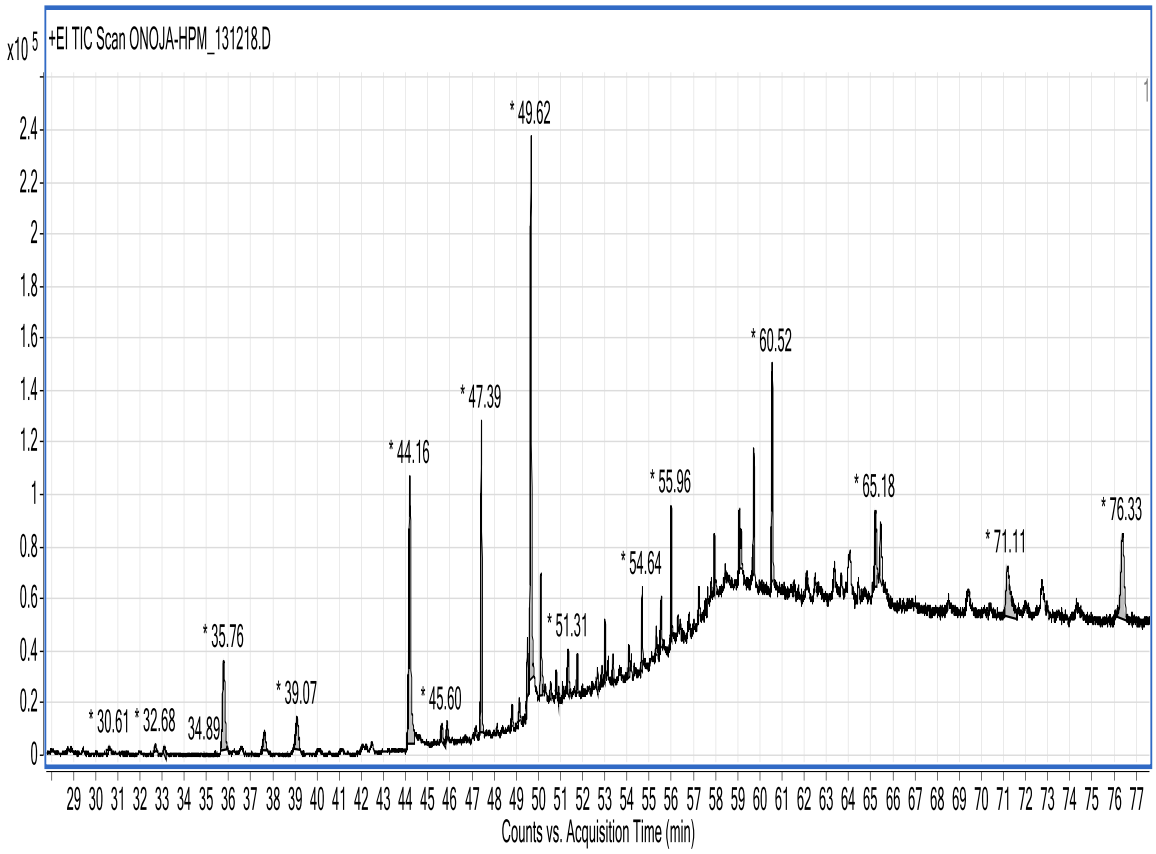

Figure 4.19: GC-MS Chromatogram of n-hexane fraction of *Phyllanthus muellerianus* (HPM) leaf

Table 4.4: Compounds identified by GC-MS analysis of *Phyllanthus muellerianus* (HPM) leaf

Retention time (min)	Molecular formula	M.W.	Compound name
30.63	$C_{14}H_{14}O_3$	230	7-Hydroxy-3-(1,1-dimethylprop-2-enyl)coumarin
35.76	$C_{20}H_{40}O$	296	3,7,11,15-Tetramethyl-2-hexadecen-1-ol
	$C_{20}H_{38}$	278	9-Eicosyne
37.64	$C_{16}H_{30}$	222	1-Hexadecyne
39.03	$C_{20}H_{40}O$	296	3,7,11,15-Tetramethyl-2-hexadecen-1-ol
45.63	$C_{15}H_{28}O_2$	240	E-10-Dodecen-1-ol propionate
47.39	$C_{19}H_{40}O_2Si$	328	Hexadecanoic acid, trimethylsilyl ester
48.80	$C_{18}H_{30}O$	262	9,12,15-Octadecatrienal
	$C_{25}H_{36}O_2$	368	6,9,12-Octadecatrienoic acid, phenylmethyl ester, (Z,Z,Z)-
49.11	$C_{15}H_{32}O$	228	1-Dodecanol, 3,7,11-trimethyl-
	$C_{16}H_{30}O$	238	7-Hexadecenal, (Z)-
49.48	$C_{18}H_{32}O_2$	280	9,12-Octadecadienoic acid (Z,Z)-
49.62	$C_{18}H_{30}O_2$	278	9,12,15-Octadecatrienoic acid, (Z,Z,Z)-
50.07	$C_{18}H_{36}O_2$	284	Octadecanoic acid
50.53	$C_{18}H_{34}O_2$	282	Oleic Acid
	$C_{21}H_{38}O_2$	322	[1,1'-Bicyclopropyl]-2-octanoic acid, 2'-hexyl-, methyl ester
	$C_{25}H_{40}O_6$	436	9,12,15-Octadecatrienoic acid, 2-(acetyloxy)-1-[(acetyloxy)methyl]ethyl ester, (Z,Z,Z)-
50.77	$C_{17}H_{31}F_3O_2$	324	3-Trifluoroacetoxypentadecane
	$C_{15}H_{28}O_2$	240	Z-8-Methyl-9-tetradecenoic acid
50.87	$C_{25}H_{40}O_2$	372	9-Octadecenoic acid (Z)-, phenylmethyl ester
51.06	$C_{19}H_{36}O$	280	12-Methyl-E,E-2,13-octadecadien-1-ol
51.31	$C_{27}H_{52}O_4Si_2$	496	9,12,15-Octadecatrienoic acid, 2-[(trimethylsilyl)oxy]-1-[[(trimethylsilyl)oxy]methyl]ethyl ester, (Z,Z,Z)-
51.73	$C_{22}H_{42}S_2Si$	398	t-Butyl-{2-[3-(2,2-dimethyl-6-methylene-cyclohexyl)-propyl]-[1,3]dithian-2-yl}-dimethyl-silane

Table 4.4: Compounds identified by GC-MS analysis of *Phyllanthus muellerianus* (HPM) leaf (contd.)

Retention time (min)	Molecular formula	M.W.	Compound name
52.63	$C_{19}H_{36}O$	280	12-Methyl-E,E-2,13-octadecadien-1-ol
52.82	$C_{18}H_{35}BrO$	346	Octadecanal, 2-bromo-
	$C_{25}H_{40}O_2$	372	9-Octadecenoic acid (Z)-, phenylmethyl ester
52.97	$C_{19}H_{36}O$	280	12-Methyl-E,E-2,13-octadecadien-1-ol
	$C_{19}H_{36}O$	280	2-Methyl-Z,Z-3,13-octadecadienol
53.11	$C_{19}H_{36}O$	280	12-Methyl-E,E-2,13-octadecadien-1-ol
53.32	$C_{19}H_{36}O$	280	12-Methyl-E,E-2,13-octadecadien-1-ol
	$C_{25}H_{40}O_2$	372	9-Octadecenoic acid (Z)-, phenylmethyl ester
54.05	$C_{25}H_{40}O_2$	372	9-Octadecenoic acid (Z)-, phenylmethyl ester
54.64	$C_{23}H_{32}O_2$	340	Phenol, 2,2'-methylenebis[6-(1,1-dimethylethyl)-4-methyl-
	$C_{21}H_{28}N_2O_2$	340	2H-3,7-Methanoazacycloundecino[5,4-b]indole-9-carboxylic acid, 5-ethyl-1,4,5,6,7,8,9,10-octahydro-, methyl ester, [5S-(5R*,7R*,9S*)]-
55.28	$C_{27}H_{54}O_4Si_2$	498	1-Monolinoleoylglycerol trimethylsilyl ether
	$C_{16}H_{34}O_7S$	370	d-Mannitol, 1-decylsulfonyl-
55.50	$C_{27}H_{54}O_4Si_2$	498	1-Monolinoleoylglycerol trimethylsilyl ether
55.96	$C_{18}H_{35}BrO$	346	Octadecanal, 2-bromo-
57.21	$C_{27}H_{54}O_4Si_2$	498	1-Monolinoleoylglycerol trimethylsilyl ether
57.91	$C_{27}H_{54}O_4Si_2$	498	1-Monolinoleoylglycerol trimethylsilyl ether
59.03	$C_{27}H_{54}O_4Si_2$	498	1-Monolinoleoylglycerol trimethylsilyl ether
59.12	$C_{27}H_{52}O_4Si_2$	496	9,12,15-Octadecatrienoic acid, 2-[(trimethylsilyl)oxy]-1-[[(trimethylsilyl)oxy]methyl]ethyl ester, (Z,Z,Z)-
59.68	$C_{30}H_{52}O$	428	2,2,4-Trimethyl-3-(3,8,12,16-tetramethyl-heptadeca-3,7,11,15-tetraenyl)-cyclohexanol
60.52	$C_{27}H_{56}$	380	Heptacosane
71.11	$C_{27}H_{54}O_4Si_2$	498	1-Monolinoleoylglycerol trimethylsilyl ether

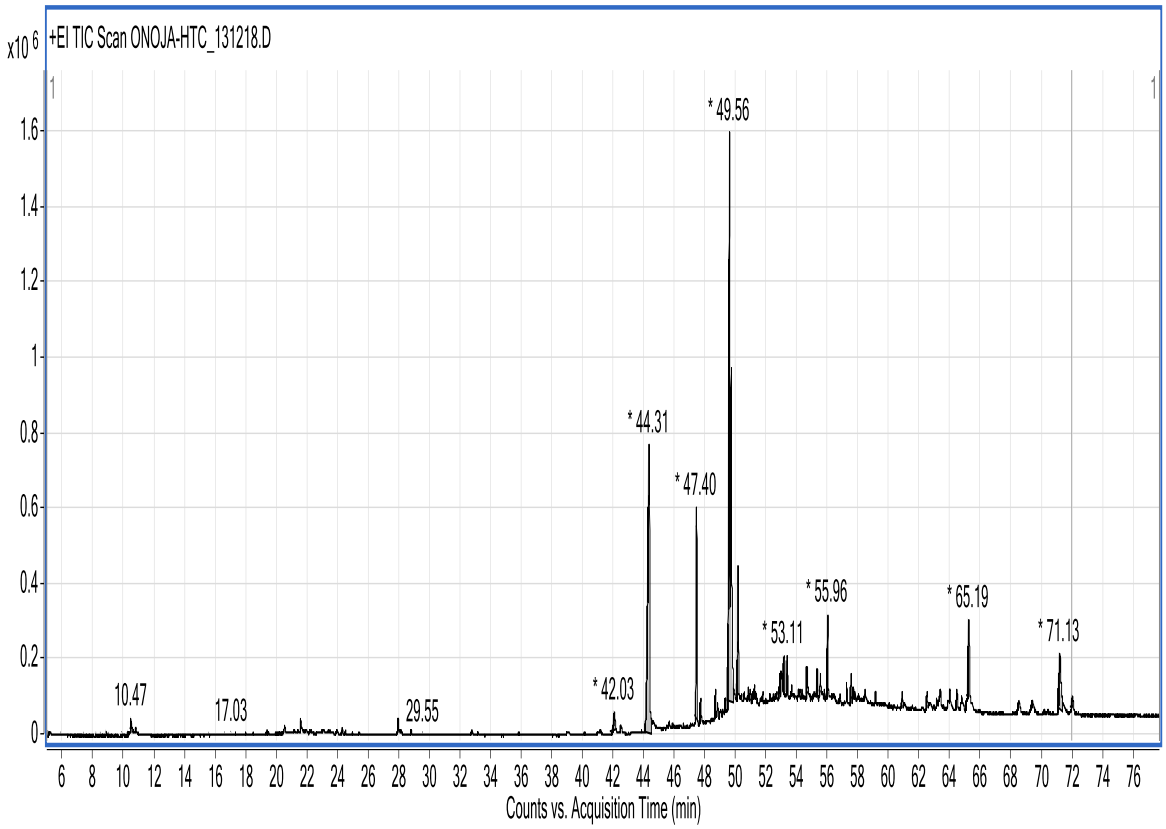

Figure 4.20: GC-MS Chromatogram of n-hexane fraction of *Tinospora cordifolia* (HTC) stem

Table 4.5: Compounds identified by GC-MS analysis of n-hexane fraction of *Tinospora cordifolia* (HTC) stem

Retention time (min)	Molecular formula	M.W.	Compound name
42.00	$C_{14}H_{28}O$	212	Tetradecanal
44.30	$C_{16}H_{32}O_2$	256	n-Hexadecanoic acid
	$C_{38}H_{68}O_8$	652	l-(+)-Ascorbic acid 2,6-dihexadecanoate
47.42	$C_{19}H_{40}O_2Si$	328	Hexadecanoic acid, trimethylsilyl ester
49.55	$C_{18}H_{32}O_2$	280	9,12-Octadecadienoic acid (Z,Z)-
50.11	$C_{18}H_{36}O_2$	284	Octadecanoic acid
	$C_{22}H_{44}O_4$	372	Octadecanoic acid, 2-(2-hydroxyethoxy)ethyl ester
53.12	$C_{20}H_{40}O_2$	312	Ethanol, 2-(9-octadecenyloxy)-, (Z)-
	$C_{20}H_{38}O_2$	310	cis-11-Eicosenoic acid
53.35	$C_{22}H_{46}O$	326	Behenic alcohol
54.63	$C_{18}H_{35}BrO$	346	Octadecanal, 2-bromo-
55.28	$C_{22}H_{46}O_3Si$	386	Hexadecanoic acid, 3-[(trimethylsilyl)oxy]propyl ester
55.98	$C_{18}H_{35}BrO$	346	Octadecanal, 2-bromo-
65.19	$C_{29}H_{48}$	396	Stigmastan-3,5-diene
	$C_{31}H_{53}ClO_2$	492	Stigmastan-3-ol, 5-chloro-, acetate, (3β,5α)-
71.16	$C_{29}H_{50}O$	414	β-Sitosterol
	$C_{29}H_{50}O$	414	γ-Sitosterol
71.99	$C_{27}H_{54}O_4Si_2$	498	1-Monolinoleoylglycerol trimethylsilyl ether

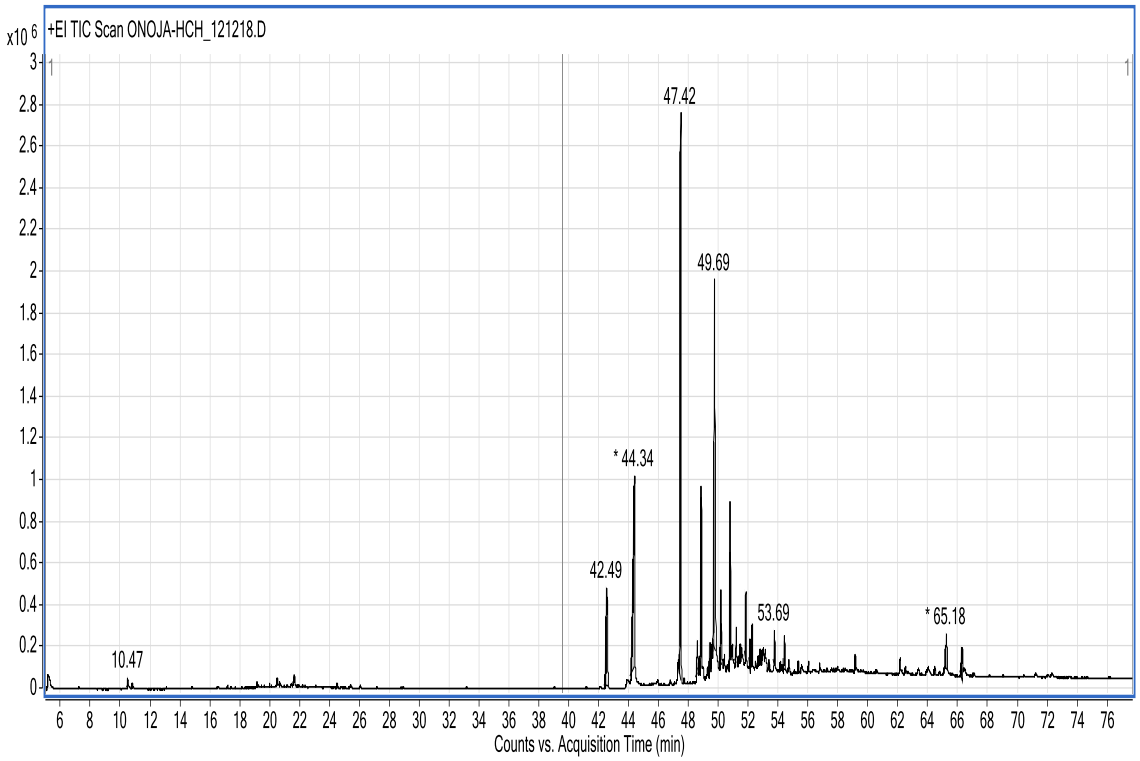

Figure 4.21: GC-MS Chromatogram of n-hexane fraction of *Cola hispida* (HCH) seed

Table 4.6: Compounds identified by GC-MS analysis of n-hexane fraction of *Cola hispida* (HCH) seed

Retention time (min)	Molecular formula	M.W.	Compound name
10.47	$C_9H_{22}OSi$	174	1-Butyl(dimethyl)silyloxypropane
	$C_{19}H_{36}O$	280	12-Methyl-E,E-2,13-octadecadien-1-ol
42.49	$C_{17}H_{34}O_2$	270	Hexadecanoic acid, methyl ester
47.42	$C_{19}H_{40}O_2Si$	328	Hexadecanoic acid, trimethylsilyl ester
48.83	$C_{19}H_{32}O_2$	292	9,12,15-Octadecatrienoic acid, methyl ester, (Z,Z,Z)-
48.53	$C_{19}H_{34}O_2$	294	Methyl 8,9-methylene-heptadec-8-enoate
48.81	$C_{19}H_{32}O_2$	292	9,12,15-Octadecatrienoic acid, methyl ester, (Z,Z,Z)-
49.38	$C_{19}H_{38}O_2$	298	Heptadecanoic acid, 16-methyl-, methyl ester
	$C_{19}H_{38}O_2$	298	Heptadecanoic acid, 10-methyl-, methyl ester
49.71	$C_{18}H_{30}O_2$	278	9,12,15-Octadecatrienoic acid, (Z,Z,Z)-
50.12	$C_{18}H_{36}O_2$	284	Octadecanoic acid
	$C_{22}H_{44}O_4$	372	Octadecanoic acid, 2-(2-hydroxyethoxy)ethyl ester
50.73	$C_{20}H_{36}O_2$	308	Methyl 9,10-methylene-octadec-9-enoate
51.13	$C_{20}H_{38}O_2$	310	Methyl 9,10-methylene-octadecanoate
	$C_{20}H_{38}O_2$	310	Cyclopropaneoctanoic acid, 2-octyl-, methyl ester
51.78	$C_{19}H_{36}O_2$	296	cis-10-Nonadecenoic acid
	$C_{18}H_{34}O_2$	282	trans-13-Octadecenoic acid
52.21	$C_{20}H_{36}O_2$	308	Methyl 9,10-methylene-octadec-9-enoate
53.69	$C_{19}H_{36}O_3$	312	Oxiraneundecanoic acid, 3-pentyl-, methyl ester, cis-
65.18	$C_{29}H_{48}$	396	Stigmastan-3,5-diene
66.24	$C_{18}H_{34}O$	266	8-Octadecenal

4.7 Characterisation of compounds isolated from *Phyllanthus muellerianus* leaf

4.7.1 Compound DPM-2

The chromatography yielded 127 fractions which were pooled together to 13 sub fractions (labeled as DPM-F1-DPM-F13). Compound **DPM-2** was obtained as a white powder from sub fraction DPM-F2 (pooled fractions 16-25) with gradient elution hexane: ethyl acetate (95:5) yielded 30 mg. It has retardation factor **(R_f)** value of 0.5 in solvent system hexane: ethyl acetate (8:2) and melting point **(M.p)**: 150.6^{o}C-151.8^{o}C. Its low resolution electron impact **(EI)** mass spectrum showed a molecular ion peak at m/z 412.3 g/mol [M+], **UV** (MeOH) λ/nm (log ε): 216.00 nm (A 0.008), 260.00 nm (A 0.114) (190-600 nm), **IR (γ_{max} ^{KBr} cm-1):** 3426.1, 2936.3, 2866.2, 2359.5, 1642.9, 1461.6, 1375.7, 1058.2, 965.4 and 592.2 and NMR data (Table 4.7). Molecular formula ($C_{29}H_{48}O$) and structure has been assigned to the substance named stigmasterol (Figure 4.22) based on the physical data and spectroscopic analysis (UV, IR, MS, ^{1}H-NMR and ^{13}C-NMR) and by comparison with reported literature (Guo *et al*., 2012).

4.7.2 Compound EPM-9A

The chromatography yielded 257 fractions which were pooled together to 18 sub fractions (labeled as EPM-F1-EPM-F18). The sub fraction EPM-F9 (pooled fractions 149-167) yielded compound **EPM-9A** (75 mg) as a white powder with the solvent system n-hexane: ethyl acetate (25:75). It has retardation factor **(R_f)** value of 0.84 in solvent system ethyl acetate: methanol (1:1), Melting point **(M.p):** 295.5^{o}C-303.7^{o}C, its low resolution electron impact **(EI)** mass spectrum showed the existence of a sterol skeleton and a molecular ion peak at m/z 414 [M+]. The exact mass was detected on FAB on the positive mode, Mass (m/z): 577.85 g/mol [M+]. **IR (γ_{max} ^{KBr} cm-1):** 3386.2, 2959.3, 2931.1, 2873.0, 1647.5, 1463.7, 1374.7, 1070.3, 1024.5, 668.2 and NMR data (Table 4.8). Molecular formula ($C_{35}H_{60}O_6$) and structure has been assigned to the substance named Daucosterol (Figure 4.23) based on the physical data and spectroscopic analysis (UV, IR, MS, ^{1}H-NMR and ^{13}C-NMR) and by comparison with reported literature (Flamini *et al*., 2001).

Table 4.7: ^{1}H and ^{13}C-NMR chemical shift values for stigmasterol (DPM-2) recorded in CDCL3 (AVANCE NEO 400 MHz)

Position	^{1}H-NMR	^{13}C-NMR
1		37.2
2		31.8
3	3.50 (m,1H)	71.79
4		42.2
5		140.7
6	5.33 (br d, 1H, J=4.8Hz)	121.7
7		31.6
8		31.6
9		50.1
10		36.1
11		21.2
12		39.76
13		42.2
14		56.85
15		24.3
16		28.90
17		56.03
18	0.68 (br s, 3H)	12.03
19	0.99 (br s, 3H)	19.38
20		36.1
21		18.7
22	5.14 (dd, 1H, J=8.4Hz, 8.4Hz)	138.3
23	4.99 (dd, 1H, J=8.8Hz, 8.4Hz)	129.2
24		51.2
25		28.90
26	0.83	21.07
27	0.79	19.01
28		23.05
29	0.81	12.23

Chemical shift values are in δ (ppm); Coupling constants are in Hz.

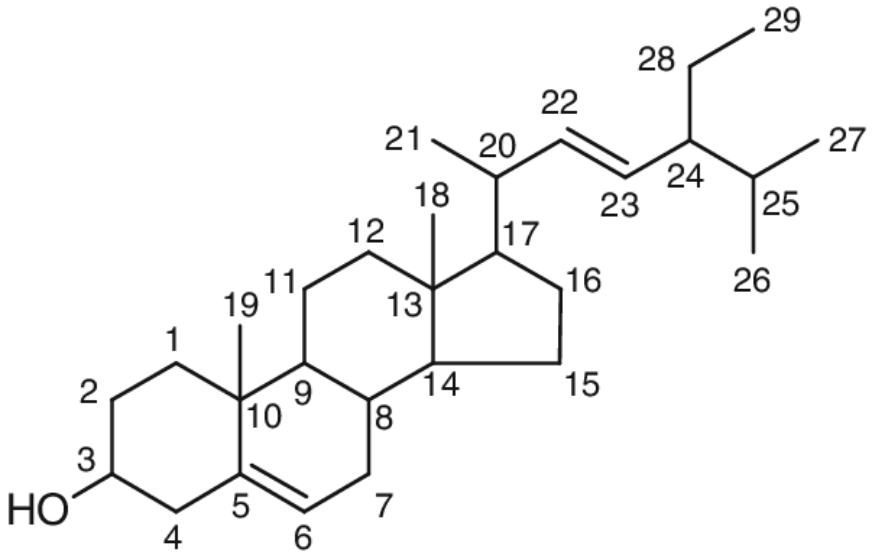

Figure 4.22: **Stigmasterol** (DPM-2)

Table 4.8: ^{1}H and ^{13}C-NMR chemical shift values for daucosterol (EPM-9A) recorded in C5D5N (AVANCE NEO 400 MHz)

Position	^{1}H-NMR	^{13}C-NMR
1		37.51
2		30.28
3		78.64
4		37.51
5		140.94
6	5.34 (br d, 1H, J=4Hz)	121.93
7		32.08
8		32.19
9		50.38
10		36.95
11		21.30
12		39.98
13		46.08
14		56.85
15		24.53
16		29.50
17		56.28
18	0.66 (br d, 3H, J=6Hz)	12.18
19	0.98 (s, 3H)	19.44
20		36.41
21		19.44
22		32.19
23		24.53
24		46.08
25		29.50
26		19.99
27		21.30
28		23.42
29		12.18
1’	5.06 (d, 1H, J=7.6Hz)	102.6
2’		75.37
3’	4.06 (t, 1H, J=8Hz, 8Hz)	78.64
4’	4.58 (d, 1H, J=10.4Hz)	71.74
5’	3.98 (m, 2H)	78.64
6’	4.28 (t, 2H, J=4.8Hz, 4.4Hz)	62.88

Chemical shift values are in δ (ppm); Coupling constants are in Hz.

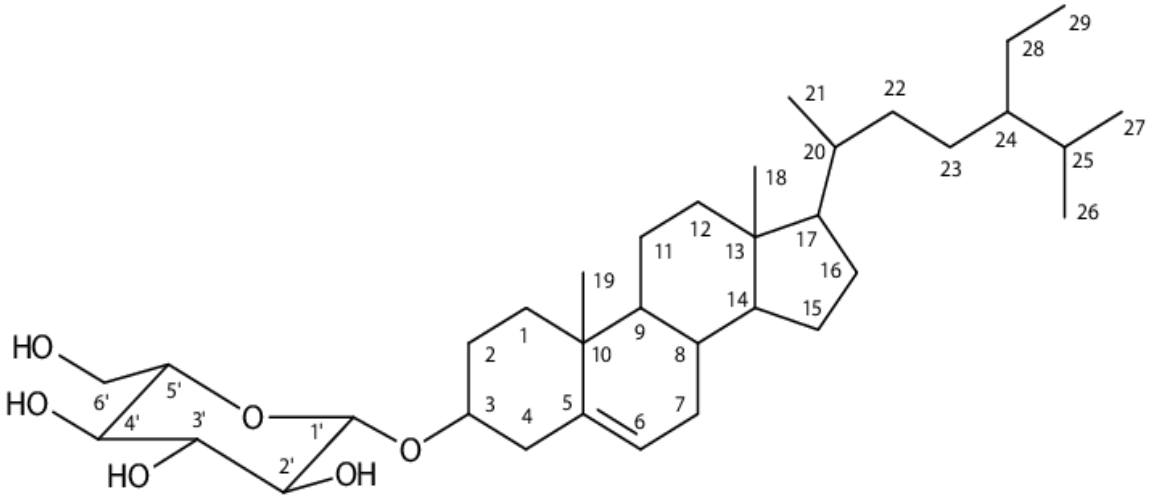

Figure 4.23: **Daucosterol (EPM-9A)**

4.8 Characterisation of compounds isolated from *Tinospora cordifolia* stem

4.8.1 Compound DTC-3

The chromatography yielded 249 fractions which were pooled together to 21 sub fractions (labeled as DTC-F1-DTC-F21). The sub fraction DTC-F3 (pooled fractions 15-32) yielded compound **DTC-3 (70 mg)** as a white amorphous powder with solvent system hexane: ethyl acetate (90:10). It has retardation factor ($\mathbf{R_f}$) value of 0.44 in solvent system hexane: ethyl acetate (4.5:0.5) and melting point (**M.p):** 80.1^{o}C-81.8^{o}C Mass (m/z): 410.2 g/mol [M+] as confirmed by LR-ESI-MS. Its low resolution electron impact **(EI)** mass spectrum showed a molecular ion peak at m/z 392.2 [M+], UV (MeOH) λ/nm (log ε): 229.00 nm (A 0.688) (190-600 nm) **IR (γ_{max} ^{KBr} cm-1):** 3314.4, 2918.9, 2849.1, 2360.0, 1467.5, 1063.2, 724.6 and NMR data (Table 4.9). Molecular formula ($C_{28}H_{58}O$) and structure has been assigned to the substance named 1-octacosanol (Figure 4.24) based on the physical data and spectroscopic analysis (UV, IR, MS, ^{1}H-NMR and ^{13}C-NMR) and by comparison with reported literature (Sadiqa *et al*., 2014).

4.8.2 Compound DTC-4

Sub fraction DTC-F4 (pooled fractions 33-48) yielded compound **DTC-4 (80 mg)** as a white powder eluted with solvent system hexane: ethyl acetate (85:15). It has retardation factor ($\mathbf{R_f}$) value of 0.6 in solvent system hexane: chloroform: ethyl acetate (4:1:1.5) and melting point (M.p): 134.4^{o}C-135.1^{o}C, Mass (m/z): 414.3 g/mol [M+], **UV** (MeOH) λ/nm (log ε): 219.00 nm (A 0.627), 270.00 nm (A 1.404) (190-600 nm) **IR (γ_{max} ^{KBr} cm-1):** 3446.3, 2936.5, 1642.3, 1462.4, 1376.6, 1058.6, 961.7, 591.7 and NMR data (Table 4.10). Molecular formula ($C_{29}H_{50}O$) and structure has been assigned to the substance named β-Sitosterol (Figure 4.25) based on the physical data and spectroscopic analysis (UV, IR, MS, ^{1}H-NMR and ^{13}C-NMR) and by comparison with reported literature (Wright *et al*., 1978).

Table 4.9: ^{1}H-NMR and ^{13}C-NMR chemical shift values for 1-octacosanol (DTC-3) recorded in CDCL3 (AVANCE NEO 500 MHz Cryoprobe)

^{1}H-NMR	^{13}C-NMR	HMBC
3.63 (t, 2H, J = 7Hz, 6.5Hz)	63.11	25.72, 32.81, 50.89
1.54 (m, 2H)	32.81	25.72, 29.35
1.26 (br s, 51H)	29.76	14.10, 22.68, 29.35, 32.81
0.86 (t, 3H, J=7Hz)	14.10	22.68, 32.81

Chemical shift values are in δ (ppm); Coupling constants are in Hz.

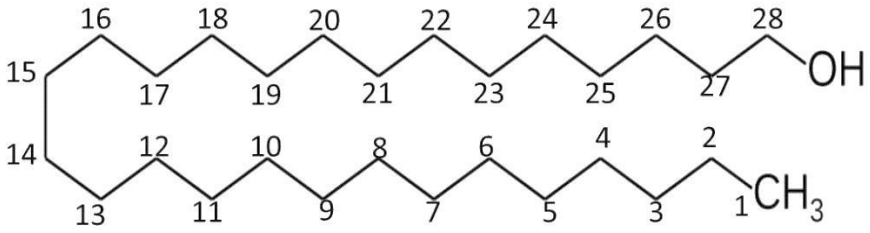

Figure 4.24: **1-Octacosanol** (DTC-3)

Table 4.10: ^{1}H and ^{13}C-NMR chemical shift values for β-Sitosterol (DTC-4) recorded in CDCL3 (AVANCE NEO 400 MHz)

Position	^{1}H-NMR	^{13}C-NMR
1		37.26
2		31.91
3	3.50 (m,1H)	71.81
4		42.31
5		138.3
6	5.32 (br d, 1H, J=5.2Hz)	121.7
7		31.88
8		31.91
9		50.14
10		36.14
11		21.21
12		39.78
13		42.31
14		56.87
15		24.30
16		28.91
17		56.07
18	0.66 (br s, 3H)	11.98
19	0.98 (br s, 3H)	19.39
20		36.14
21	0.89	18.78
22		33.96
23		26.10
24		45.85
25		29.17
26	0.80	21.07
27		19.81
28		23.07
29	0.84	12.23

Chemical shift values are in δ (ppm); Coupling constants are in Hz.

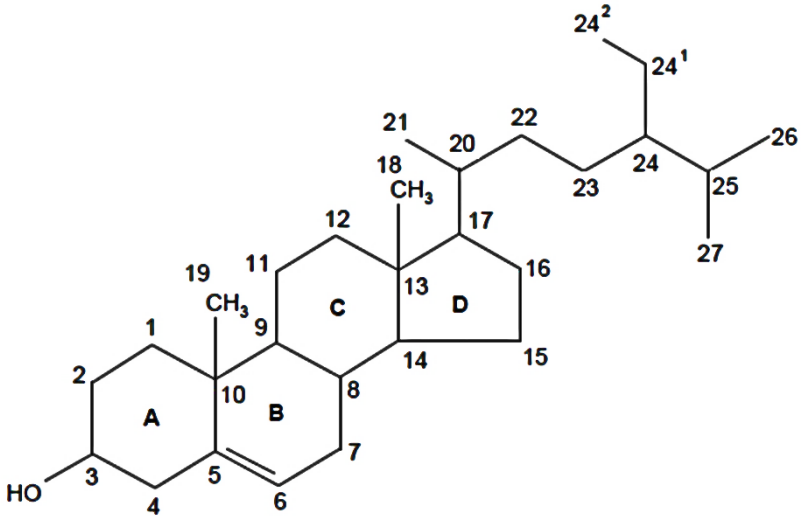

Figure 4.25: **β-Sitosterol (DTC-4)**

4.8.3 Compound ETC-11

The chromatography yielded 252 fractions which were pooled together to 34 sub fractions (labeled as EA-1-EA-34) based on their TLC profile using solvent system 4:3:2:1 (Hex: DCM: EA: MeOH). Sub fraction EA-11 (pooled fractions 77-80) eluted with hexane: dichloromethane (1:3) yielded **ETC-11** as a yellow compound. It has retardation factor (**R_f**) value of 0.5 in solvent system ethyl acetate: acetone (3.5:1.5). EI-MS m/z 275.2 g/mol [M]+; UV (MeOH) λ/nm (log ε): 248.00 nm (A 1.132), 267.00 nm (A 0.906), 304.00 nm (A 0.313), 416.00 nm (A 0.394) (230 nm- 600 nm) **IR (γ_{max} ^{KBr} cm-1):**3428.0, 2960.7, 2923.9, 2856.0, 1648.7, 1569.4, 1414.3, 1260.8, 1092.5, 1021.3, 865.7 and NMR data (Table 4.11) Molecular formula ($C_{17}H_9NO_3$) and structure has been assigned to the substance named Liriodenine (Figure 4.26) based on the physical data and spectroscopic analysis (UV, IR, MS, ^{1}H-NMR and ^{13}C-NMR) and by comparison with reported literature (Hamid *et al*., 2015).

4.8.4 Compound ETC-14

Compound **ETC-14** was obtained as a white powder with N-formylaporphine skeletons was obtained from ethyl acetate fraction (sub fraction EA-14 (pooled fractions 98-102)) with solvent system n-hexane: dichloromethane (1:3) yielded 410 mg. It has retardation factor **(R_f)** value of 0.57 in solvent system hexane: ethyl acetate (1:1) and melting point **(M.p)**:252.9^{o}C-260.2^{o}C, Mass (m/z): 293.2 g/mol [M+], **UV** (MeOH) λ/nm (log ε): 214.00 nm (A 0.448), 229.00 nm (A 0.397), 273.00 nm (A 0.335), 315.00 nm (A 0.067) (start wavelength 200-stop wavelength 600 nm) **IR (γ_{max} ^{KBr} cm-1):** 3045.8, 2877.1, 1658.0, 1423.8, 1221.4, 1041.2, 933.8, 775.3, 734.7, 643.9 and NMR data (Table 4.12). Molecular formula ($C_{18}H_{15}NO_3$) and structure has been assigned to the substance named (-)-N-formylanonaine (Figure 4.27) based on the physical data and spectroscopic analysis (UV, IR, MS, ^{1}H-NMR and ^{13}C-NMR) and by comparison with reported literature (Hui-Min *et al*., 2010).

Table 4.11: ^{1}H (AVANCE NEO 400 MHz) and ^{13}C-NMR (AV-III-HD 800 MHz Cryo-Probe) chemical shift values for Liriodenine (ETC-11) recorded in CD3OD

Position	^{1}H-NMR	^{13}C-NMR
1		168.2
1a		122.5
2		152.1
3	7.42 (1H, s, H-3)	102.3
3a		
4	8.02 (1H, d, J=5.2 Hz, H-4)	124.3
5	8.74 (1H, d, J=5.2 Hz, H-5)	143.11
6a		
7		181.67
7a		130.1
8	8.47 (1H, dd, J=8Hz, 1.2 Hz, H-8)	127.2
9	7.64 (1H, t, J = 7.2 Hz, 6.8 Hz, H-9)	127.7
10	7.87 (1H, ddd, 1.6 Hz, 1.6 Hz, H-10)	133.5
11	8.79 (1H, d, J=7.6 Hz, H-11)	126.7
11a		
-OCH_2O-	6.47 (2H, s)	102.8

Chemical shift values are in δ (ppm); Coupling constants are in Hz.

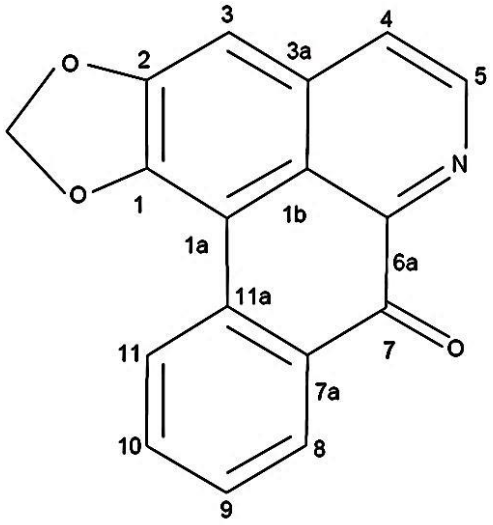

Figure 4.26: **Liriodenine (ETC-11)**

Table 4.12: ^{1}H and ^{13}C-NMR chemical shift values for (-)-N-formylanonaine (ETC-14) recorded in C5D5N (AVANCE NEO 400 MHz)

Position	^{1}H-NMR	^{13}C-NMR
1		143.6
1a		117.4
2		147.5
3	6.60 (s, 1H)	108.1
3a		127.4
4	2.60 (dd,1H, J=4.4, 12Hz;H4α), 3.01 (m,1H;H4β)	29.8
5	3.68 (dddd, 1H, J=4.4Hz;H5α), 3.37 (dd, 1H, J=4.4Hz;H5β)	41.81
6a	5.19 (dd, 1H, J=4.4, 14Hz)	49.53
7	3.15 (ddd, 1H, J=12.4Hz;H7α), 2.84 (dd,1H, J=4.4, 14Hz;H7β)	41.81
7a		135.2
8	7.28 (d, 1H, J=0.8Hz)	128.2
9	7.32 (m, 1H)	127.7
10	7.43 (m, 1H)	127.6
11	8.23 (d, 1H, J=8Hz)	127.5
11a		131.1
N-CHO	8.37 (s, 1H)	162.3
-OCH_2O-	6.11 and 6.02 (each d, 1H, J=1.2Hz)	101.5

Chemical shift values are in δ (ppm); Coupling constants are in Hz.

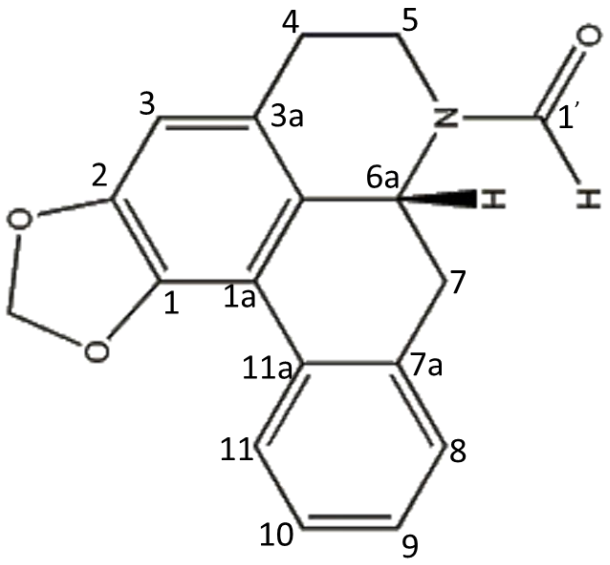

Figure 4.27: **(-)-N-formylanonaine (ETC-14)**

4.8.5 Compound ETC-20

Compound **ETC-20** was obtained as a crystal and also as a white amorphous powder from sub fraction EA-16 - EA-24 (pooled fractions 113-165) which yielded 8,161 mg. It has retardation factor ($\mathbf{R_f}$) value of 0.41 in solvent system *n*-hexane: ethyl acetate (8:2). It has melting point (**M.p):** 192.7^{o}C-196.7^{o}C, Mass (m/z): 358.3 g/mol [M+], **UV** (MeOH) λ/nm (log ε): 214.00 nm (A 0.245) (200- 600 nm) **IR (γ_{max} ^{KBr} cm-1):** 3503.5, 3127.6, 2970.4, 2936.6, 2875.6, 1746.9, 1703.3 1502.6, 1152.3, 1025.0, 913.4, 871.2, 791.9 and NMR data (Table 4.13). Molecular formula ($C_{20}H_{22}O_6$) and structure has been assigned to the substance named Columbin (Figure 4.28) based on the physical data and spectroscopic analysis (UV, IR, MS, ^{1}H-NMR and ^{13}C-NMR) and by comparison with reported literature (Rathnasamy *et al*., 2016).

4.8.6 Compound ETC-SF-25-7B

The chromatography yielded 279 fractions which were pooled together to 22 sub fractions (labeled as ETC-SF-25-1-ETC-SF-25-22). Compound **ETC-SF-25-7B** was obtained as a white powder isolated from sub fraction ETC-SF-25-7 (pooled fractions 73-89) with solvent system hexane: ethyl acetate (60:40) to yield 430 mg. It has retardation factor **($\mathbf{R_f}$)** value of 0.73 in solvent system hexane: ethyl acetate (4:6). Melting point (**M.p):**199.3^{o}C-202.1^{o}C, Mass (m/z): 374.2 g/mol [M+], **UV** (MeOH) λ/nm (log ε): 214.00 nm (A 0.163) (200- 600 nm) **IR (γ_{max} ^{KBr} cm-1):** 3549.8, 3451.6, 3397.0, 2944.5, 2888.2, 1756.5, 1707.3, 1506.1, 1159.3, 1031.9, 922.3, 807.3 and NMR data (Table 4.14). Molecular formula ($C_{20}H_{22}O_7$) and structure has been assigned to the substance named 8-hydroxycolumbin (Figure 4.29) based on the physical data and spectroscopic analysis (UV, IR, MS, ^{1}H-NMR and ^{13}C-NMR) and by comparison with reported literature (Oguakwa *et al*., 1986).

Table 4.13: ^{1}H and^{13}C-NMR chemical shift values for Columbin (ETC-20) recorded in CD3OD (AVANCE AV-400 MHz)

Position	^{1}H-NMR	^{13}C-NMR
1	5.28 (br d, 1H, J=4.8Hz)	75.53
2	6.53 (dd, 1H, J=5.2, 8 Hz)	131.45
3	6.25 (dd, 1H, J=1.6, 8 Hz)	137.02
4		82.09
5		36.25
6a	1.73 (dd, 1H, J=8, 14.8 Hz)	27.08
6b	1.44 (m, 1H)	27.08
*7a	2.56 (m, 2H)	18.48
7b	2.06 (m, 1H)	18.48
*8	2.56 (m,1H)	45.35
9		38.56
10	1.83 (br s, 1H)	47.96
11a	2.40/1.97 (dd, 1H, J=4.4, 14.8 Hz)	42.35
11b	1.97 (dd, 1H, J=12, 14.8 Hz)	42.35
12	5.57 (dd, 1H, J=4, 12 Hz)	72.78
13		126.72
14	7.59 (br s, 1H)	141.47
15	7.49 (br t, 1H, J=1.6, 3.2 Hz)	145.00
16	6.55 (br s, 1H)	109.68
17		176.77
18		177.26
19	0.99 (br s, 3H)	24.52
20	1.21 (br s, 3H)	28.14

*Overlapped protons, Chemical shift values are in δ (ppm); Coupling constants are in Hz.

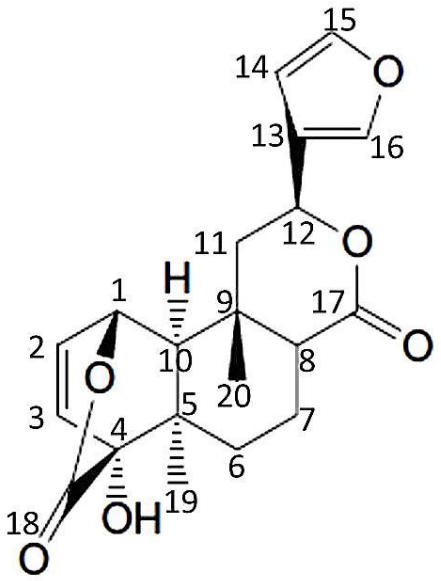

Figure 4.28: **Columbin (ETC-20)**

Table 4.14: ^{1}H-NMR (AVANCE-III-AV-400 MHz CD3OD) and ^{13}C-NMR (AVANCE NEO-300 MHz CD3OD) chemical shift values for 8-hydroxycolumbin (ETC-SF-25-7B)

Position	^{1}H-NMR	^{13}C-NMR
1	5.34 (d, 1H, J=4.8Hz)	75.29
2	6.56 (dd, 1H, J=5.2Hz)	131.50
3	6.26 (dd, 1H, J=1.6, 7.6Hz)	137.35
4		82.40
5		37.23
6	1.70 (m, 2H)	27.89
7a	1.59 (m, 1H)	27.89
7b	3.01 (m, 1H)	27.89
8		41.03
9		38.55
10	1.82 (br s, 1H)	48.42
11a	2.10 (dd, 1H, J=6.8, 15.6Hz)	37.24
11b	2.42 (dd, 1H, J=12, 14.8Hz)	37.24
12	5.56 (dd, 1H, J=5.6, 11.6Hz)	73.05
13		127.05
14	7.57 (br s, 1H)	141.41
15	7.49 (b t, 1H, J=1.6Hz)	145.00
16	6.53 (br s, 1H)	109.73
17		175.24
18		177.24
19	1.03 (br s, 3H)	20.68
20	1.16 (br s, 3H)	24.90

Chemical shift values are in δ (ppm); Coupling constants are in Hz.

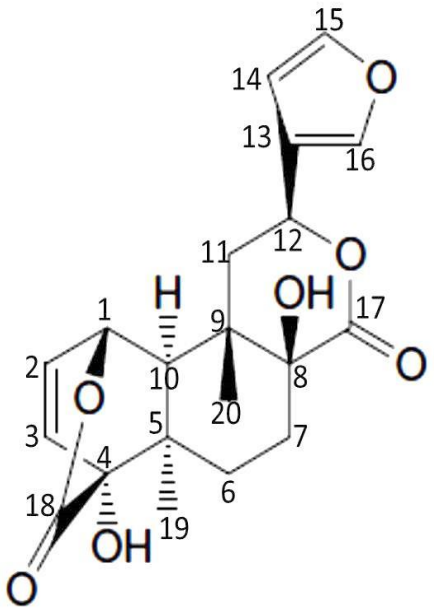

Figure 4.29: **8-hydroxycolumbin** (ETC-SF-25-7B)

4.8.7 Compound ETC-SF-25-8

Compound **ETC-SF-25-8** was isolated as a white crystalline solid (1,160 mg) from sub fraction ETC-SF-8 (pooled fractions 90-112) eluted with the solvent system hexane: ethyl acetate (55:45). It has retardation factor ($\mathbf{R_f}$) value of 0.73 in solvent system hexane: ethyl acetate (4:6). Melting point (**M.p):** 230.9^{o}C-254.6^{o}C, Mass (m/z): 374.2 g/mol [M+], **UV** (MeOH) λ/nm (log ε): 214.00 nm (A 0.208) (200- 600 nm) **IR (γ_{max} ^{KBr} cm-1):** 3510.3, 3144.2, 3083.1, 2972.4, 2937.4, 1762.2, 1705.9, 1503.5, 1458.8, 1387.3, 1203.8, 1158.3, 1063.1, 1025.3, 878.7 and NMR data (Table 4.15). Molecular formula **(**$C_{20}H_{22}O_7$) and structure has been assigned to the substance named Tinosporide (Figure 4.30) based on the physical data and spectroscopic analysis (UV, IR, MS, ^{1}H-NMR and ^{13}C-NMR) and by comparison with reported literature (Rathnasamy *et al*., 2016).

4.8.8 Compound ETC-SF-25-8B

Compound **ETC-SF-25-8B** was obtained as a white powder isolated from sub fraction ETC-SF-8 (pooled fractions 90-112) yielded 60 mg. It has retardation factor ($\mathbf{R_f}$) value of 0.73 in solvent system hexane: ethyl acetate (4:6). Melting point (**M.p):** 256.0^{o}C-261.2^{o}C, Mass (m/z): 390.3 g/mol [M+], **UV** (MeOH) λ/nm (log ε): 215.00 nm (A 0.313), 220.00 nm (A 0.319) (200- 600 nm) **IR (γ_{max} ^{KBr} cm-1):** 3486.1, 3150.6, 1754.1, 1716.6, 1507.4, 886.6 and NMR data (Table 4.16). Molecular formula ($C_{20}H_{22}O_8$) and structure has been assigned to the substance named Tinosporicide (Figure 4.31) based on the physical data and spectroscopic analysis (UV, IR, MS, ^{1}H-NMR and ^{13}C-NMR) and by comparison with reported literature (Sultan, 1992).

Table 4.15: ^{1}H-NMR (δ, AVANCE AV-500 MHz CD3OD) and ^{13}C-NMR (δ, AVANCE AV-600 MHz CD3OD) chemical shift values for Tinosporide (ETC-SF-25-8)

Position	^{1}H-NMR	^{13}C-NMR
1	4.97 (d, 1H, J=2.5Hz;H1)	72.3
2	3.86 (dd, 1H, J=3Hz;H2)	50.5
3	3.63 (d, 1H, J=4.00Hz;H3)	52.1
4		82.2
5		35.7
6		27.8
7a		17.7
7b		17.7
8	2.56 (m, 2H;H8)	44.8
9		41.9
10	2.06 (s, 2H;H10)	46.9
11a	2.34 (dd, 1H, J=4.0, 14.5Hz;H11a)	41.9
11b	1.94 (dd, 1H, J=12, 15Hz;H11b)	41.9
12	5.69 (dd, 1H, J=4, 12Hz;H12)	72.3
13		126.6
14	6.56 (d, 1H, J=1Hz;H14)	109.69
15	7.50 (t, 1H, J=1.5Hz;H15)	145.0
16	7.60 (s, 1H;H16)	141.0
17		176.7
18		174.0
19	1.21 (s, 3H;H19)	28.2
20	1.18 (s, 3H;H20)	23.3

Chemical shift values are in δ (ppm); Coupling constants are in Hz.

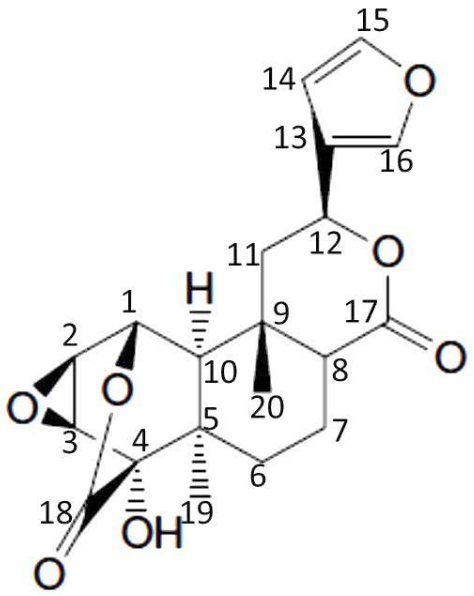

Figure 4.30: **Tinosporide** (ETC-SF-25-8)

Table 4.16: ^{1}H-NMR (AVANCE-III-AV-400 MHz CD3OD) and ^{13}C-NMR (AVANCE NEO-400 MHz CD3OD) chemical shift values for Tinosporicide (ETC-SF-25-8B)

Position	^{1}H-NMR	^{13}C-NMR
1	5.36 (d, 1H, J=2Hz)	71.09
2	4.00 (dd, 2H, J =4.4Hz)	50.45
3	3.43 (d, 1H, J =4.8Hz)	27.50
4		81.83
5		41.82
8	2.81 (dd, 1H, J=11.6, 14.4 Hz)	36.55
9		40.18
11a	2.30 (dd, 1H, J=5.6, 14.4 Hz)	36.55
11b	2.07-2.02 (m, 3H)	27.96
12	5.98 (dd, 1H, J=5.2, 11.2Hz)	71.48
13		126.68
14	6.68 (d, 1H, J=1.2Hz)	109.54
15	7.59 (d, 1H, J = 2Hz)	144.30
16	7.7 (br s,1H)	140.45
17	1.53 (br s, 3H)	21.23
18 (C=O)		174.47
19	1.64 (br s, 3H)	23.99
20 (C=O)		172.75

Chemical shift values are in δ (ppm); Coupling constants are in Hz.

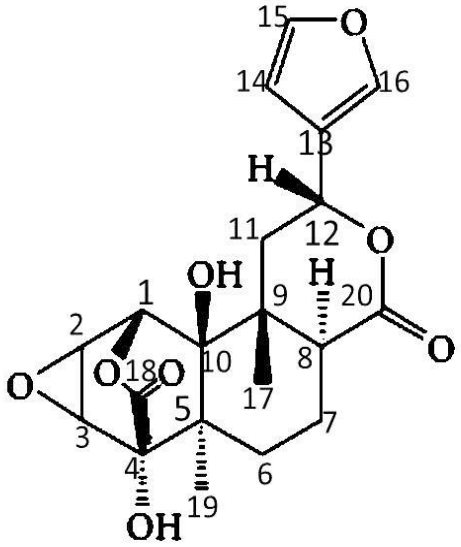

Figure 4.31: **Tinosporicide** (ETC-SF-25-8B)

4.8.9 Compound ETC-SF-25-9

The compound **ETC-SF-25-9** was isolated as a crystal from sub fraction ETC-SF-9 (pooled fractions 113-125) eluted with hexane: ethyl acetate (50:50) of ethyl acetate fraction which yielded 54 mg. It has retardation factor ($\mathbf{R_f}$) value of 0.25 in solvent system ethyl acetate: methanol (4:1). Melting point (M.p):183.3^{o}C-186.2^{o}C, LR EI-MS: m/z: 341.1 g/mol [M+]. The molecular ion peak for corydine is at m/z 341.1[M+]. **UV** (MeOH) λ/nm (log ε): 249.00 (2.42), 268 (2.72), 286 (2.69) nm (190-600 nm). IR (Liquid technique) cm^{-1}: 3951.9, 3877.7, 3464.6, 3202.6, 2942.1, 2833.8, 1592.8, 1462.2, 1425.4, 1369.8, 1319.8, 1285.2, 1239.5, 1135.8, 1102.5, 1075.0, 951.9, 808.3, 648.3 and NMR data (Table 4.17). Empirical formula ($C_{20}H_{23}NO_4$) and structure has been assigned to the substance named Corydine (Figure 4.32) based on the physical data and spectroscopic analysis (UV, IR, MS, ^{1}H-NMR and ^{13}C-NMR) and by comparison with reported literature (Singh and Chaudhuri, 2015).

4.8.10 Compound ETC-SF-25-19A

The compound **ETC-SF-25-19A** was isolated as an orange colour compound from the sub fraction ETC-SF-19 (pooled fractions 228-239) of ethyl acetate fraction eluted as a deep yellow eluate with eluent ethyl acetate (100%) yielded 25 mg. It has retardation factor **($\mathbf{R_f}$)** value of 0.3 in solvent system hexane: ethyl acetate: methanol (1.5:8.5:1.5). Melting point (M.p):226.5^{o}C-230.7^{o}C, LR EI-MS: m/z: 351.0 [M+]. **UV** (MeOH) λ/nm (log ε): 221.00 nm (A 0.915), 244.00 nm (A 1.378), 273.00 nm (A 1.454) (190- 600 nm). **IR (γ_{max} KBr cm-1):** 3926.7, 3840.4, 3434.7, 2932.9, 2833.6, 1645.9, 1594.1, 1509.5, 1459.6, 1358.5, 1238.6, 1142.6, 881.4 and NMR data (Table 4.18). Molecular formular ($C_{20}H_{17}NO_5$) and structure has been assigned to the substance named Oxoglaucine (Figure 4.33) based on the physical data and spectroscopic analysis (UV, IR, MS, ^{1}H-NMR and ^{13}C-NMR) and by comparison with reported literature (Ohiri *et al*., 1982).

Table 4.17: ^{1}H and ^{13}C-NMR chemical shift values for corydine (ETC-SF-25-9) recorded in CD3OD (AVANCE NEO 400 MHz)

Position	^{1}H-NMR	^{13}C-NMR
1		143.7
1a		121
2		150.5
3	6.85 (1H, s)	112.61
3a		126.7
4		29.65
5		53.7
6a		62.37
7		36.35
7a		131.1
8	6.88 (d, 2H, J = 9.6 Hz)	112.61
9	6.93 (d, 1H, J = 8 Hz)	112.89
10		153.1
11		144.7
11a		129.4
N-CH_3	2.52 (s, 3H)	43.89
2-OCH_3	3.85 (s, 3H)	56.71
10-OCH_3	3.88 (s, 3H)	56.71
11-OCH_3	3.64 (s, 3H)	62.37

Chemical shift values are in δ (ppm); Coupling constants are in Hz.

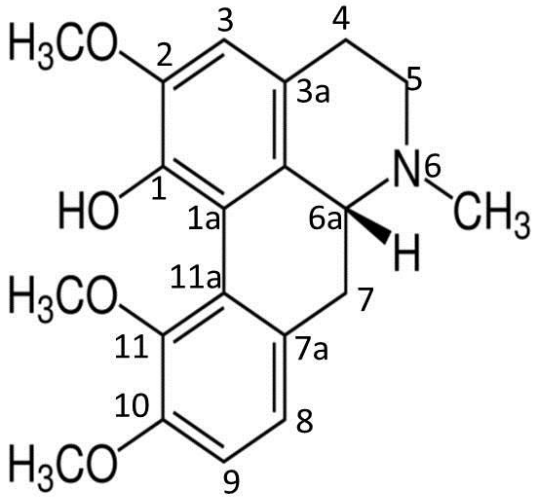

Figure 4.32: **Corydine** (ETC-SF-25-9)

Table 4.18: ^{1}H (AVANCE-III AV-400 MHz) and ^{13}C-NMR (AVANCE NEO 400 MHz) chemical shift values for oxoglaucine (ETC-SF-25-19A) recorded in CD3OD

Position	^{1}H-NMR	^{13}C-NMR
1		155.6
1a		122.5
2		158.6
3	7.42 (s, 1H)	107.8
4	7.93 (d, 1H, J=5.2Hz)	125.5
5	8.692 (d,1H, J=5.2 Hz)	144.9
6a		145.6
7		182.3
7a		137.3
8	8.705 (s, 1H)	111.6
9		150.9
10		155.6
11	7.82 (s,1H)	110.3
11a		127.3
1-OCH_3	4.03 (s, 3H)	61.09
2-OCH_3	4.09 (s, 3H)	56.85
9-OCH_3	3.97 (s, 3H)	56.31
10-OCH_3	4.02 (s, 3H)	56.52

Chemical shift values are in δ (ppm); Coupling constants are in Hz.

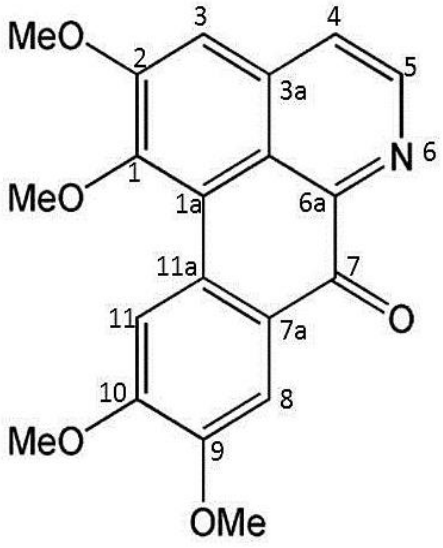

Figure 4.33: **Oxoglaucine** (ETC-SF-25-19A)

4.8.11 Characterisation of compound ETC-SF-26-4

The chromatography yielded 78 fractions which were pooled together to 7 sub fractions (labeled as EA-26-1- EA-26-7). The eluent 100% ethyl acetate eluted light yellow eluates EA-26-4 (pooled fractions 32-43) which contain a white armourphous solid known as compound **ETC-SF-26-4** (60 mg) soluble in pyridine. It has retardation factor ($\mathbf{R_f}$) value of 0.8 in solvent system methanol: ethyl acetate (3:4). Melting point (**M.p):** 144.1^{o}C-145.2^{o}C, Mass (m/z): 653.2 g/mol [M+]. **IR (γ_{max} ^{KBr} cm-1):** 3816.0, 3424.0, 2920.0, 2850.0, 1618.7, 1551.9, 1468.0, 1072.5, 721.1 and NMR data (Table 4.19). Molecular formula ($C_{40}H_{78}NO_5$) and structure has been assigned to the substance named re l - (2 S , 3 S , 4R, 1 6E) - 2 - [(2 'R) - 2 ' - hydroxy nonadecanoylamino]-heneicosadec-16-ene-1,3,4-triol (Figure 4.34) based on the physical data and spectroscopic analysis (UV, IR, MS, ^{1}H-NMR and ^{13}C-NMR) and by comparison with reported literature (Maia *et al*., 2010).

4.8.12 Compound MTC-8

The chromatography yielded 168 fractions which were pooled together to 17 sub fractions (labeled as MTC-F1- MTC-F17). The eluent 100% ethyl acetate eluted golden yellow eluate with white powder known as compound **MTC-8** (25 mg) from sub fraction MTC-F8 (pooled fractions 69-85)**.** It has retardation factor **($\mathbf{R_f}$)** value of 0.84 in solvent system ethyl acetate: methanol (1:1). Melting point **(M.p):** 295.5^{o}C-303.7^{o}C, its low resolution electron impact **(EI)** mass spectrum showed the existence of a sterol skeleton and a molecular ion peak at m/z 414 [M+]. The exact mass was detected on FAB on the positive mode, Mass (m/z): 577.85 g/mol [M+], **IR (γ_{max} ^{KBr} cm-1):** 3386.2, 2959.3, 2931.1, 2873.0, 1647.5, 1463.7, 1374.7, 1070.3, 1024.5, 668.2 and NMR data (Table 4.20). Molecular formula ($C_{35}H_{60}O_6$) and structure has been assigned to the substance named Daucosterol (Figure 4.35) based on the physical data and spectroscopic analysis (UV, IR, MS, ^{1}H-NMR and ^{13}C-NMR) and by comparison with reported literature (Flamini *et al*., 2001).

Table 4.19: ^{1}H and ^{13}C-NMR chemical shift values for re l - (2 S , 3 S , 4R, 1 6E) - 2 - [(2 ’R) - 2 ’ - h y d ro x y nonadecanoylamino]-heneicosadec-16-ene-1,3,4-triol (ETC-SF-26-4) recorded in C5D5N (AVANCE-III AV-400 MHz)

Position	^{1}H-NMR	^{13}C-NMR
1	4.53 (dd, 1H, J=6.4Hz), 4.44 (dd, 1H, J=4.8Hz)	62.06
2	5.12 (m, 1H)	53.00
3	4.37 (dd,1H, J=6Hz)	76.81
4	4.29 (d,1H,J=6.4Hz)	73.03
5	2.26 (m,1H), 1.96 (m,1H)	34.17
6	1.75 (m, 3H)	26.66
7-14	1.24 -1.42	30.01-30.34
15	2.03 (m, 1H)	32.13[a]
16	5.64 (td, J=15.4Hz; 5.4Hz)	131.30[b]
17	5.52 (td, J=15.4Hz; 5.8Hz)	131.11[b]
18	2.03 (m)	34.17
19	1.24 -1.42	32.13
20	1.24 -1.42	22.94
21	0.85 (dd, 5H, J=4.8Hz, 5.2Hz)	14.24
1’		175.23
2’	4.62 (m, 1H)	72.48
3’	2.22 (m), 2.03 (m)	35.73
4’	1.24 -1.42	26.66
5-16’	1.24 -1.42	30.01-30.34
17’	1.24 -1.42(m)	32.13
18’	1.24 -1.42(m)	22.94
19’	0.85 (dd, 5H, J=4.8Hz, 5.2Hz)	14.24
N-H	8.59 (d, 1H, J=9.2Hz)	150.24
HO-1	6.70 (d, 2H, J=6.4Hz)	-
HO-3	6.70 (d, 2H, J=6.4Hz)	-
HO-4	6.22 (d, 1H, J=6.4Hz)	-
HO-2’	7.63 (d, 1H, J=5.2Hz)	135.80

Chemical shift values are in δ (ppm); Coupling constants are in Hz.

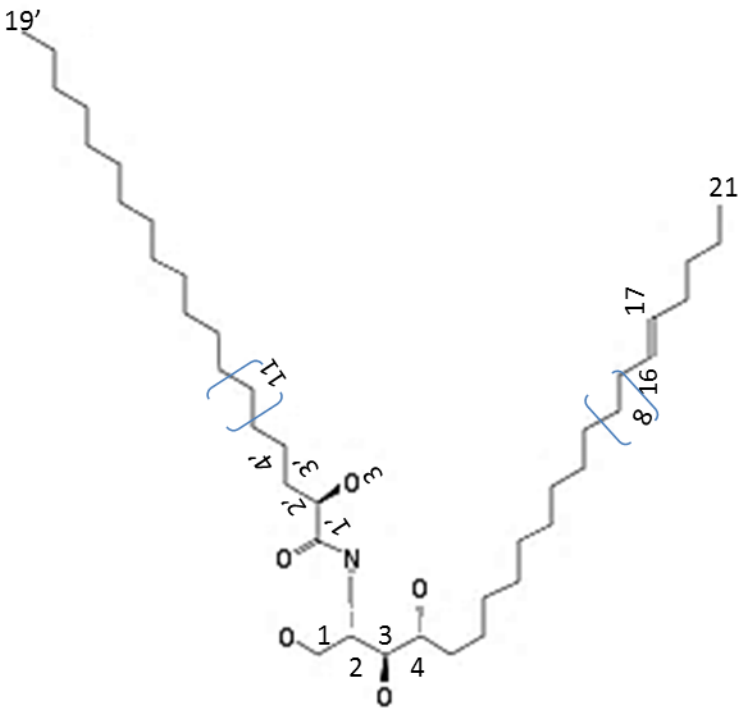

Figure 4.34: **re l - (2 S , 3 S , 4R, 1 6E) - 2 - [(2 ’R) - 2 ’ - h y d ro x y nonadecanoylamino]-heneicosadec-16-ene-1,3,4-triol (ETC-SF-26-4)**

Table 4.20: ^{1}H and ^{13}C-NMR chemical shift values for daucosterol (MTC-8) recorded in C5D5N (AVANCE NEO 400 MHz)

Position	^{1}H-NMR	^{13}C-NMR
1		37.51
2		30.28
3		78.64
4		37.51
5		140.94
6	5.34 (br d, 1H, J=4Hz)	121.93
7		32.08
8		32.19
9		50.38
10		36.95
11		21.30
12		39.98
13		46.08
14		56.85
15		24.53
16		29.50
17		56.28
18	0.66 (br d, 3H, J=6Hz)	12.18
19	0.98 (s, 3H)	19.44
20		36.41
21		19.44
22		32.19
23		24.53
24		46.08
25		29.50
26		19.99
27		21.30
28		23.42
29		12.18
1’	5.06 (d, 1H, J=7.6Hz)	102.6
2’		75.37
3’	4.06 (t, 1H, J=8Hz, 8Hz)	78.64
4’	4.58 (d, 1H, J=10.4Hz)	71.74
5’	3.98 (m, 2H)	78.64
6’	4.28 (t, 2H, J=4.8Hz, 4.4Hz)	62.88

Chemical shift values are in δ (ppm); Coupling constants are in Hz.

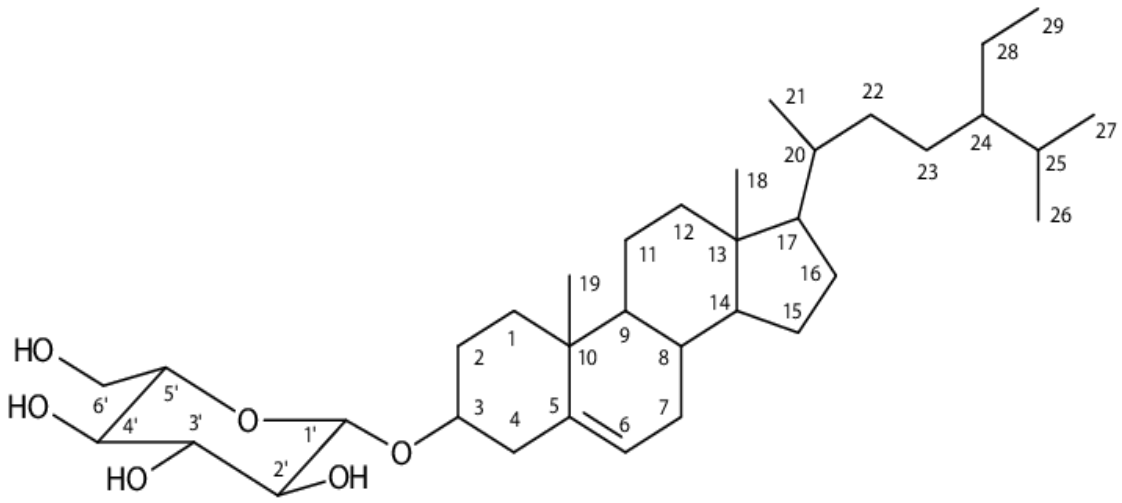

Figure 4.35: **Daucosterol** (MTC-8)

4.8.13 Compound MTC-14A

Sub fraction MTC-F13 (pooled fractions 116-127) and MTC-F14 (pooled fractions 128-140) eluted with solvent system ethyl acetate: methanol (400:100 to 350:150) yielded compound **MTC-14A** as a yellow powder from aqueous methanol fraction (280 mg). It has retardation factor ($\mathbf{R_f}$) value of 0.25 solvent system ethyl acetate: methanol (4:6). Melting point (**M.p):** 228.5^{o}C-231.7^{o}C, **EI-MS** m/z 351.2 g/mol [M]+ (calcd for $C_{21}H_{22}NO_4$ $^{+}$ 352.1543); **UV** (MeOH) λ/nm (log ε): 220.00 nm (A 0.365), 275 nm (A 0.712), 346.00 nm (A 0.947) (start wavelength 190-stop wavelength 600 nm) **IR (γ_{max} ^{KBr} cm-1):**3421.1, 2949.5, 2847.5, 1606.2, 1517.1, 1379.9, 1275.7, 1242.8, 1142.9, 1109.4, 1020.4, 814.3 and NMR data (Table 4.21). Empirical formula ($C_{21}H_{22}NO_4$) and structure has been assigned to the substance Palmatine (Figure 4.36) based on the physical data and spectroscopic analysis (UV, IR, MS, ^{1}H-NMR and ^{13}C-NMR) and by comparison with reported literature (Ling-Ling *et al*., 2014).

4.9 Characterisation of compounds isolated from *Cola hispida* seed

4.9.1 Compound DCH-14

The chromatography yielded 151 fractions which were pooled together to 20 sub fractions (labeled as DCH-F1- DCH-F20). Compound **DCH-14** was obtained as a white powder from dichloromethane fraction (sub fraction DCH-F14 (pooled fractions 97-103) with eluent ethyl acetate 100% which yielded 20 mg. It has retardation factor **($\mathbf{R_f}$)** value of 0.84 in solvent system ethyl acetate: methanol (1:1), Melting point **(M.p):** 295.5^{o}C-303.7^{o}C, its low resolution electron impact **(EI)** mass spectrum showed the existence of a sterol skeleton and a molecular ion peak at m/z 414 [M+]. The exact mass was detected on FAB on the positive mode, Mass (m/z): 577.85 g/mol [M+], **IR (γ_{max} ^{KBr} cm-1):** 3386.2, 2959.3, 2931.1, 2873.0, 1647.5, 1463.7, 1374.7, 1070.3, 1024.5, 668.2 and NMR data (Table 4.22). Molecular formula ($C_{35}H_{60}O_6$) and structure has been assigned to the substance named Daucosterol (Figure 4.37) based on the physical data and spectroscopic analysis (UV, IR, MS, ^{1}H-NMR and ^{13}C-NMR) and by comparison with reported literature (Flamini *et al*., 2001).

Table 4.21: ^{1}H and ^{13}C-NMR chemical shift values for palmatine (MTC-14A) recorded in CD3OD (AVANCE NEO 400 MHz)

Position	^{1}H-NMR	^{13}C-NMR
1	7.66 (1H, s, H-1)	109.9
2		153.8
3		150.9
4	7.04 (1H, s, H-4)	112.2
4a		128.10
5	3.29 (2H, t, J = 6.0 Hz, H-5)	27.8
6	4.93 (2H, t, J = 8.0 Hz, H-6)	56.6
8	9.75 (1H, s, H-8)	146.4
8a		121.2
9		139.8
10		151.9
11	8.10 (1H, d, J = 9.2 Hz, H-11)	128.1
12	7.99 (1H, d, J = 9.2 Hz, H-12)	124.4
12a		130.1
13	8.79 (1H, s, H-13)	121.2
13a		135.3
13b		120.5
2-OCH_3	3.93 (3H, s, 2-OCH3)	56.9
3-OCH_3	3.98 (3H, s, 3-OCH3)	57.3
9-OCH_3	4.10 (3H, s, 9-OCH3)	57.6
10-OCH_3	4.20 (3H, s, 10-OCH3)	62.5

Chemical shift values are in δ (ppm); Coupling constants are in Hz.

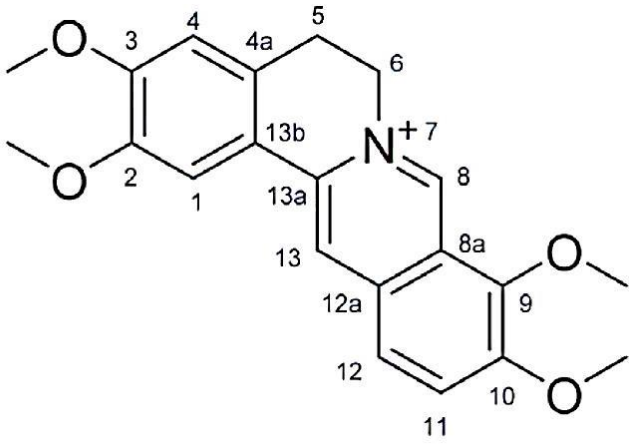

Figure 4.36: **Palmatine (MTC-14A)**

Table 4.22: ^{1}H and ^{13}C-NMR chemical shift values for daucosterol (DCH-14) recorded in C5D5N (AVANCE NEO 400 MHz)

Position	^{1}H-NMR	^{13}C-NMR
1		37.51
2		30.28
3		78.64
4		37.51
5		140.94
6	5.34 (br d, 1H, J=4Hz)	121.93
7		32.08
8		32.19
9		50.38
10		36.95
11		21.30
12		39.98
13		46.08
14		56.85
15		24.53
16		29.50
17		56.28
18	0.66 (br d, 3H, J=6Hz)	12.18
19	0.98 (s, 3H)	19.44
20		36.41
21		19.44
22		32.19
23		24.53
24		46.08
25		29.50
26		19.99
27		21.30
28		23.42
29		12.18
1’	5.06 (d, 1H, J=7.6Hz)	102.6
2’		75.37
3’	4.06 (t, 1H, J=8Hz, 8Hz)	78.64
4’	4.58 (d, 1H, J=10.4Hz)	71.74
5’	3.98 (m, 2H)	78.64
6’	4.28 (t, 2H, J=4.8Hz, 4.4Hz)	62.88

Chemical shift values are in δ (ppm); Coupling constants are in Hz.

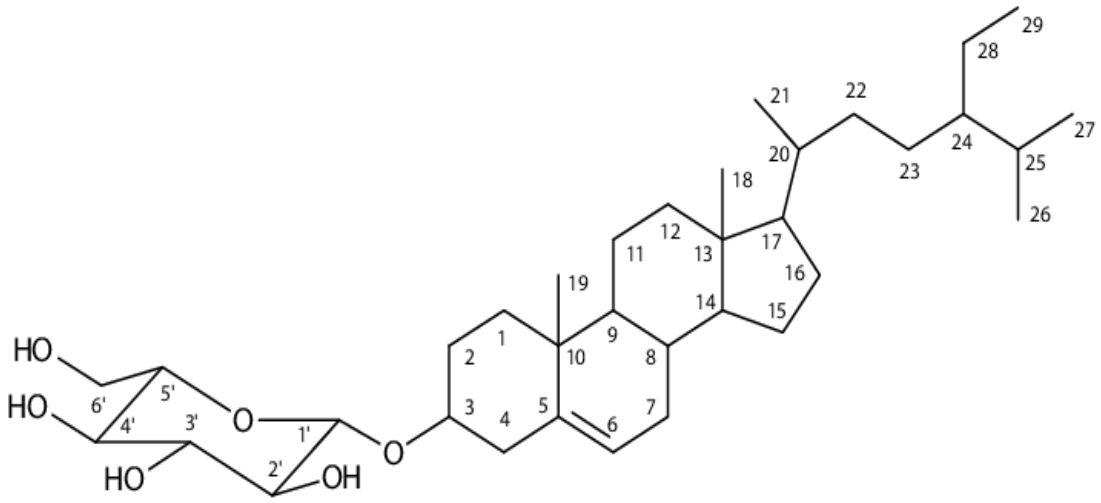

Figure 4.37: **Daucosterol** (DCH-14)

4.9.2 Compound ECH-6A

The chromatography yielded 389 fractions which were pooled together to 20 sub fractions (labeled as ECH-F1- ECH-F20). The compound **ECH-6A** was obtained as a white powder from ethyl acetate fraction (sub fraction ECH-F6 (pooled fractions 48-62) in solvent system hexane: dichloromethane (1:7) yielded 23 mg. It has retardation factor ($\mathbf{R_f}$) value of 0.6 in solvent system hexane: chloroform: ethyl acetate (4:1:1.5). Melting point (M.p): 134.4^{o}C-135.1^{o}C, Mass (m/z): 414.3 g/mol [M+]. **UV** (MeOH) λ/nm (log ε): 219.00 nm (A 0.627), 270.00 nm (A 1.404) (190-600 nm) **IR (γ_{max} ^{KBr} cm-1):** 3446.3, 2936.5, 1642.3, 1462.4, 1376.6, 1058.6, 961.7, 591.7 and NMR data (Table 4.23). Molecular formula ($C_{29}H_{50}O$) and structure has been assigned to the substance named β-Sitosterol (Figure 4.38) based on the physical data and spectroscopic analysis (UV, IR, MS, ^{1}H-NMR and ^{13}C-NMR) and by comparison with reported literature (Wright *et al*., 1978).

4.9.3 Compound ECH-9I

Compound **ECH-9I** was was obtained as oil, isolated from ethyl acetate fraction (Sub fraction ECH-F9 (pooled fractions 96-116) which yielded 125 mg with solvent system hexane: dichloromethane (1:9). It has retardation factor ($\mathbf{R_f}$) value of 0.65 in solvent system hexane: ethyl acetate (3:7). Melting point **(M.p)**: 112.5^{o}C-113.2^{o}C, Mass (m/z): 126.1 g/mol [M+], **UV** (MeOH) λ/nm (log ε): 229.00 nm (A 1.659), 262.00 nm (A 2.527), 271.00 nm (A 2.553), **IR** (γ_{max} ^{NEAT} cm^{-1}): 3389.7, 2930.5, 2846.2, 1678.5, 1522.9, 1398.9, 1281.4, 1192.8, 1023.6, 812.6, 776.8, 616.7 and NMR data (Table 4.24). Molecular formula ($C_6H_6O_3$) and structure has been assigned to the substance 5-hydroxymethylfurfural (Figure 4.39) based on the physical data and spectroscopic analysis (UV, IR, MS, ^{1}H-NMR and ^{13}C-NMR) and by comparison with reported literature (Prasenjit and Paresh, 2013).

Table 4.23: ^{1}H and ^{13}C-NMR chemical shift values for β-Sitosterol (ECH-6A) recorded in CDCL3 (AVANCE NEO 400 MHz)

Position	^{1}H-NMR	^{13}C-NMR
1		37.26
2		31.91
3	3.50 (m,1H)	71.81
4		42.31
5		138.3
6	5.32 (br d, 1H, J=5.2Hz)	121.7
7		31.88
8		31.91
9		50.14
10		36.14
11		21.21
12		39.78
13		42.31
14		56.87
15		24.30
16		28.91
17		56.07
18	0.66 (br s, 3H)	11.98
19	0.98 (br s, 3H)	19.39
20		36.14
21	0.89	18.78
22		33.96
23		26.10
24		45.85
25		29.17
26	0.80	21.07
27		19.81
28		23.07
29	0.84	12.23

Chemical shift values are in δ (ppm); Coupling constants are in Hz.

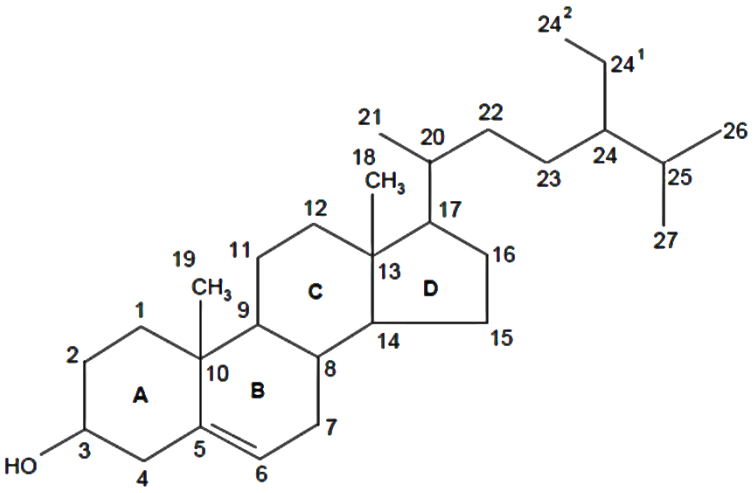

Figure 4.38: **β-Sitosterol** (ECH-6A)

Table 4.24: ^{1}H-NMR (AVANCE-III-AV-400 MHz) and ^{13}C-NMR (AVANCE NEO 300 MHz) chemical shift values for 5-Hydroxymethylfurfural (ECH-9I) recorded in CD3OD

^{1}H-NMR	^{13}C-NMR	HMBC
9.51 (s, 1H, CHO, H-2)	179.43	57.57, 124.89, 163.11
7.37 (d, 1H, J = 3.6 Hz, H-3)	124.89	110.88, 153.76, 163.11, 179.43
6.57 (d, 1H, J = 3.6 Hz, H-4)	110.88	57.57, 124.89, 153.76, 163.11, 179.43
4.60 (s, 3H, CH_2OH, H-5)	57.57	110.88, 124.89, 153.76, 163.11

Chemical shift values are in δ (ppm); Coupling constants are in Hz.

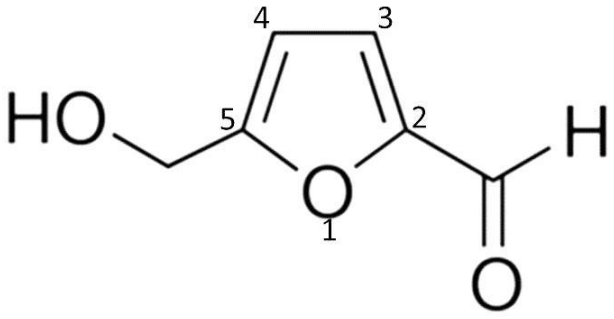

Figure 4.39: **5-Hydroxymethylfurfural** (ECH-9I)

4.9.4 Compound ECH-12

Compound **ECH-12** was obtained as a white powder isolated from ethyl acetate fraction (Sub fraction ECH-F12 (pooled fractions 138-195)) yielded 31 mg with solvent system dichloromethane: methanol (98:2) soluble in pyridine. It has retardation factor **(R_f)** value of 0.93 in solvent system methanol: water (3:2), Mass (m/z): 189.1 g/mol [M+]. **IR (γ_{max} ^{KBr} cm-1):** 3415.4, 3108.8, 2965.1, 2842.2, 2757.9, 1680.0, 1590.1, 1385.7, 1346.0, 1311.4, 827.5 and NMR data (Table 4.25). Molecular formula ($C_{10}H_7NO_3$) and structure has been assigned to the substance 2-hydroxyquinoline-4-carboxylic acid (Figure 4.40) based on the physical data and spectroscopic analysis (UV, IR, MS, ^{1}H-NMR and ^{13}C-NMR) and by comparison with reported literature (Zhiwei *et al*., 2017).

4.10: Biological activities of isolated compounds

4.10.1: Acetylcholinesterase inhibitory activity of isolated compounds

Oxoglaucine (Oxoaporphinoid alkaloid) isolated from ethyl acetate fraction of *Tinospora cordifolia* stem exhibited the highest AChE inhibitory activity (IC_{50} of 0.803±0.09 mg/mL) compared to eserine (IC_{50} = 0.531±0.34 mg/mL). Also, other alkaloids like palmatine ((IC_{50} = 0.837±0.07mg/mL), liriodenine (IC_{50} = 0.807±0.07 mg/mL), N-formylanonaine (IC_{50} = 0.819±0.06 mg/mL) showed good acetylcholinesterase inhibitory potentials (Figure 4.41).

4.10.1.1: Molecular docking study of compounds on acetylcholinesterase residue

Molecular docking revealed hydrophobic, hydrogen bonding and π -stacking interactions among tested compounds and the active site of AChE, which justified their high inhibitory potentials (Figure 4.42-4.54).

Table 4.25: ^{1}H-NMR (AVANCE AV-400 MHz) and ^{13}C-NMR (AV-III-HD 800 MHz Cryo-Probe) chemical shift values for 2-Hydroxyquinoline-4-carboxylic acid (ECH-12) recorded in C5D5N

^{1}H-NMR	**^{13}C-NMR**	**HMBC**
8.82 (1H, d, J = 8.1Hz, H-5)	127.73	130.85, 140.78, 150.09
7.67 (1H, s, H-2)	124.88	117.60, 169.05
7.55–7.48 (2H, m, H6-7)	115.95, 130.85	117.60, 122.32, 127.73, 124.88, 140.78, 149.98
7.25–7.21 (1H, m, H-8)	122.32	115.95, 117.60
13.27 (1H, br.s, COOH, H-11)	169.05	-

Chemical shift values are in δ (ppm); Coupling constants are in Hz.

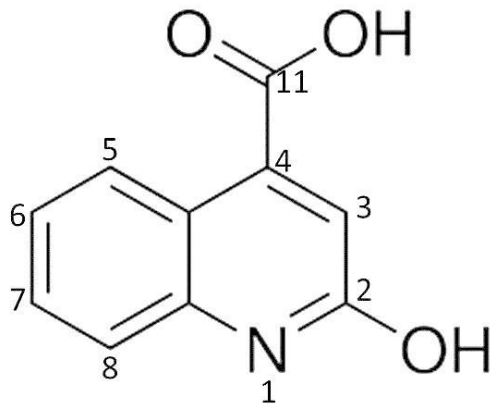

Figure 4.40: **2-Hydroxyquinoline-4-carboxylic acid** (ECH-12)

4.10.2: Prolyl endopeptidase inhibitory activity

The compound stigmasterol isolated from dichloromethane fraction of *Phyllanthus muellerianus* leaf demonstrated the highest PEP inhibitory activity (IC_{50} = 0.773±2.9 mM, 68% inhibition) compared to bacitracin (IC_{50} = 0.125±1.5 Mm, 99% inhibition) followed by oxoglaucine an oxoaporphine alkaloid from *Tinospora cordifolia* (IC_{50} = 0.780±3.1Mm, 65% inhibition) and corydine (IC_{50} = 0.788±3.1Mm, 60.3% inhibition) (Figure 4.55).

4.10.2.1: Molecular docking studies of active compounds on prolyl endopeptidase residue

In the molecular docking, figure 4.56 depicts the comparison of the crystal (cyan) and the simulated pose (magenta) of cognate ligand from PDB: 3IVM. The top ranked conformation of stigmasterol and oxoglaucine with the PEP enzyme shows hydrophobic interactions with Tyr458, Tyr483, Ala561, Val562, and Ile673 as well as hydrogen bonds interactions, respectively stabilizing the ligands in the binding pocket of enzyme which justify its activity (Figure 4.57-4.59).

4.10.3: Metal chelating activity of isolated compounds

Oxoglaucine also showed good metal chelating potential with IC_{50} of 0.216±0.00 mg/mL alongside stigmasterol and 5-hydroxymethylfurfural which had IC_{50} of 0.283±0.00 mg/mL and 0.295±0.01 mg/mL at 1 mg respectively compared to standard EDTA with IC_{50} of 0.045±0.11 mg/mL (Figure 4.60). The tested compounds demonstrated the abilities to lower brain metal ions and targeting Aβ/metal ions interactions which might offer a large potential to chelation therapy.

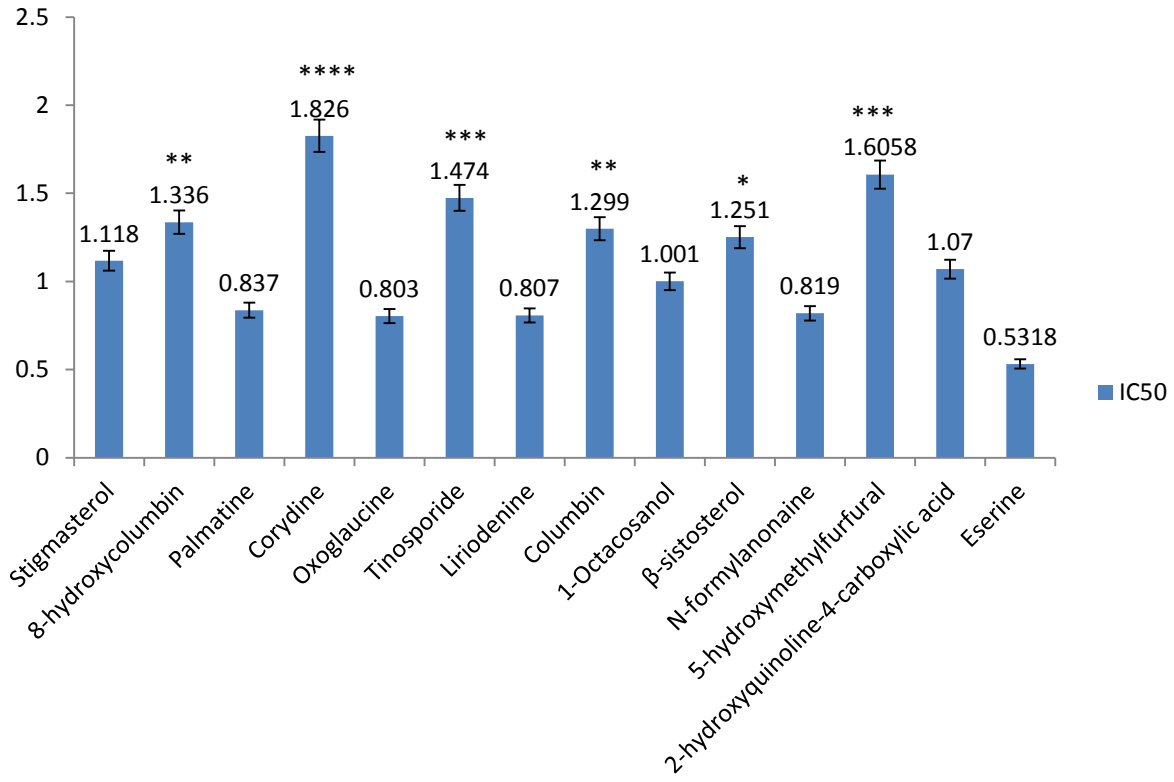

Figure 4.41: Acetylcholinesterase inhibitory activity of compounds isolated from *Phyllanthus muellerianus* leaf, *Tinospora cordifolia* stem and *Cola hispida* seed at 1 mg/mL (IC_{50}±SD (mg/mL)

Values are presented as mean ± standard deviation (n=3).

Comparison of each compounds with standard (Eserine) was done and level of significant difference represented with *, **, *** and ****. Extracts with no asterisks are not significantly (NS) different from the standard

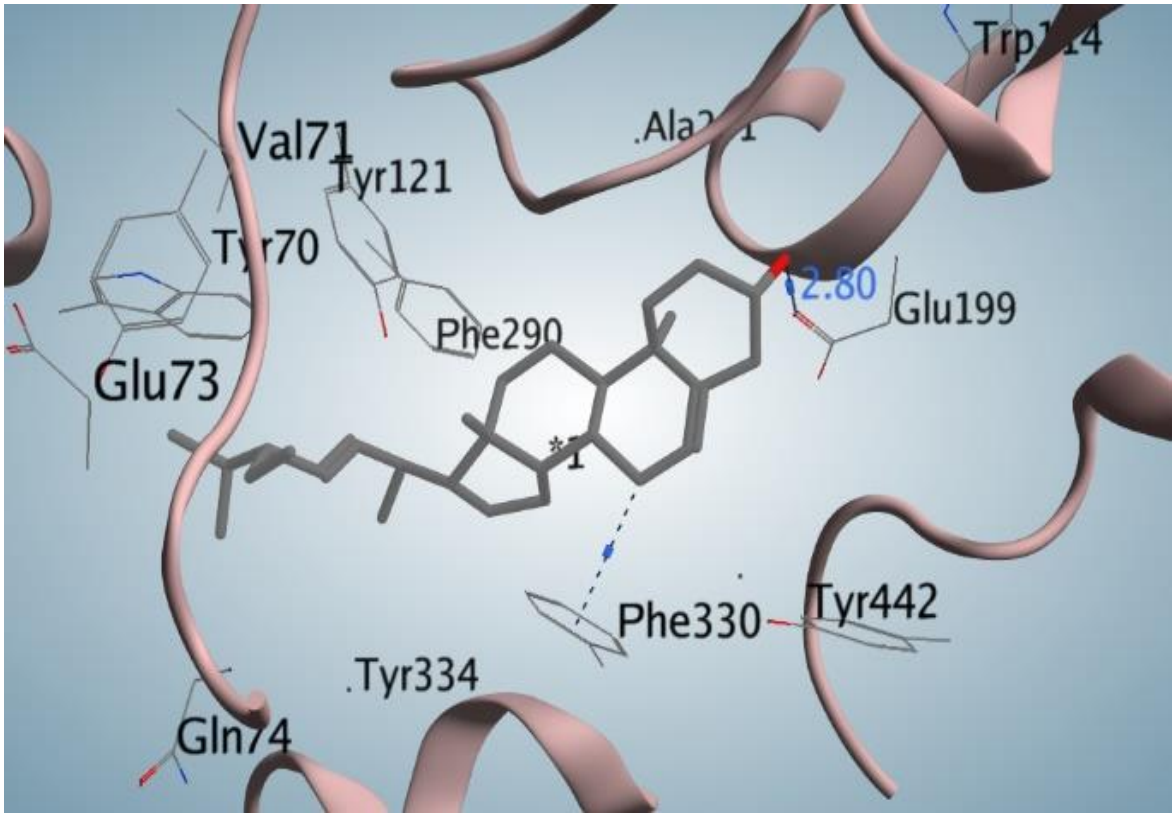

Figure 4.42. The simulated poses of the compound Stigmasterol. Hydrogen bonds are presented in blue lines. Grey sticks show the ligand while the acetylcholinesterase residues are shown as pink ribbons. The images were rendered using MOE 2015.01.08.

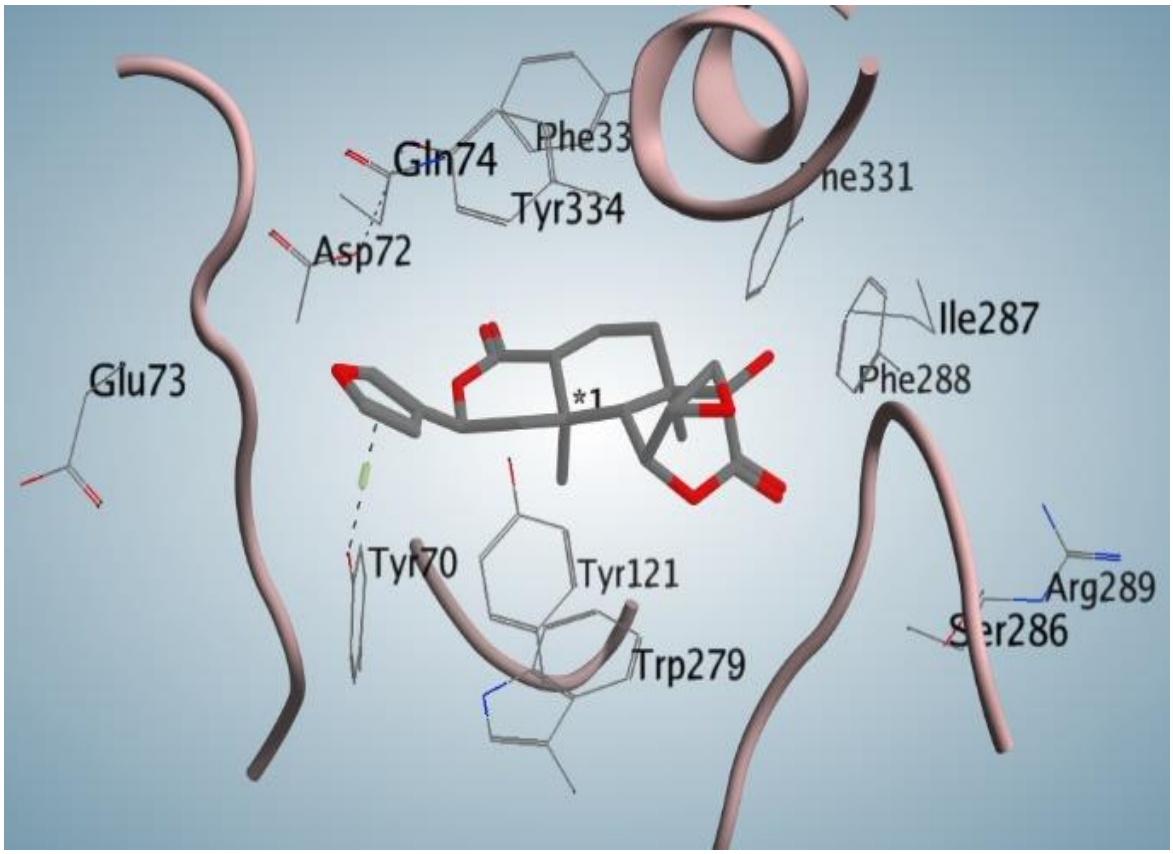

Figure 4.43. The simulated poses of the compound 8-Hydroxycolumbin. Hydrogen bonds are presented in blue lines. Grey sticks show the ligand while the acetylcholinesterase residues are shown as pink ribbons. The images were rendered using MOE 2015.01.08.

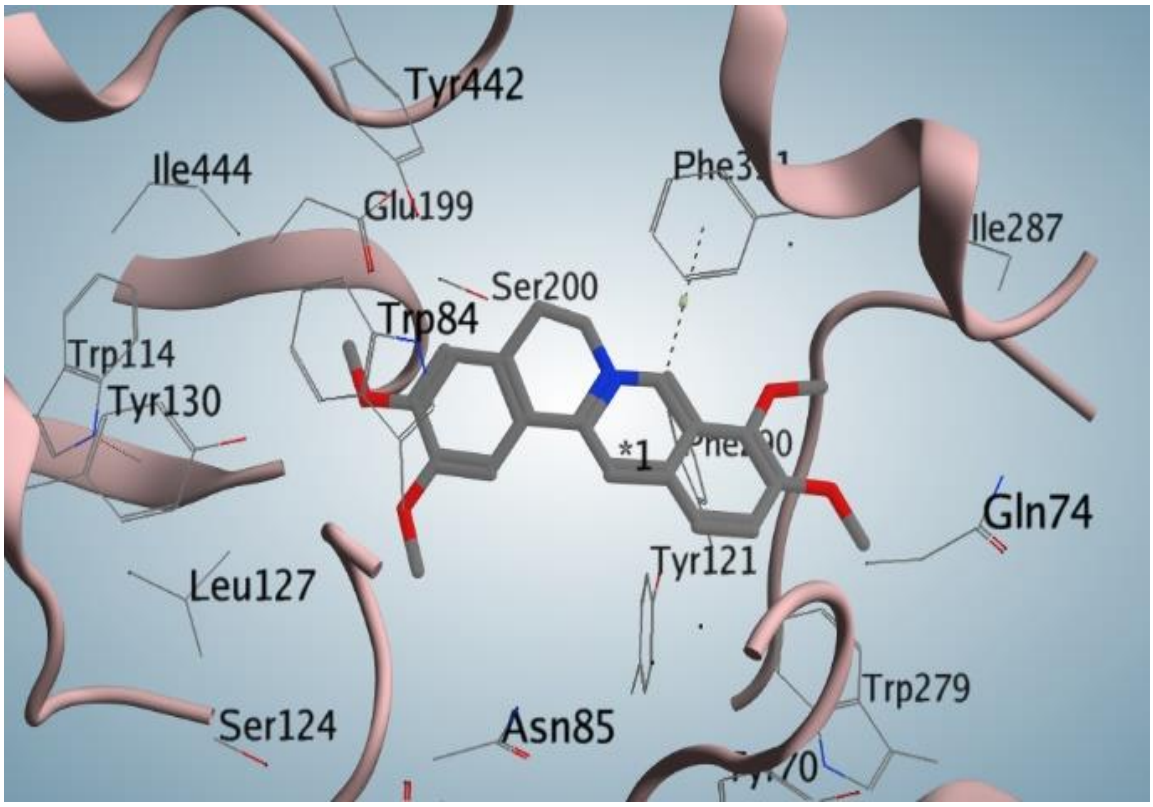

Figure 4.44. The simulated poses of the compound Palmatine. Hydrogen bonds are presented in blue lines. Grey sticks show the ligand while the acetylcholinesterase residues are shown as pink ribbons. The images were rendered using MOE 2015.01.08.

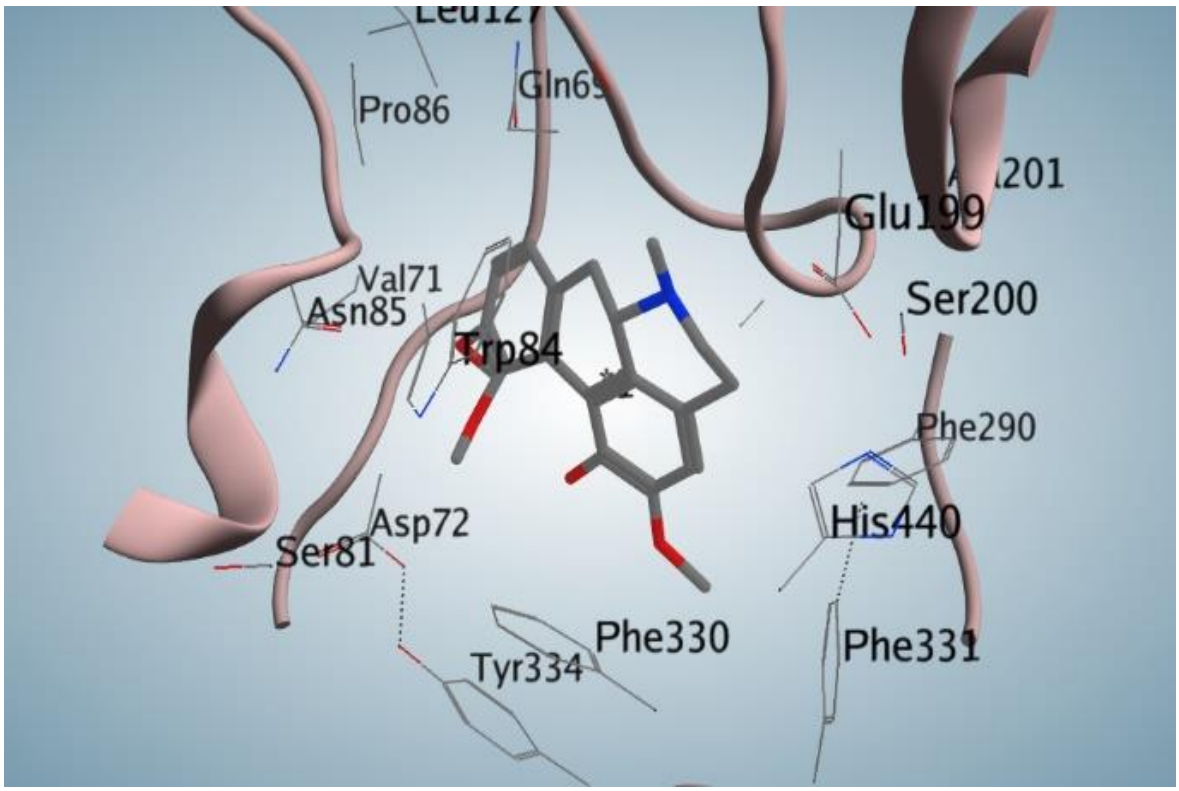

Figure 4.45. The simulated poses of the compound Corydine. Hydrogen bonds are presented in blue lines. Grey sticks show the ligand while the acetylcholinesterase residues are shown as pink ribbons. The images were rendered using MOE 2015.01.08.

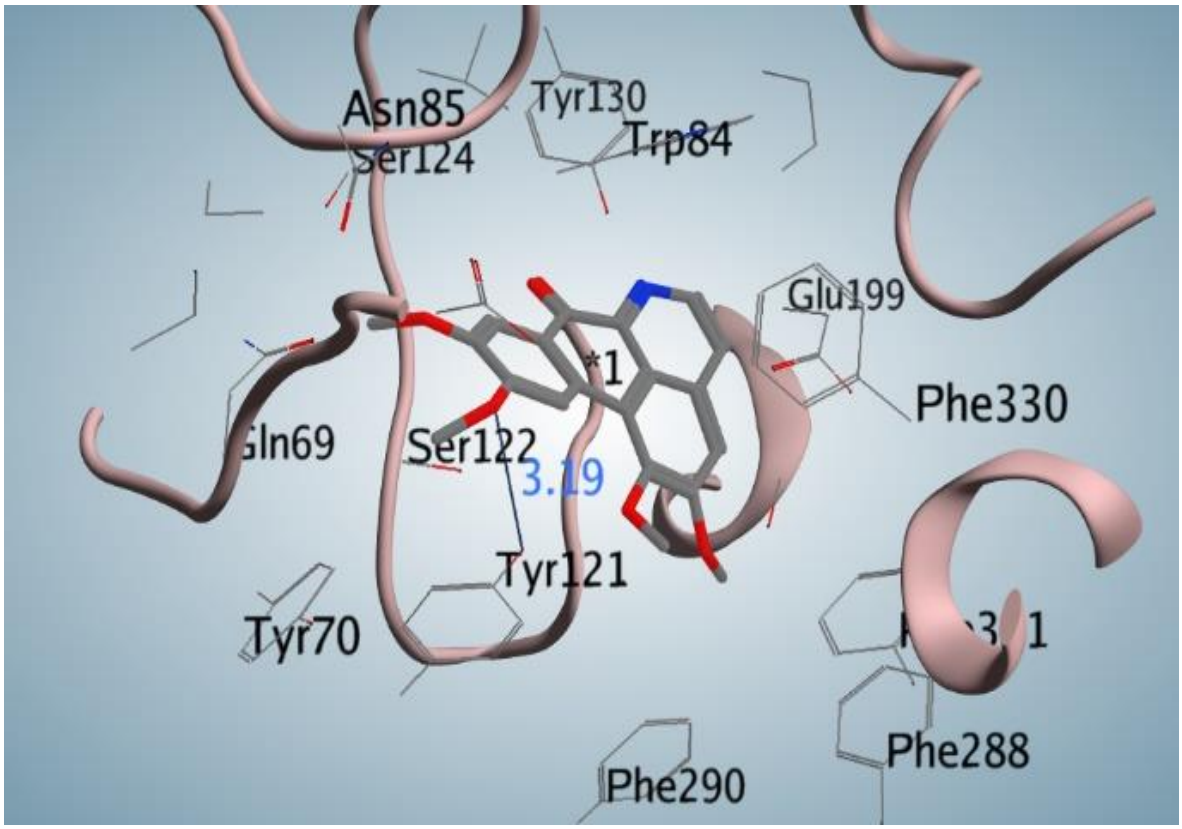

Figure 4.46. The simulated poses of the compound Oxoglaucine. Hydrogen bonds are presented in blue lines. Grey sticks show the ligand while the acetylcholinesterase residues are shown as pink ribbons. The images were rendered using MOE 2015.01.08.

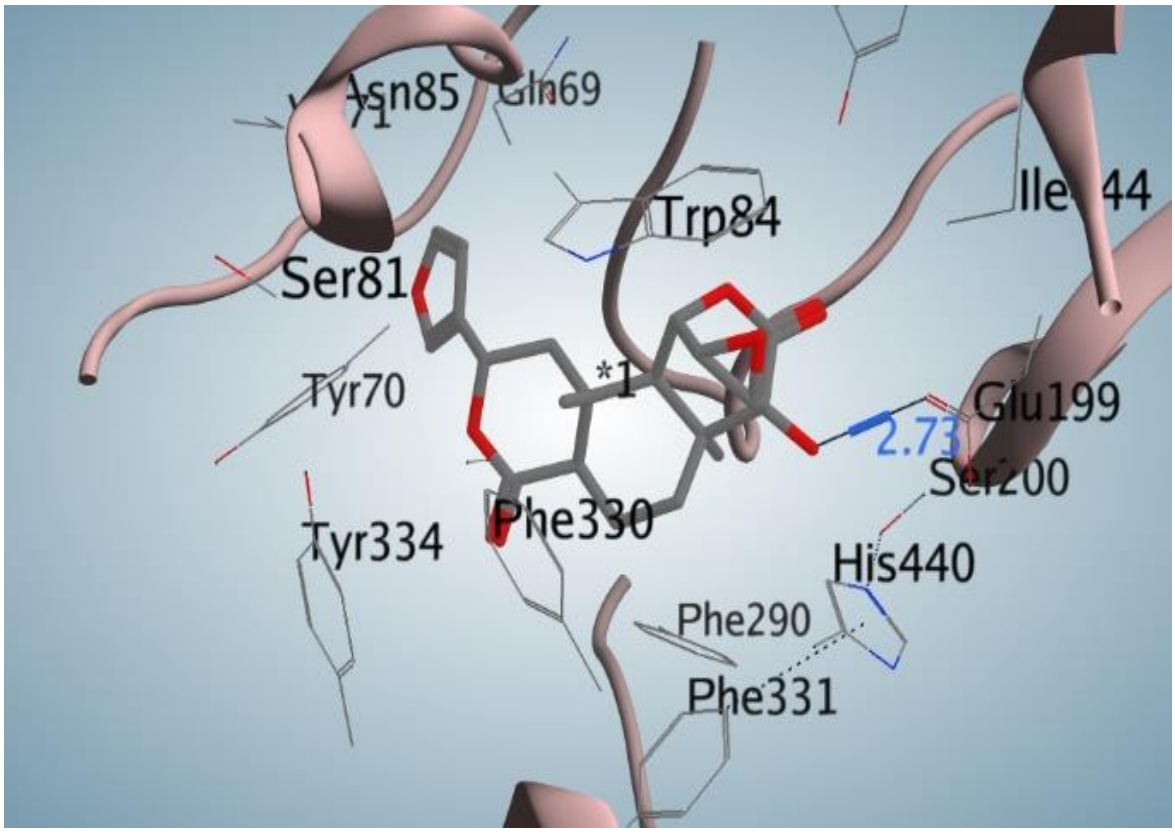

Figure 4.47. The simulated poses of the compound Tinosporide. Hydrogen bonds are presented in blue lines. Grey sticks show the ligand while the acetylcholinesterase residues are shown as pink ribbons. The images were rendered using MOE 2015.01.08.

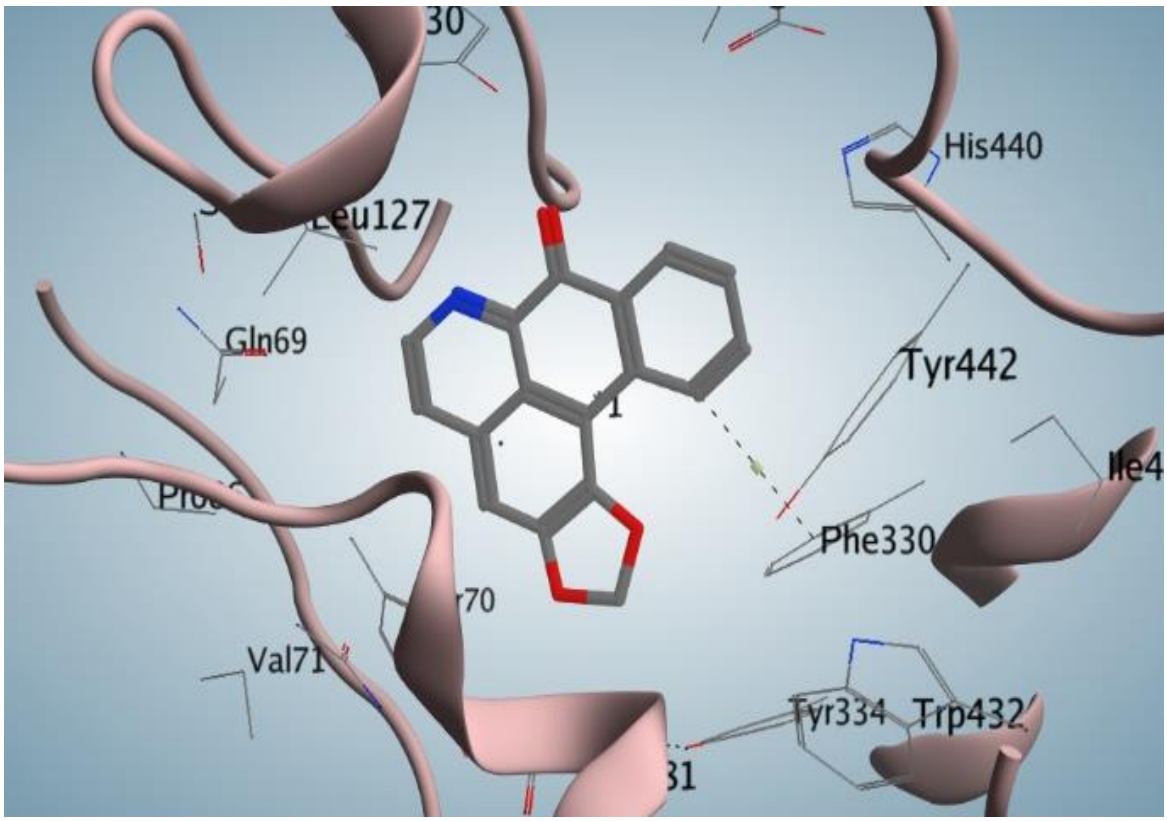

Figure 4.48. The simulated poses of the compound Liriodenine. Hydrogen bonds are presented in blue lines. Grey sticks show the ligand while the acetylcholinesterase residues are shown as pink ribbons. The images were rendered using MOE 2015.01.08.

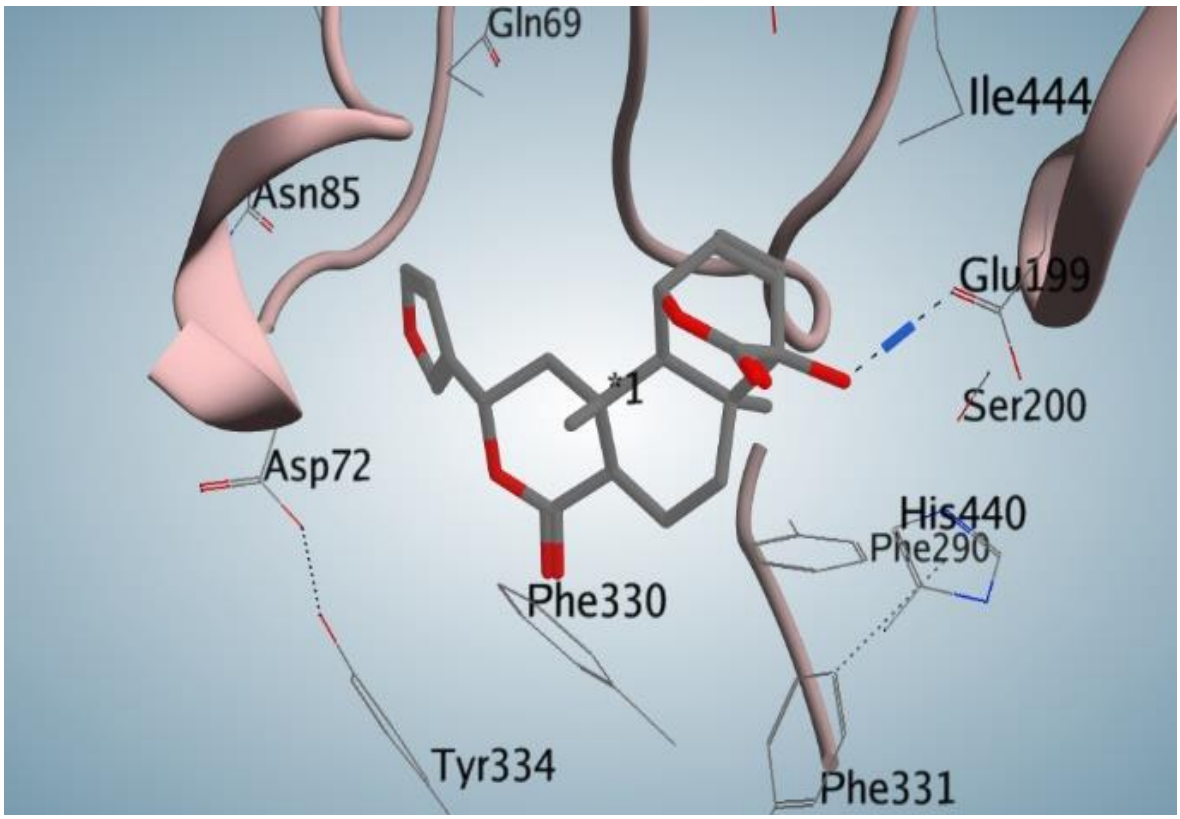

Figure 4.49. The simulated poses of the compound Columbin. Hydrogen bonds are presented in blue lines. Grey sticks show the ligand while the acetylcholinesterase residues are shown as pink ribbons. The images were rendered using MOE 2015.01.08.

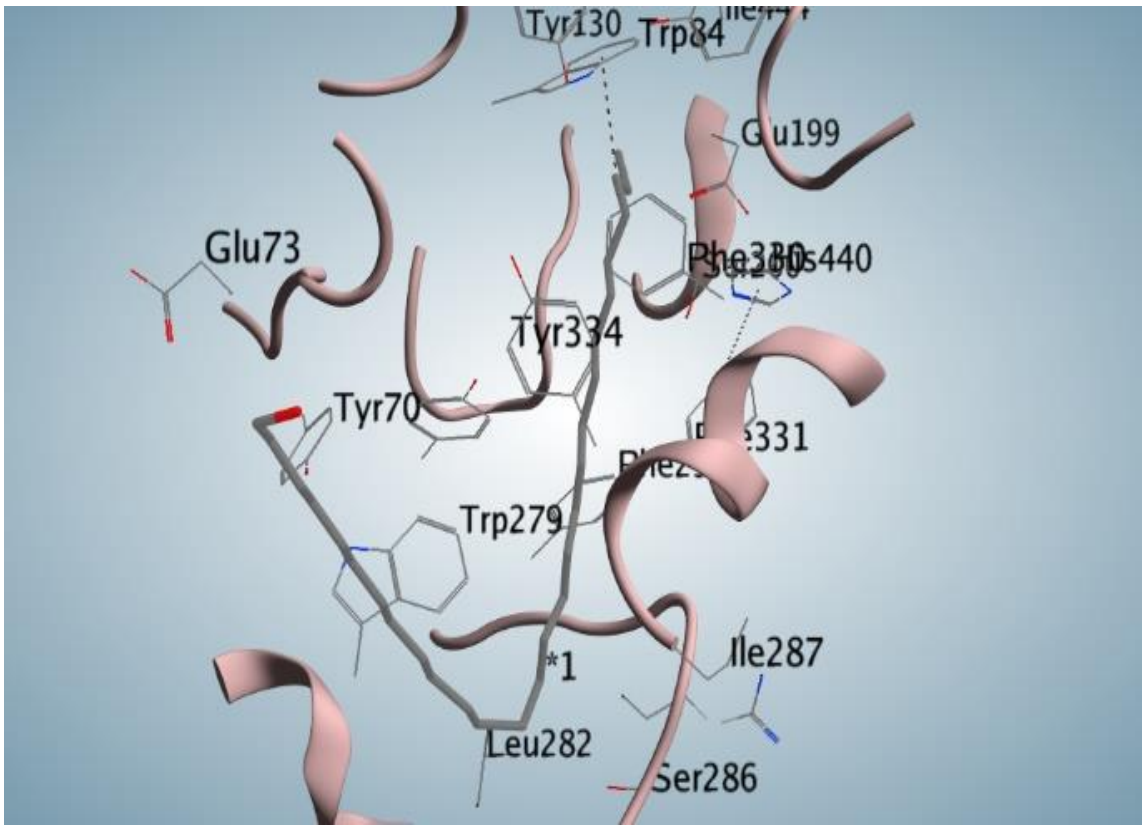

Figure 4.50. The simulated poses of the compound 1-Octacosanol. Hydrogen bonds are presented in blue lines. Grey sticks show the ligand while the acetylcholinesterase residues are shown as pink ribbons. The images were rendered using MOE 2015.01.08.

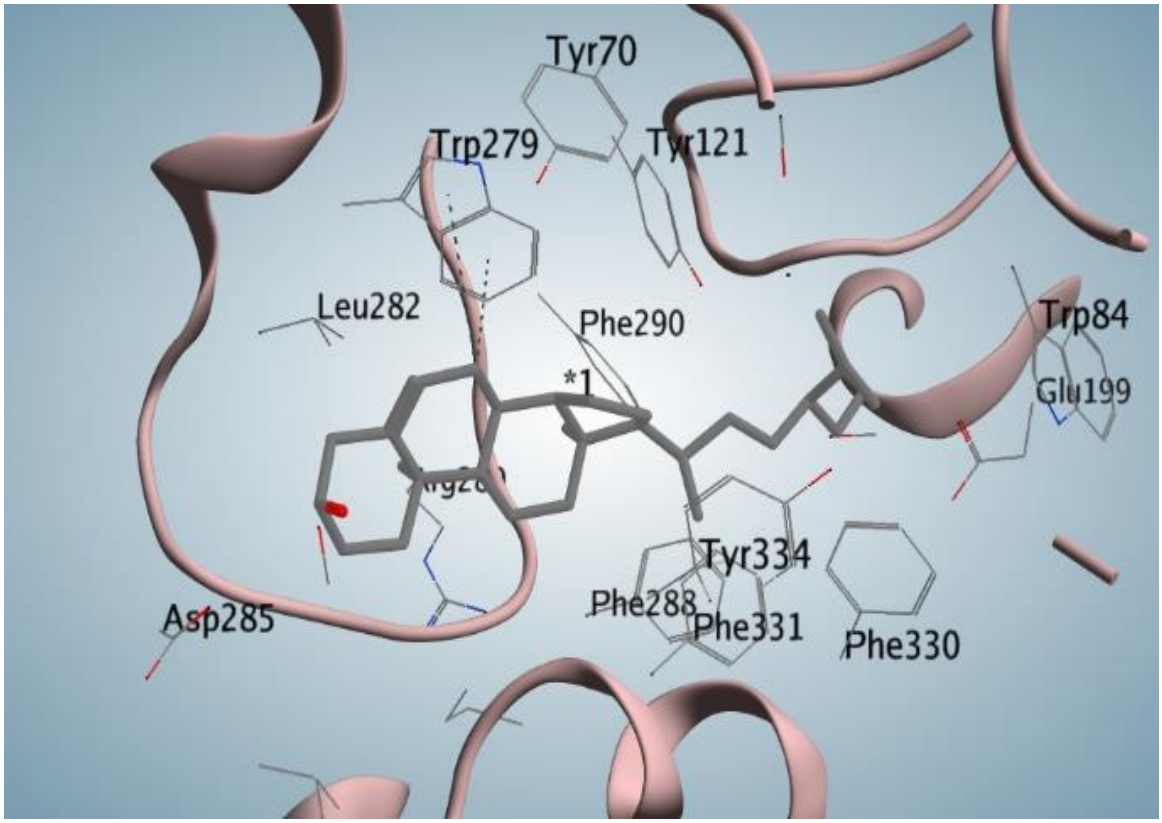

Figure 4.51. The simulated poses of the compound β-sitosterol. Hydrogen bonds are presented in blue lines. Grey sticks show the ligand while the acetylcholinesterase residues are shown as pink ribbons. The images were rendered using MOE 2015.01.08.

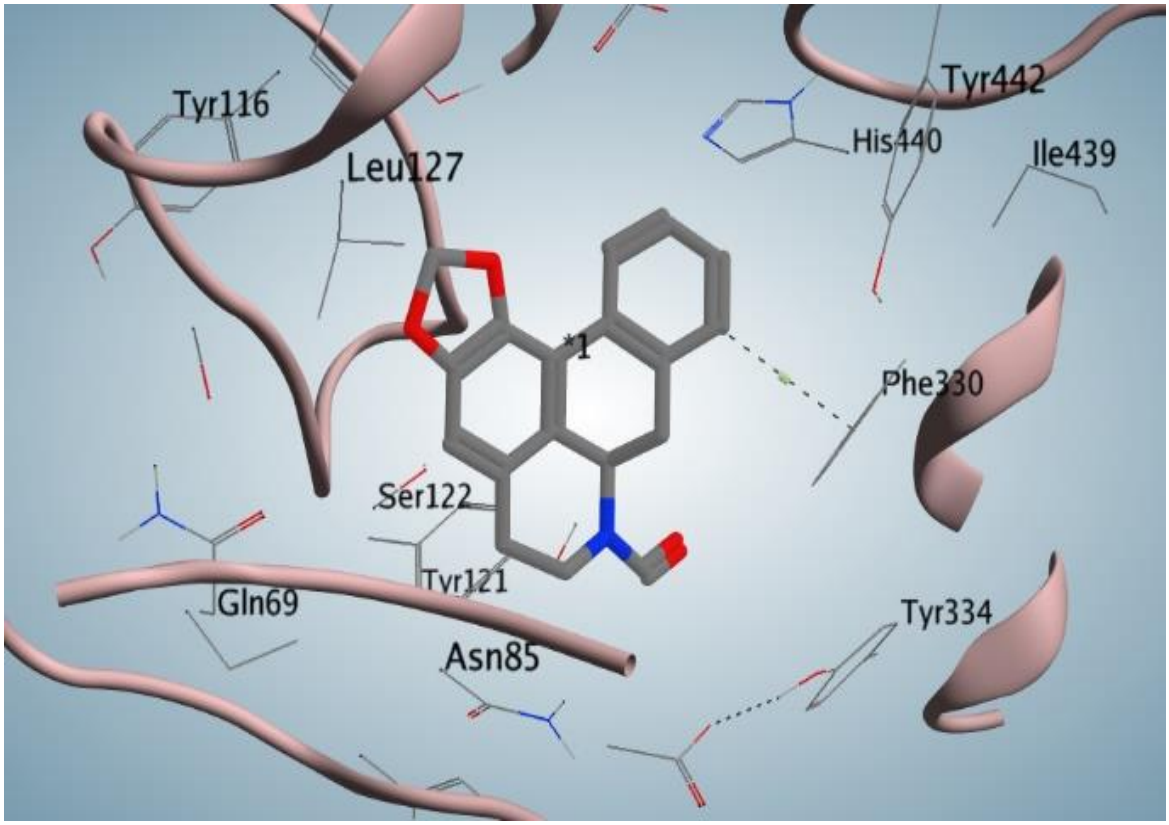

Figure 4.52. The simulated poses of the compound -(-N)-Formylanonaine. Hydrogen bonds are presented in blue lines. Grey sticks show the ligand while the acetylcholinesterase residues are shown as pink ribbons. The images were rendered using MOE 2015.01.08.

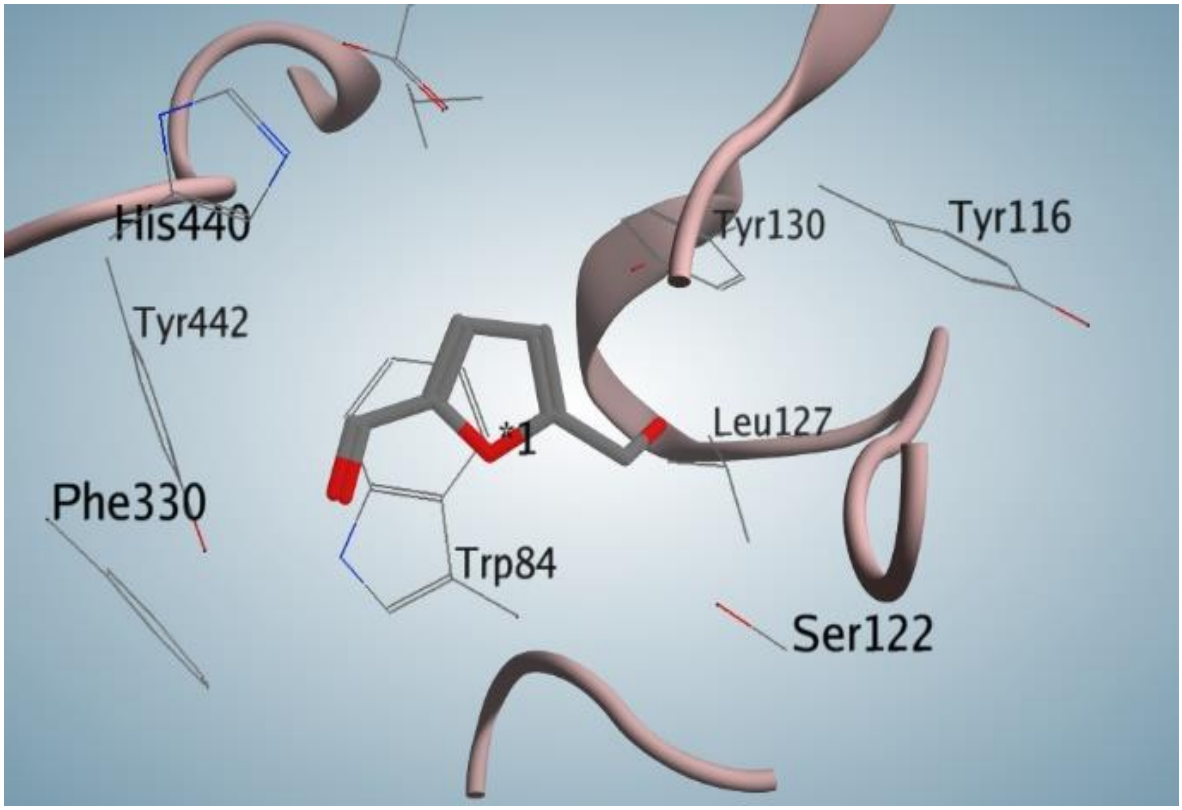

Figure 4.53. The simulated poses of the compound 5-Hydroxymethylfurfural. Hydrogen bonds are presented in blue lines. Grey sticks show the ligand while the acetylcholinesterase residues are shown as pink ribbons. The images were rendered using MOE 2015.01.08.

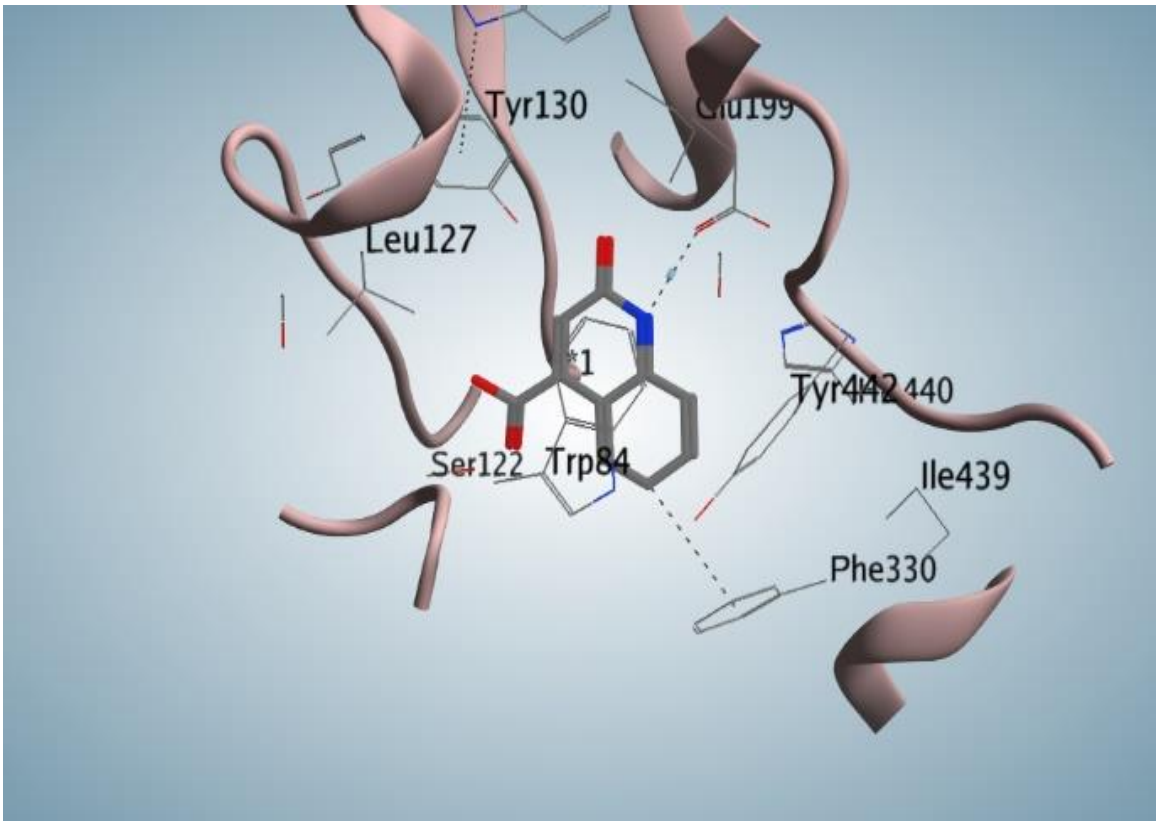

Figure 4.54. The simulated poses of the compound 2-hydroxyquinoline-4-carboxylic acid. Hydrogen bonds are presented in blue lines. Grey sticks show the ligand while the acetylcholinesterase residues are shown as pink ribbons. The images were rendered using MOE 2015.01.08.

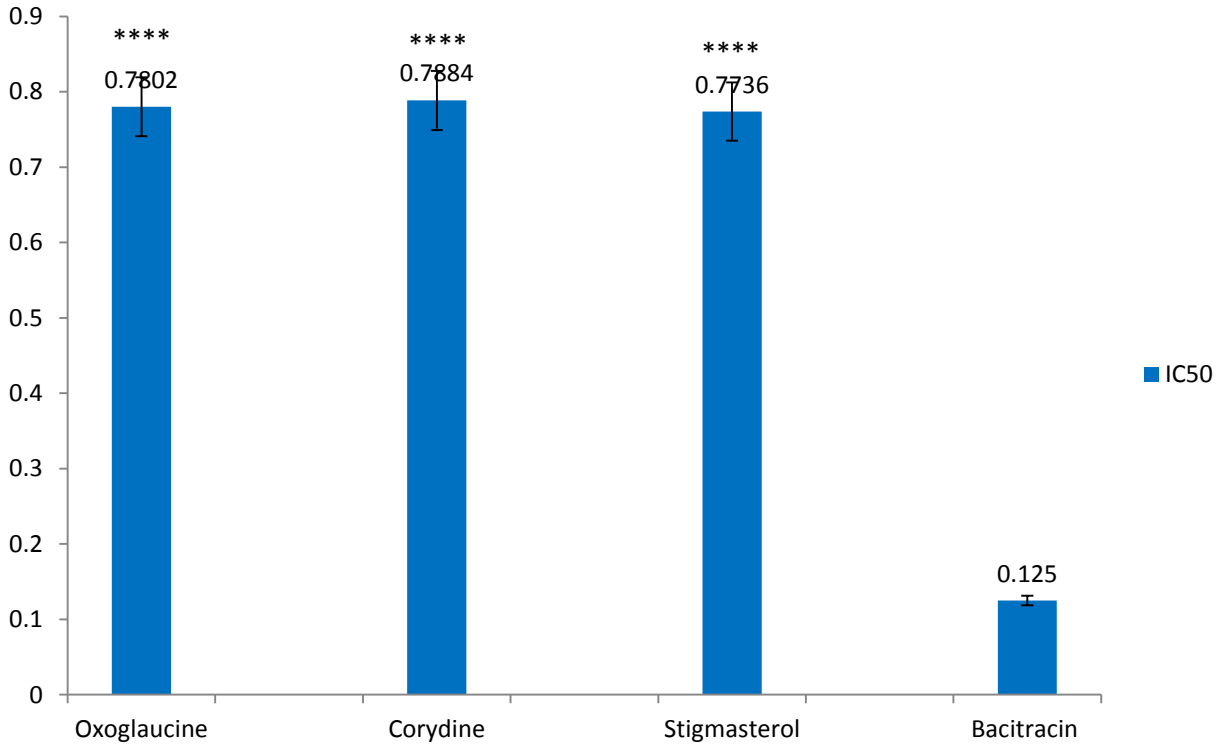

Figure 4.55: Prolyl endopeptidase inhibitory activity of compounds isolated at 1mM (IC_{50}±SEM (mM)

Values are presented as mean ± standard error of mean (n=3).

Comparison of each compounds with standard (Bacitracin) was done and level of significant difference represented with *, **, *** and ****. Extracts with no asterisks are not significantly (NS) different from the standards

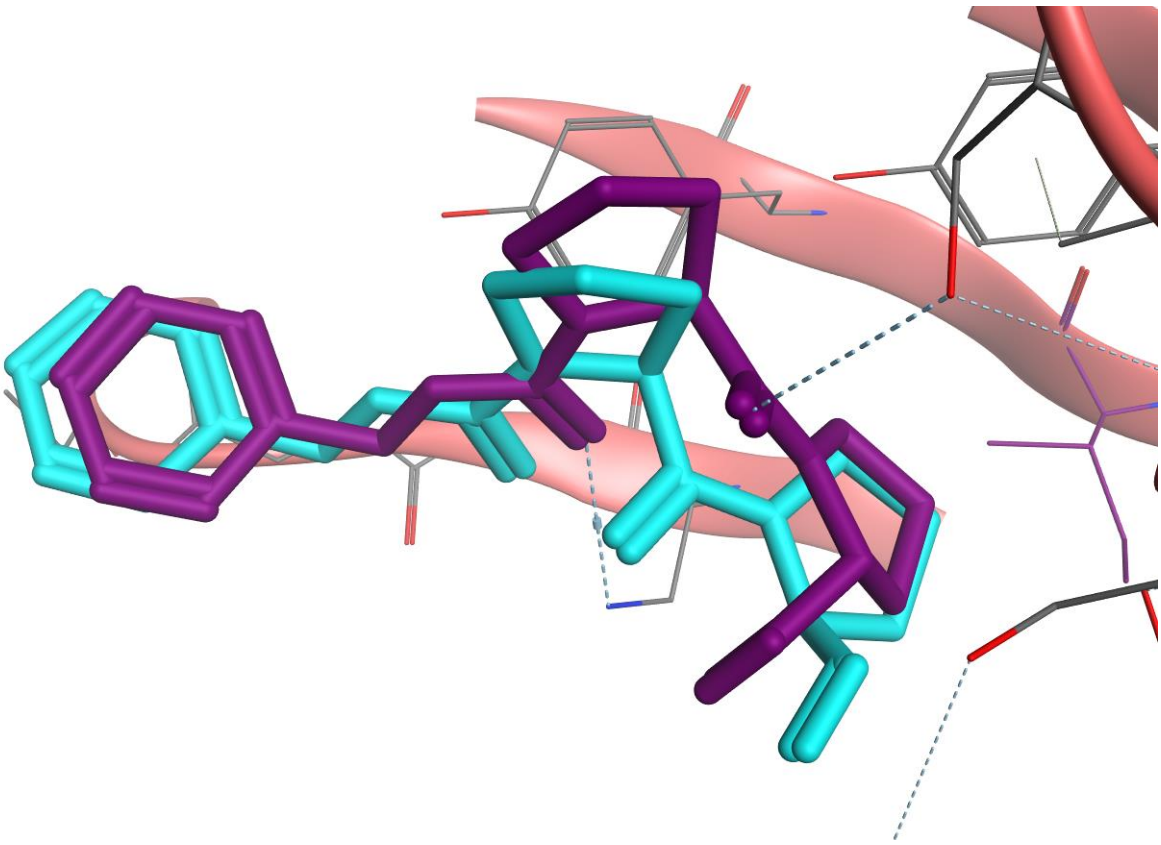

Figure 4.56: Comparison of the crystal (cyan) and the simulated pose (magenta) of cognate ligand from PDB: 3IVM complexed with an inhibitor N-benzyloxycarbonyl-L-prolyl-L-prolinal

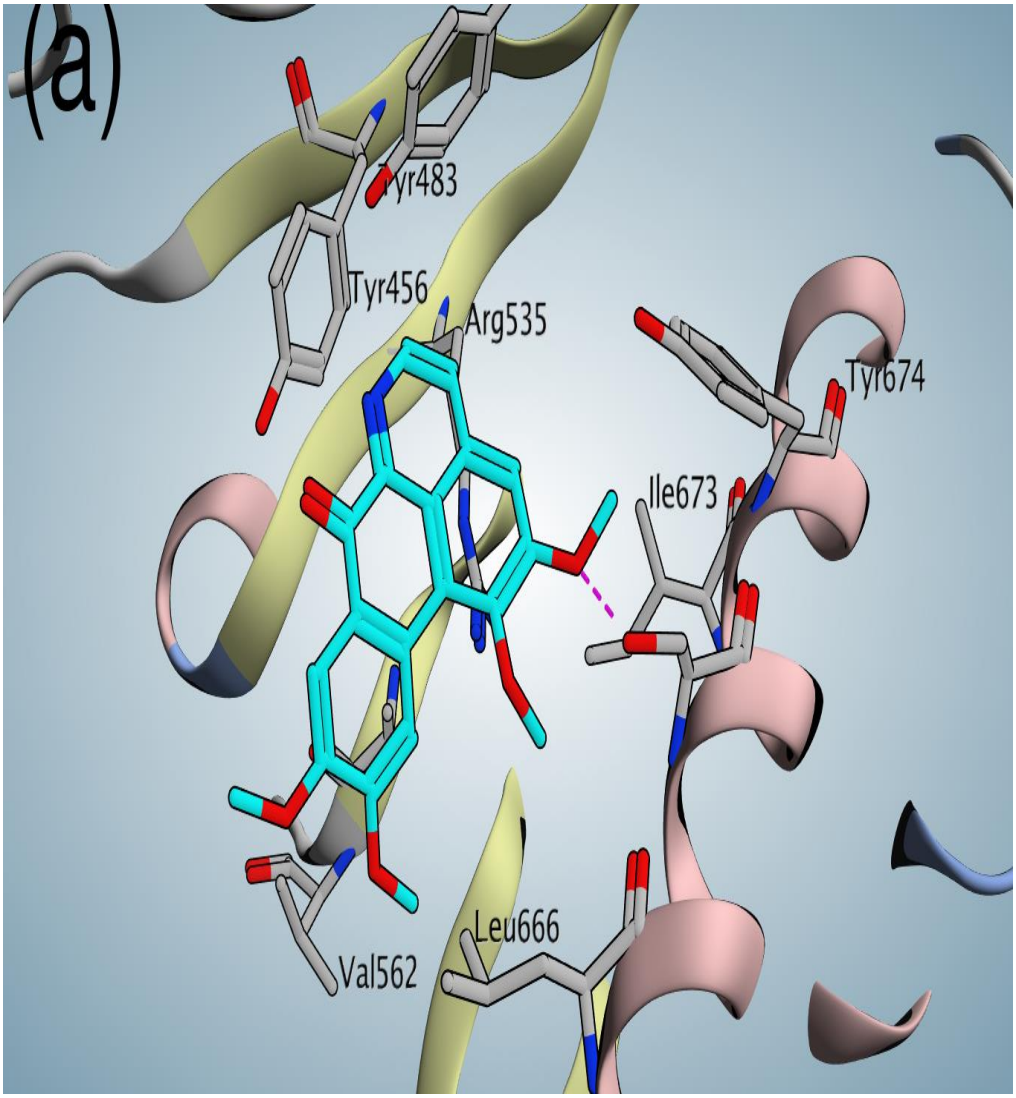

Figure 4.57. The simulated poses of the compound Oxoglaucine (a). Hydrogen bonds are presented in red dashed lines. Cyan sticks show the ligand while the PEP residues are shown as grey sticks. The images were rendered using MOE 2018.0101.

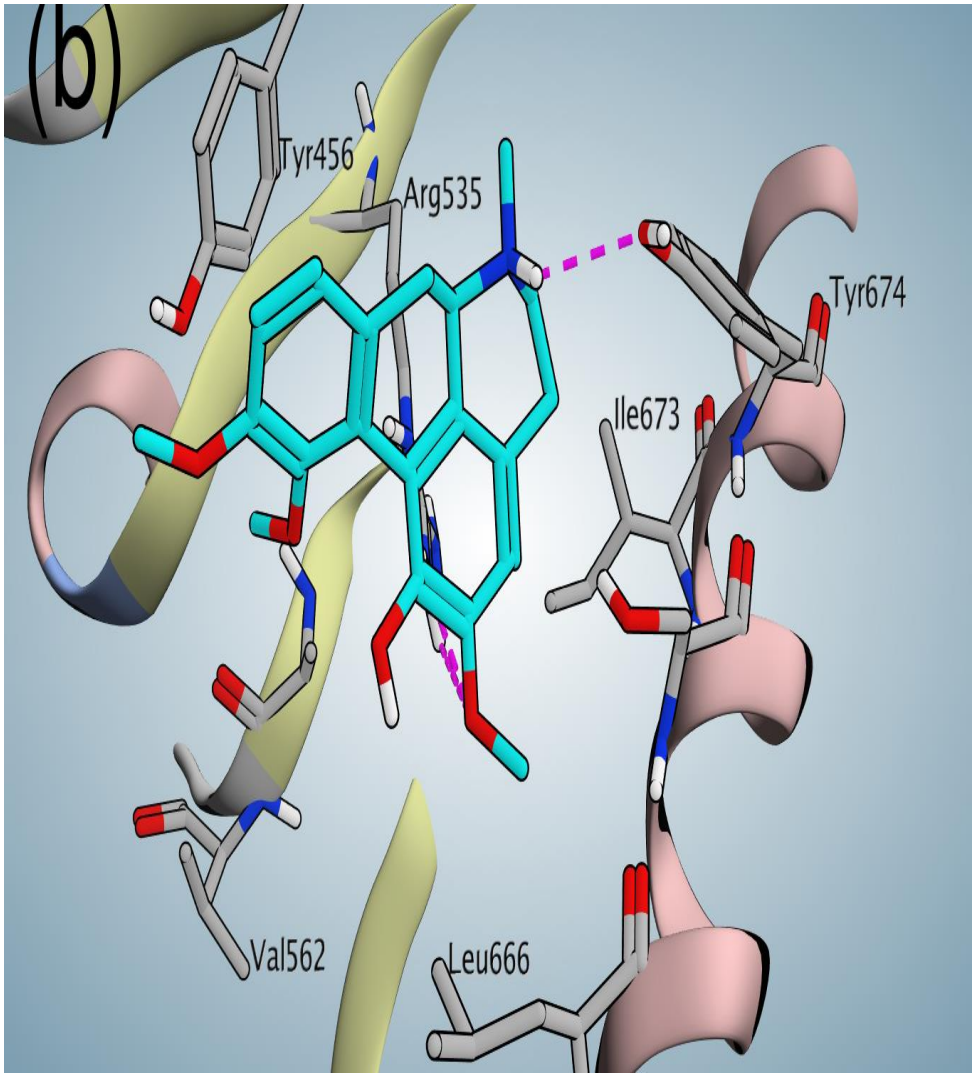

Figure 4.58. The simulated poses of the compound Corydine (b). Hydrogen bonds are presented in red dashed lines. Cyan sticks show the ligand while the PEP residues are shown as grey sticks. The images were rendered using MOE 2018.0101.

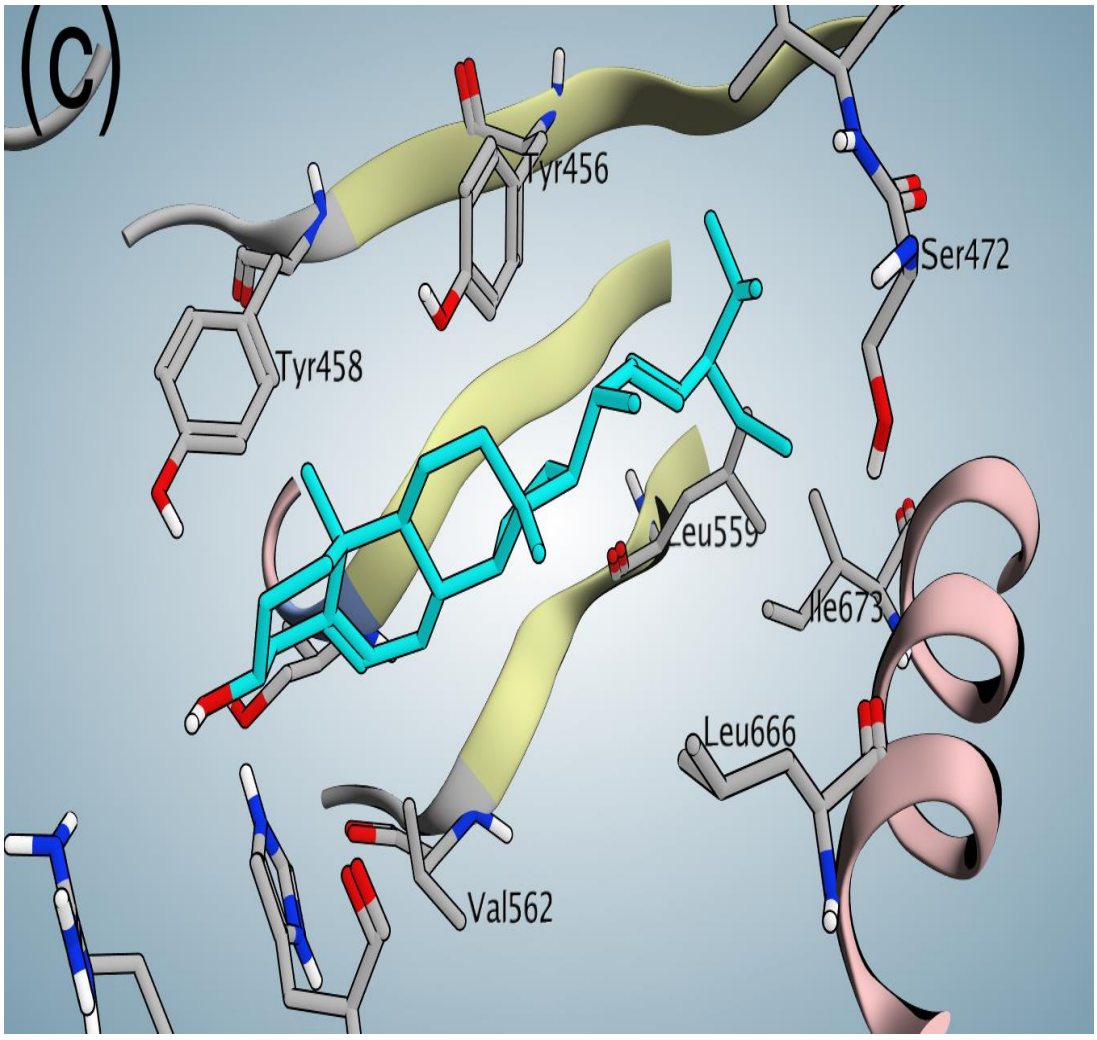

Figure 4.59. The simulated poses of the compound Stigmasterol (c). Hydrogen bonds are presented in red dashed lines. Cyan sticks show the ligand while the PEP residues are shown as grey sticks. The images were rendered using MOE 2018.0101.

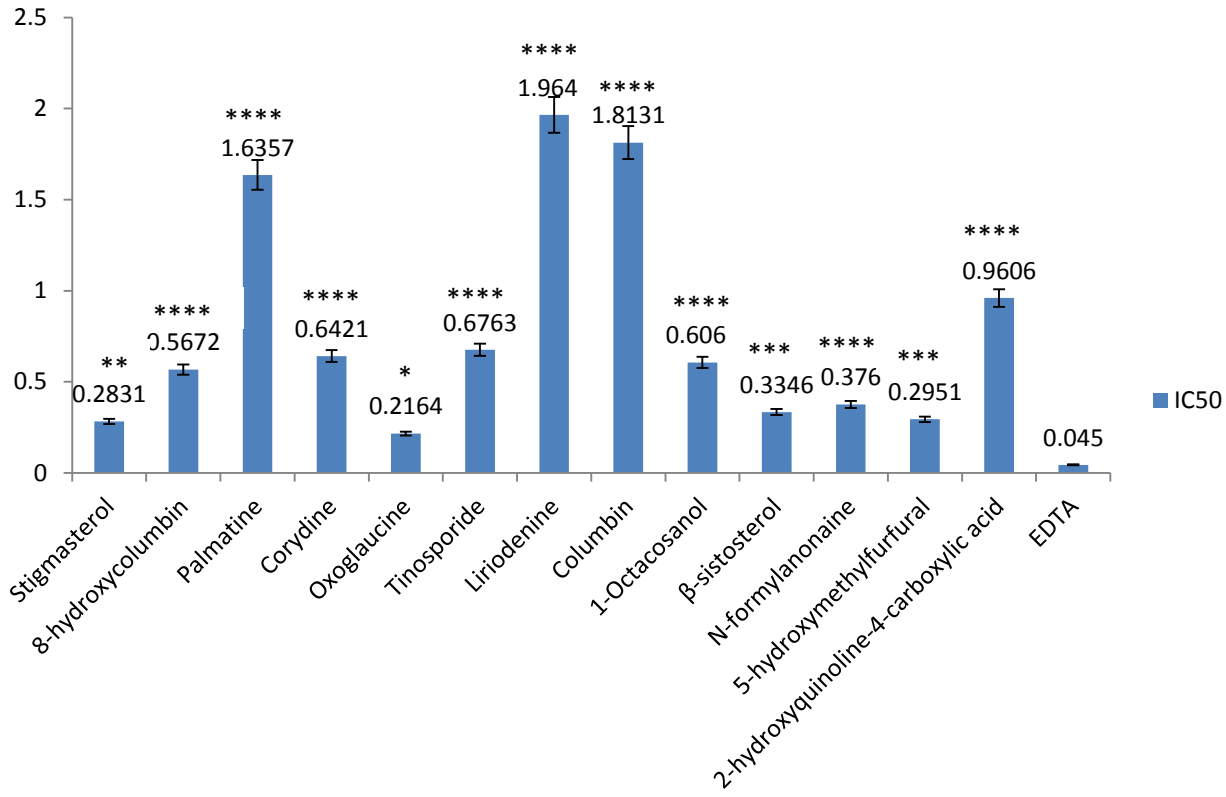

Figure 4.60: Metal chelating activity of compounds isolated from *Phyllanthus muellerianus* leaf, *Tinospora cordifolia* stem and *Cola hispida* seed at 1 mg/mL (IC_{50}±SD (mg/mL)

Values are presented as mean ± standard deviation (n=3).

Comparison of each compounds with standard (EDTA) was done and level of significant difference represented with *, **, *** and ****. Extracts with no asterisks are not significantly (NS) different from the standard

CHAPTER FIVE

5.0 DISCUSSION, CONCLUSION AND RECOMMENDATION

5.1 Preliminary study on acetylcholinesterase inhibitory activities of the ten selected medicinal plant extracts

The present study began with a preliminary investigation of ten (10) selected Nigerian medicinal plants namely; *Tinospora cordifolia, Stephania dinklagei*, *Phyllanthus amarus*, *Cleome rutidosperma*, *Spilanthes filicaulis*, *Strophanthus hispidus*, *Gongronema latifolium*, *Cola hispida*, *Phyllanthus muellerianus* and *Hedranthera barteri* representing species in plant families such as Apocynaceae, Menispermaceae, Malvaceae, Euphorbiaceae, Asteraceae, Phyllantaceae, Cleomaceae that has been reported in literature from ethnobotanical survey conducted in some parts of Southwest Nigeria as memory enhancing and antiaging agents (Elufioye *et al*., 2012, Sonibare and Ayoola, 2015). However, there is paucity of scientific evidence to justify their efficacy. The chemical constituents of most of these plants are unknown and may have either dangerous effects or positive effect on human health. On the other hand, some plants, which are not reported to be used in herbal medicine, might also possess potential activity.

A number of scientific researches have been carried out on the benefit of medicinal herbs in the treatment of neurodegenerative disorders. Amongst these are *Salvia officinalis* (Lamiaceae) reported to contain the antioxidants carnosic acid and rosmarinic acid. These compounds are thought to protect the brain from oxidative damage. Extract from the licorice root is reported to treat or even prevent brain cell death in diseases like Alzheimer's and its associated symptoms (Bilge and Ilkay, 2005). One of the research plants, *Tinospora cordifolia* belonging to the family Menispermaceae has been previously reported and proving to possess memory improving effect in animals with memory deficits (Malve *et al*., 2014). Also, administration of *Tinospora cordifolia* increases the cognitive function in

patients with AD (Lannert and Hoyer, 1998). *Emblica officinalis* belongs to the family Euphorbiaceae exhibited significant improvement in memory retention of young and aged rats in a dose-dependent manner. It reversed the diazepam and scopolamine induced amnesia. As a memory enhancer and reversal of memory deficits, *Emblica officinalis* plays an important role in the treatment of memory deficits and AD (Mani and Milind, 2007).

The result showed that three of the ten plants namely *Phyllanthus muellerianus* leaves (Euphorbiaceae), *Tinospora cordifolia* stem (Menispermaceae) and *Cola hispida* seed (Malvaceae) demonstrated good acetylcholinesterase (hAChE) inhibitory activity *in vitro*. *Phyllanthus muellerianus* leaves showed the highest acetylcholinesterase (hAChE) inhibitory activity with IC_{50} value of 3.70 ± 0.70 μg/mL as compared to standard drug Galanthamine (IC_{50} of 0.758 ± 0.057 μg/mL) followed by *Cola hispida* with IC_{50} value of 26.9 ± 7.8 μg/mL at 200 μg/mL. Since most of the AChE inhibitors are known to contain nitrogen, the higher activity of these extracts may be due to their rich alkaloidal content (Orhan *et al*., 2004). The acetylcholinesterase inhibitory activities displayed by the tested plants validate the folkloric use of species of respective plant families in the improvement of memory and other cognitive functions.

5.2 The Percentage yield of crude extracts and fractions

The percentage yields of extracts were calculated both for the crude methanolic extracts and partitioned fractions. The highest percentage yield was obtained from the seed of *Cola hispida* extract (11.58%) followed by methanolic extract of *Phyllanthus muellerianus* leaf (7.15%). In the partitioned fractions, it was observed that ethyl acetate fraction of *Phyllanthus muellerianus* leaf has the highest yield at 41% from 250 g of methanolic extract. Ethyl acetate fraction of *Tinospora cordifolia* has the highest yield at 54% from 170 g of methanolic extract. Aqueous fraction of *Cola hispida* gave the highest yield of 65.4% from 470 g of methanolic extract. n-hexane and dichloromethane fractions of *Cola hispida* gave low yield of 1.42% and 1.31%, respectively. The percentage yields of the extracts could be attributed to so many factors such as mode of plant extraction, solvent used, maturity of plant, genetic and evolution, the growing conditions and region, physiological variations, time of plant collection, season of collection and generally environmental factors such as rainfall, temperature, mineral elements and humidity (Figueiredo *et al*., 2008).

5.3 Qualitative phytochemical Screening

The result of the phytochemical screening showed that *Phyllanthus muellerianus* and *Tinospora cordifolia* contains alkaloids, tanins, flavonoids, anthraquinones, saponin, phenols, glycosides, terpenoids and steriod showing various degree of abundance. Alkaloids, glycosides, flavonoids and terpenoids were detected in *Cola hispida* crude extract while tanins, phenol and steroid were not detected. The result showed that *Tinospora cordifolia* has relatively high amount of alkaloid and terpenoids present in them. Season of collection, time of plant collection, genetic profile and generally abiotic and biotic environmental factors could also determine the presence or absence of the phytochemicals (Cirak and Radusiene, 2019).

5.4 Anti-cholinesterase inhibitory activities of plant crude extracts and fractions of *Phyllanthus muellerianus* leaf, *Tinospora cordifolia* stem and *Cola hispida* seed

Plants have been used since ancient times in traditional medicinal systems for the treatment of memory dysfunction. Medicinal plants have been proven to be rich in plethora of bioactive compounds which could be used in managing various diseases that threaten human health. Currently, new drugs that can improve memory and learning or delay the neurodegenerative process are essential in conditions such as Alzheimer's disease. Since natural products are multi-target and multi-functional in nature, they would provide additional benefit such as synergistic and additive effects usually required in the management of complex diseases such as AD thereby enhancing the facuties of learning and memory. Bores *et al*. (1996) reported that natural products are the richest resources for new anticholinesterase drugs. Studies carried out on some species have resulted in the identification of compounds which are currently either in clinical use or templates for other drug discovery e.g. Galanthamine, an alkaloid isolated from *Galanthus nivalis* L. (Amaryllidaceae). Galanthamine was approved by FDA in 2004 for use as an acetylcholinesterase inhibitor in the treatment of AD (Jones *et al*., 2006), Rivastigmine which was synthesized from the lead compound physostigmine derived from *Physostigma venenosum* and approved in 2000 by US-FDA (Lopez *et al*., 2002), Also, Huperzine A, an

alkaloid isolated from *Huperzia serrata* is sold as a food supplement used for memory enhancement and to treat symptoms of AD in China (Marston *et al*., 2002).

The acteylcholinesterase is a biologically important enzyme that hydrolyzes acetylcholine, an important neurotransmitter in the brain considered to play role in the pathology of Alzhiemer's disease (Herbert *et al*., 1995). One of the most imperative tactics for treatment of this disease involves the enhancement of acetylcholine level in the brain using AChE inhibitors. Therefore, Inhibition of acetylcholinesterase, the key enzyme in the breakdown of acetylcholine, is considered one of the treatment strategies against several neurological disorders including Alzheimer's as reported by (Enz *et al*., 1993).

In this study, the methanol extracts of *Phyllanthus muellerianus* leaf, *Tinospora cordifolia* stem and *Cola hispida* seed, its derived fractions (*n*-hexane, dichloromethane, ethyl acetate and aqueous methanol) at various concentrations were tested for their anticholinesterase inhibitory activities using Ellman's colorimetric method and β-naphtyl acetate and fast blue B salt (NA-FB) methods *in vitro*. The principle involves the measurement of the rate of production of thio-choline as acetylthiocholine is hydrolysed. This is accomplished by the continuous reaction of the thiol group with DTNB to produce the yellow anion of 5-thio-2-nitro-benzoic acid (TNB). In the NA-FB method, the enzyme hydrolyzes the substrate β-naphthyl acetate to naphthol and acetate. Naphthol is allowed to react with fast blue B. This reaction resulted in the development of a stable purple color (diazonium dye). The colour intensity is proportional to enzyme activity. All the test samples showed concentration dependent cholinesterase inhibition in both Ellman's colorimetric method and β-naphtyl acetate and fast blue B salt (NA-FB) assay method. Standard curves were generated and calculation of the 50% inhibitory concentration (IC_{50}) values was done using Microsoft Excel. All data was expressed as mean ± S.D. and of triplicate parallel measurements. The extract/compound that inhibits the hydrolysis of substrate by 50% was determined. The smaller the IC_{50} value, the higher the enzyme inhibitory activity (Prieto *et al.*, 1999). The AChE inhibition potential of ethyl acetate fraction of *Cola hispida* seed and *Phyllanthus muellerianus* at 5 mg/mL were most prominent with IC_{50} values of 0.656±0.24 mg/mL and 0.742±0.12 mg/mL, respectively when compared to the standard eserine at 0.01mg/mL (IC_{50} value of 0.007±0.00 mg/mL) in the Ellman's method. The ethyl acetate fraction of

Phyllanthus muellerianus leaf, *Tinospora cordifolia* stem and *Cola hispida* seed at 5 mg/mL in the NA-FB assay method showed IC_{50} values of 0.258±0.10 mg/mL, 1.604±0.04 mg/mL and 2.220±0.02 mg/mL, respectively when compared to the standard eserine at 0.01mg/mL (IC_{50} value of 0.014±0.00 mg/mL). The implication of the findings is that the ethyl acetate fraction of *Cola hispida* and *Phyllanthus muellerianus* has the potential to increase the half-life of acetylcholine in the brain thereby improving learning and memory because of their potential to inhibit acetylcholinesterase which causes the degradation of acetylcholine.

5.5 Anti-oxidant activities of plant crude extracts and fractions of *Phyllanthus muellerianus* leaf, *Tinospora cordifolia* stem and *Cola hispida* seed.

5.5.1 Metal chelating activity

Metal ions have been revealed to aberrantly accrue in the brain with aging as well as in the course of several neurodegenerative disorders as well as AD (Filiz *et al*., 2008). Particularly, the interplay of metal-protein interactions with oxidative stress was recently highlighted by several laboratories (Sayre *et al*., 2001). Therefore, metal chelation therapy may now be considered as a promising clinical approach to AD treatment (Valko *et al*., 2005). Studies have implicated physiological transition metals such as iron (Fe), copper (Cu) and zinc (Zn) and prooxidant non-physiological elements, such as aluminum (Al) as key factors in the pathophysiology of Alzheimer's disease (Zatta *et al*., 2002). Indeed, very high levels of Cu (400 μM) and Zn (1 mM) were found in amyloid plaques and AD neuropil regions in comparison to healthy brain (70 μM Cu and 350 μM Zn) (Lovell *et al*., 1998). Remarkably, this latter study exposed that divalent cations increase in the early phase of AD, while trivalent metal ions start increasing significantly in the later phase of AD, mainly in frontal cortex and hippocampus (Rao *et al.*, 1999).

As the demand for new and more effective drugs for AD treatment continues to grow, pharmacological strategies aimed at lowering brain metal ions and targeting Aβ/metal ions interactions might offer a large potential to chelation therapy. Studies on neuronal degeneration in the brains of patients with AD show that hippocampus is one of the primary regions affected during the early stages of the disease (Seabrook *et al*., 1999). Neurotoxic heavy metals like Pb (Monterio *et al*., 1991) and Cd (Stohs and Bagchi, 1995) are known to disrupt structural features of the cells also in this region of the brain. Studies suggest that

curcumin significantly reduces Pb- and Cd-induced neurotoxicity in rat hippocampal neurons (Dairam *et al*., 2007) and increased hippocampal neurogenesis in chronically stressed rats (Xu *et al*., 2007). The use of phytochemical products as an alternative strategy for the amelioration in neurotoxic mechanisms has been gaining a lot of consideration recently (Joseph *et al*., 2005).

In this study, the dichloromethane and ethyl acetate fractions of *Tinospora cordifolia* stem at 5 mg/mL concentration showed good metal chelating activity by inhibition of ferrozine–Fe^{+2} complex formations with IC_{50} values of 0.199±0.08 mg/mL and 0.273±0.12 mg/mL, respectively as compared to the ethyl acetate fractions of *Phyllanthus muellerianus* leaf (IC_{50}= 1.538±0.13 mg/mL) and *Cola hispida* seed (IC_{50}= 0.624±0.05 mg/mL) as compared to the standard vitamin C at 0.1mg/mL (IC_{50} value of 0.019±0.00 mg/mL). The dichloromethane and ethyl acetate fraction of *Tinospora cordifolia* stem through its antioxidant property demonstrated the abilities to lower brain metal ions and targeting A*β*/metal ions interactions which might offer a large potential to chelation therapy.

5.5.2 Radical scavenging activity using DPPH

A number of studies show that free radical damage and oxidative stress is involved in age related neurodegenerative diseases. Likewise, there are numerious studies which have examined the beneficial role of antioxidants to either reduce or block neuronal death occurring in the pathophysiology of these disorders (Ramassamy, 2006).

The plant kingdom offers a wide range of secondary metabolite displaying antioxidant potentials especially plant polyphenols that can defend against a number of diseases that is related to oxidative stress and free radical-induced damage (Vladimir-Knežević *et al*., 2012, Teixeira *et al*., 2013). Compounds such as serotonin (5-hydroxytryptamine), flavonoids, quercetin, and simple alkylphenols have been shown to prevent membrane lipid peroxidation and protect neuronal cells against oxidative cell death *in vitro* (Moosmann *et al*., 1997). Vitamin E also reported to rescue the neuronal cytotoxicity induced by aluminum in AβPP transgenic mice and reduce Aβ deposition in the brain by reducing isoprostane levels (Praticò *et al*., 2002).

The DPPH (1,1-diphenyl-2-picrylhydrazyl radicals) test is a broadly used method to assess the free radical scavenging activity of plant extracts and compounds. This method is based on the reduction of methanolic DPPH (2,2 diphenyl-1-hydrazine) solution in the presence of antioxidant resulting in the formation of non-radical DPPH-H by the reaction. The stable DPPH were reduced by the extracts and thus changing the color from purple to yellow to varying degrees depending on the presence of antioxidant compounds which can donate electron or hydrogen atom. The degree of discoloration designates the scavenging power of the extracts.

DPPH radical scavenging based antioxidant potential of the extracts was assessed using the IC_{50} parameter. Here, IC_{50} means the concentration of antioxidant required for 50% scavenging of 1,1-diphenyl-2-picrylhydrazyl radicals in the specified time. The smaller the IC_{50} value, the higher antioxidant activity of the plant extracts (Prieto *et al.*, 1999). In DPPH (1,1-diphenyl-2-picrylhydrazyl) radical scavenging assay, at 5 mg/mL concentration, ethyl acetate fraction of *Tinospora cordifolia* stem has the highest radical scavenging activity (IC_{50} = 0.419±0.03 mg/mL) as compared to the ethyl acetate fractions of *Phyllanthus muellerianus* leaf (IC_{50} = 1.005±1.07 mg/mL) and *Cola hispida* seed (IC_{50} = 1.427±0.64 mg/mL) when compared to the standard vitamin C at 0.01mg/mL (IC_{50} = 0.008±0.00 mg/mL). The high free radical scavenging activity of *Tinospora cordifolia* is an indication of its hydrogen donating ability, which might be due to the presence of rich source of polyphenols, possessing −OH groups the potent H_2 donors (Conforti *et al*., 2005).

5.5.3 Total antioxidant capacity

The phosphomolybdate method was based on the reduction of Mo (VI) to Mo (V) by the antioxidant compound and the formation of a green phosphate/Mo (V) complex at acidic pH with a maximal absorption at 695 nm. The phosphomolybdate method is quantitative since the total antioxidant activity is expressed as ascorbic acid equivalent (Kumaran, 2007).

In this research, the total antioxidant capacity was higher in dichloromethane fraction of *Phyllanthus muellerianus* leaf with value of 217.52±16.01 mg/g ascorbic acid equivalent/g of extract at 0.1-0.01 mg/mL concentration (R^2=0.9748) than in dichloromethane fractions of *Tinospora cordifolia* stem and *Cola hispida* seed with values of 69.71±10.05 mg/g and

79.58±9.07 mg/g, respectively. Also, the ethyl acetate fraction of *Phyllanthus muellerianus* leaf showed a high value of 118.154±19.13 mg/g when compared to ethyl acetate fractions of *Tinospora cordifolia* stem and *Cola hispida* seed with values of 68.229±4.89 mg/g and 95.569±6.82 mg/g, respectively. The high antioxidant capacity of dichloromethane fraction of *Phyllanthus muellerianus* leaf could be attributed to the presence of polyphenols such as tanins, flavonoids which could be relevant in the therapeutic action of this plant.

5.5.4 Ferric reducing antioxidant power

The antioxidants present in the methanol crude extracts and other fractions of *Phyllanthus muellerianus* leaf, *Tinospora cordifolia* stem and *Cola hispida* seed caused their reduction of the colourless Fe3+-ferricyanide (TPTZ–Fe (III)) complex to its blue ferrous coloured (TPTZ–Fe (II)) owing to action of electron donating in the presence of antioxidant and thus proved the reducing power. The ferric reducing power activity of methanol extracts and other fractions seem to be due to presence of polyphenols. The reducing capacity of plant extract may serve as a significant indicator of its antioxidant power. Like the DPPH radical scavenging activity, the reducing power increased with increasing concentration and also higher absorbance of the reaction mixture specifies a higher reducing potential. Therefore, the reducing activity of ferrous ion was higher in ethyl acetate fraction of *Phyllanthus muellerianus* leaf with value of 36.190±3.33 mg/g ascorbic acid equivalent/g of extract at 0.1-0.01 mg/mL (R^2=0.9968) followed by dichloromethane fraction of *Tinospora cordifolia* stem with value of 28.617±3.63 mg/g and ethyl acetate fraction of *Cola hispida* seed with value of 14.813±2.71 mg/g ascorbic acid equivalent/g of extract. The result indicates that the high ferric reducing potential of ethyl acetate fraction of *Phyllanthus muellerianus* leaf may be due to its ability to donate electron or hydrogen by the −OH group of polyphenols present in the extract (Irshad *et al*., 2012).

5.6 GC-MS analysis of hexane fraction of *Phyllanthus muellerianus*, *Tinospora cordifolia* and *Cola hispida*

Gas chromatography-mass spectroscopy (GC-MS) is the most powerful and widely used technique for the analysis of complex mixtures (Hirschfeld, 1980). GC-MS analysis is best used to make an effective identification of bioactive constituents of volatile matter, long

chain, branched chain hydrocarbons, alcohols acids, esters, etc. This analysis will provide a representative spectral output of all the compounds that get separated from the sample. Peak area (%), retention time (RT), molecular formula and molecular weight (MW) were used for the confirmation of phytochemical compounds.

The GC-MS analysis of *n*-hexane fraction of *Phyllanthus muellerianus* leaf reveals major compounds present which are 3,7,11,15-Tetramethyl-2-hexadecen-1-ol (RT 35.76; 33.95%), Hexadecanoic acid, trimethylsilyl ester (RT 47.39;52.62%), Octadecanoic acid (RT 50.07;22.51%), Heptacosane (RT 60.52; 33.69%), 6,9,12-Octadecatrienoic acid, phenylmethyl ester, (Z,Z,Z)- (RT 48.80;4.26%), 9,12,15-Octadecatrienoic acid, (Z,Z,Z)- (RT 49.62;100%), Phenol, 2,2'-methylenebis[6-(1,1-dimethylethyl)-4-methyl- (RT 54.64;14.06%), Octadecanal, 2-bromo-(RT 55.96;15.67%).

The GC-MS analysis of *n*-hexane fraction of *Tinospora cordifolia* stem reaveals major compounds present which are n-Hexadecanoic acid (RT 44.30;49.79%), Hexadecanoic acid, trimethylsilyl ester (RT 47.42;16.58%), 9,12-Octadecadienoic acid (Z,Z)- (RT 49.55;100%), Octadecanoic acid (RT 50.11;5.89%), Octadecanal, 2-bromo-(RT 54.63;3.14%), Hexadecanoic acid, 3-[(trimethylsilyl) oxy]propyl ester (RT 55.28;1.61%), Stigmastan-3,5-diene (RT 65.19;8.76%), β-Sitosterol (RT 71.16;14.37%).

GC-MS analysis of *n*-hexane fraction of *Cola hispida* seed shows the presence of the following compounds Hexadecanoic acid, methyl ester (RT 42.49;35.54%), Hexadecanoic acid, trimethylsilyl ester (RT 47.42;97.32%), 9,12,15-Octadecatrienoic acid, methyl ester, (Z,Z,Z)- (RT 48.81;30.94%), Methyl 8,9-methylene-heptadec-8-enoate (RT 48.53;7.28%), Heptadecanoic acid, 16-methyl-, methyl ester (RT 49.38;4.74%), 9,12,15-Octadecatrienoic acid, (Z,Z,Z)- (RT 49.69;100%), Octadecanoic acid (RT 50.12;13.04%), Methyl 9,10-methylene-octadec-9-enoate (RT 50.73;21.82%).

GC-MS analyses of plant extracts showed the presence of a wide range of compounds associated with antioxidant and acetylcholinesterase (AChE) inhibitory properties. Knowledge of those phytochemicals could form drug leads for the synthesis of new pharmacological agents in the treatment or management of neurodegenerative diseases such as Alzheimer's disease. The GC-MS revealed the ubiquitousness of octadecanoic acid and hexadecanoic acid in the three selected plants.

5.7 Characterisation of compounds isolated

Chromatographic analysis such as column chromatography of the plant extracts from *Phyllanthus muellerianus* leaf, *Tinospora cordifolia* stem and *Cola hispida* seed led to the isolation of nineteen (19) compounds. Thin layer chromatography profile in several solvent systems gave single spots to ascertain its purity. Two (2) compounds namely Stigmasterol and Daucosterol was isolated and identified from *Phyllanthus muellerianus* also reported for the first time. Chromatographic analyses of the fractions of *Tinospora cordifolia* afforded thirteen (13) compounds identified as β-sitosterol, Daucosterol, Columbin , Tinosporide, Tinosporicide, 8-hydroxycolumbin, Oxoglaucine, Corydine, Liriodenine, N-formylanonaine, Palmatine, 1-octacosanol, rel-(2s,3s,4r,16e)-2-[(2'r)-2'-hydroxynonadecanoylamino]-heneicosadec-16-ene-1,3,4-triol.

Oxoglaucine and rel-(2s,3s,4r,16e)-2-[(2'r)-2'-hydroxynonadecanoylamino]-heneicosadec-16-ene-1,3,4-triol are reported for the first time in the genus Tinospora, while liriodenine is reported for the first time in the species.

Four (4) compounds namely β-Sitosterol, 5-hydroxymethylfurfural, 2-hydroxyquinoline-4-carboxylic acid, daucosterol was isolated and reported for the first time from *Cola hispida*.

Stigmasterol is a class of organic compound stigmastane. Its low resolution electron impact (EI) mass spectrum showed major fragmentation at m/z (%): 412.3 (100.0), 396.3 (35.6), 381.3 (18.0), 369.3 (25.0), 351.2 (35.1), 337.3 (5.2), 329.3 (19.9), 314.2 (27.9), 300.2 (42.4), 283.2 (13.0), 271.2 (51.8), 255.2 (87.9), 241.1 (11.4), 231.1 (24.2), 213.1 (46.8), 199.1 (21.2), 185.1 (17.4), 173.1 (20.5), 159.0 (58.3), 145.0 (57.4), 133.0 (47.0), 119.0 (35.8), 107.0 (50.9), 95.0 (47.6), 81.0 (66.6), 69.0 (52.9), 55.0 (78.6), 43.0 (32.9). ^{1}H-NMR spectra showed the presence of two methyl sinlgets at δ 0.68, and 0.99; three methyl doublets that appeared at δ 0.83-0.76. ^{1}H-NMR spectra also showed protons at δ 4.99 (dd, 1H, J=8.8Hz, 8.4Hz), δ 5.14 (dd, 1H, J=8.4Hz, 8.4Hz) and δ 5.33 (br d, 1H, J=4.8Hz) suggesting the presence of three protons corresponding to that of a trisubstituted and a disubstituted olefinic bond which suggested presence of at least two double bonds. The proton corresponding to the H-3 of a sterol moiety appeared as multiplets at δ 3.50 suggested presence of an α-proton typical of sterols hydroxylated at C-3. ^{13}**C-NMR-**(δ, AVANCE NEO 400 MHz **CDCL3**) showed the presence of twenty nine carbons. Polarization transfer experiments (DEPT) were

carried out with last polarization angles at 135^0, 90^0 to determine the multiplicity of each carbon atom. The above spectral data supported the presence of sterol skeleton having a hydroxyl group at C-3 (δ 71.79) position with two double bonds at C-5/C-6 (δ 140.7/121.7) and C-22/C-23 (δ 138.3/129.2).This indicated the presence of two double bonds. One carbon resonance was in the oxygenated aliphatic region (δ 71.79). The physical and spectral data are consistent to the reported literature values (Guo *et al*., 2012).

Daucosterol, a steroid saponin was obtained as a white powder. Its low resolution electron impact (EI) mass spectrum showed the existence of a sterol skeleton and a molecular ion peak at m/z 414 [M+]. The ^{1}H-NMR spectrum of daucosterol reveals an olefinic proton signal of H-6 at δ 5.34 (br d, 1H, J=4Hz) and methyl signals at δ 0.66 (s) and δ 0.99 (s). The signal at δ 5.06 (d, *J* = 7.6Hz) suggested the presence of one anomeric proton. The chemical shift and coupling constant of this proton suggested axial-axial coupling thus showing that the sugar moiety was *β*-linked to the aglycone. The ^{13}C-NMR (δ, AVANCE NEO 400 MHz **C5D5N**) showed the presence of thirty five carbons. Polarization transfer experiments (DEPT) were carried out with last polarization angles at 135^0, 90^0 to determine the multiplicity of each carbon atom. It also reveals that the olefinic proton resonate at δ 121.9 while the C-3 (β-linkage) signal resonate at δ 78.64 suggesting that the sugar moiety was linked to the oxygen at C-3 of the aglycone. The presence of a sugar moiety was further confirmed by the signal at δ 102.6 which was assigned to the anomeric carbon. The signals for the other sugar carbons were observed at δ 75.37, 78.64, 71.74 and 62.88. These chemical shifts confirmed that the sugar moiety was glucose. Accordingly, the structure was elucidated as daucosterol (β-sitosterol-3-*O*-β-D-glucoside) by comparison of the spectral data, as described in the literature (Flamini *et al*., 2001). Daucosterol is reported for the first time from the species *Tinospora cordifolia, Cola hispida* and *Phyllanthus muellerianus*.

1-octacosanol is a straight-chain aliphatic 28-carbon primary fatty alcohol. Its low resolution electron impact (EI) mass spectrum showed major fragmentation at m/z (%): 392.2 (6.3), 364.3 (3.5), 334.2 (1.8), 308.1 (2.1), 292.2 (2.2), 264.1 (2.9), 250.1 (2.6), 223.0 (3.3), 195.1 (4.2), 181.0 (5.7), 167.1 (7.7), 153.1 (11.2), 139.0 (14.7), 125.0 (31.8), 111.0 (55.5), 97.0 (92.0), 83.0 (100.0), 69.0 (73.5), 57.0 (96.6), 43.0 (71.5). The methylene group carrying the hydroxy (OH) on ^{1}H-NMR resonated at 3.63 ppm with coupling constant of

7Hz attached to a methylene carbon at 63.11 ppm, while the methyl (-CH_3) resonated at 0.86 ppm on ^{1}H-NMR which is found attached to carbon around 14.10 ppm. Other methylene group resonated around 1.54 ppm and 1.26 ppm on ^{1}H-NMR. ^{13}**C-NMR-**(δ, AVANCE-III-AV-400 MHz **CDCL3**) shows that at δ (ppm) 14.10 (-CH_3), 22.68 (-CH_2), 25.72 (-CH_2), 29.60 (-CH_2 X21), 31.91 (-CH_2), 32.81 (-CH_2), 63.11 (-CH_2OH). The spectra and physical data were in complete concurrence with the literature (Sadiqa *et al*., 2014).

β-Sitosterol is a class of organic compound stigmastane. Its low resolution electron impact (EI) mass spectrum showed major fragmentation at m/z (%): 414.3 (100.0), 396.3 (65.1), 381.3 (34.7), 369.2 (21.1), 351.3 (29.1), 329.3 (38.4), 315.2 (16.0), 303.3 (41.1), 289.2 (14.7), 271.2 (40.0), 255.1 (84.6), 241.1 (10.7), 231.1 (28.7), 213.1 (56.3), 199.1 (21.3), 173.1 (26.3), 159.0 (46.7), 145.0 (50.3), 133.1 (39.8), 119.0 (31.3), 107.0 (11.8), 95.0 (43.8), 81.0 (45.9), 69.0 (33.7), 55.0 (51.9). The ^{1}H-NMR spectra of β-sitosterol showed the presence of six methyl signals that appeared as two methyl sinlgets at δ 0.66, and δ 0.98; three methyl doublets that appeared at δ 0.80, 0.82, and 0.90. The ^{1}H-NMR spectra of also showed one olefinic proton at δ 5.32. The ^{1}H-NMR spectra also showed a proton corresponding to the proton connected to the C-3 hydroxy group which appeared as multiplets at δ 3.50. The ^{13}C-NMR reveals that the proton connected to the C-3 hydroxy group resonate at δ 71.81 while the aromatic/olefinic proton was attached to carbon at δ 138.3/121.72. This indicates the presence of a double bond. The ^{13}C-NMR together with COSY, HMQC and HMBC showed twenty nine carbon signal including six methyls, eleven methylenes, ten methane and three quaternary carbons. Thus, the compound was assigned as β-sitosterol that was consistent to the reported literature values (Wright *et al*., 1978).

Liriodenine belongs to the class of oxoaporphine alkaloids. LREI-MS of Liriodenine run on Instrument (JEOL JMS600H-1) revealed: m/z (%): 275.2 (100.0), 247.2 (18.3), 219.1 (11.4), 188.1 (12.4), 162.1 (6.0), 81.0 (3.2). The proton NMR revealed the presence of one methylenedioxy group and seven aromatic protons. In the ^{1}H-NMR spectrum of liriodenine showed a proton singlet signal of methylenedioxy signal at δ 6.47, a pair of doublets with coupling constant of 5.2 Hz in the aromatic region at δ 8.02 and 8.74 are characteristic for H-4 and H-5 of an oxoaporphine structure. In the aromatic region, the four aromatic regions at δ 8.47, 7.64, 7.87 and 8.79 were assigned to H-8, H-9, H-10 and H-11, respectively. **^{13}C-NMR (**δ, AV-III-HD 800 MHz Cryo-Probe CD3OD**)** showed the presence of seventeen (17)

carbons, one carbonyl groups (C=O) attached to C-7 at 181.67 ppm while the methylenedioxy group (-O-CH_2-O-) was attached to carbon at δ 102.80. Polarization transfer experiments (DEPT) were carried out with the last polarization pulse angle θ 90^0, 135^0 to determine the multiplicity of each carbon. DEPT-HSQC reveals the aromatic proton at 7.42 ppm was attached (C-102.39 ppm), 8.02 ppm (C-124.38 ppm), 8.74 ppm (C-143.11 ppm), 8.47 ppm (C-127.27 ppm), 7.64 ppm (C-127.72 ppm), 7.87 ppm (C-133.59 ppm), 8.79 ppm (C-126.79 ppm). The spectra and physical data were in complete concurrence with the literature (Hamid *et al*., 2015).

(-)-N-formylanonaine belongs to class of aporphines was obtained as a white powder but when dissolved in solvents like pyridine or methanol and allow to dry turns into a crystal like compound. The infrared (IR) **(γ_{max} ^{KBr} cm^{-1})** spectrum showed absorptions at 1658.0 cm^{-1} indicating the (N-CHO). The EI mass spectrum indicated other major peaks include m/z (%) 276.3 (2.5), 262.3 (6.0), 248.2 (18.6), 235.1 (100.0), 204.2 (9.3), 178.2 (21.6), 151.2 (9.0), 88.1 (9.7). ^{1}H- NMR (δ, AVANCE NEO 400 MHz C5D5N) showed a singlet at 8.37 ppm (N-CHO proton) and a doublet with coupling constant of 8Hz at 8.23 ppm on proton (C-11), an also three aromatic protons which appears downfield at 7.43 ppm (m, 1H), 7.32 ppm (m, 1H) and 7.28 ppm (d, 1H, J=0.8Hz) assigned to C-10, C-9 and C-8, respectively. Doublet doublet at 5.19 ppm corresponding to C-6a (J=4.4, 14Hz), while two doublets for the methyenedioxy protons appeared at 6.11 ppm and 6.02 ppm. The ^{13}C-NMR spectrum (δ, AVANCE NEO 400 MHz C5D5N) of N-formylanonaine showed the presence of 18 carbons. Polarization transfer experiments (DEPT) were carried out with the last polarization pulse angle θ 90^0, 135^0 to determine the multiplicity of each carbon. The presence of carbonyl group was confirmed by the signal at 162.3 ppm. The resonance at 101.5 ppm was assigned to the –OCH_2O- carbon. The aromatic methine carbons afforded signals at 128.2 ppm, 127.7 ppm, 127.6 ppm and 127.5 ppm (C-8, C-9, C-10 and C-11carbon atom, respectively), while the quaternary carbons appeared at 135.2 ppm (C-7a), 131.1 ppm (C-11a), 127.4 ppm (C-3a) and 127 (C-1b). The spectra and physical data were in complete concurrence with the literature (Hui-Min *et al*., 2010).

Columbin is a diterpenoid of the clerodane series or a furanoid diterpenoid. Its low resolution electron impact (EI) mass spectrum showed other major fragmentation at m/z 340.2(1.4), 314.2 (22.9), 296.2 (8.2), 268.2 (4.2), 246.2 (53.9), 231.1(79.2), 220.1(16.4),

204.1(43.0), 190.1(20.5), 161.0(23.8), 152.0 (77.7), 121.0 (53.5), 107.0 (100.0), 94.0 (33.9), 81.0 (21.6), 54.9 (11.9), 40.96 (10.5). The IR spectra of columbin compound displayed bands pertinent to lactone moiety around (1746.9 cm^{-1}, 1703.3 cm^{-1}) and hydroxyl moiety around (3503.5 cm^{-1}). In the proton NMR, signals at δ 7.59, 7.49 and 6.55 obtained were allocated to the β-substituted furan moiety. Also singlets accounting for three protons each at δ 0.99 and δ 1.21 were duly assigned to the tertiary methyl are attached to C-19 and C-20, respectively. The resonance at δ 5.57 was ascribed to the proton at C-12 bearing the furan moiety. The ^{13}C-NMR (δ, AVANCE AV-400 MHz **CD3OD**) showed the presence of twenty carbons. ^{13}C-NMR also reveals two carbonyl groups (C=O) attached to C-18 and C-17 around δ 177.26 and δ 176.77, respectively. The protonated carbons of the furan ring gave signals at 109.68 (C-16), 141.47 (C-14) and 145.00 (C-15) ppm, while the signal of the quaternary carbon (C-13) of the furan ring appeared at 126.72 ppm. The spectra and physical data were in complete concurrence with the literature (Rathnasamy *et al*., 2016).

8-hydroxycolumbin is a diterpenoid of the clerodane series or a furanoid diterpenoid. Its low resolution electron impact (EI) mass spectrum showed other major fragmentation appeared at m/z (%) 356.3 (1.0), 330.3 (3.8), 312.2 (1.5), 263.2 (32.7), 245.2 (12.8), 234.2 (64.4), 204.1 (48.0), 192.1 (74.4), 169.1 (52.5), 124.0 (100.0), 109.0 (67.3), 81.0 (38.2), 43.9 (20.2). The IR spectra of 8-hydroxycolumbin compound displayed three strong bands pertinent to lactone moiety around (1756.5 $cm^{-1}$and 1707.3 cm^{-1}) and hydroxyl moiety around (3549.8 cm^{-1}). In the ^{1}H-NMR, signals at δ 7.57, 7.49 and 6.53 obtained were allocated to the β-substituted furan moiety. Also singlets accounting for three protons each at δ 1.03 and δ 1.16 were duly assigned to the tertiary methyl are attached to C-19 and C-20, respectively. The resonance at δ 5.56 was ascribed to the proton at C-12 bearing the furan moiety. The ^{13}C-NMR (δ, AVANCE AV-400 MHz CD3OD) showed the presence of twenty carbons. ^{13}C-NMR also reveals two carbonyl groups (C=O) attached to C-18 and C-17 around δ 177.24 and δ 175.24, respectively. The protonated carbons of the furan ring gave signals at δ 109.73 (C-16), 145.00 (C-15) and 141.41 (C-14) ppm, respectively while the signal of the quaternary carbon (C-13) of the furan ring appeared at 127.05 ppm. The spectra and physical data were in complete concurrence with the literature (Oguakwa *et al*., 1986).

Tinosporide belongs to class of a furanoid deterpenoid. Its low resolution electron impact (EI) mass spectrum showed other major fragmentation appeared at m/z (%) 328.3(4.1),

316.2(3.3), 275.2(23.4), 259.2, 192.2, 181.1, 135.1, 124.1, 107.1, 94.1, 81.1, 55.0. The **IR** bands at 1762.2, 1705.9 cm^{-1} showed the presence of a d-lactone. Also bands for hydroxyl (3510.3 cm^{-1}) and epoxide (3083.1 cm^{-1}) were detected. The ^{1}H-NMR displayed signals at 7.60 ppm (1H, br s), 7.50 ppm (1H, br s) and 6.56 ppm (1H, br s) assignable to the protons of the β-substituted furan moiety. Two angular methyls were observed as singlets at 1.16 ppm and 1.21 ppm. The signals at 5.69 ppm (dd, 1H, J=4, 12Hz) was assigned to the C-12 proton, bearing the b-substituted furan moiety. The signals at the aliphatic region 2.34 ppm (dd, 1H, J=4.0, 14.5Hz;H11a), 1.94 ppm (dd, 1H, J=12, 15Hz;H11b) were attributed to the C-11 methylene protons. The signals at 4.97 ppm (d, 1H, J=2.5Hz), 3.86 ppm (dd, 1H, J=3Hz), 3.63 ppm (d, 1H, J=4.00Hz) were given to protons on C-1, C-2 and C3 of ring A, respectively. From the ^{13}C-NMR and DEPT-135 experiments of Tinosporide**,** six methyls, three methylenes, six methines, four furanoid carbons, three quarternary carbons and two lactone carbonyls were detected. The spectra and physical data were in complete concurrence with the literature (Rathnasamy *et al*., 2016).

Tinosporicide is a diterpenoid of the clerodane series or a furanoid diterpenoid. Tinosporicide showed a UV spectrum characteristics for furanoid deterpenoids with λ_{max} (methanol) at 215 nm (A 0.313), 220.00 nm (A 0.319). The IR spectrum (KBr) showed the presence of a hydroxyl group (ν_{max} 3486.1, 3150.6 cm^{-1}), lactone C=O (ν_{max} 1754.1, 1716.6 cm^{-1}) and furan ring (ν_{max} 1507.4, 886.6 cm^{-1}). Its low resolution electron impact (EI) mass spectrum showed other major fragmentation at m/z 345.3 (loss of $C_{19}H_{21}O_6$), 291.2 (loss of $C_{16}H_{19}O_5$), 252.1 (loss of $C_{13}H_{16}O_5$), 124.0 (loss of $C_8H_{12}O$), 95.0 (loss of C_6H_7O), 81.0 (C_5H_5O). The presence of two methyl group C-5 (C-19 protons) and C-9 (C-17 protons) was evident from the presence of two sharp, three proton singlets appearing at 1.64 ppm and 1.53 ppm, respectively. The chemical shift of the methyl group at C-9 is observed at high field due to the influence of the furan ring on the same side of the C-9 methyl group. The coupled system of protons was confirmed by COSY experiments. Strong cross peak was observed linking C-12 proton at 5.98 ppm with C-11a (2.30 ppm) and C-11b (2.06 ppm) in the COSY experiment. The coupling constant between C-11a and C-11b was found to be 14.4Hz which was due to the germinal coupling between them. Irradiation at 5.98 ppm (C-12 proton) resulted in each of the double doublets at 2.30 ppm (C-11a proton) and 2.06 ppm (C-11b proton) collapsing to simple doublets. Three other protons resonated to a doublet at 5.36 ppm with coupling constant of (J = 2Hz), a double doublet at 4.00 ppm (J = 4.4Hz) and a

doublet at 3.43 ppm (J = 4.8Hz) which were assigned to C-1, C-2 and C-3 protons, respectively. The three downfield signals in the aromatic region were assigned to the furan ring at 7.70 ppm (C-16), 7.59 ppm (C-15) and 6.68 ppm (C-14). ^{13}**C- NMR-**(δ, AVANCE NEO-400 MHz **C5D5N**) spectrum showed the presence of twenty carbons. Two sharp signals at 23.99 and 21.23 ppm were identified as the methyl carbons (C-5 methyl and C-9 methyl), respectively. The presence of two carbonyl group was confirmed by signals at 174.47 and 172.75 ppm which was assigned to C-18 and C-20, respectively. The protonated carbons of the furan ring gave signals at δ 140.45 (C-16), 144.30 (C-15) and 109.54 (C-14), respectively while the signal of the quaternary carbon (C-13) of the furan ring appeared at 126.68 ppm. The hydroxyl (OH) bearing quaternary carbons resonated at 71.4 and 81.83 ppm which were assigned to C-10 and C-4, respectively. The presence of an epoxide group in tinosporicide was indicated by the presence of OH signals at δ 50.45 and δ 27.50 which were assigned to C-2 and C-3, respectively. The spectra and physical data were in complete concurrence with the literature (Sultan, 1992).

Corydine a rare isoquinoline alkaloid, LR EI-MS (JEOL 600H1) reveals m/z (%): 341.1 (89.0), 340.2 (54.0), 326.1 (100.0), 324.1 (66.6), 311.2 (29.1), 310.1 (83.9), 295.1 (35.0), 280.2 (11.8), 268.1 (9.4), 252.1 (5.2), 181.2 (2.4), 155.1 (6.7), 44.0 (2.1), 42.1 (2.7). The ^{1}H-NMR analysis suggested an aporphine alkaloid due to multiplet signals around the upfield region of the spectra (2.33-3.19 ppm) and to aromatic protons around the downfield regions at δ 6.938/6.918 and δ 6.880/6.856 which appear as doublet each. ^{1}H-NMR also reveals presence of three methoxy group (-OCH_3) which resonate at 3.88 ppm, 3.85 ppm and 3.64 ppm. A methyl attached to the nitrogen (N-CH_3) was observed around 2.52 ppm. ^{13}C-NMR (AVANCE NEO 400 MHz, CD3OD) showed the presence of twenty carbons. DEPT-HSQC reveals the attachment of the three methoxy group at position 62.37 ppm (-OMe), 56.71 ppm (-OMe) and 56.42 ppm (-OMe). Also reveals one Nitrogen attached to methyl (N-Me) at 43.89 ppm. On HMBC, the methoxyl groups were attached to C-10, C-2 and C-11 at 153.10, 150.56 and 144.71, respectively. Corydine a rare isoquinoline alkaloid has been previously reported for the first time from *Tinospora cordifolia*, cultivar of Central Institute of Medicinal and Aromatic Plants (CIMAP) Gene bank, Lucknow, India (Singh and Chaudhuri, 2015).

Oxoglaucine is a new aporphinoid alkaloid. LREI-MS of oxoglaucine run on Instrument (JEOL 600H1) revealed: m/z (%): 351.0 (100.0), 336.1 (75.4), 320.2 (34.1), 308.1 (45.8), 292.2 (22.9), 277.1 (14.9), 264.1 (9.7), 250.1 (9.1), 234.1 (4.5), 222.1 (11.7), 207.2 (5.9), 194.1 (5.6), 175.6 (11.7), 165.1 (3.0), 151.1 (10.6), 136.1 (16.6), 125.1 (4.0), 110.1 (4.4), 96.1 (2.9), 88.0 (3.4), 69.1 (3.5), 44.0 (6.6), The aromatic protons resonated at 8.70 ppm, 8.69 ppm, 7.93 ppm, 7.82 ppm and 7.42 ppm. ^{1}H-NMR also reveals presence of four methoxy group (-OCH_3) which resonate at 3.97 ppm, 4.02 ppm, 4.03 ppm and 4.09 ppm. ^{13}C-NMR (AVANCE NEO 400 MHz, CD3OD) showed the presence of twenty carbons. DEPT-HSQC reveals the proton and carbon attachments. proton 8.70 ppm (C-111.60 ppm), 8.69 ppm (C-144.94 ppm), 7.93 ppm (C-125.56 ppm), 7.82 ppm (C-110.36 ppm), 7.42 ppm (C-107.87 ppm), 4.09 ppm (C-56.85 ppm), 4.03 ppm (61.09 ppm), 4.02 ppm (C-56.52 ppm) and 3.97 ppm (C-56.31 ppm). The four methoxy's resonated at 61.09 ppm (-OMe), 56.85 ppm (-OMe), 56.52 ppm (-OMe), 56.31 ppm (-OMe). ^{13}C-NMR also reveals the presence of one carbonyl groups (C=O) attached to C-7 at 182.38 ppm. The four methoxy's are attached to carbons around 150.9 ppm, 153.0 ppm, 155.6 ppm and 158.62 ppm. The isolation of Oxoglaucine was once reported from *Chasmanthera dependens* Hochst family Menispermaceae (Ohiri *et al*., 1982). Oxoglaucine is therefore been reported for the first time in *Tinospora cordifolia* and from the genus Tinospora.

re l - (2 S , 3 S , 4R, 1 6E) - 2 - [(2 'R) - 2 ' - hydroxy nonadecanoylamino]-heneicosadec-16-ene-1,3,4-triol a new compound belonging to a class of ceramides has been reported for the first time in Menispermaceae. Its low resolution electron impact (EI) mass spectrum on JEOL MS Route instrument showed major fragmentation at m/z (%): 774.4 (1.8), 760.5 (4.0), 732.5 (8.4), 718.5 (6.0), 693.3 (12.4), 679.4 (23.9), 665.3 (43.7), 647.3 (26.1), 620.3 (9.1), 592.3 (7.2), 524.3 (2.0), 467.1 (10.5), 453.2 (21.4), 439.2 (60.4), 422.2 (30.4), 408.2 (72.3), 394.2 (44.1), 384.1 (71.2), 370.1 (39.7), 357.0 (100.0), 339.1 (75.6), 308.1 (16.0), 298.1 (4.7), 280.0 (13.5), 265.1 (25.1), 226.1 (11.6), 125.0 (11.9), 97.0 (29.3), 83.0 (45.6), 69.0 (44.9), 59.9 (81.0), 43.0 (67.4). Its IR spectrum revealed several broad peaks in the range of 3816.0-3424.0 cm^{-1} characteristic of bonded N-H or O-H stretching, the amide carbonyl at 1618.7 cm^{-1}, followed by the N-H bending at 1551.9 cm^{-1}. The long aliphatic chain was characterized by a band at 721.1 cm^{-1}. The ^{1}H-NMR spectrum showed characteristic signal for an amide proton at δ 8.59 (d, 1H, J=9.2Hz), resonances for

four hydroxyl groups at δ 7.63, 6.70 (d, 2H, J=6.4Hz) and 6.22 (d, 1H, J=6.4Hz), all appearing as broad singlet; a signal at δ 5.12 (m, H-2) for a methine bonded to a nitrogen; signals at δ 4.53 (dd, J=6.4Hz, H-1a) and 4.44 (dd, 1H, J=4.8Hz, H-1b) for a hydroxymethylene, as well as signals at δ 4.62 (m, 1H,H-2´), 4.37 (dd,1H, J=6Hz, H-3) and 4.29 (d,1H,J=6.4Hz, H-4) corresponding to three oxymethines. Additionally, signals for a double bond at δ 5.64 (td, J=15.4 and 5.4 Hz, H-16) and 5.52 (td, J=15.4 and 5.8 Hz, H-17), two terminal methyl at δ 0.85 (dd, 5H, J=4.8Hz, 5.2Hz, 3H-19´/3H-21) and several methylene hydrogens at δ 2.26-1.24 corresponding to two aliphatic chains were also observed. The COSY spectrum revealed coupling for the methine attached to the nitrogen (H-2) with the oxymethylene (2H-1) and an oxymethine (H-3) protons, and the latter with the oxymethine H-4. As expected, the ^{13}C-NMR spectra exhibited three downfield carbon signals at δ 175.23 (C-1'), 131.30 (C-16) and 131.11 (C-17) corresponding to a carbonyl amide and a double bond, respectively. Signals for a nitrogenated methine at δ 53.00 (C-2), an oxymethylene at δ 62.06 (C-1) and three oxymethynes at d 76.81 (C-3), 73.03 (C-4) and 72.48 (C-2'). In addition, several carbon signals in the range of δ 35.73-22.94 related to methylene groups and a carbon signal at 14.28 corresponding to two terminal methyls were also deduced from ^{13}C-NMR spectra, suggesting that compound was a ceramide. The unequivocal positions of the hydroxyl groups were deduced based on the HMBC spectrum in which the proton signal at δ 8.59 (NH) showed correlations with the carbonyl (C-1') and the nitrogenated methine (C-2), while the proton signal at δ 5.12 (H-2) exhibited correlations with the carbon signals at δ 62.06 (C-1), 76.81 (C-3) and 73.03 (C-4). Furthermore, HMBC correlation between the proton signal at δ 4.62 (H-2´) and the carbonyl (C-1') confirmed the presence of a side chain of a α-hydroxy fatty acid. re l - (2 S , 3 S , 4R, 1 6E) - 2 - [(2 'R) - 2 ' - hydroxy nonadecanoylamino]-heneicosadec-16-ene-1,3,4-triol belonging to a class of ceramides is been reported for the first time in *Tinospora cordifolia* and from the genus Tinospora. The spectra and physical data were in complete concurrence with the literature (Maia *et al*., 2010).

Palmatine is protoberberine isoquinoline alkaloids. LR-EI-MS of palmatine run on Instrument (JEOL 600H2) revealed: m/z (%): 351.2 (94.2), 336.2 (100.0), 321.2 (30.2), 308.2 (14.4), 292.2 (22.4), 278.2 (11.7), 264.2 (3.2), 248.1 (5.7), 236.2 (2.8), 220.2 (4.7), 206.2 (2.9), 191.2 (2.2), 176.1 (4.1), 145.2 (2.0), 102.2 (4.3), 95.6 (4.5), 89.1 (2.4), 46.1

(5.1), 44.1 (8.1). The proton NMR reveals the presence of four methoxy (-OCH_3) groups which resonated at 3.93 ppm, 3.98 ppm, 4.10 ppm and 4.20 ppm. The aromatic protons resonated as a singlet at 7.04 ppm, as a singlet at 7.66 ppm, as a doublet at 7.99 ppm with coupling constant of 9.2 Hz, as a doublet at 8.10 ppm with coupling constant of 9.2 Hz, as a singlet at 8.79 ppm and as a singlet at 9.75 ppm. The signals at δ 8.10 (1H, d, J = 9.2 Hz, H-11) and δ 7.99 (1H, d, J = 9.2 Hz, H-12) indicated a pair of *ortho* –coupled aromatic protons. There were also two methylene signals at δ 4.93 (2H, t, J = 8.0 Hz, H-6) and δ 3.29 (2H, t, J = 6.0 Hz, H-5) which were shown to be coupled on the ^{1}H-^{1}H COSY spectrum. The appearing of these methylene signals downfield indicated the presence of an electron withdrawing centre such as nitrogen or oxygen. Electron withdrawing groups cause a shift of methylene signals from δ 1.3-0.8 downfield. The ^{13}C-NMR spectrum (δ, AVANCE NEO-400 MHz CD3OD) of palmatine showed the presence of 21 carbons. The ^{13}C-NMR spectrum confirmed presence of aromatic carbons. There were six signals attributable to hydrogenated aromatic carbons at δ 146.4, 121.2, 124.4, 128.1, 109.9 and 112.2. The signal at δ 146.4 indicated a carbon was next to an electron withdrawing centre. The methylene carbon signal downfield at δ 56.6 confirmed presence of nitrogen atom. The other methylene carbon signal appeared at δ 27.8. There were also nine quaternary carbon signals which could be identified on the HSQC spectrum. These had no protons attached to them and they appeared at δ 153.8, 150.9, 128.1, 121.2, 143.6, 151.9, 139.8, 130.1, 135.3 and 120.5. The methoxy (-OCH3) groups are attached to carbon at 56.9 ppm, 57.3 ppm, 62.5 ppm and 57.6 ppm on DEPT-HSQC but are attached to carbon at 153.8 ppm, 150.9 ppm, 151.9 ppm and 146.4 ppm, respectively on HMBC. These enabled determination of the exact positions of the methoxy groups on the aromatic rings system. DEPT-HSQC revealed that the aromatic protons are attached to the following carbons 7.04 ppm singlet (C-112.2 ppm), 7.66 ppm singlet (C-109.9 ppm), 8.10 ppm doublet (C-128.1 ppm), 7.99 ppm doublet (C-124.4 ppm), 8.79 ppm singlet (C-121.2 ppm) and 9.75 ppm singlet (C-146.4 ppm). The spectra and physical data were in complete concurrence with the literature (Ling-Ling *et al*., 2014).

5-hydroxymethylfurfural is a member of the class of furans that is furan which is substituted at positions 2 and 5 by formyl and hydroxymethyl substituents, respectively. Its low resolution electron impact (EI) mass spectrum on JEOL 600H-1 instrument showed major fragmentation at m/z (%): 126.1 (63.9), 109.0 (19.2), 97.0 (100.0), 81.0 (5.8), 69.1

(45.2), 53.0 (22.7), 41.0 (97.0). ^{1}H- NMR reveals the presence of an aldehyde (CHO) which resonate around 9.51 ppm as a singlet, the methylene hydroxygroup (OH) resonate around 4.60 ppm as a singlet, while the furan ring resonate as a doublet, 1H each with a coupling constant of 3.6 Hz around 7.37 ppm and 6.57 ppm, respectively. ^{13}C- NMR-(δ, AVANCE NEO 300 MHz CD3OD): showed the presence of six carbons. Polarization transfer experiments (DEPT) were carried out with last polarization angles at 135^{0}, 90^{0} to determine the multiplicity of each carbon atom. DEPT 135^{0} reveals the presence of one methylene (CH_2) at 57.57 ppm and five methine groups (CH) which resonate around δ 179.4, 163.1, 153.6, 124.9 and 110.8. DEPT-HSQC reveals that proton 9.51 ppm is attached to carbon at 179.43 ppm (CHO), 7.37 ppm doublet with coupling constant of 3.6 Hz is attached to carbon at 124.8 ppm, 6.57 ppm also a doublet with coupling constant of 3.6 Hz is attached to carbon at 110.8 ppm which account for the furan ring and proton 4.60 ppm attached to carbon 57.57 ppm (OH). The molecule consists of a furan ring, containing both aldehyde and alcohol functional groups. This compound is reported for the first time in the species *Cola hispida*.

2-hydroxyquinoline-4-carboxylic acid is a quinolinemonocarboxylic acid. It is a conjugate acid of a 2-oxo-1,2-dihydroquinoline-4-carboxylate. Its low resolution electron impact (EI) mass spectrum on JEOL 600H-1 instrument showed major fragmentation at m/z (%): 189.1 (100.0), 172.1 (2.6), 161.1 (26.7), 144.1 (55.0), 132.1 (4.5), 117.1 (50.7), 104.0 (2.7), 89.0 (19.4), 75.0 (3.9), 63.0 (9.3), 50.9 (3.7), Its IR spectrum revealed several broad peaks in the range of 3415.4-3108.8 cm^{-1} characteristic of bonded N-H or O-H stretching. ^{1}H- NMR reveals the position of the acid which resonate at δ 13.2 (-COOH), the aromatic protons resonate around δ 7.66 as broad singlet, δ 7.55-7.48 as multiplets, δ 7.25-7.21 multiplets and at δ 8.82 as doublet with coupling constant of 8Hz which is a characteristics of quinoline ring. ^{13}C-NMR-(δ, AV-III-HD 800 MHz Cryo-Probe CD5D5N) showed the presence of ten carbons. ^{13}C-NMR also revealed that the acid is attached to carbon at δ 169.05. DEPT-HSQC reveals that proton at 8.82 ppm is attached to carbon at 127.73 ppm, proton at 7.66 ppm is attached to carbon at 124.88, proton at 7.55-7.48 ppm is attached to carbon at δ 115.95, δ 130.85 and proton at 7.25-7.21 ppm is attached to carbon at 122.32 ppm. The spectra and physical data were in complete concurrence with literature (Zhiwei *et al*., 2017). This compound is reported for the first time in the species *Cola hispida*.

5.8 Biological activities of isolated compounds

5.8.1 Acetylcholinesterase inhibitory activity of isolated compounds

Many studies described alkaloids as the main compounds capable of inhibiting AChE enzyme (Ortega *et al*., 2004). Studies have pointed out several new classes of secondary metabolites as potent inhibitors of AChE enzyme, such as flavonoids (Hillhouse *et al*., 2004), flavones (Sawasdee *et al*., 2009), as well as steroids, terpenoids, oils, and other phenolic compounds (Ji and Zhang, 2008).

In this study, the compounds isolated were evaluated for their acetylcholinesterase (AChE) inhibitory activities. Oxoglaucine (Oxoaporphinoid alkaloid) isolated from ethyl acetate fraction of *Tinospora cordifolia* stem exhibited the highest AChE inhibitory activity (IC_{50} of 0.803±0.09 mg/mL) compared to eserine (IC_{50} = 0.532±0.34 mg/mL). Liriodenine and N-formylanonaine also belonging to the class of aporphine alkaloids also demonstrated good acetylcholinesterase inhibitory activity with IC_{50} of 0.807±0.07 mg/mL and 0.819±0.06 mg/mL, respectively at 1 mg/mL. Also, a protoberberine isoquinoline alkaloid known as palmatine isolated from aqueous methanol fraction also showed considerable inhibition of acetylcholinesterase with IC_{50} of 0.837±0.07 mg/mL. This indicates that alkaloid compounds have the potential to increase the half-life of acetylcholine in the brain thereby improving learning and memory as compared to other classes of compounds isolated.

5.8.1.1 Molecular docking study on Anticholinesterase

New molecular modeling tactics, driven by rapidly improving computational platforms, have allowed many success stories for the use of computer-assisted drug design in the discovery of new mechanism- or structure-based drugs. Berberine, an isoquinoline alkaloid isolated from the dried rhizome of *Rhizoma coptidis* showed promising cholinesterase inhibitory potentials with mostly hydrophobic interactions with the enzyme (Ji *et al*., 2012). The possible interactions among geissospermine (indole-indoline alkaloid) isolated from *Geissospermum vellosii* and AChE of the Pacific electric ray were studied by molecular docking; hydrogen bonds, hydrophobic interactions and p-p stacking were involved (Araujo *et al.,* 2011). Infractopicrin an indole alkaloid isolated from *Cortinarius infractus* binds preferentially to the oxyanion hole of the AChE enzyme by p-p interactions with the aromatic residues (Geissler *et al*., 2010).

Molecular modeling studies were carried out in order to probe the binding mode of putative inhibitors against *Tetronarce californica* (Pacific electric ray) acetylcholinesterase (AChE). In this connection, a PDB (PDB ID:10CE) complexed with an inhibitor MF268 (physostigmine analogue 8-(cis-2,6-dimethylmorpholino)octylcarbamoyleseroline) was chosen and the compounds were docked using the coordinates of the cognate ligand (Fukuto, 1990).

The top ranked docked pose of stigmasterol is extensively stabilized with numerous hydrophobic interactions and also a hydrogen bond with GLU 199 (1.77). The top ranked pose of 8-hydroxycolumbin forms numerous hydrophobic interactions with ASP 72, TRP 84 , PHE 330 and a number of hydrogen bonds with TYP70 (2.76), GLU73 (2.66), PHE 288 (2.04), ARG289 (2.47) and PHE 331(2.82). The top ranked docked pose of palmatine forms a hydrogen bond with the side chain of TYR 130 (2.86). A number of hydrophobic interactions are also formed with Phe 330 and TYR 334. The top ranked docked pose of corydine shows a hydrophobic bond with TRP 84 and a salt bridge with GLU 199. The top-ranked simulated pose of oxoglaucine is characterised with a hydrogen bond with TYR 121 (3.19). The ligand also mediates a hydrophobic interaction with TRP 84 which stabilizes the interaction. The top ranked docked pose of tinosporide forms a number of hydrophobic interaction and hydrogen bonds with Glu 199. The top ranked docked pose of liriodenine forms a hydrophobic interaction with TRP 84 and pi-stacking interactions with TRP 84 and PHE 330. The top ranked docked pose of columbin show that there are four hydrophobic interactions of columbin with ASP 72, TRP 84A, Phe 330A as well as another hydrogen bond with GLU199 (1.77). The top ranked docked pose of 1-octacosanol forms a number of hydrophobic interactions with TRP 84, TRP279, LEU 282 and PHE 331 which stabilize it in binding pocket. The top ranked dock pose of β-sitosterol forms hydrophobic interactions with TRP279, PHE 290, PHE 330, PHE 331 and TRY 334. The top ranked docked pose of –(-N)-formylanonaine forms hydrophobic interactions with TRP 84 and PHE 330. There are also two pi-stacking interactions with TRP 84 and one with PHE 330. The top ranked docked pose of 5-hydroxymethylfurfural forms a Pi Stacking interaction with TRP 84. The top ranked docked pose of 2-hydroxyquinoline-4-carboxylic acid forms a number of hydrophobic interactions and hydrogen bonds with GLU199 (3.00) and TYR 130 (2.86) and pi-stacking interactions with TRP84 and PHE330. Free-energy scores show strong affinity of the inhibitors for the enzyme binding pocket. The estimated free energy of binding (ΔG)

for the target molecule, AChE with stigmasterol, 8-hydroxycolumbin, palmatine, corydine, oxoglaucine, tinosporide, liriodenine, columbin, 1-octacosanol, β-sitosterol, –(-N)-formylanonaine, 5-hydroxymethylfurfural and 2-hydroxyquinoline-4-carboxylic were found to be -7.32, -7.18, -7.25, -7.45, -7.55, -7.49, -6.18, -7.13, -7.65, -7.42, -6.33, -4.45 and -5.27 kcal/mol, respectively. This is an indication that the tested compounds can improve memory and learning or delay the neurodegenerative process essential in conditions such as Alzheimer's disease due to their abilities to bind to the catalytic/inhibitor site with moderate energy and thus proposedly mediate competitive inhibition of the enzyme. The binding affinity of the compounds tested with AChE are comparable to that of the approved standard drugs by US-FDA like donepezil (Aricept), rivastigmine (Exelon), galantamine (Reminyl) and tacrine (Cognex) which have estimated free energy of binding to be 3.58, -5.61, -7.86 and -6.95 kcal/mol, respectively in a study conducted by (Jagmohan *et al*., 2011).

5.8.2 Prolyl endopeptidase inhibitory activity

Prolyl endopeptidase (PEP) is a serine protease which is known to play a role in degradation of proline containing neuropeptides involved in the processes of learning and memory. There are many proline containing biologically active peptides, often neuropeptides. Because proline is the only amino acid with a secondary amine group, it confers special secondary structure to peptides, and its presence in the peptide chain confers resistance to degradation by most proteases. Thus, prolyl endopeptidase (PEP) has been considered to be the specific hydrolyser of proline containing neuropeptides (García-Horsman *et al*., 2007). It is found widely distributed among various organs, particularly in the brain of patients with amnestic disorders (Irazusta *et al*., 2002). PEP inhibitors are expected to exert their beneficial effects by increasing the brain levels of those neuropeptides which may improve and restore cognitive functions and protect vulnerable nerves against damage and cell death (Umemura *et al*., 1999, Vendeville *et al*., 1999). Therefore, they are considered to have therapeutic potential against Alzheimer's disease. Inhibition of prolyl endopeptidase (PEP) is also considered a promising strategy for AD treatment. Berberine a natural alkaloid isolated from *Rhizoma coptidis* has been reported to inhibit PEP in a dose-dependent manner (Tarrago *et al*., 2007).

In this study, the amount of p-nitroaniline (yellow) released is been measured spectrophotometrically and the compounds that inhibits the hydrolysis of substrate (Z-Gly-

pNA) by 50% was determined. Stigmasterol isolated from dicholoromethane fraction of *Phyllanthus muellerianus* leaf showed good prolyl endopeptidase inhibitory activity with IC_{50} value of 0.773±2.9 mM higher than oxoglaucine and corydine isolated from ethyl acetate fraction of *Tinospora cordifolia* stem which showed IC_{50} value of 0.780±3.1 mM and 0.788±3.17 mM at 1mM, respectively when compared with the standard Bacitracin with IC_{50} value of 0.125±1.5 mM. This indicates that the compounds tested have the potentials to prevent cleavage of proline containing neuropeptides in the brain thereby improving learning and memory.

5.8.2.1 Molecular docking study on Prolyl endopeptidase

Molecular modeling studies were carried out in order to examine the binding mode of active compounds against proline endopeptidase (PEP). In this connection, a homologous PDB was chosen and the compounds; Oxoglaucine, Corydine and Stigmasterol were docked using the coordinates of the cognate ligand. Prior to docking simulation, the redocking studies of cognate ligand were performed. The evaluation of Root Mean Square Deviation (RMSD) between Cartesian coordinates of the simulated and crystal pose serve as gold standard for the efficiency of a target. In our case, the RMSD between the two poses was found to be less than 1.5 Å.

The active site of the Proline Endopeptidase is part of a larger pocket that is virtually bounded by Phe461 and Arg579 (Li *et al*., 2010b). The top ranked docked pose of Oxoglaucine is characterised by two hydrogen bonds, with Tyr483 (2.93) and Ser670 (1.9). The ligand also mediates hydrophobic interactions with Tyr483 and with side chain of Arg535 which stabilize the interaction. The compound also forms a pi-cation interaction with the guanidium nucleus of Arg535 (3.92). The top-ranked simulated pose of Corydine as evident from the aporphine ring system exhibited hydrophobic contacts with the surrounding residues; Tyr456, Val473, Ile673 and Tyr674. These hydrophobic interactions accelerate the process of complexation (Young *et al*., 2007). The polar atoms of the ligand mediate hydrogen bonding interaction with the side chain of Arg535. Moreover, a hydrogen bond is also observed in between the hydroxyl group of Tyr674 and the N atom of aporphine. The contact is further stabilized by a special π-Cation Interactions between the guanidium nucleus of Arg535 and the ligand. The top ranked conformation of stigmasterol with the PEP enzyme shows hydrophobic interactions with Tyr458, Tyr483, Ala561, Val562, and

Ile673 stabilizing the ligand in the binding pocket. The estimated free energy of binding (ΔG) for the target molecule, PEP with stigmasterol, corydine, oxoglaucine were found to be -7.75, -6.56 and -6.60 kcal/mol, respectively as compared to standard bacitracin (-12.22 kcal/mol). This indicates that the docked compounds have the potentials to prevent cleavage of proline containing neuropeptides in the brain thereby improving learning and memory due to their ability to bind effectively to the active site of enzyme and cause an inhibition of PEP.

5.8.3 Metal chelating activity of isolated compounds

Metal-chelating activity is one of the antioxidant mechanisms since it reduces the concentration of the transition metal that catalyzes lipid peroxidation. Currently, several lipophilic metal chelators, such as clioquinol and its derivative PBT2, have been subjected to clinical trials, which have shown encouraging results in some AD patients (Faux *et al*., 2010). Ferrozine can quantitatively for complexes with ferrous iron yielding a red colour. However, in the presence of chelating agents, there is disruption of the formation of the complexes which leads to decrease in the red colour. Measurement of the colour gives estimation of the binding affinity of the co-existing chelators. Among the compound evaluated for their metal chelating potentials, oxoglaucine isolated from ethyl acetate fraction of *Tinospora cordifolia* stem gave good metal chelating activity with IC_{50} of 0.216±0.00 mg/mL alongside stigmasterol and 5-hydroxymethylfurfural which had IC_{50} of 0.283±0.00 mg/mL and 0.295±0.01 mg/mL at 1 mg respectively compared to standard EDTA with IC_{50} of 0.045±0.11 mg/mL. Overall, the results of antioxidant assay illustrate that oxoglaucine through its antioxidant property can effectively attenuate the ROS-mediated neuronal death in Alzheimer's disease.

5.9 Conclusion and recommendations

5.9.1 Conclusion

Alzheimer disease is a neurodegenerative disease currently without any effective treatment. Cholinesterase and prolyl endopeptidase inhibitors can alleviate symptoms, improving cognitive function due to their ability to increase acetylcholine half-life and prevent cleavage of neuropeptides, respectively in the brain. Nature is a source of new bioactive compounds and a source of inspiration for the synthesis of new ones with anti-cholinesterase

and anti-prolyendopeptidase activity with low side effect. The three plants selected *Phyllanthus muellerianus, Tinospora cordifolia* and *Cola hispida* displayed potent anti-cholinesterase and anti-proly endopeptidase activity. The research validates the folkloric use of plants in the family Euphorbiaceae, Menispermaceaae and Malvaceae in Nigerian ethnomedicine in the treatment of neurodegenerative disorders.

This research has also made possible the isolation and identification of nineteen compounds as possible cholinesterase and prolyl endopeptidase inhibitors from selected Nigerian medicinal plants. *Tinospora cordifolia* stem afforded thirteen (13) compounds identified as β-sitosterol, daucosterol, columbin, tinosporide, tinosporicide, 8-hydroxycolumbin, oxoglaucine, corydine, liriodenine, N-formylanonaine, palmatine, 1-octacosanol, rel-(2s,3s,4r,16e)-2-[(2'r)-2'-hydroxynonadecanoylamino]-heneicosadec-16-ene-1,3,4-triol. Oxoglaucine an oxoaporphine alkaloid and rel-(2s,3s,4r,16e)-2-[(2'r)-2'-hydroxynonadecanoylamino]-heneicosadec-16-ene-1,3,4-triol a ceramide are reported for the first time in the genus Tinospora while liriodenine is reported for the first time in the species. Four (4) compounds namely β-Sitosterol, 5-hydroxymethylfurfural, 2-hydroxyquinoline-4-carboxylic acid and β-Sitosterol glucoside (daucosterol) were isolated and reported for the first time from *Cola hispida*. Two (2) compounds namely stigmasterol and daucosterol was isolated and reported for the first time from *Phyllanthus muellerianus*.

Oxoglaucine, a new compound isolated from *Tinospora cordifolia* and stigmasterol isolated from *Phyllanthus muellerianus* showed high acetylcholinesterase and prolyl endopeptidase inhibitory activities compared to standards eserine and bacitracin, respectively. Oxoglaucine and stigmasterol can improve memory and learning or delay the neurodegenerative process essential in conditions such as Alzheimer's disease due to their abilities to bind to the catalytic/inhibitor site with moderate energy and thus proposedly mediate competitive inhibition of the enzyme. The two biomolecules could serve as potential leads for novel drug development for the management of Alzheimer's disease.

5.9.2 Contribution to Knowledge

1. The justification of the ethnomedicinal use of the research plants in the management of neurodegenerative diseases such as AD has been established.

2. Two compounds namely stigmasterol and daucosterol were isolated and reported for the first time from *Phyllanthus muellerianus*.
3. Oxoglaucine an oxoaporphine alkaloid is reported for the first time in the genus Tinospora while liriodenine is reported for the first time in the species *Tinospora cordifolia*.
4. re l - (2 S , 3 S , 4R, 1 6E) - 2 - [(2 ’R) - 2 ’ - hydroxy nonadecanoylamino]-heneicosadec-16-ene-1,3,4-triol a new compound belonging to a class of ceramides has been reported for the first time in Menispermaceae.
5. Four compounds namely β-Sitosterol, 5-hydroxymethylfurfural, 2-hydroxyquinoline-4-carboxylic acid and β-Sitosterol glucoside (Daucosterol) were isolated and reported for the first time from *Cola hispida*.
6. The molecular docking studies of the isolated compounds on PDB ID: 10CE (acetylcholinesterase) and 3IVM (prolyl endopeptidase) are been reported for the first time.

5.9.3 Recommendations

Following the outcome of the research, the following recommendations are presented:

i) The documentation of indigenous knowledge in Nigerian ethnomedicine should be encouraged because this knowledge can be passed on from generation to generation which may lead to several drug discoveries and Nigerian traditional medical practitioners should be trained in modern methods that could enhance their practice.

ii) Further investigation showing the pharmacokinetics (PK) and pharmacodynamics (PD) of the isolated acetylcholinesterase and prolyl endopeptidase inhibitory compounds needs to be conducted. Both together influence dosing, benefit and adverse effects.

iii) Further exploration of *Phyllanthus muellerianus, Tinospora cordifolia* and *Cola hispida* for isolation of potential bioactive compounds is recommended.

REFERENCE

Abou-Donia, A.H., Darwish, F.A., Toaima, S.M., Shawky, E., Takla, S.S. 2014. A new approach to develop a standardized method for assessment of acetylcholinesterase inhibitory activity of different extracts using HPTLC and image analysis. *Journal of Chromatography B* 955: 50-57.

Aburjal, T., Darwish, R.M., Al-Khalil, S., Mahgzah, A., Al-Abbdi, A. 2001. Screening of antibiotic resistant inhibitors from local plant materials against two different strains of *Pseudomonas aeruginosa*. *Journal of Ethnopharmacology* 76: 39-44.

Agyare, C., Lechtenberg, M., Deters, A., Petereit, F., Hensel, A. 2011. Ellagitannins from *Phyllanthus muellerianus* (Kuntze) Exell.: Geraniin and furosin stimulate cellular activity, differentiation and collagen synthesis of human skin keratinocytes and dermal fibroblasts. *Phytomedicine* 18.7: 617–624.

Agyare, C., Asase, A., Niehues, M., Lechtenberg, M., Deters, A., Hensel, A. 2009. Ethnopharmacological survey and *in vitro* confirmation of ethnopharmacological use of medicinal plants used for wound healing in Bosomtwe–Atwima–Kwanwoma area. *Ghana Journal of Ethnopharmacology* 125: 393–403.

Ahmad, V.U., Khan, A., Farooq, U., Kousar, F., Khan, S.S., Nawaz, S.A., Abbasi, M.A., Choudhary, M.I. 2005. Three new cholinesterase-inhibiting *cis*clerodane diterpenoids from *Otostegia limbata*. *Chemical and Pharmaceutical Bulletin* 53: 378–381.

Ahmad, V.U., Hussain, J., Hussan, H., Farooq, U., Akber, E., Nawaz, S.A., Choudary, M.I. 2004. Tow ceramides from *Tanacetum artemesioides*. Zeitschrift fur Naturforschung B-*A Journal of Chemical Sciences* 59: 329-333.

Akhondzadeh, S., Noroozian, M. 2002. Alzheimer's disease: pathophysiology and pharmacotherapy. *Drugs* 4: 1167-1172.

Ali, R., Sadoqi, M., Moller, S., Boutajangout, A., Mezei, M. 2018. Molecular dynamics and docking studies on acetylcholinesterase (AChE) inhibitors. *Biophysical Journal* 114.3: 340a.

Alzheimer's Association. 2015. *Alzheimer's Disease Facts and Figures*. *Alzheimer's and Dementia* 11.3: 332.

Alzheimer's Disease International. 2015. World Alzheimer Report. London.

Alzheimer's Disease International. 2004. *Drug Treatment in Dementia*. Fact Sheet 8. Updated April 2000. Last accessed March 09.

American Psychiatric Association. 1994. Diagnostic and statistical manual of metal disorders (4t' ed) Washington, DC, *American Psychiatric Association* 123-126,684.

Andrisano, V., Bartolini, M., Gotti, R., Cavrini, V., Felix, G. 2001. Determination of inhibitors' potency (IC_{50}) by a direct high performance liquid chromatographic method on an immobilized acetylcholinesterase column. *Journal of Chromatography B* 753: 375–383.

Appiah-Opong, R., Nyarko, A. K., Dodoo, D., Gyang, F. N., Koram, K. A., Ayisi, N. K. 2011. Antiplasmodial activity of extracts of *Tridax procumbens* and *Phyllanthus amarus* in *in vitro Plasmodium falciparum* culture systems. *Ghana Medical Journal* 45.4: 143–150.

Aqil, F., Khan, M.S., Owais, M., Ahmad, I. 2005. Effect of certain bioactive plant extracts on clinical isolates of ß-lactamase producing methicilin resistant *Staphylococcus aureus*. *Journal of Basic Microbiology* 45: 106-114.

Araújo, J.Q., Lima, J.A., Angelo da, C. P., Ricardo, B. A., Albuquerque, M.G. 2011. Docking of the alkaloid geissospermine into acetylcholinesterase: A natural scaffold targeting the treatment of Alzheimer's disease. *Journal of Molecular Modeling* 17:1401–1412.

Arbonnier, M. 2004. *Trees, Shrubs and lianas of West African dry zones*. CIRAD, Margraf Publishers, France.

Arendt, T., Bruckner, M.K., Lange, M., Bigl, V. 1992. Changes in acetylcholinesterase and butyrylcholinesterase in Alzheimer's disease resemble embryonic development-a study of molecular forms. *Neurochemistry International* 21: 381-396.

Attack, J.R., Perry, E.K., Bonham, J.R., Candy, J.M., Perry, R.H. 1986. Molecular forms of acetylcholinesterase and butyrylcholinesterase in the aged human central nervous system. *Journal of Neurochemistry* 47: 263-277.

Balandrin, M.F., Klocke, J.A., Wurtele, E.S., Bollinger, W.H. 1985. Natural plant chemicals: Sources of industrial and medicinal materials. *Science* 228:1154-1160.

Ballard, C.G. 2001. Advances in the treatment of Alzheimer's disease: benefits of dual cholinesterase inhibition. *European Neurology* 47.1: 64-70.

Barelli, H., Pelit, A., Hirsch, E., Wilk, S., De Nanteuil, G., Morain, P., Checler, F. S. 1999. 17092-1, a highly poleni, specific and celi permanent inhibitor of human proline endopeptidase. *Biochemical and Biophysical Research Communications* 257: 657-661.

Barrett, A.J., Rawlings, N.D. 1992. Oligopeptidases, and the emergence of the prolyl oligopeptidase family. *Biological Chemistry HoppeSeyler* 373: 353-360.

Barnes, C.A., Meltzer, J., Houston, F., Orr, G., McGann, K., Wenk, G.L. 2000. Chronic treatment of old rats with donepezil or galantamine: effects on memory, hippocampal plasticity and nicotinic receptors. *Neuroscience* 99.1: 17-23.

Bar-On, P., Millard, C.B., Harel, M., Dvir, H., Enz, A., Sussman, J.L., Silman, I. 2002. Kinetic and structural studies on the interaction of cholinesterases with the anti-Alzheimer drug rivastigmine. *Biochemistry* 41.11: 3555-3564.

Bartolucci, C., Perola, E., Cellai, L., Brufani, M., Lamba, D. 1999. "Back door" opening implied by the crystal structure of a carbamoylated acetylcholinesterase. *Biochemistry* 38: 5714–5719.

Benzie, I.F.F., Strain, J.J. 1999. Ferric reducing/antioxidant power assay: direct measure of total antioxidant activity of biological fluids and modified version for simultaneous measurement of total antioxidant power and ascorbic acid concentration, in: L. Packer (Ed.), Methods in Enzymology, 299: Oxidants and Antioxidants, Academic Press, Orlando, FL: 15–27.

Bilge, S., Ilkay, O. 2005. Discovery of drug candidates from some Turkish plants and conservation of biodiversity. *Pure and Applied Chemistry* 77:53-64.

Blennow, K., de Leon, M.J., Zetterberg, H. 2006. Alzheimer's disease. *Lancet* 368: 387–403.

Blennow, K. 2004. CSF biomarkers for mild cognitive impairment. *Journal of Internal Medicine* 256: 224–234.

Blois, M.S. 1958. Antioxidant determinations by the use of a stable free radical. *Nature* 181: 1199–1200.

Bores, G.M., Huger, F.P., Petko, W., Mutlib, A.E., Camacho, F., Rush, D.K., Selk, D.E., Wolf, V., Kosley, R.W., Davis, L., Vargas, H.M. 1996. Pharmacological evaluation of novel Alzheimer's disease therapeutics: acetylcholinesterase inhibitors related to galanthamine. *Journal of Pharmacology and Experimental Therapeutics* 277.2: 728-38.

Bossy-Wetzel, E., Schwarzenbacher, R., Lipton, S.A. 2004. Molecular pathways to neurodegeneration. *Nature Medicine* 10: S2-9.

Brand-Williams, W., Cuvelier, M.E., Berset, C. 1995. Use of a free radical method to evaluate antioxidant activity. *Food Science Technology* 28: 25–30.

Bratt, A.M., Kelly, M.E., Domeney, A.M., Naylor, R.J., Costall, B. 1996. Acute and chronic arecoline: Effects on a scopolamine-induced deficit in complex maze learning. *Pharmacology biochemistry and Behaviour* 53: 713-721.

Briskin, D.P. 2000. Medicinal plants and phytomedicines, linking plant biochemistry and physiology to human health. *American Society of Plant Physiology* 124: 507-514.

Brusotti, G. Cesari, I. Gilardoni, G. 2012. Chemical composition and antimicrobial activity of *Phyllanthus muellerianus* (Kuntze) Excel essential oil. *Journal of Ethnopharmacology* 142.3: 657–662.

Burkill, H. M. 2000. *The Useful plants of West Tropical Africa.* Vol. 5. 2nd ed. Royal Botanic Gardens, Kew. 686.

Burkill, H.M. 1985. *The useful plants of west tropical Africa*, Vol 5, Royal Botanic Gardens, Kew.

Bustamam, A., Ibrahim, S., al zubairi, A.S., Manal, M.E.T., Syam, M.M. 2008. Zerumbone: A natural compound with anticholinesterase activity. *American Journal of Pharmacology and Toxiology* 3: 209-211.

Butterfield, D.A., Lauderback, C.M. 2002. Lipid peroxidation and protein oxidation in Alzheimer's disease brain: potential causes and consequences involving amyloid beta-peptide-associated free radical oxidative stress. *Free Radical Biology and Medicine* 32.11: 1050–1060.

Butterfield, D.A., Sue, G., Gerald, M., Giulio M. P. 2002. Amyloid beta-peptide and amyloid pathology are central to the oxidative stress and inflammatory cascades under which Alzheimer's disease brain exists. *Journal of Alzheimer's Disease* 4.3: 193–201.

Chang, H.M., But, P.P. 2001. *Pharmacology and Application of Chinese Materia Medica* (vols. 1), World Sceintific, *Singapore* 551-553.

Changwong, N., Sabphon, C., Ingkaninan, K., Sawasdee, P. 2012. Acetyl- and butyryl-cholinesterase inhibitory activities of mansorins and mansonones. *Phytotherapy Research* 26: 392–396.

Choudhary, M.I. 2005. Juliflorine: a potent natural peripheral anionicsite- binding inhibitor of acetylcholinesterase with calcium-channel blocking potential, a leading candidate for Alzheimer's disease therapy. *Biochemical* and *Biophysical Research Communications* 332: 1171–1177.

Choudhary, M.I., Nawaz, S.A., ul-Haq, Z., Lodhi, M.A., Ghayur, M.N., Jalil, S., Riaz, N., Yousuf, S. 2005. Withanolides, a new class of natural cholinesterase inhibitors with calcium antagonistic properties. *Biochemical* and *Biophysical Research Communications* 334: 276–287.

Cirak, C., Radusiene, J. 2019. Factors affecting the variation of bioactive compounds in *Hypericum* species. *Biologia Futura* 70: 198–209.

Colovic, M. B., Krstic, D. Z., Lazarevic-Pasti, T. D., Bondzic, A. M., Vasic, V. M. 2013. Acetylcholinesterase Inhibitors:Pharmacology and Toxicology. *Current Neuropharmacology* 11: 315-335.

Conforti, F., Loizzo, M.R., Statti, G.A., Menichini, F. 2005. Comparative radical scavenging and antidiabetic activities of methanolic extract and fractions from *Achillea ligustica* ALL. *Biological and Pharmaceutical Bulletin* 28:1791–4.

Çulhaog˘lu, B., Gönül Yapar A., Tuncay Dirmenci C. 2013. Bioactive constituents of *Salvia chrysophylla* Stapf. *Natural Product Research* 27: 438–447.

Cygler, M., Schrag, J.D., Sussman, J.L., Harel, M., Silman, I., Gentry, M.K., Doctor, B.P. 1993. Relationship between sequence conservation and three-dimensional structure in a large family of esterases, lipases, and related proteins. *Protein Science* 2.3: 366-382.

Dairam, A., Limson, J.L., Watkins, G.M., Antunes, E., Daya, S. 2007. Curcuminoids, curcumin, and demethoxycurcumin reduce lead-induced memory deficits in male wistar rats. *Journal of Agricultural and Food Chemistry* 55: 1039–1044.

Dalziel, J.M. 1937. *The Useful Plants of West Africa.* London, Crown Oversea Agent for the Colonies, 158.

Daniel, M. 2006. *Medicinal Plants: Chemistry and Properties*. vol.2, Science Publication, 24-36.

Darvesh, S., Grantham, D.L., Hopkins, D.A. 1998. Distribution of butyrylcholinesterase in the human amygdala. *Journal of Comparative Neurology* 393: 374-390.

Davis, K.L., Mohns, R.C., Maria, D. 1996. Cholinergic markers in elderly patients with early sings of Alzheimer's disease. *The Journal of American Medical Association* 281: 1401-1406.

De-Oliveria, A.M., Conserva, L.M., De-Souza Ferro, J.N., De-Almeida Brito, F., LyraLemos, R.P., Barreto, E. 2012. Antinociceptive and anti-inflammatory effects of octacosanol from the leaves of sabiceagrisea var. Grisea in mice. *International Journal of Molecular Sciences* 13: 1598-1611.

Dhingra, D., Goyal, P.K. 2008. Evidences for the involvement of monoaminergic and GABAergic systems in antidepressant-like activity of *Tinospora cordifolia* in mice. *Indian Journal of Pharmaceutical Sciences* 70.6: 761-67.

Dhuley, J.N. 1997. Effect of some Indian herbs on macrophage functions in ochratoxin A treated mice. *Journal of Ethnopharmacology* 58: 15-29.

Dickson, D.W. 1997. The pathogenesis of senile plaques. *Journal of Neuropathology & Experimental Neurology* 56: 321-339.

Dinis, T.C.P., Madeira, V.M.C., Almeida, M.L.M. 1994. Action of phenolic derivates (acetoaminophen, salycilate and 5-aminosalycilate) as inhibitors of membrane lipid peroxidation and as peroxyl radical scavengers. *Archives of Biochemistry* and *Biophysics* 315: 161-169.

Doughari, J.H., Sunday, D. 2008. Antibacterial activity of *Phyllanthus muellerianus*. *Pharmaceutical Biology* 46: 400–405.

Drug Treatment in Dementia. Fact Sheet 8. Updated April 2000. Last accessed March 09, 2004. Alzheimer's disease International.

Dua, J.S., Prasad, D.N., Tripathi, A.C., Gupta, R. 2009. Role of traditional medicine in neuropsychopharmacology. *Asian Journal of Pharmaceutical and Clinical Research* 2.2: 72-6.

Duke, J. A. 2001. *Handbook of Nuts*: Herbal Reference Library. CRC Press, 360.

Ekholm, M., Konschin, H. 1999. Comparative model building of human butyrylcholinesterase. *Journal* of *Molecular Structure* 467.2: 161-172.

Ellman, G.L., Courtney, K.D., Andres, V., Featherstone, R.M. 1961. A new and rapid colorimetric determination of acetylcholinesterase activity. *Biochemical Pharmacology* 7: 88–95.

Elufioye, T.O., Obuotor, E.M., Agbedahunsi, J.M., Adesanya, S.A., 2013. Acetyl andbutyryl cholinesterase inhibitory effect of *Peltophorum pterocarpum* (DC) Backerex K. Heyne (family Legumonosae). *Journal of Pharmacognosy* and *Phytotherapy* 5: 77–82.

Elufioye, T.O., Oladele, A.T., Cyril-Olutayo, C.M., Agbedahunsi, J.M., Adesanya, S.A. 2012. Ethnomedicinal Study and Screening of Plants Used for Memory Enhancement and Antiaging in Sagamu, Nigeria. *European Journal of Medicinal Plants* 2.3: 262-275.

Enz, A., Amstuz, R., Boddeke, H., Gmelin, G., Malanowski, J. 1993. Brain selective inhibition of acetylcholinesterase: a novel approach to therapy for Alzheimer's disease. *Progress in Brain research* 98: 431-438.

Faux, N.G., Ritchie, C.W., Gunn, A., Rembach, A., Tsatsanis, A., Bedo, J. 2010. PBT2 rapidly improves cognition in Alzheimer's disease: Additional phase II analyses. *Journal of Alzheimer's Disease* 20: 509–16.

Ferreira, A., Proença C., Serralheiro, M.L.M., Araújo, M.E.M. 2006. The *in vitro* screening for acetylcholinesterase inhibition and antioxidant activity of medicinal plants from Portugal. *Journal of Ethnopharmacology* 108.1: 31-37.

Figueiredo, A.C., Barroso, J.G., Pedro, L.G., Scheffer, J.J. 2008. Factors affecting secondary metabolite production in plants: volatile components and essential oils. *Flavour and Fragrance Journal* 23: 213–226.

Filiz, G., Price, K.A., Caragounis, A., Du, T., Crouch, P.J., White, A.R. 2008.The role of metals in modulating metalloprotease activity in the AD brain. *European Biophysics Journal* 37: 315–321.

Flamini, G., Antognoli, E., Morelli, I. 2001. Two flavonoids and other compounds from the aerial part of *Centaurea bracteata* from Italy. *Phytochemistry* 57: 559-564.

Formichi, P., Battisti, C., Radi, E., Federico, A. 2006. Cerebrospinal fluid tau, A beta, and phosphorylated tau protein for the diagnosis of Alzheimer disease. *Journal of Cellular Physiology* 208: 39–46.

Fortette, F., Rigaud, A.S., Morin, M., Gisselbrecht, M., Bert, P. 1995. Assessing vascular dementia. *Netherlands Journal* of *Medicine* 47.4: 185-195.

Fowler, D.G. 2006. *Traditional fever remedies: A list of Zambian plants*. University of Chicago Press: 1427 E. 60th Street Chicago, IL 60637 USA.

Friedland, R.P., Wilcock, G.K. 2000. Dementia. In: Evans, J.G., Williams, T.F., Beattie, B.L., Michel, J.P., Wilcock (Ed.) Oxford text book of geriatric medicine, 2nd edition, Oxford University Press, 922-932.

Fukami, T., Yokoi, T. 2012. The emerging role of human esterases. *Drug Metabolism* and *Pharmacokinetics* 27: 466–477.

Fukuchi, K., Accavitti-Loper, M.A., Kim, H.D., Tahara, K., Cao, Y., Lewis, T.L., Caughey, R.C., Kim, H. 2006. Amelioration of amyloid load by anti-Ab single-chain antibody in Alzheimer mouse model. *Biochemical* and *Biophysical Research Communications* 344: 79–86.

Fukuto, T. R. 1990. Mechanism of action of organophosphorus and carbamate insecticides. *In Environmental Health Perspectives* 87: 245-254.

García-Horsman, J.A., Männistö, P.T., Venäläinen, J. I. 2007. On the role of prolyl oligopeptidase in health and disease. *Neuropeptides* 41: 1–24.

Geissler, T., Brandt, W., Porzel, A., Schlenzig, D., Kehlen, A., Wessjohann, L., Arnold, N. 2010. Acetylcholinesterase inhibitors from the toadstool *Cortinarius infractus*. *Bioorganic* & *Medicinal Chemistry* 18: 2173–2177.

Geula, C., Mesulam, M.M. 1996. Systematic regional variations in the loss of cortical cholinergic fibres in Alzheimer's disease. *Cerebral Cortex* 6: 165-177.

Geula, C., Mesulam, M.M. 1999. Cholinergic system in Alzheimer's disease. In: Terry, R.D., Katzman, R., Bick, K.L., Sisodia, S.S. (Ed.) Alzheimer's disease. Second edition, Lippincott Williams and Wilkins, 269-292.

Geula, C., Schatz, C.R., Mesulam, M.M. 1993. Differential localization of NADPH diaphorase and calbindin-D28k within the cholinergic neurons of the basal forebrain, striatum and brainstem in the rat, monkey, baboon and human. *Neuroscience* 54: 461-476.

Giacobini, E. 2000. Cholinesterase inhibitors: from the Calabar bean to Alzheimer's therapy. In: Giacobini E (Ed.) Cholinesterases and cholinesterase inhibitors. London: *Martin Dunitz* 181-226.

Gnaju, L., Karan, D., Chanda, S., Srivastava, K.K., Sawhney, R.C., Selvamurthy, W. 2003. Immunomodulatory effects of agents of plant origin. *Biomedicine and pharmacology* 57: 296-300.

Gnatt, A., Ginzberg, D., Lieman-Hurwitz, J., Zamir, R., Zakut, H., Soreq, H. 1991. Human acetylcholinesterase and butyrylcholinesterase are encoded by two distinct genes. *Cellular and Molecular Neurobiology* 11.1: 91-104.

Govind, P., Madhuri, S. 2010. Pharmacological Activities of *Ocimum Sanctum* (Tulsi): A Review. *International Journal of Pharmaceutical Sciences Review and Research* 5.1: 61-65.

Greenblatt, H.M., Kryger, G., Lewis, T., Silman, I., Sussman, J.L. 1999. Structure of acetylcholinesterase complexed with (-)-galanthamine at 2.3 A resolution. *FEBS Lett*er 463.3: 321-326.

Greig, N.H., Utsuki, T., Yu, Q., Zhu, X., Holloway, H.W., Perry, T.A., Lee, B., Ingram, K.D., Lahiri, D.K. 2001. A new therapeutic target in Alzheimer's disease treatment: attention to butyrylcholinesterase. *Current Medical Research* and *Opinion* 17.2: 1-6.

Gudala, K., Bansal, D., Schifano, F., Bhansali, A. 2013. Diabetes mellitus and risk of dementia: A meta-analysis of prospective observational studies. *Diabetes Investigation* 4.6: 640–50.

Guo, J.W., Chen, J.M., Lin, L., Xu, F. 2012. Five chemical constituents of the ethyl acetate fraction from ethanol extract of *Semen litchi*. *Journal of Medicinal Plants Research* 6.11: 168-170.

Gupta, Y.K., Briyal, S., Gulati, A. 2010. Therapeutic potential of herbal drugs in cerebral ischaemia. *Indian Journal of Physiology* and *Pharmacology* 54.2: 99-122.

Haam, J., Yakel, J.L. 2017. Cholinergic modulation of the hippocampal region and memory function. *Journal of Neurochemistry* 142.2: 111–121.

Hall, W.C., Fitzpatrick, D., Klatt, L.L., Raczkowski, 1989. Cholinergic innovation of the superior colliculus in the cat. *Journal of Comparative Neurology* 287: 495-514.

Hallanger, A.E., Levey, A.I., Lee, H.J., Rye, D.B., Wainer, B.H. 1987. The origins of cholinergic and other subcortical afferents to the thalamus in the rat. *Journal of Comparative Neurology* 262: 105-124.

Hamid, H.A. Yusoff, M.M., Liu, M., Karim, M.R. 2015. α-Glucosidase and α-amylase inhibitory constituents of *Tinospora crispa*: Isolation and chemical profile confirmation by ultra-high performance liquid chromatography-quadrupole time-of-flight/mass spectrometry. *Journal of functional foods* 16: 74–80.

Hanks, G.R. 2002. *Narcissus and daffodil: the genus Narcissus*. In: Hanks GR (Ed.) Taylor & Francis Ltd: London. 428.

Harel, M., Schalk, I., Ehret-Sabattier, L., Bouet, F., Goeldner, M., Hirth, C., Axelsen, P., Silman, I., Sussman, J. 1993. Quaternary ligand binding to aromatic residues in the active-site gorge of acetylcholinesterase. *Proceedings of the National Academy of Sciences* 90: 9031-9035.

Heins, J., Welker, P., Schönlein, C., Born, I., Hartrodt, B., Neubert, K., Barth, A. 1988. Mechanism of proline-specific proteinases:(I) Substrate specificity of dipeptidyl peptidase IV from pig kidney and proline-specific endopeptidase from *Flavobacterium meningosepticum*. *Biochimica et Biophysica Acta (BBA)-Protein Structure and Molecular Enzymology* 954: 161–169.

Heiss, W.D., Zeiler, K. 1978. Drug influence on cerebral circulation. *Pharmacotherapie* 1: 137-144.

Heo, H.J., Kim, M.J., Lee, J.M., Choi, S.J., Cho, H.Y., Hong, B., Kim, H.K., Kim, E., Shin, D.H. 2004. Naringenin from *Citrus junos* has an inhibitory effect on acetylcholinesterase and a mitigating effect on amnesia. *Dementia and Geriatric Cognitive Disorders* 17: 151–157.

Herbert, L.E., Scherr P.A., Beckeff L.A. 1995. Age-specific incidence of Alzheimer's disease in a community population. *JAMA* 273: 1354-1359.

Hillhouse, B. J., Ming, D. S., French, C. J., Towers, G. H. N. 2004. Acetylcholine esterase inhibitors in *Rhodiola rosea*. *Pharmaceutical Biology* 42.1: 68–72.

Hirschfeld, T. 1980. The hyphenated method. *Journal of Analytical Chemistry* 52: 297A–303A.

Hnatyszyn, O., Broussalis, A., Herrera, G. 1999. Argentine plant extracts active against polymerase and ribonucleaseHactivities of HIV-1 reverse transcriptase. *Phytotherapy Research* 13.3: 206–209.

Hodges, J.R. 2006. Alzheimer's centennial legacy: origins, landmarks and the current status of knowledge concerning cognitive aspects. *Brain* 129: 2811-2822.

Hostettmann, K., Borloz, A.U., Marston, A. 2006. Natural product inhibitors of acetylcholinesterase. *Current Organic Chemistry* 10: 825-847.

Houghton, P., Agbedahunsi, J., Adegbulugbe, A. 2004. Alkaloids from two Nigerian crinum species and their acetylcholinesterase inhibitory activity. *Journal of Pharmacy and Pharmacology* 56: S77-S78

Houghton, P.J., Howes, M.J. 2005. Natural Products and Derivatives affecting neurotransmission relevant to alzheimer's and parkinson's disease. *Neurosignals* 14: 6-22.

Houghton, P.J., Ren, Y., Howes, M.J. 2006. Acetylcholinesterase inhibitors from plants and fungi. *Natural Product Reports* 23: 181-199.

Howes, M.J.R., Nicolette, S.L.P., Houghton, P.J. 2003. Plant with traditional uses and activities, relevant to the management of alzheimer's disease and other cognitive disorders. *Phytotherapy Research* 17: 1-18.

Howes, M-JR., Houghton, P.J. 2003. Plants used in Chinese and Indian traditional medicine for improvement of memory and cognitive function. *Pharmacology Biochemistry and Behavior* 75.3: 513-527.

Huang, S.Y., Zou, X. 2010. Advances and challenges in protein-ligand docking. *International Journal of Molecular Sciences* 11: 3016–3034.

Hui-Min Wanga, Chung-Yi Chen, Chun-Yen Chen, Mei-Ling Ho, Yi-Ting Chou, Hou-Chien Chang, Chih-Hung Lee, Chau-Zen Wang, I-Ming Chu. 2010. (-)-N-Formylanonaine from *Michelia alba* as a human tyrosinase inhibitor and antioxidant. *Bioorganic & Medicinal Chemistry* 18: 5241–5247.

Hung, T.M., Luan, T.C., Vinh, B.T., Cuong, T.D., Min, B.S. 2011. Labdane-type diterpenoids from *Leonurus heterophyllus* and their cholinesterase inhibitory activity. *Phytotherapy Research* 25: 611–614.

Ingkanian, K., Phenga, P., Yuenyongsawad, S., Khohara. 2006. Acetylcholinesterase inhibitors from *Stephania venosa* tuber. *The Journal of Pharmacy and Pharmacology* 58: 695-700.

Ingkaninan, K., Best, D., Heijden, V.D., Hofte, A.J.P., Karabatak, B., Irth, H., Tjaden, U.R., Greef, V.D., Verpoorte, R. 2000. High-performance liquid chromatography with on-line coupled UV, mass spectrometric and biochemical detection for

identification of acetylcholinesterase inhibitors from natural products. *Journal of Chromatography A* 872: 61–73.

Ingkaninan, K., Temkitthawon, P., Chuenchom, K., Yuyaem, T., Thongnoi, W. 2003. Screening for acetylcholinesterase inhibitory activity in plants used in Thai traditional rejuvenating and neurotonic remedies. *Journal of Ethnopharmacology* 89: 261-264.

Irazusta, J., Larrinaga, G., Gonzalez-Maeso, J., Gil, J., Meana, J.J., Casis, L. 2002. Distribution of prolyl endopeptidase activities in rat and human brain. *Neurochemistry International* 40: 337–345.

Irazusta, J., Silveira, P.F., Gil, J., Varona, A., Casis, L. 2001. Effects of hydrosal~ne treatments on prolyl endopeptidase activity in rat tissues. *Regulatory Peptides* 101: 141-147.

Irshad, M., Zafaryab, M., Singh, M., Rizvi, M.M. 2012. Comparative analysis of the antioxidant activity of *Cassia fistula* extracts. *International Journal of Medicinal Chemistry* 2012: 157125.

Iuvone, D., Gerova, D., Chervenkov, T., Yankov, T. 2005. Polyphenol and antioxidant capacity of Bulgarian medicinal plants. *Journal of Ethnopharmacology* 96: 145-150.

Jagmohan, S., Ramanathan, K., Rao, S. 2011. Identification of Potential Inhibitors against acetylcholinesterase associated with alzheimer's diseases: A molecular docking approach. *Journal of Computational Methods* in *Molecular Design* 1.1: 44-51.

Jana, U., Chattopadhyay, R.N., Shw, B.P.1999. Preliminary studies on anti-inflammaory activity of *Zingiber officinale* Rosc., *Vitex negundo* Linn. and *Tinospora cordifolia* (Willid) Miers in albino rats. *Indian Journal* of *Pharmacology* 31.3: 232-233.

Ji, H.F., Shen, L. 2012. Molecular basis of inhibitory activities of berberine against pathogenic enzymes in Alzheimer's disease. *The Scientific World Journal* 2012: 823201.

Ji, H.F., Zhang, H.Y. 2008. Multipotent natural agents to combat alzheimer's disease. Functional spectrum and structural features. *Acta Pharmacologica Sinica* 29.2: 143–151.

Ji, R.W., Zhang, H.Y. 2005. A new strategy to combat alzheimer's disease, combinig radical scavenging potential with metal-protein attenuating ability in one molecule. *Bioorganic and Medicinal Chemistry Letters* 15: 21-24.

Jones, W.P., Chin, Y.W., Kinghorn, A.D. 2006. The role of pharmacognosy in modern medicine and pharmacy. *Current Drug Targets* 7: 247-264.

Joseph, J.A., Shukitt-Hale, B., Casadesus, G. 2005. Reversing the deleterious effects of aging on neuronal communication and behavior: beneficial properties of fruit polyphenolic compounds. *American Journal* of *Clinical Nutrition* 81: 313S–316S.

Kabuto, H., Asanuma, M., Nishibayashi, S., Lida, M., Ogawa, N. 1997. Chronic administration of Oren-gedoku-to (TJ15) inhibits ischemia-induced changes in brain indoleamine metabolism and muscarinic receptor binding in the Mongolian gerbil. *Neurochemical Research* 22: 33-36.

Kang, S.Y., Lee, K. Y., Sung, S. H., Park, M. J., and Kim, Y. C. 2001. Coumarins isolated from *Angelica gigas* inhibit acetylcholinesterase: structure-activity relationships. *Journal of Natural Products* 64: 683–685.

Kato, T., Okada, M., Nagatsu, T. 1980b. Distribution of post-proline cleaving enzyme in human brain and the peripheral tissues. *Molecular* and *Cellular Biochemistry* 32: 117–121.

Katsayal, U.A., Lamal, R.S. 2009. Preliminary Phytochemical and antibacterial screening of the ethanolic stem bark extract of *Phyllanthus muellerianus*. *Nigerian Journal of Pharmaceutical Sciences* 8: 121-125.

Kennedy, C. 2009. *Guduchi: The one who protects the body*. California College of Ayurveda. Ayurveda Research papers.

Khare, C.P. 2007. *Indian Medicinal Plants*, An Illustrated Dictionary, *Springer* 223.

Khosa, R.L., Prasad, S. 1971. Pharmacognostical studies on Guduchi (*Tinospora cordifolia* Miers). *Indian Journal* of *Medical* Research 6: 261-269.

Kim, J.K., Choi, S.J., Bae, H., Kim, C.R., Cho, H.Y., Kim, Y.J., Lim, S.T., Kim, C.J., Kim, H.K., Peterson, S., Shin, D.H. 2011. Effects of methoxsalen from *Poncirus trifoliata* on acetylcholinesterase and trimethyltin-induced learning and memory impairment. *Bioscience, Biotechnology*, and *Biochemistry* 75: 1984–1989.

Kim, J.Y., Lee, W.S., Kim, Y.S., Curtis-Long, M.J., Lee, B.W., Ryu, Y.B., Park, K.H. 2011. Isolation of cholinesterase-inhibiting flavonoids from *Morus lhou*. *Journal of Agricultural and Food Chemistry* 59: 4589–4596.

Kirtikar, K.R., Basu, B.D. 1975. *Indian Medicinal Plants*. Edn 2, Vol. 1, M/S Bishen Singh, Mahendra Pal Singh.

Kitchen, D.B., Decornez, H., Furr, J.R., Bajorath, J. 2004. Docking and scoring in virtual screening for drug discovery: methods and applications. *Nature Reviews Drug Discovery* 3: 935-949.

Kochler S. L. 1986. *Tropical Crops. A Textbook of Economic Botany*. Macmillan Publishers. 301-302.

Kosasa, T., Kuriya, Y., Matsui, K., Yamanishi, Y. 2000. Inhibitory effect of orally administered donepezil hydrochloride (E2020), a novel treatment for Alzheimer's disease, on cholinesterase activity in rats. *European Journal of Pharmacology* 389.2-3: 173-179.

Kumar, P.V., Shashidhara, S., Kumar, M.M., Sridhara, B.Y. 2000. Effect of *Luffa echinata* on lipid peroxidation and free radical scavenging activity. *Journal of Pharma Pharmacology* 52: 891-8.

Kumar, V.P., Chauhan, N.S., Padh, H., Rajani, M. 2006. Search for antibacterial and antifungal agents from selected Indian medicinal plants, *Journal of Ethnopharmacology* 107: 182-188.

Kumaran, K. 2007. Estimation of total flavonoid content in propolis by two complementary colorimetric methods. *Journal of Food and Drug Analysis* 10: 178–182.

Lannert, H., Hoyer, S. 1998. Intracerebroventricular administration of streptozotocin causes long-term diminutions in learning and memory abilities and in cerebral energy metabolism in adult rats. *Behavioural Neuroscience* 112: 1199-1208.

Lautenschlager, N.T., Cupples, L.A., Rao, V.S., Auerbach, S.A., Becker, R., Burke, J. 1996. Risk of dementia among relatives of alzheimer's disease patients in the mirage study: What is in store for the oldest old?. *Neurology* 46.3: 641–50.

Lawandi, J., Gerber-Lemaire, S., Juillerat-Jeanneret, L., Moitessier, N. 2010. Inhibitors of prolyl oligopeptidases for the therapy of human diseases: Defining diseases and inhibitors. *Journal of Medicinal Chemistry* 53: 3423–3438.

Lee, H.P., Zhu, X., Casadesus, G., Castellani, R.J., Nunomura, A., Smith, M.A., Lee, H., Perry, G. 2010. Antioxidant approaches for the treatment of alzheimer's disease. *Expert Review* of *Neurotherapeutics* 10: 1201–1208.

Lee, S. H., Jaganath, I. B., Wang, S.M., Sekaran, S. D. 2011. Antimetastatic effects of *Phyllanthus* on human lung (A549) and breast (MCF-7) cancer cell lines. *PLoS ONE* 6.6: Article ID e20994.

Lee, S., Han, S., Kim, H.M., Lee, J.M., Mok, S.Y., Lee, S. 2011. Isolation and identification of phytochemical constituents from *Taraxacum coreanum*. *Journal of Korean Society* for *Applied Biological Chemistry* 54: 73-78.

Lengauer, T., Rarey M. 1996. Computational methods for bimolecular docking. *Current Opinion in Structural Biology* 6: 402-406.

Lenta, B.N., Vonthron-Sénécheau C, Weniger B, Devkota KP., Ngoupayo, J., Kaiser, M., Naz, Q., Choudhary, M.I., Tsamo, E., Sewald, N. 2007. Leishmanicidal and

cholinesterase inhibiting activities of phenolic compounds from *Allanblackia monticola* and *Symphonia globulifera*. *Molecules* 12: 1548–1557.

Li, G., Sokal, I., Quinn, J.F., Leverenz, J.B., Brodey, M., Schellenberg, G.D., Kaye, J.A., Raskind, M.A., Zhang, J., Peskind, E.R., Montine, T.J. 2007. CSF tau/Abeta42 ratio for increased risk of mild cognitive impairment: a follow-up study. *Neurology* 69.7: 631–9.

Li, J.R., Wilk, E., Wilk, S. 1996. Inhibition of prolyl oligopeptidase by Fmoc-aminoacylpyrrolidine-2-nitriles. *Journal of Neurochemistry* 66: 2105-2112.

Li, M., Chen, C., Davies, D. R., Chiu, T. K. 2010a. Induced-fit mechanism for prolyl endopeptidase. *Journal of Biological Chemistry*, 285.28.: 21487–21495.

Li, M., Chen, C., Davies, D. R., Chiu, T. K. 2010b. Induced-fit mechanism for prolyl endopeptidase. *Journal of Biological Chemistry* 285.28: 21487–21495.

Ling-Ling Yu, Rong-Tao Li, Yuan-Bao Ai, Wei Liu, Zhang-Shuang Deng, Zhong-Mei Zou. 2014. Protoberberine Isoquinoline Alkaloids from *Arcangelisia gusanlung*. *Molecules* 19: 13332-13341.

Liu, J.S., Zhu, Y.L., Yu, C.M., Zhou, Y.Z., Han, Y.Y., Wu, F.W., Oi, B.F. 1986. The structures of huperzine A and B, two new alkaloids exhibiting marked anticholinesterase activity. *Canadian Journal of Chemistry* 64.4: 837-839.

Liu, Y., Nair, M.G. 2010. An efficient and economical MTT assay for determining the antioxidant activity of plant natural product extracts and pure compounds. *Journal of Natural Products* 73.7: 1193-1195.

Lo, Y.C., Teng, C.M., Chen, C.F., Chen, C.C., Hong, C.Y. 1994. Magnolol and honokiol from *Magnolia officinalis* protect rat heart mitochondria against lipid peroxidation. *Biochemical Pharmacology* 47: 549-553.

Loffler, T., Lee, S.K., Noldner, M., Chatterjee, S.S., Hoyer, S., Schliebs, R. 2001. Effect of *Ginkgo biloba* extract (EBG 761) on glucose metabolism-related markers in streptozotocin-damaged rat brain. *Journal of Neural Transmission* 108: 1457-1474.

Loizzo, M.R., Menichini, F., Conforti, F., Tundis, R., Bonesi, M., Saab, A.M., Statti, G.A., Cindio, B., Houghton, P.J., Menichini, F., Frega, N.G. 2009. Chemical analysis, antioxidant, anti-inflammatory and anticholinesterase activities of *Origanum ehrenbergii* Boiss and *Origanum syriacum* L. essential oils. *Food Chemistry* 117: 174-180.

Lopez, S., Bastida, J., Viladomat, F., Codina, C. 2002. Acetylcholinesterase inhibitory activity of some Amaryllidaceae alkaloids and *Narcissus* extracts. *Life Science* 71: 2521-2529.

López-Vallejo, F., Caulfield, T., Martínez-Mayorga, K., Giulianotti, M.A., Houghten, R.A., Nefzi, A., Medina-Franco, J.L. 2011. Integrating virtual screening and combinatorial chemistry for accelerated drug discovery. *Combinatorial Chemistry & High Throughput Screening* 14: 475–487.

Lovell, M.A., Robertson, J.D., Teesadale, W.J., Campbell, J.L., Markesberry, W.R. 1998. Copper, iron and zinc in Alzheimer's disease senile plaques. *Journal of the Neurological Sciences* 158: 47–52.

Loy, C.T., Schofield, P.R., Turner, A.M., Kwok, J.B.J. 2014. Genetics of dementia. *Lancet* 383: 828–40.

Lu, Y.H., Du, C.B., Liu, J.W., Wei, D.Z. 2001. Neuroprotective effects of *Hypericum perforatum* on trauma induced by hydrogen peroxide in PC 12 cells. *The American Journal of Chinese Medicine* 32: 397-405.

Maes, M., Goossens, F., Lin, A.H., De Meester, I., Van Gastel, A., Scharpe, S. 1998. Effects of psychological stress on serum prolyl endopeptidase and dipeptidyl peptidase IV activity in humans: higher serum prolyl endopeptidase activity is related to stress-induced anxiety, *Psychoneuroendocrinology* 23: 485-495.

Mahley, R.W., Weisgraber, K.H., Huang, Y. 2006. Apolipoprotein E4: A causative factor and therapeutic target in neuropathology, including Alzheimer disease. *Proceedings of the National Academy of Sciences of the United States of America* 103.15: 5644–51.

Maia, A.V., Veras, M.L., Braz-Filho, R., Lopes, N.P., Silveiraa, E.R., Pessoa, O.D.L. 2010. New Ceramides from *Acnistus arborescens*. *Journal of the Brazilian Chemical Society* 21.5: 867-871.

Malve, H., Raut, S., Marathe, P., Rege, N. 2014. Effect of combination of *Phyllanthus emblica*, Tinospora cordifolia and Ocimum sanctum on spatial learning and memory in rats. *Journal of Ayurveda and Integrative Medicine* 5: 209-215.

Mani, V., Milind, P. 2007. Memory enhancing activity of *Emblica officinalis* Gaertn: An ayurvedic preparation. *Physiology* & *Behavior* 91: 46-54.

Manjusha, G.V., Rajathi, K., Alphonse, J.K.M., Meera, K.S. 2011. Antioxidant potential and antimicrobial activity of *Andrographis paniculata* and *Tinospora cordifolia* against pathogenic organisms. *Journal* of *Pharmacy Research* 4.2: 452-5.

Marston, A., Kissling, J., Hostettmann, K. 2002. A rapid TLC bioautographic method for the detection of acetylcholinesterase and butyrylcholinesterase inhibitors in plants. *Phytochemical Analysis* 13: 51-54.

Mary, N.K., Babu, B.H., Padikkala, J. 2003. Antiatherogenic effect of Caps HT2, a herbal Ayurvedic medicine formulation. *Phytomedicine* 10.6-7: 474-82.

Mason, R.P., Olmstead, E.G., Jacob, R.F. 2000. Antioxidant activity of the monoamine oxidase B inhibitor Lazabemide. *Biochemistry Pharmacology* 60: 709-716.

Mathew, S., Kuttan, G. 1997. Antioxidant activity of *Tinospora cordifolia* and its usefulness in the amelioration of cyclophosphamide induced toxicity. *Journal* of *Experimental* & *Clinical Cancer Research* 16.4: 407-411.

Meng, X.Y., Zhang, H.X., Mezei, M., Cui, M. 2011. Molecular docking: A powerful approach for structure-based drug discovery. *Current Computer-Aided Drug Design* 7: 146–157.

Mesulam, M.M., Geula, C. 1988. Nucleus basalis (Ch4) and cortical cholinergic innervation in the human brian: observations based on the distribution of acetylcholinesterase and choline acetyltransferase. *Journal of Comparative Neurology* 275: 216-240.

Mesulam, M.M. 2000. Neuroanatomy of cholinesterases in the normal human brain and in Alzheimer's disease. In: Giacobini E (Ed.) Cholinesterase and cholinesterase inhibitors. *Martin Dunitz Ltd, UK* 121-137.

Mesulam, M.M., Geula, C. 1988. Nucleus basalis (Ch4) and cortical cholinergic innervation in the human brain: observations based on the distribution of acetylcholinesterase and choline acetyltransferase. *Journal of Comparative Neurology* 275: 216-240.

Mesulam, M.M., Geula, C., Bothwell, M.A., Hersh, L.B. 1989. Human reticular formation: cholinergic neurons of the pedunculopontine and laterodorsal tegmental nuclei and some cytochemical comparisons to forebrain cholinergic neurons. *Journal of Comparative Neurology* 281: 611-633.

Mesulam, M.M., Geula, C., Brimijoin, S., Smiley, J.F. 1995. Butyrylcholinesterase immunochemistry in human cerebral cortex. *Society of Neuroscience Abstract* 21: 1976.

Minotti, G. and Aust, S. D. 1987. An investigation into thee mechanism of citrate-Fe2+-dependent lipid peroxidation. *Free Radical Biology and Medicine* 3.6: 379–387.

Monterio, H.P., Bechara, E.J., Abdalla, D.S. 1991. Free radicals involvement in neurological porphyrias and lead poisoning. *Molecular* and *Cellular Biochemistry* 103: 73–83.

Moosmann, B., Uhr, M., Behl, C. 1997. Neuroprotective potential of aromatic alcohols against oxidative cell death. *FEBS Letters* 413.3: 467-72.

Mukeshwar, P., Surendra, K. C., Manoj, K.V., Rohit, S. 2012. *Tinospora cordifolia*: A Climbing shrub in health care management. *International Journal* of *Pharma* and *Bio* Sciences 3.4: 612 – 628.

Mukherjee, P.K., Kumar, V., Mal, M., Houghton, P.J. 2007a. Acetylcholinesterase inhibitors from plants. *Phytomedicine* 14: 289-300.

Nadkarni, K.M. 1976. *Indian Materia Medica* (*3rd Edn, Vol 1*) *popular prakashan*, Bombay, 296.

Nagai, T., Mc Geer, P.L., Peng, J.H., Dolman, C.E. 1983. Choline acetyltransferase immunohistochemistry in brains of Alzheimer's disease patients and controls. *Neuroscicience Letter* 36: 195-199.

Nagaraja, P.K., Kammar, K.F., Devi, S. 2007. Modulation of morphology and some gluconeogenic enzymes activity by *Tinospora cordifolia* (Willd.) in diabetic rat kidney. *Biomed Research* 18: 179-83.

Nair, P.K.R., Rodrigueza, S., Ramachandrana, R., Alamoa, A., Melnicka, S.J., Escalona, E., Garcia, P.I., Wnukb, S.F., Ramachandrana, C. 2004. Immune stimulating properties of a novel polysaccharide from the medicinal plant *Tinospora cordifolia*. *International Immunopharmacology* 4: 1645–1659.

Nalini, K., Karanth, K.S., Rao, A., Aroot, A.R. 1995. Effects of *Celastrus paniculatus* on passive avoidance performance and biogenic amine turnover in albino rats. *Journal of Ethnopharmacology* 47: 101-108.

Nascimento, G.G.F., Locatelli, J., Freitas, P.C., Silva, G.L. 2000. Antibacterial activity of plant extracts and phytochemicals on antibiotic-resistant bacteria. *Brazilian Journal of Microbiology* 31: 247-256.

Ndjonka, D., Bergmann, B., Agyare, C. 2012. *In vitro* activity of extracts and isolated polyphenols from West African medicinal plants against *Plasmodium falciparum*. *Parasitology Research* 111.2: 827–834.

Nightingale, S.L. 1997. Donepezil approved for treatment of Alzheimer's disease. *JAMA* 277: 10.

Nolte, H.J., Rosenberry, T.L., Neumann, E. 1980. Effective charge on acetylcholinesterase active sites determined from the ionic strength dependence of association rate constants with cationic ligands. *Biochemistry* 19.16: 3705-3711.

Nordberg, A. 2000. The effect of cholinesterase inhibitors studied with brain imaging. In: Giacobini E, (Ed.) Cholinesterase and cholinesterase inhibitors. *Martin Duntz, London* 237-247.

Ofokansi, K.C., Eze, A.O., Uzor, P.F. 2011. Evaluation of the antimicrobial activity of the aqueous and methanolic leaf extracts of *Mitacarpus villosus* with amoxicillin. *African Journal* of *Pharmaceutical Research* and *Development* 3: 43-47.

Ogane, N., Giacobini, E., Messamore, E. 1992a. Preferential inhibition of acetylcholinesterase molecular forms in rat brain. *Neurochemical Research* 17.5: 489-495.

Oguakwa, J.U., Galeffi, C., Nicoletti, M., Messana, I., Barini-Bettolo, G.B. 1986. Research on African medicinal plants, XI., 8-hydroxy columbin, a new furanoid diterpene from *Chasmanthera dependens*. *Planta Medica* 3: 198–199.

Ohiri, F.C., Verpoorte, R., Baerheim-Svendsen, A. 1982. Alkaloids from *Chasmanthera dependens*. *Planta Medica* 46.4: 228-30.

Ollis, D.L., Cheah, E., Cygler, M., Dijkstra, B., Frolow, F., Franken, S.M., Hazel, M., Remington, S.J., Silman, I., Schrag, J. 1992. The a/ß hydrolase fold. *Protein Engineering* 5.3: 197-211.

Orhan, I., Asian, M. 2009. Appraisal scopolamine-induced antiamnesia effect in mice and *in vitro* antiacetylcholinesterase and antioxidant activities of some traditionally used lamiaceae plants. *Journal of Ethnopharmacology* 122: 327-332.

Orhan, İ. 2002. *lnvestigation of acetylcholinesterase inhibitory activity of some plants growing in Turkey*, Ph.D. Thesis, Institute of Health Sciences, Gazi University, Ankara.

Orhan, I., Kartal, M., Naz, Q., Yilmaz, G., Kan, Y., Konuklugil, B., Sener, B., Choudhary, M.I. 2007. Antioxidant and anticholinesterase evaluation of selected Turkish Salvia species. *Food Chemistry* 103: 1247–54.

Orhan, I., Sener, B., Choudhary, M.I., Khalid, A. 2004. Acetylcholinesterase and butyrylcholinesterase inhibitory activity of some Turkish medicinal plants. *Journal of Ethnopharmacology* 91: 57-60.

Ortega, M. G., Agnese, A. M., Cabrera, J. L. 2004. Anticholinesterase activity in an alkaloid extract of *Huperzia saururus. Phytomedicine* 11.6: 539–543.

Otoguro, K., Kuno, F., Omura, S. 1997. Arisugacins, selective acetylcholinesterase inhibitors of microbial origin. *Pharmacology* & *Therapeutics* 76: 45–54.

Pacheco, G., Palacios-Esquivel, R., Moss, D.E. 1995. Cholinesterase inhibitors proposed for treating dementia in Alzheimer's disease: selectivity towards human brain acetylcholinesterase compared with butyrylcholinesterase. *Journal of Pharmacology and Experimental Therapeutics* 274.2: 767-770.

Palpu, P., Rao, C.V., Kishore, K., Gupta, Y.K., Kartik, R., Govindrajan, R. 2008. *Herbal formulation as memory enhancer in Alzheimer condition*. Council of Scientific and Industrial Research. United States Patent 7429397.

Park, C.H., Choi, S.H., Koo, J.W., Seo, J.H., Kim, H.S., Jeong, S.J., Suh, Y.H. 2002. Novel cognitive improving and neuroprotective activites of *Polygala teniufolia* willdenow extract, BT-11. *Journal of Neuroscience Reseach* 70: 484-493.

Perry, E.K., Haroutunian, V., Davis, K.L., Levy, R., Lantos, P., Eagger, S., Honavar, M., Dean, A., Griffiths, M., McKeith, I.G. 1994. Neocortical cholinergic activities differentiate Lewy body dementia from classical Alzheimer's disease. *NeuroReport* 5.7: 747-749.

Perry, E.K., Perry, R.H., Blessed, G., Tomplinson, B.E. 1978a. Changes in brain cholinesterases in senile dementia of Alzheimer's type. *Neuropathology* and *Applied Neurobiology* 4: 273-277.

Perry, E.K., Perry, R.H., Smith, C.J., Purohit, D., Bonham, J., Dick, D.J., Candy, J.M., Edwardson, J.A., Fairbairn, A. 1986b. Cholinergic receptors in cognitive disorders. *Canadian Journal of Neurological Sciences* 13.4: 521-527.

Perry, N.S. 2000. *In vitro* inhibition of human erythrocyte acetylcholinesterase by *Salvia lavandulaefolia* essential oil and constituent terpenes. *Journal of Pharmacy and Pharmacology* 52: 895–902.

Perry, N.S., Houghton, P.J., Jenner, P., Keith, A., Perry, E.K. 2002. *Salvia lavandulaefolia* essential oil inhibits cholinesterase *in vivo*. *Phytomedicine* 9: 48-51.

Perry, N.S., Houghton, P.J., Theobald, A**.**, Jenner, P., Perry, E.K. 2000. *In vitro* inhibition of human erythrocyte acetylcholinesterase by *Salvia lavandulaefolia* essential oil and constituent terpenes. *Journal of Pharmacy and Pharmacology* 52: 895–902.

Perry, N.S.L., Houghton, P.J., Sampson, J., Theobald, A.E., Hart, S., Lis-Balchin, M., Hoult, J.R.S., Evans, P., Jenner, P., Milligan, S., Perry, E.K. 2001. *In vitro* activities of *S. lanvadulaefolia* (Spanish sage) relevant to the treatment of alzheimer's disease. *Journal of Pharmacy and Pharmacology* 53: 1347-1356.

Pettersen, E. F., Goddard, T. D., Huang, C. C., Couch, G. S., Greenblatt, D. M., Meng, E. C., Ferrin, T. E. 2004. UCSF Chimera - A visualization system for exploratory research and analysis. *Journal of Computational Chemistry* 25.13: 1605-12.

Picollo, M.I., Toloza, A.C., Mougabure, C.G., Zygadlo, J., Zerba, E. 2008. Anticholinesterase and pediculicidal activities of monoterpenoids. *Fitoterapia* 79: 271–278.

Prasenjit, B., Paresh, L. D. 2013. Influence of properties of SAPO's on the one-pot conversion of mono-, di- and poly-saccharides into 5-hydroxymethylfurfural. *Royal Society of Chemistry Advances* 3.38: 17156-17165.

Praticò, D., Clark, C.M., Liun, F., Rokach, J., Lee, V.Y., Trojanowski, J.Q. 2002. Increase of brain oxidative stress in mild cognitive impairment: a possible predictor of alzheimer disease. *Archieves of Neurology* 59.6: 972-6.

Prieto, P., Pineda, M., Aguilar, M. 1999. Spectrophotometric quantitation of antioxidant capacity through the formation of a phosphomolybdenum complex: specific application to the determination of vitamin E. *Analytical Biochemistry* 269: 337–341.

Prince, R.J., Pennington, R.A., Sine, S.M. 2002. Mechanism of tacrine block at adult human muscle nicotinic acetylcholine receptors. *Journal of General Physiology* 123.3: 369-393.

Puntel, R. L., Nogueira, C. W., Rocha, J. B. T. 2005. Krebs cycle intermediates modulate thiobarbituric acid reactive species (TBARS) production in rat brain *in vitro*. *Neurochemical Research* 30.2: 225–235.

Rachel, F., Melissa, T. 2011. Alzheimer's disease Current treatment options and future developments. *Formulary journal modern medicine* 46: 268-284.

Rahman, A., Zareen, S., Choudhary, M. I., Ngounou, F. N., Yasin, A., Parvez, M. 2002. Terminalin A, a novel triterpenoid from *Terminalia glaucescens*. *Tetrahedron Lett*er 43: 6233-6236.

Rajkapoor, B. Sankari, M. Sumithra, M. 2007. Antitumor and cytotoxic effects of *Phyllanthus polyphyllus* on ehrlich ascites carcinoma and human cancer cell lines. *Bioscience, Biotechnology and Biochemistry* 71.9: 2177–2183.

Ramassamy, C. 2006. Emerging role of polyphenolic compounds in the treatment of neurodegenerative diseases: a review of their intracellular targets. *European Journal Pharmacology* 5: 51–64.

Ramasamy, S., Wahab, N., Zainal Abidin, N., Manickam, S., Zakaria, Z. 2012. Growth inhibition of human gynecologic and colon cancer cells by *Phyllanthus watsonii* through apoptosis induction. *PLoS ONE* 7.4: Article ID e34793.

Rao, K.S.J., Rao, R.V., Shanmugavelu, P., Menon, R.B. 1999. Trace elements in Alzheimer's disease brain: A new hypothesis. *Alzheimers Representative* 2: 241–246.

Rathnasamy, R., Ravikumar, R., Sambasivam, M., Thinagarbabu, R., Aravind, S. 2016. Isolation and Characterisation of clerodane diterpenoids from the traditional medicinal plant -*Tinospora glabra (*Burm. f.*)* Merrill. *Der Pharmacia Lettre* 8.8: 280-287.

Rawal, A.K., Muddeshwar, M.G., Bisis, S.K. 2012. *Rubia cordifolia, Fagonia cretica* linn and *Tinospora cordifolia* exert neuroprotection by modulating the antioxidant system. *International Journal of Pharma Biological Science* 3.4: 612 – 628.

Rawlings, N.D., Barrett, A.J. 1994. Families of serine peptidases. *Methods Enzymology* 244: 19–61.

Rawlings, N.D., Morton, F.R., Kok, C.Y., Kong, J., Barrett, A.J. 2008. MEROPS: the peptidase database. *Nucleic Acids Research* 36: 320–325.

Rice-Evans, C.A., Nicholas, J.M., George, P. 1996. Structureantioxidant activity relationships of flavonoids and phenolic acids. *Free Radical Biology and Medicine* 20: 933–956.

Richard, M., Yaakov, S. 2012. Epidemiology of Alzheimer Disease. *Cold Spring Harb Perspect in Medicine* 2.8: a006239.

Robak, J., Grygleweski, R.J. 1998. Flavonoids are scavengers of superoxide anions. *Biochemical Pharmacology* 37: 837-45.

Sadiqa, F., Kehkashan, K., Sadia-Zikr-Ur-Rehman, Zulfiqar, A., Samreen, S., Viqar, U.A., Munawwer, R., Muhammed, A.M., Shaheen, F. 2014. Isolation and Phytochemicals from *Cordia rothii* (Boraginaceae) and evaluation of their Immunodulatory properties. *Record of Natural Products* 8.1: 51-55.

Saleem, M., Nazir, M., Akhtar, N. 2009. New phthalates from *Phyllanthus muellerianus* (Euphorbiaceae). *Journal of Asian Natural Products Research* 11.11: 974–977.

Samuelsson, G. 2004b. *Drugs of Natural Origin*: A Text Book of Pharmacognosy, Aotekarsocieteten- Swedish Pharmaceutical Society, Swedish Pharmaceutical Press, Stockholm, Sweden, 342.

Sancheti, S., Um, B.H., Seo, S.Y. 2009. 1,2,3,4,6-penta-*O*galloyl-D-glucose: A cholinesterase inhibitor from *Terminalia chebula*. *South African Journal of Botany* 72.2: 285-288.

Sarter, M., Bruno, J.P. 1997. Cognitive functions of cortical acetylcholine: toward a unifying hypothesis. *Brain Research Reviews* 23.1–2: 28–46.

Sawasdee, P., Sabphon, C., Sitthiwongwanit, D., Kokpol, U. 2009. Anticholinesterase activity of 7-methoxyflavones isolated from *Kaempferia parviflora*. *Phytotherapy Research* 23.12: 1792–1794.

Sayre, L.M., Smith, M.A., Perry, G. 2001. Chemistry and biochemistry of oxidative stress in neurodegenerative disease. *Current Medicinal Chemistry* 8:721-738.

Schliebs, R., Arendt, T. 2011. The cholinergic system in aging and neuronal degeneration. *Behavioural Brain Research* 221: 555–563.

Seabrook, G.R., Rosahl, T.W. 1999. Transgenic animals relevant to alzheimer's disease. *Neuropharmacology* 38: 1–17.

Selkoe, D. 2001. Alzheimer's disease: genes, proteins, and therapy. *Physiological Review* 81.2: 741-766.

Selkoe, D.J. 1999. Translating cell biology into therapeutic advances in alzheimer disease. *Nature* 399.6738: A23–31.

Sermboonpaisarn, T., Sawasdee, P. 2012. Potent and selective butyrylcholinesterase inhibitors from *Ficus foveolata*. *Fitoterapia* 83: 780–784.

Sheng, R., Lin, X., Zhang, J., Chol, K.S., Huang, W., Yang, B., He, Q., Hu, Y. 2009. Design, synthesis and evaluation of flavonoid derivatives as potent AChE inhibitors. *Bioorganic* & *Medicinal Chemistry* 17: 6692–6698.

Shinoda, M., Toide, K., Ohsawa, I., Kohsaka, S. 1997. Specific inhibitor for prolyl endopeptidase suppresses the generation of amyloid beta protein in NG108-15 cells. *Biochemical* and *Biophysical Research Communications* 235: 641–645.

Shinotoh, H. 1999. PET study of cholinergic system in the brain. *Rinsho Shinkeigaku* 39.1: 33-35.

Siddiqui, M.F., Levey, A.I. 1999. Cholinergic therapies in Alzheimer's disease: *Drugs of future* 24: 417-444.

Silverman, R.B., Holladay, M.W., 2014. *The Organic Chemistry of Drug Design and Drug Action*. Academic press, 2–4.

Singh, D., Chaudhuri, P.K. 2015. (+) Corydine from the stems of *Tinospora cordifolia*. *Asian Journal of Chemistry* 27.4: 1567.

Singh, J., Sinha, K., Sharma, A., Mishra, N.P., Khanuja, S.P. 2003. Traditional uses of *Tinospora cordifolia* (Guduchi). *Journal of Medicinal Aromatic Plant Science* 25: 748-51.

Singh, R.K. 2005. *Tinospora cordifolia* as an adjuvant drug in the treatment of hyper-reactive malarious splenomegaly: Case reports. *Journal of Vector Borne Disease* 42: 36-8.

Singh, N., and Rajini, P. S. 2004. Free radical scavenging activity of an aqueous extract of potato peel. *Food Chemistry* 85.4: 611-616.

Singhal, A.K., Naithani, V., Bangar, O.P. 2012. Medicinal plants with a potential to treat Alzheimer and associated symptoms. *International Journal of Nutrition, Pharmacology, Neurological Diseases* 2.2: 84-91.

Siram, S., Patel, M.A., Patel, K.V., Punjani, N.H. 2004. *Compendium on Medicinal Plants*. Gujarat SA, ed Ahmedabad, India, Agricultural University, 1–54.

Smauelsson, G. 2004c. *Drugs of Natural Origin*: A Text Book of Pharmacognosy Aotekarsocieteten- Swedish Pharmaceutical Society, Swedish Pharmaceutical Press, Stockholm, Sweden, 265.

Smith, D.H., Johnson, V.E., Stewart, W. 2013. Chronic neuropathologies of single and repetitive TBI: Substrates of dementia?. *Nature Reviews Neurology* 9.4: 211–21.

Snape, M.F., Misra, A., Murray, T.K., De Souza, R.J., Williams, J.L., Cross, A.J., Green, A.R. 1999. A comparative study in rats of the in vitro and in vivo pharmacology of the acetylcholinesterase inhibitors tacrine, donepezil and NXX-066. *Neuropharmacology* 38.1: 181-193.

Sofowora A. 1993. *Medicinal plants and Traditional Medicine in Africa*. 2nd Ed. Sunshine House, Ibadan, Nigeria: Spectrum Books Ltd; *Screening Plants for Bioactive Agents* 134-156.

Sonibare, M.A., Ayoola, I.O. 2015. Medicinal plants used in the treatment of neurodegenerative disorders in some parts of Southwest Nigeria. *African Journal of Pharmacy and Pharmacology* 9.38: 956-965.

Soreq, H., Zaku, H. 1993. *Human cholinesterases and acetylcholinesterase*. Academic Press, New York, 328.

Stohs, S.J., Bagchi, D. 1995. Oxidative mechanisms in the toxicity of metal ions. *Free Radical Biology and Medicine* 18: 321–336.

Sultan, A. 1992. Isolation and structural studies on the chemical constituents of *Tinospora malabarica* and *Nigella Sativa*. Ph.D. Thesis, Pakistan Research Repository, University of Karachi, Karachi.

Sung, S.H., Kang, S.Y., Lee, K.Y., Park, M.J., Kim, J.H., Park, J.H., Kim, Y.C., Kim, J., Kim, Y.C. 2002. (+)-a-Viniferin, a stilbene trimer from *Caragana chamlague*, inhibits acetylcholinesterase. *Biological and Pharmaceutical Bulletin* 25: 125–127.

Sur, S.J., Koo, B.S., Jin, U.H., Hwang, M.J., Kim, C.H. 2006. Pharmacological characterisation of orally active cholinesterase inhibitory activity of *Prunus persia* L. Batsch in rats. *Journal of Molecular Neuroscience* 29: 101-107.

Suresh, P.S., Kumar, A., Kumar, R., Singh, V.P. 2008. An *in silico* [correction of *in silico*] approach to bioremediation: laccase as a case study. *Journal of Molecular Graphics & Modelling* 26.5: 845–9.

Sussman, J.L., Harley, M., Frolow, F., Oefner, C., Goldman, A., Toker, L., Silman, I. 1991. Atomic structure of acetylcholinesterase from *Torpido Californica*: a prototypic acetylcholine-binding protein. *Sceince* 253.5022: 872-879.

Tarrago, T., Kichik, N., Seguí, J., Giralt, E. 2007. The natural product berberine is a human prolyl oligopeptidase inhibitor. *ChemMedChem* 2.3: 354–359.

Teixeira, J., Silva, T., Andrade, P.B., Borges, F. 2013. Alzheimer's disease and antioxidant therapy: How long how far?. *Current Medicinal Chemistry 20*: 2939–2952.

Thal, L.J. 1999. *Clinical trials in Alzheimer's disease*. In: Terry RD, Katzman R, Bick KL, Sisoda SS. (Ed.) Alzheimer's disease. 2°d edition, Lippincott Williams and Wilkins, USA: 423-439.

Toide, K., Shinoda, M., Miyazaki, A. 1998. A novel prolyl endopeptidase inhibitor, JTP-4819 its behavioral and neurochemical properties for the treatment of Alzheimer's disease. *Annual Review of Neuroscience* 9: 17-29.

Toide, K., Shinoda, M., Iwamoto, Y., Fujiwara, T., Okamiya, K., Uemura, A. 1997. A novel prolyl endopeptidase inhibitor, JTP4819, with potential for treating Alzheimer' disease. *Behavioural Brain Research* 83: 147-151.

Trease, G.E. and Evans, W.C. 1996. *A textbook of Pharmacognosy*, 14th ed. London: Bailliere Tindall Ltd, 612.

Tyler, V.E. 1994. *Herbs of choice; the therapeutic use of phytomedicinals*. Haworth Press Inc. USA: 1-15.

Umemura, K., Kondo, K., Ikeda, Y., Nishimoto, M., Hiraga, Y., Yoshida, Y., Nakashirna, M. 1999. Pharmakokinetics and safety of Z-321, a novel specific orally active prolyl endopeptidase inhibitor, in healthy male volunteers. *Clinical Pharmacology* 39: 462-470.

Upadhaya, A.K., Kumar, K., Kumar, A., Mishra, H.S. 2010. *Tinospora cordifolia* (Willd.) Hook. F. and Thoms. (Guduchi)-alidation of the Ayurvedic pharmacology through experimental and clinical studies. *International Journal of Ayurveda Research* 1: 112-121.

Urbain, A., Marston, A., Grilo, L.S., Bravo, J., Purev, O., Purevsuren, B., Batsuren, D., Reist, M., Carrupt, P.A., Hostettmann, K. 2008. Xanthones from *Gentianella amarella* ssp. *acuta* with acetylcholinesterase and monoamine oxidase inhibitory activities. *Journal of Natural Product* 71: 895–897.

Urbain, A.A., Marston, A., Queiroz, E.F., Ndjoko, K. 2004. Xanthones from *Gentiana campestris* as new acetylcholinesterase inhibitors. *Planta Medica* 70: 1011–1014.

Uriarte-Pueyo, I., Calvo, M.I. 2011. Flavonoids as acetylcholinesterase inhibitors. *Current Medicinal Chemistry* 18: 5289–5302.

Venäläinen, J.I., Juvonen, R.O., Männistö, P.T. 2004. Evolutionary relationships of the prolyl oligopeptidase family enzymes. *European Journal Biochemistry* 271: 2705–2715.

Vladimir-Knežević, S., Blaženković, B., Bival Štefan, M., Babac, M. 2012. Plant polyphenols as antioxidants influencing the human health. In *Phytochemicals as Nutraceuticals–Global Approaches to Their Role in Nutrition and Health*; Rao, V., Ed.: InTech: Rijeka, Croatia, 155–180.

Valko, M., Morris, H., Cronin, M.T. 2005. Metals, toxicity and oxidative stress. *Current Medicinal Chemistry* 12: 1161–1208.

Vasudevan, M. and Parle, M. 2007. Memory enhancing activity of Anwala churna (*Emblica officinalis* Gaertn.): an Ayurvedic preparation. *Physiology and Behavior* 91.1: 46–54.

Vasudevan, M., Parle, M. 2006. Pharmacological actions of *Thespesia populnea* relevant to Alzheimer's disease. *Phytomedicine* 13: 677–687.

Vendeville, S., Bourel, L., Davioud-Charvet, E., Grellier, P., Deprez, B., Segheraert, C. 1999. Automated parallel synthesis of a tetrahydroisoquinolin-based library: potential prolyl endopeptidase inhibitors. *Bioorganic & Medicinal Chemistry Letters* 9: 437-442.

Vinutha, B., Prashanth, D., Salma, K., Sreeja, S.L., Pratiti, D., Padmaja, R., Radhika, S., Amit, A., Venkateshwarlu, K., Deepak, M. 2007. Screening of selected Indian medicinal plants for acetylcholinesterase inhibitory activity. *Journal of Ethnopharmacology* 109.2: 359-363.

Volkova, R.I., Kireeva, E.G., Mikhel'son, M., Muske, G.A. 1976. Enzymatic hydrolysis and reversible binding of suberyldicholine by cholinesterases. *Voprosy Meditsinskoi Khimii* 22.1: 64-71.

Wallen, E.A., Christiaans, J.A., Forsberg, M.M., Venalainen, J.I., Mannisto, P.T., Gynther. 2002. Dicarboxylic acid bis (Lprolyl-pyrrolidine) arnides as prolyl oligopeptidase inhibitors. *Journal of Medicinal Chemistry* 45: 4581-4584.

Wallin, A.K., Wattmo, C., Minthon, L. 2011. Galantamine treatment in Alzheimer's disease: response and long-term outcome in a routine clinical setting. *Neuropsychiatry Disease Treatment* 7: 565–576.

Walter, R., Shlank, H., Glass, J.D., Schwartz, I.L., Kerenyi, T.D. 1971. Leucylglycinamide released from oxytocin by human uterine enzyme. *Science* 173: 827–829.

Wang, H.X., Xu, W., Pei, J.J. 2012. Leisure activities, cognition and dementia. *Molecular Basis of Disease* 1822.3: 482–91.

Wang, Y.H., Wan, Q.L., Gu, C.D., Luo, H.R., Long, C. 2012. Synthesis and biological evaluation of lycorine derivatives as dual inhibitors of human acetylcholinesterase and butyrylcholinesterase. *Chemistry Central Journal* 6: 96.

Wild, S., Roglic, G., Green, A., Sicree, R., King, H. 2004. Global prevalence of diabetes: estimates for 2000 and projections for 2030. *Diabetes Care* 27: 1047–1053.

Wilson, G.L., Lill, M.A. 2011. Integrating structure-based and ligand-based approaches for computational drug design. *Future Medicinal Chemistry* 3: 735–750.

World Health Organization. 2012. Role of acetylcholinesterase inhibitors. Available at http://www.who.int/entity/mental_health/mhgap/evidence/resource/dementia_q1.pdf

Wright, J.L.C., McInnes, A.G., Shimizu, S., Smith, D.G., Walter, J.A. 1978. Identification of C-24 alkyl epimers of marine sterols by ^{13}C nuclear magnetic resonance spectroscopy. *Canadian Journal of Chemistry* 56: 1898-1903.

Xu, Y., Ku, B., Cui, L., Li, X., Barish, P.A., Foster, T.C., Ogle, W.O. 2007. Curcumin reverses impaired hippocampal neurogenesis and increases serotonin receptor 1A mRNA and brain-derived neurotrophic factor expression in chronically stressed rats. *Brain Research* 1162: 9–18.

Yamaguchi, K., Mori, H., Nishimura, M. 1995. A novel isoenzyme of ascorbate peroxidase localized on glyoxysomal and leaf peroxisomal membranes in pumpkin. *Plant Cell Physiology* 36: 1157–1162.

Yilmaz, A., Pinar Caglar, T. Dirmenci, Nezhun Gören. 2012. A novel isopimarane diterpenoid with acetylcholinesterase inhibitory activity from *Nepeta sorgerae*, an endemic species to the Nemrut mountain. *Natural Product Communications* 7: 693–696.

Yoa, Z., Drieu, K., Papadopoulos, V. 2001. The *Ginkgo biloba* extract EGb761 rescues the PC12 neuronal cells from β-amyloid-induced cell death by inhibiting the formation of β-amyloid-derived diffusible neurotoxic ligands. *Brain Research* 889: 181-190.

Yoshida, K., Nakajima, S., Ootani, T., Saito, A., Amano, N., Takano, K., Uchiyama, Y., Haruki, E. 1996. Serum prolyl endopeptidase activities of patients with senile dementia of the Alzheimer type and of those with vascular dementia. *Journal of Clinical Biochemistry and Nutrition* 21: 227-235.

Yoshimoto, T., Fischl, M., Olowski, R.C., Walter, R. 1978. Post-proline cleaving enzyme and post-proline dipeptidyl aminopeptidase. Comparison of two peptidases with high specificity for proline residues. *Journal of Biological Chemistry* 253.10: 3708-16.

Yoshimoto, T., Walter, R., Tsuru, D. 1980. Proline specific endopeptidase from Flavobacterium. *Journal of Biological Chemistry* 255: 4786-4792.

Yoshimoto, T., Orlowski, R.C., Walter, R. 1977. Post-proline cleaving enzyme: identification as serine protease using active site specific inhibitors. *Biochemistry* 16: 2942-2948.

Young, T., Abel, R., Kim, B., Berne, B. J., Friesner, R. A. 2007. Motifs for molecular recognition exploiting hydrophobic enclosure in protein–ligand binding. *Proceedings of the National Academy of Sciences* 104.3: 808–813.

Yuriev, E., Agostino, M., Ramsland, P.A. 2011. Challenges and advances in computational docking: 2009 in review. *Journal* of *Molecular Recognition 24*: 149–164.

Zatta, P., Kiss, T., Suwalsky, M., Berthon, G. 2002. Aluminium (III) as a promoter of cellular oxidation. *Coordination Chemistry Reviews* 228: 263–270.

Zhang, Y., Kua J., McCammon, J.A. 2002. Role of the catalytic triad and oxyanion hole in acetylcholinesterase catalysis: an ab initio QM/MM study. *Journal of the American Chemical Society* 124.35: 10572–10577.

Zhang, J.Y., Pu, S.B., Qian, S.H., Liu, D., Wang, K.C. 2011. Studies on the chemical constituents in fruits of *Acanthopanax gracilistylus*. *Zhong Yao Cai* 34: 226-229.

Zhao, Q., Tang, X.C. 2002. Effects of huperzine A on acetylcholinesterase isoforms *in vitro*: comparison with tacrine, donepezil, rivastigmine and physostigmine. *European Journal of Pharmacology* 445.2-3: 101-107.

Zhao, Y., Ling ku, Y., Hao, X.J., Lee, S.S. 2000. Preparation of analogues of territrem B, a potent AChE inhibitor. *Tetrahedron* 56: 8901–8913.

Zhiwei, S., Zhonghui, M., Li, Y., Buming, L., Sheng-Xiang, Q. 2017. N-containing phytochemicals from the seeds of *Brucea javanica*. *Chemistry of Natural Compounds* 53.4: 799-801.

Zhou, H.X., Wlodek, S.T., McCammon, J.A. 1998. Conformation gating as a mechanism for enzyme specificity. *Proceedings of the National Academy of* Sciences *of the United States of America* 95.16: 9280-9283.

Zhu, X., Greig, N.H., Holloway, H.W., Whittaker, N.F., Brossi, A., Yu, Q. 2000. A practical conversion of natural physostigmine into the potent butyrylcholinesterase inhibitor *N*1,*N*8-bisnorcymserine. *Tetrahedron Lett*ers 41: 4861–4864.

Zhu, Z., Zheng, T., Homer, R.J., Kim, Y-K., Chen, N.Y., Cohn, L., Hamid, Q., Elias, J.A. 2004. Acidic mammalian chitinase in asthmatic Th2 inflammation and IL-13 pathway activation. *Science* 304.5677: 1678-1682.

Appendix 1: Spectroscopic analysis of Stigmasterol

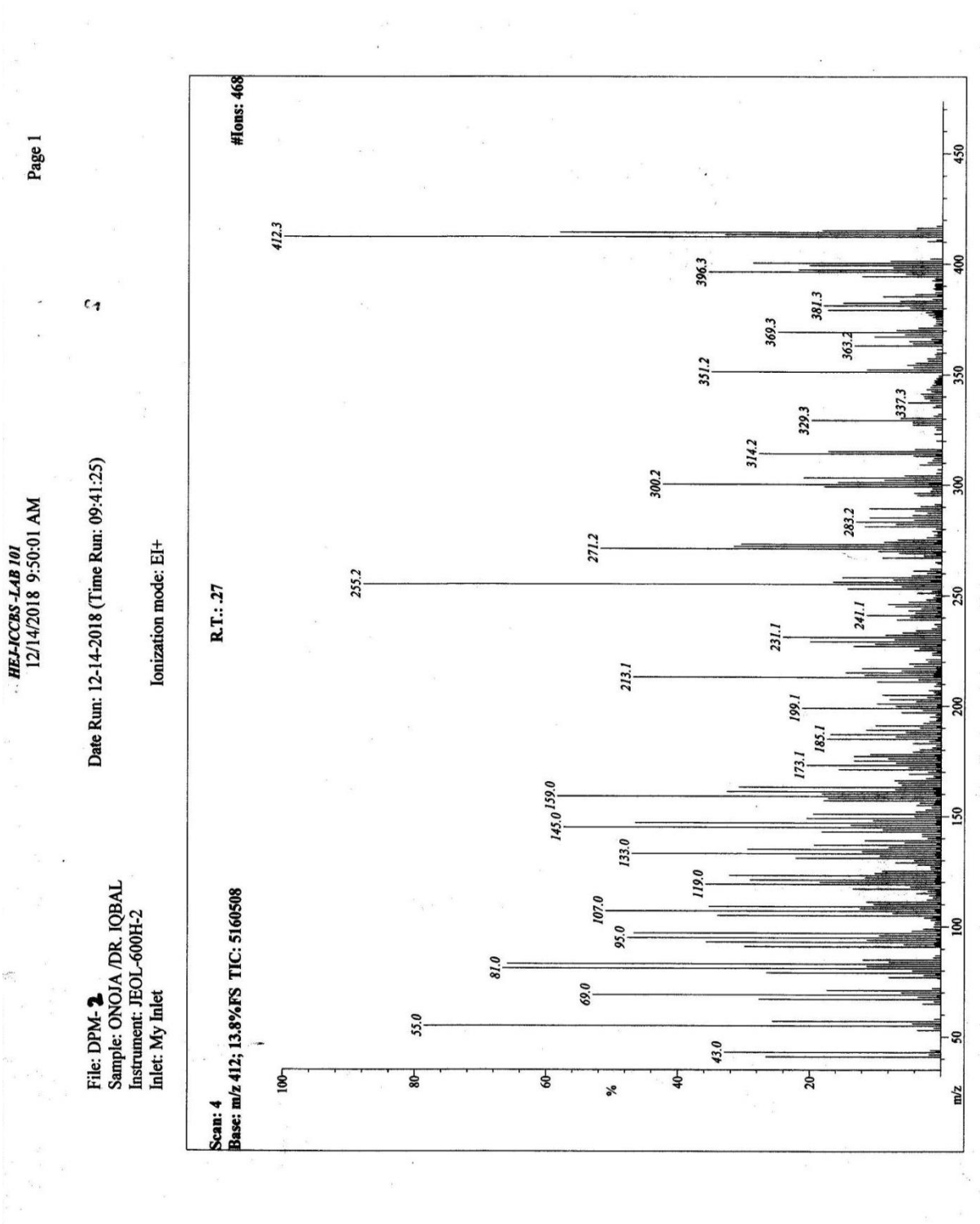

EI-MS spectra of Stigmasterol

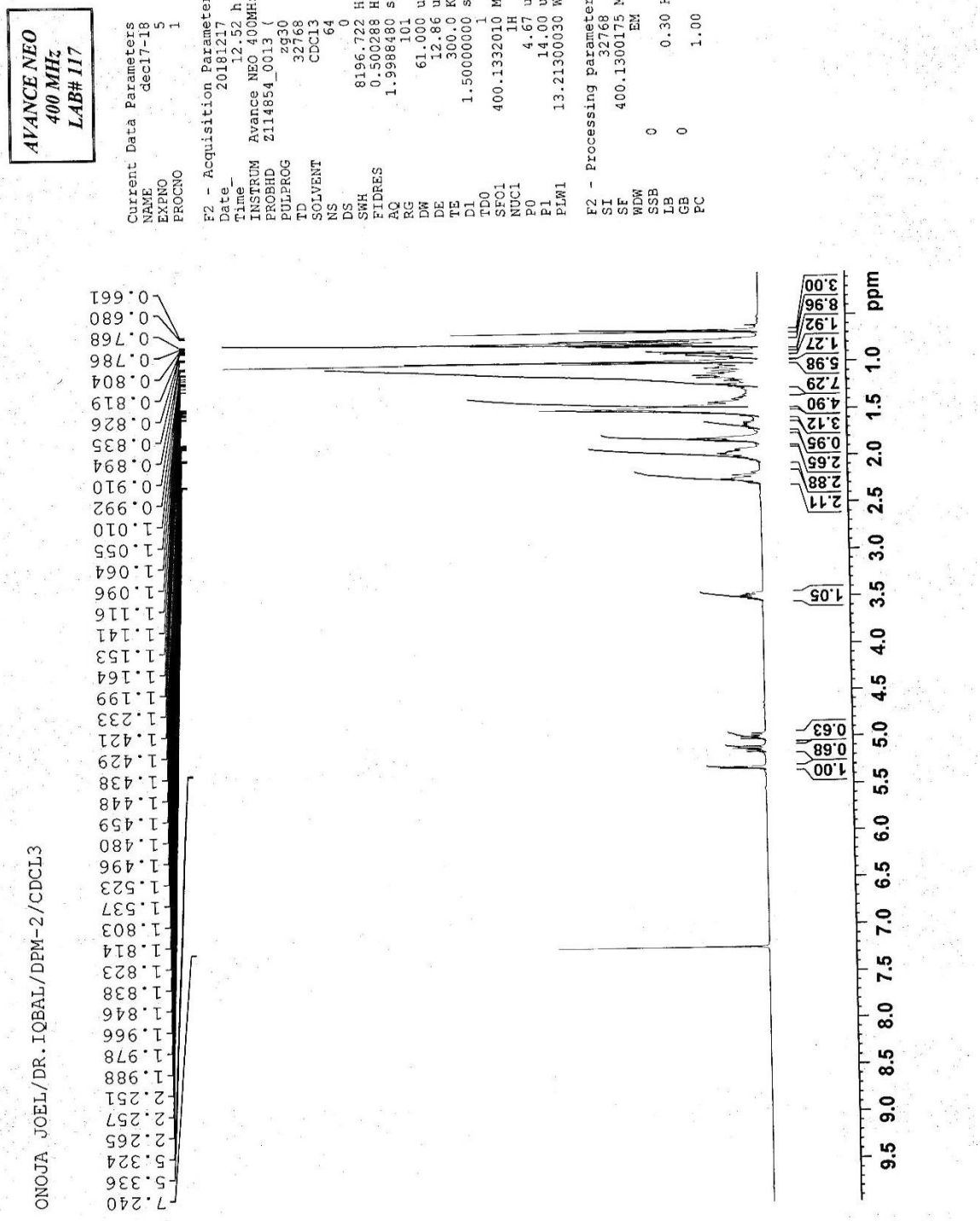

^{1}H-NMR spectra of Stigmasterol

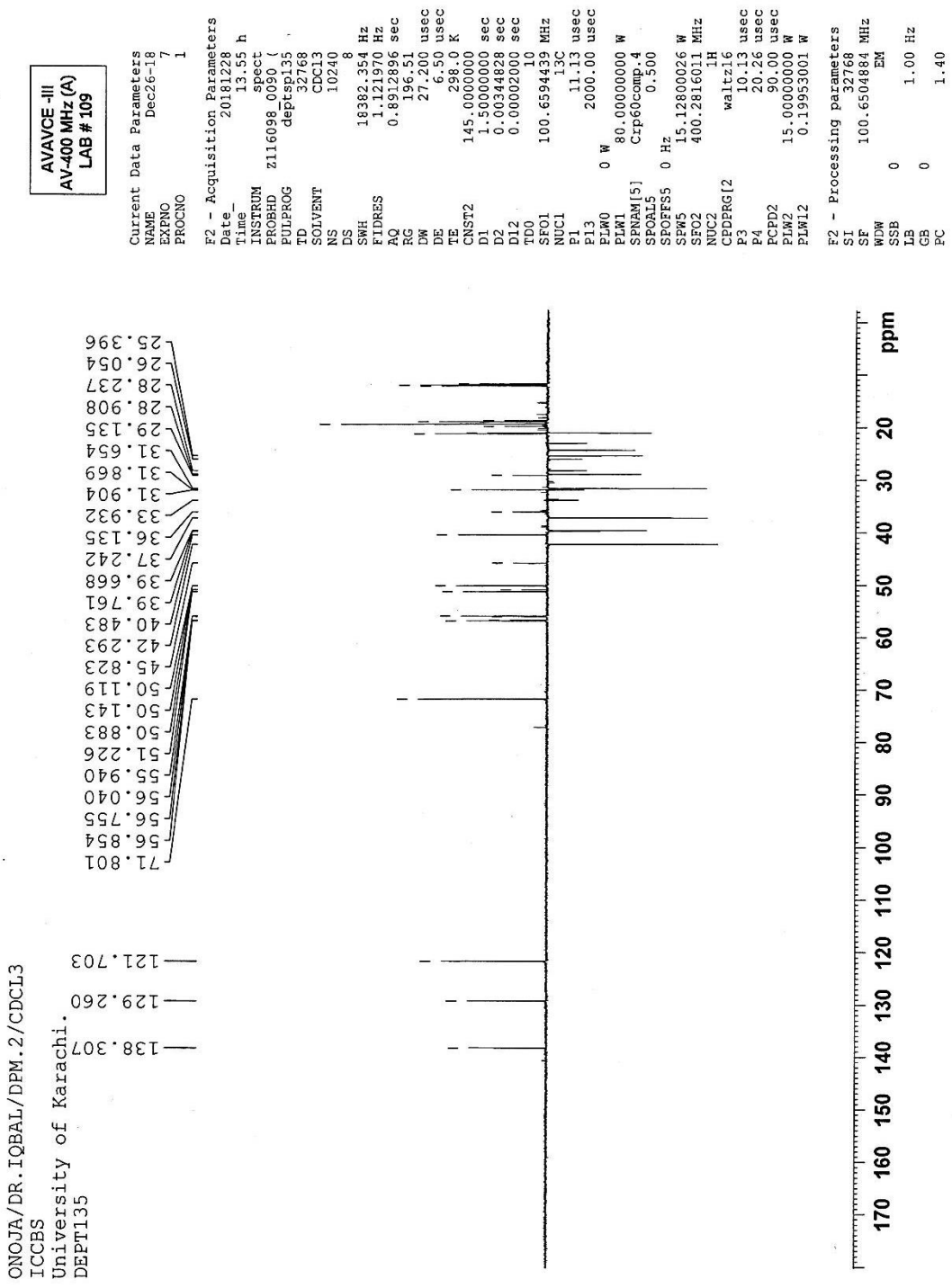

DEPT 135 spectra of Stigmasterol

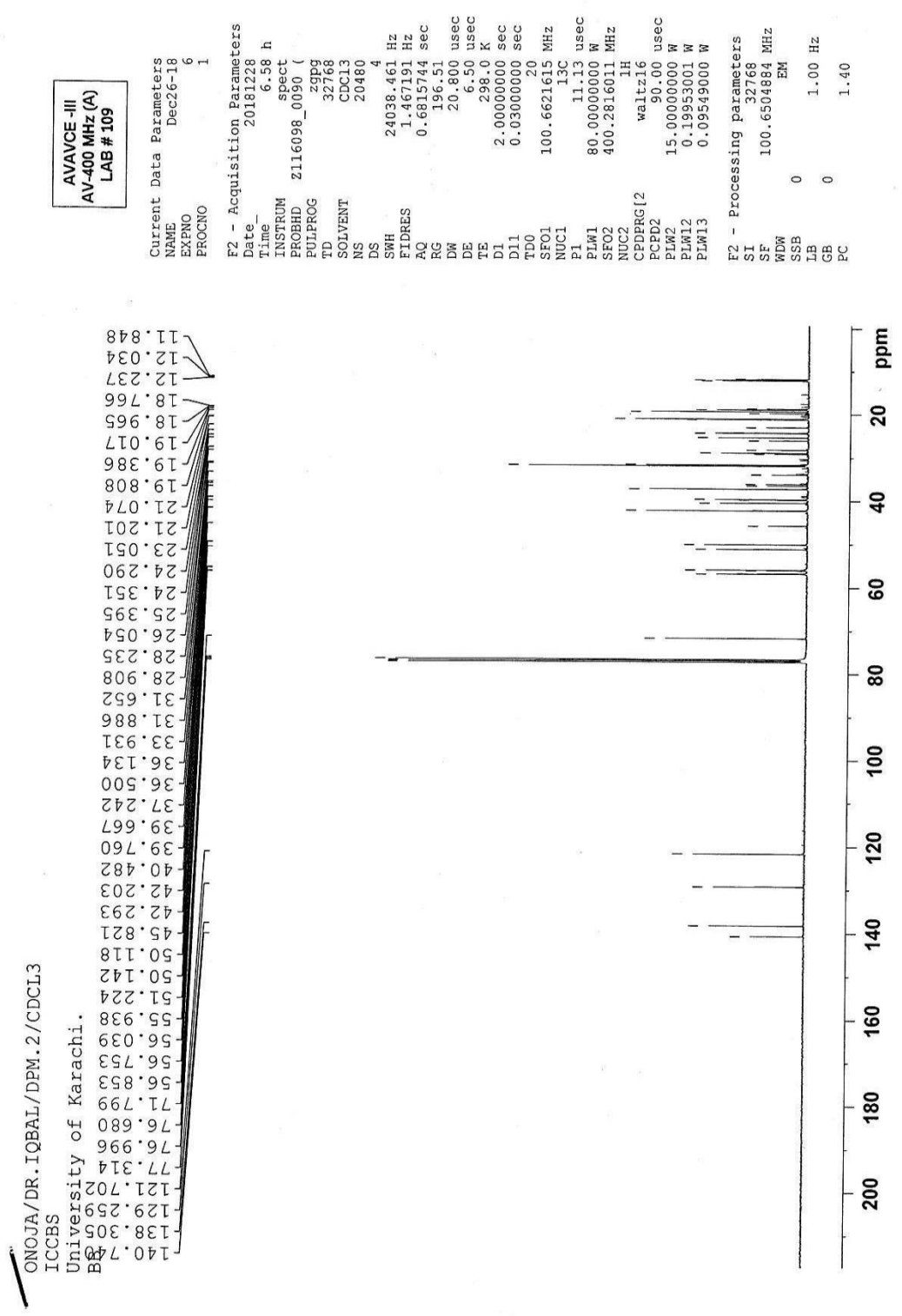

BB spectra of Stigmasterol

Appendix 2: Spectroscopic analysis of Daucosterol

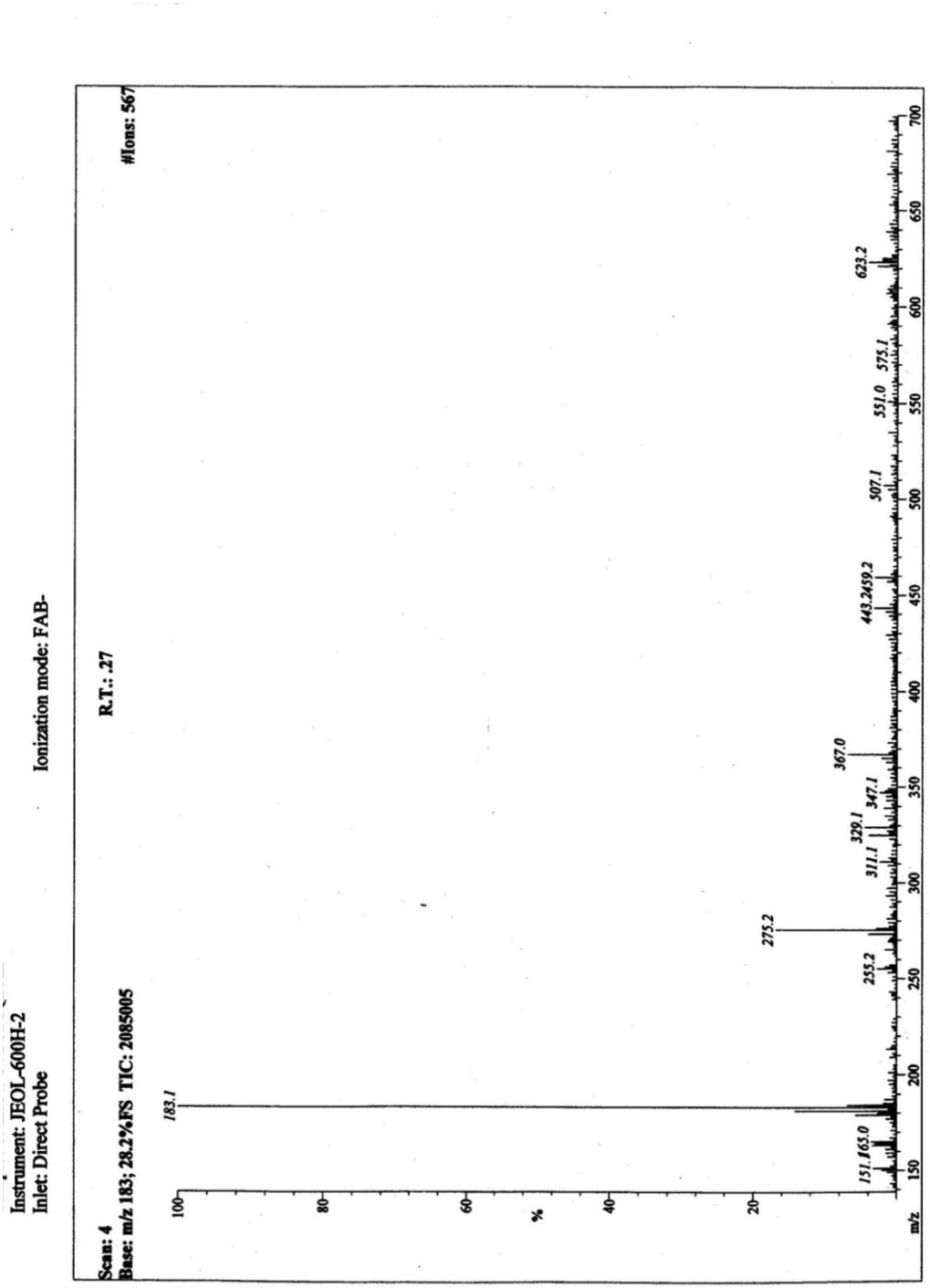

FABN spectra of Daucosterol

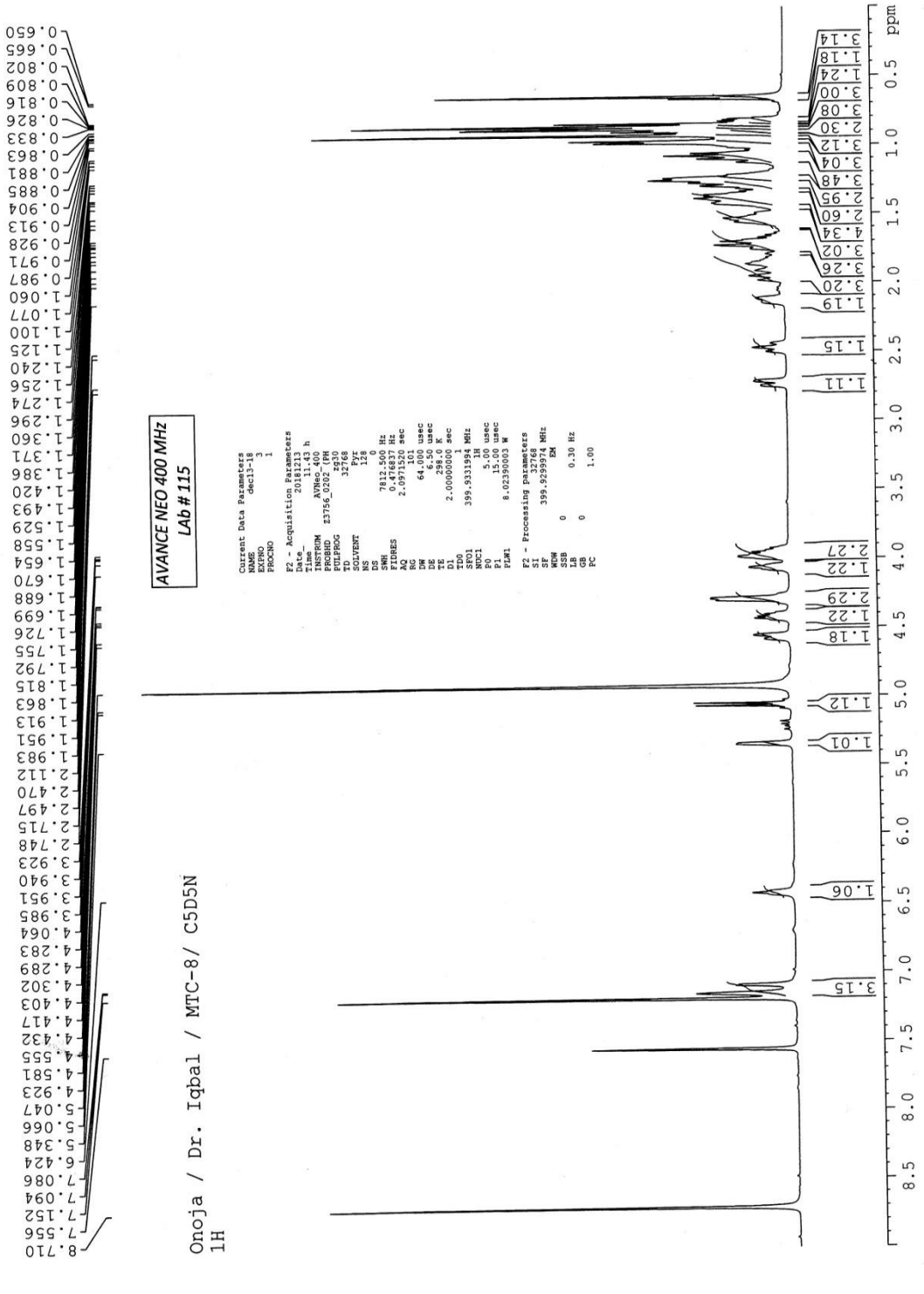

[1]H-NMR spectra of Daucosterol

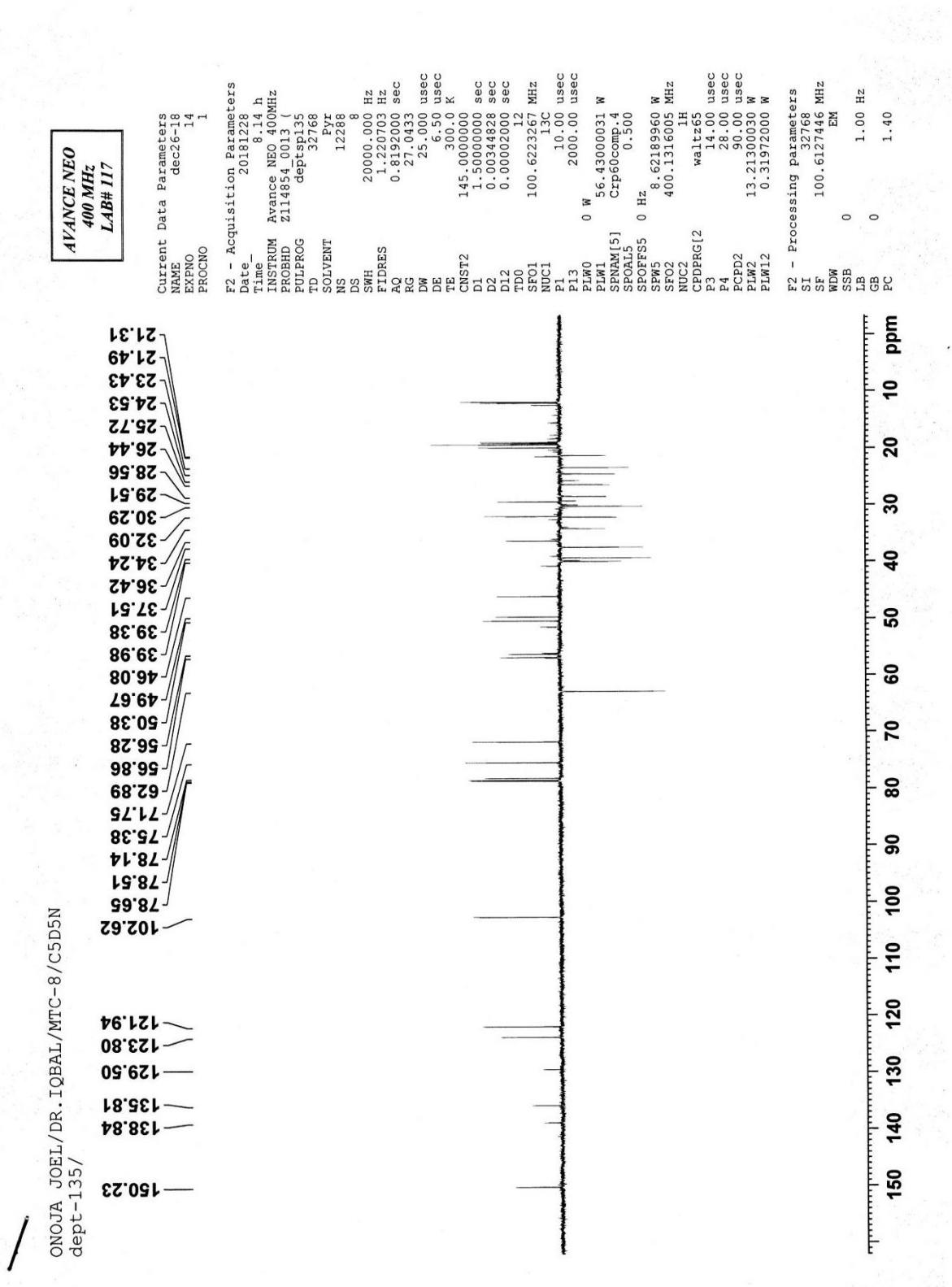

DEPT 135 spectra of Daucosterol

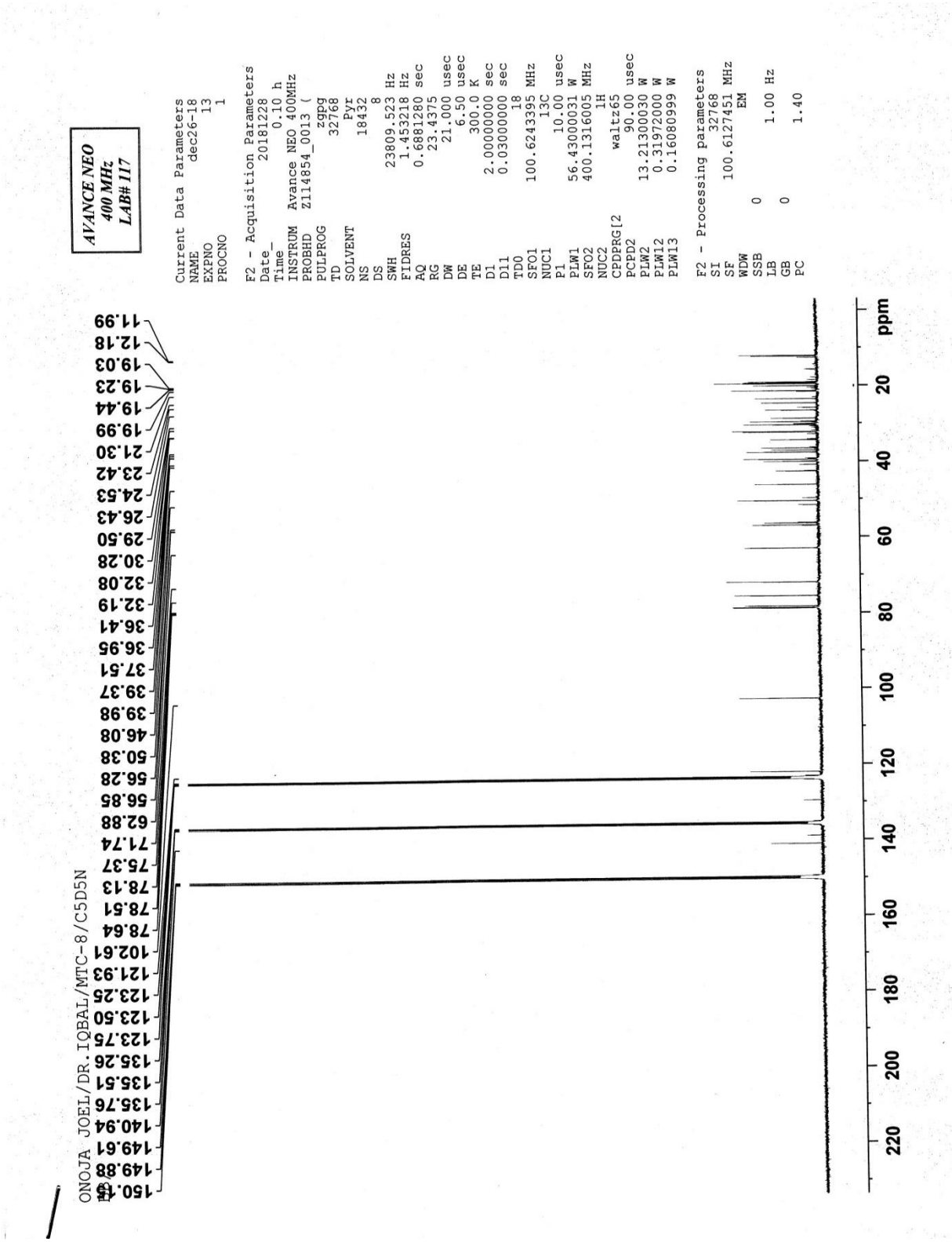

BB spectra of Daucosterol

Appendix 3: Spectroscopic analysis of 1-octacosanol

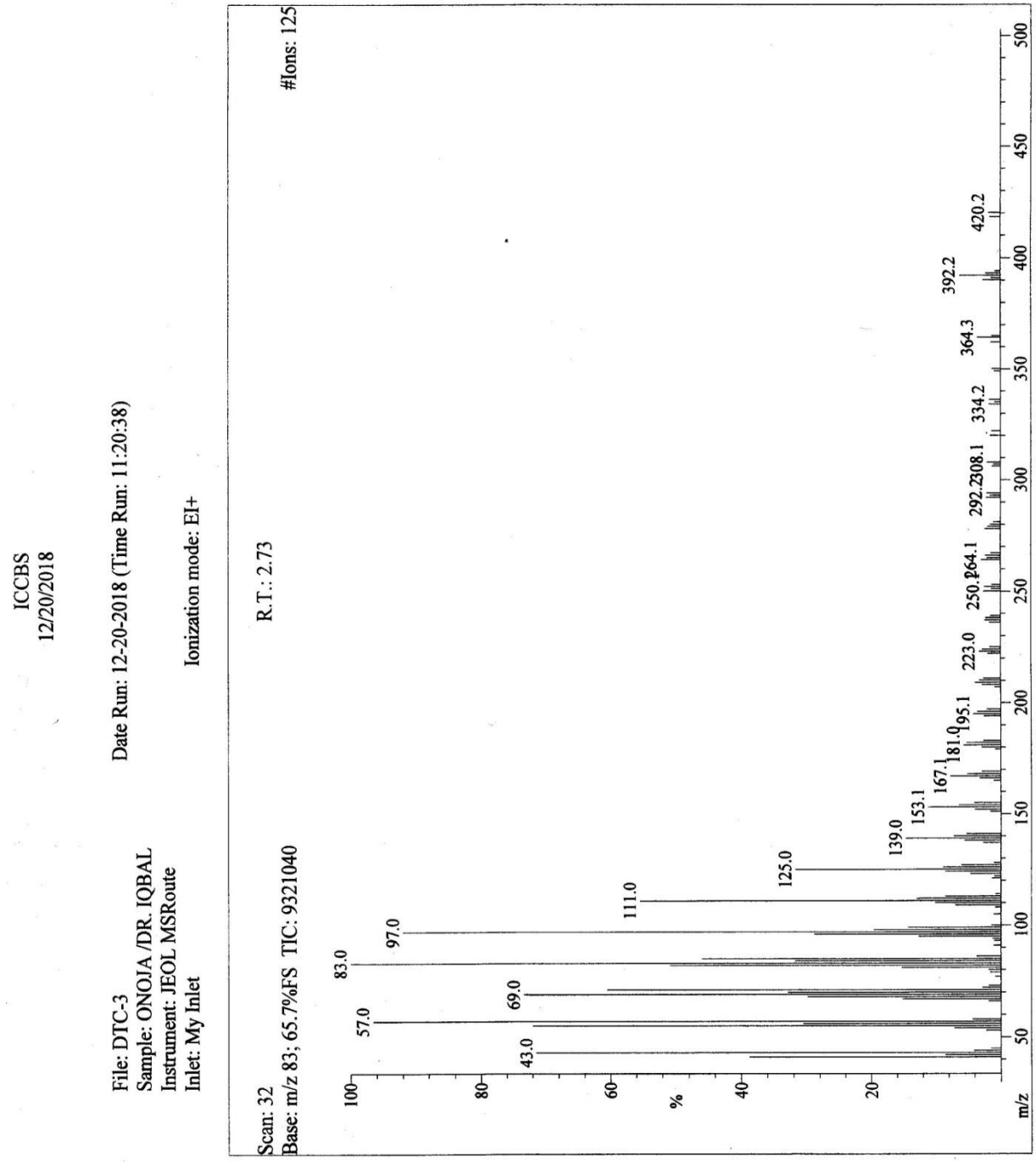

EI-MS spectra of 1-Octacosanol

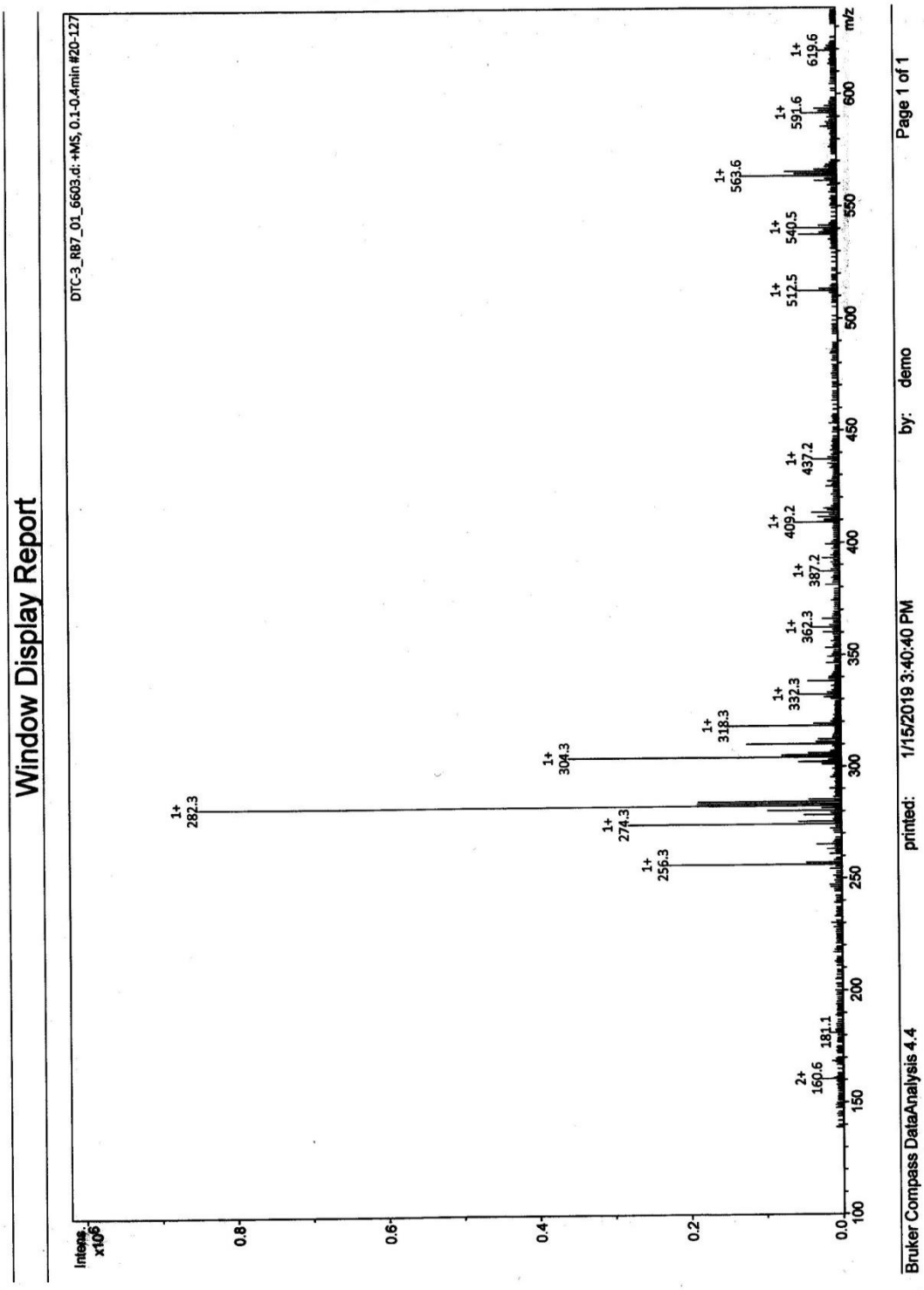

ESI-MS spectra of 1-Octacosanol

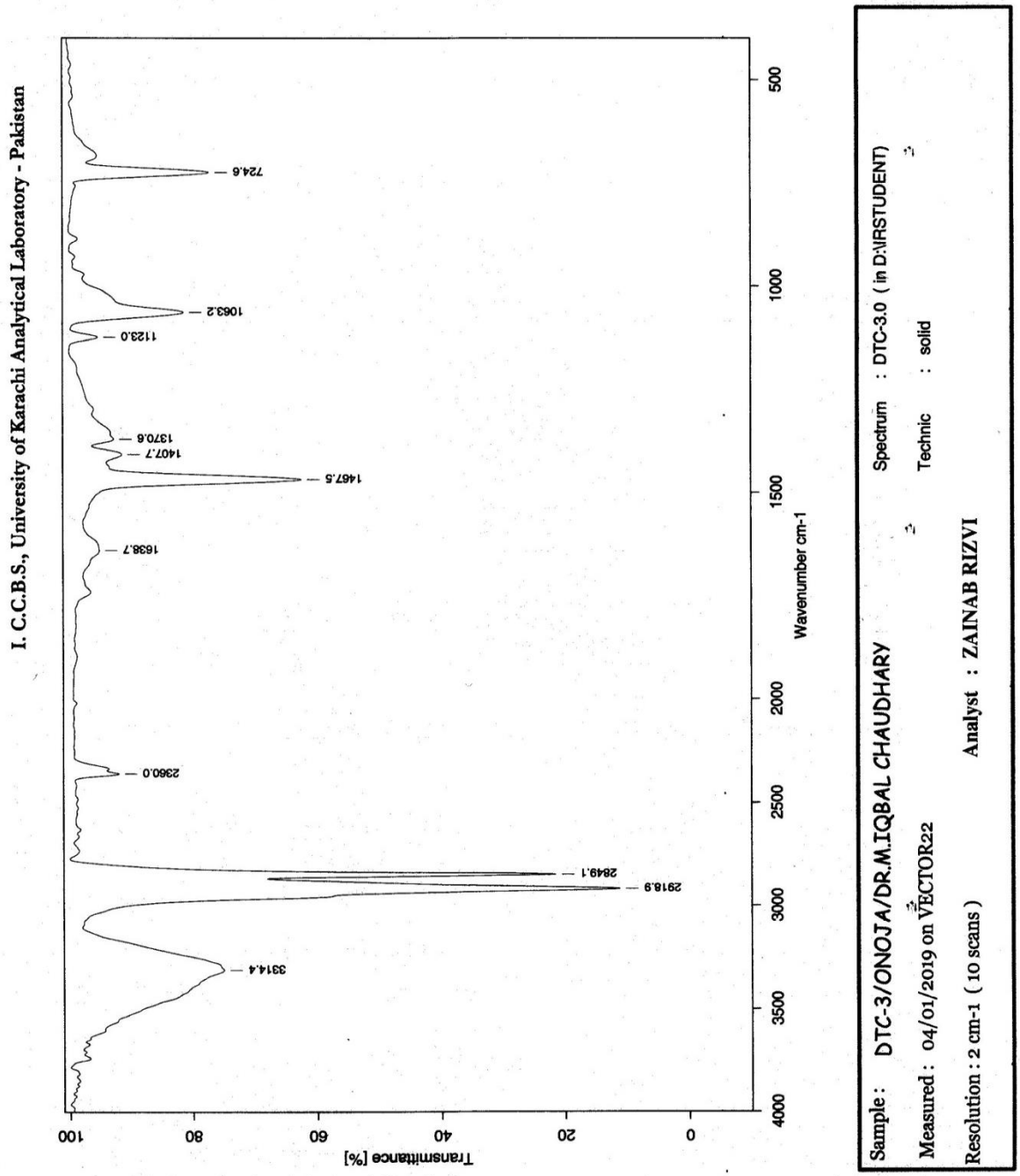

FT-IR spectra of 1-Octacosanol

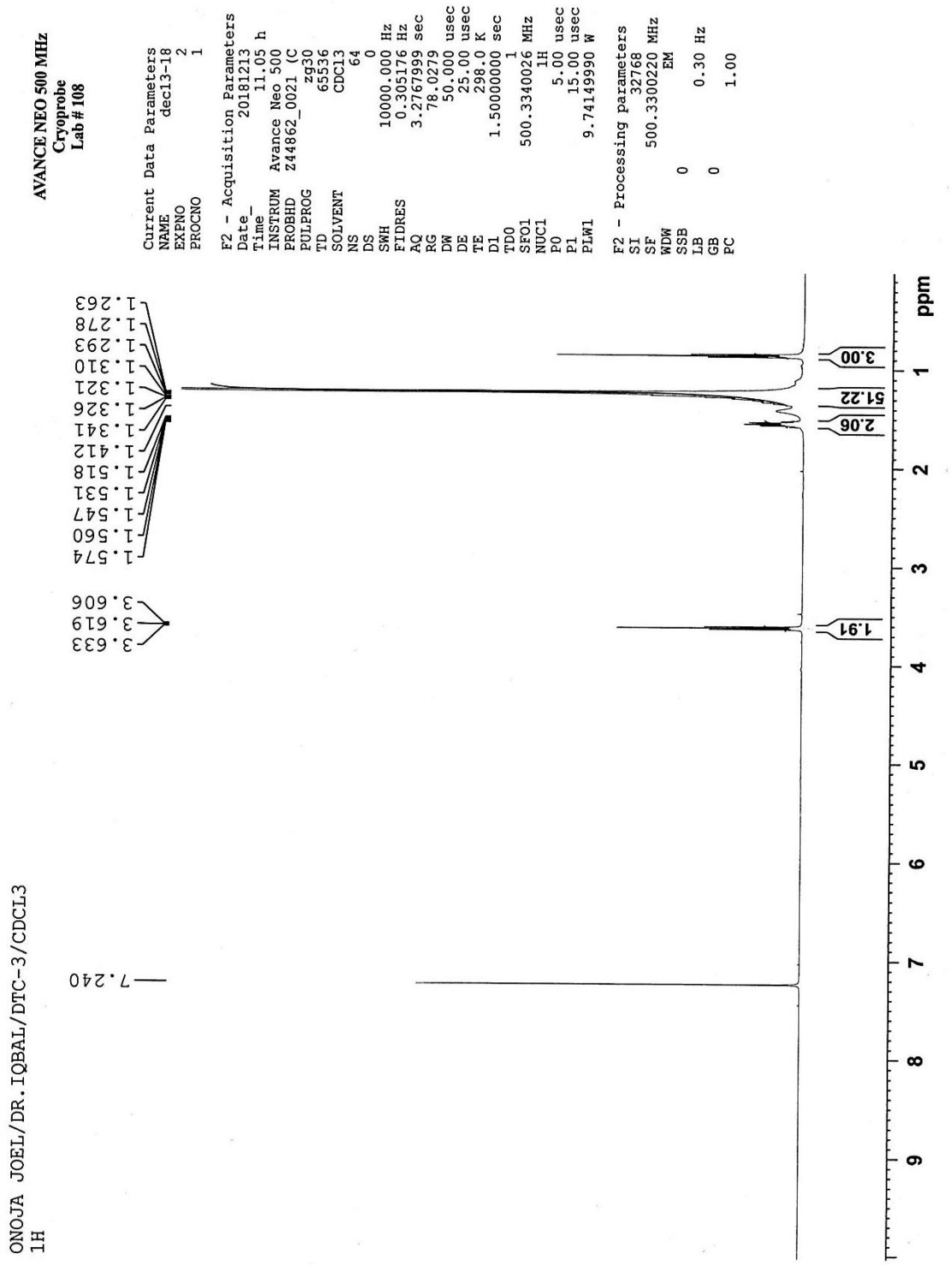

[1]H-NMR spectra of 1-Octacosanol

DEPT 135 spectra of 1-Octacosanol

DEPT 90 spectra of 1-Octacosanol

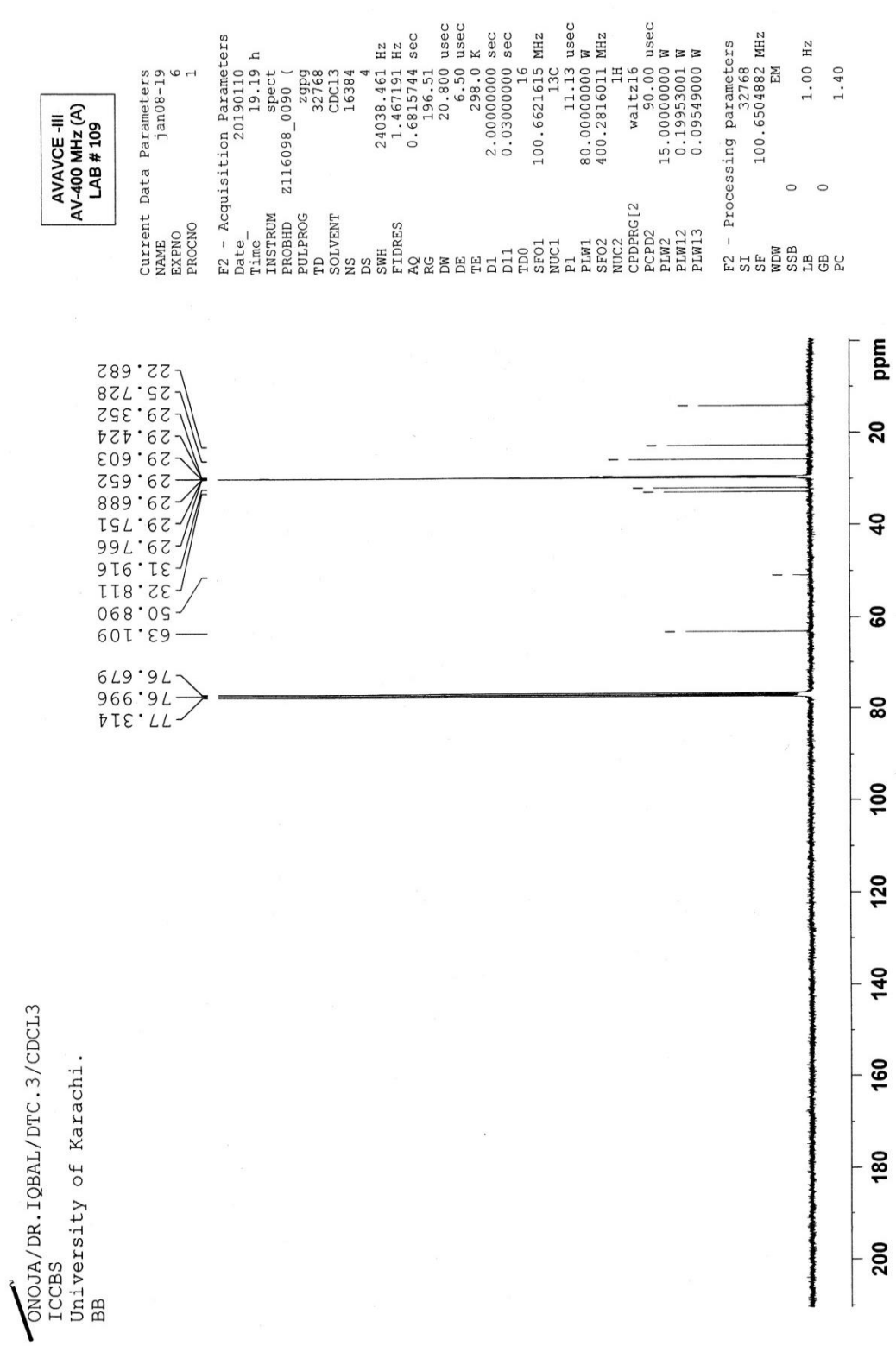

BB spectra of 1-Octacosanol

Appendix 4: Spectroscopic analysis of β-Sitosterol

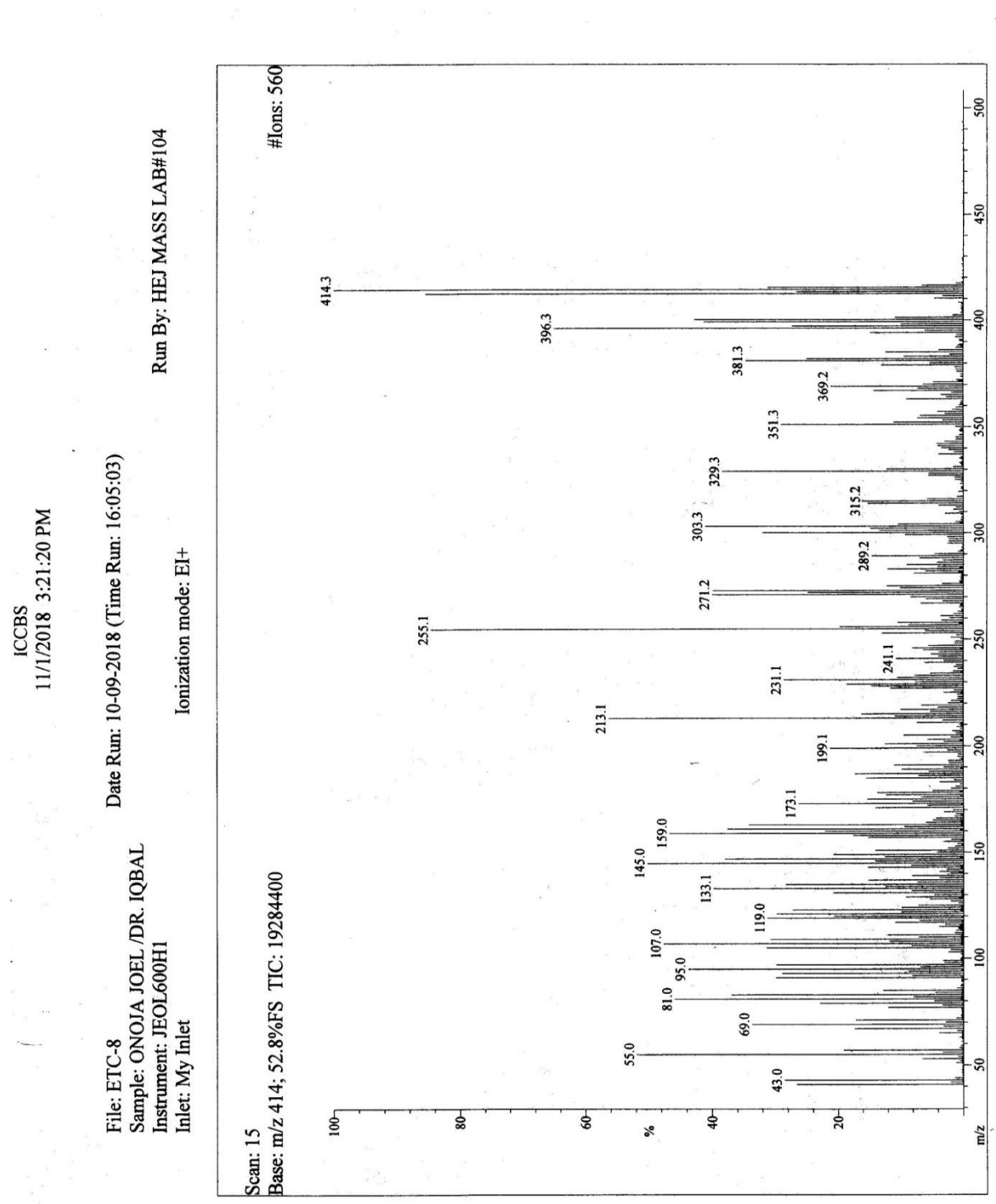

EI-MS spectra of β-sitosterol

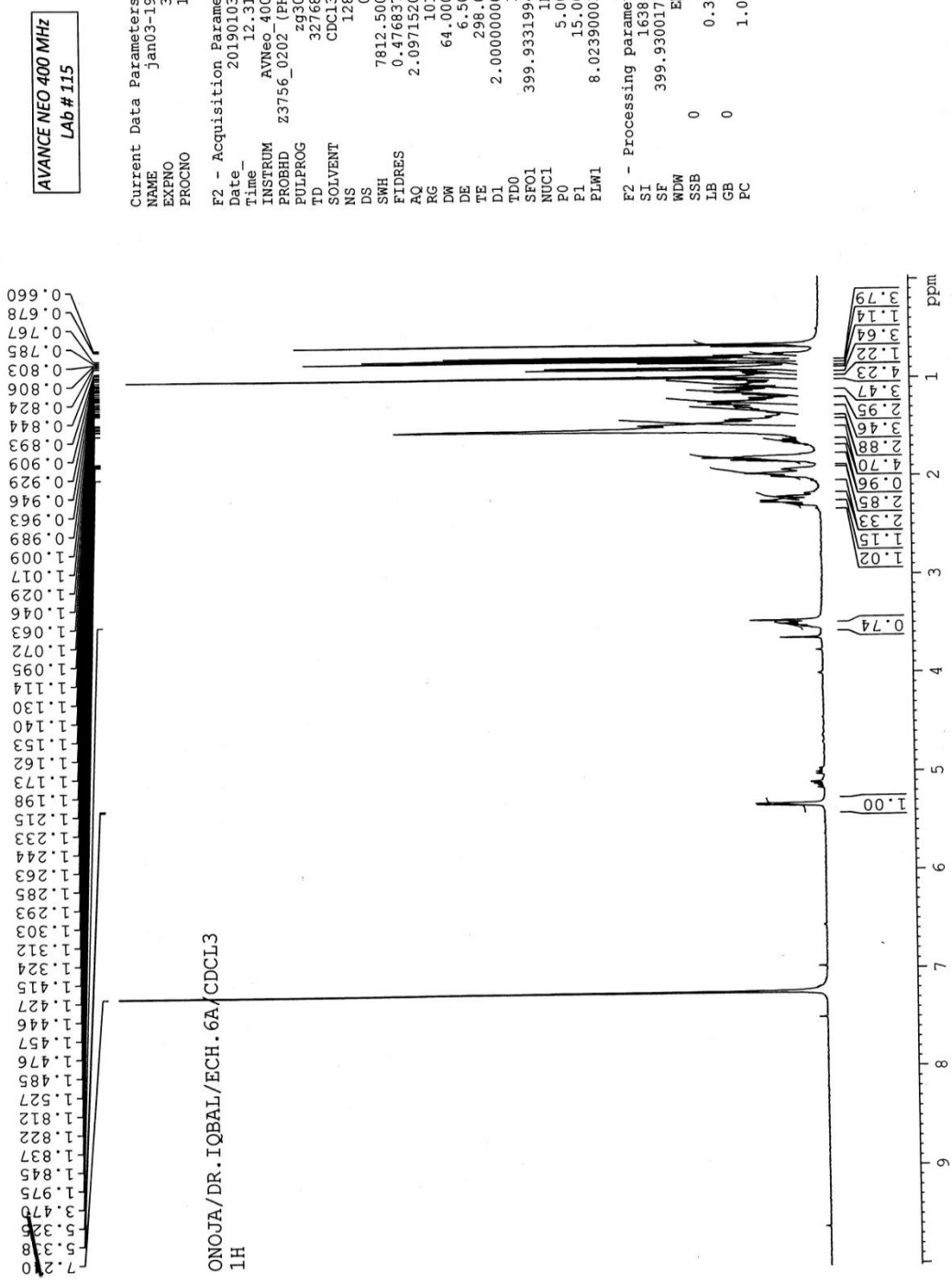

[1]H-NMR spectra of β-sitosterol

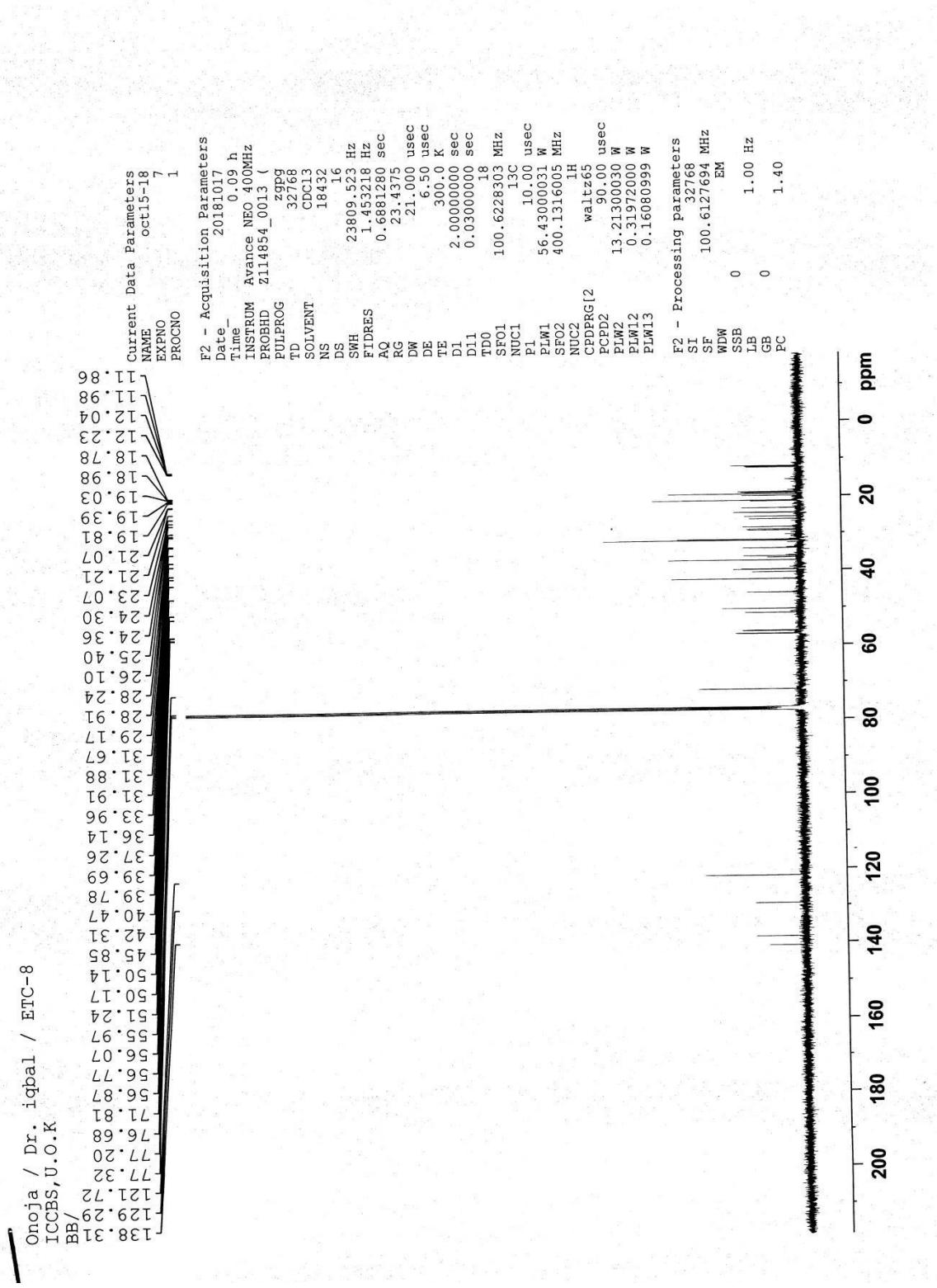

BB spectra of β-sitosterol

Appendix 5: Spectroscopic analysis of (-)-N-formylanonaine

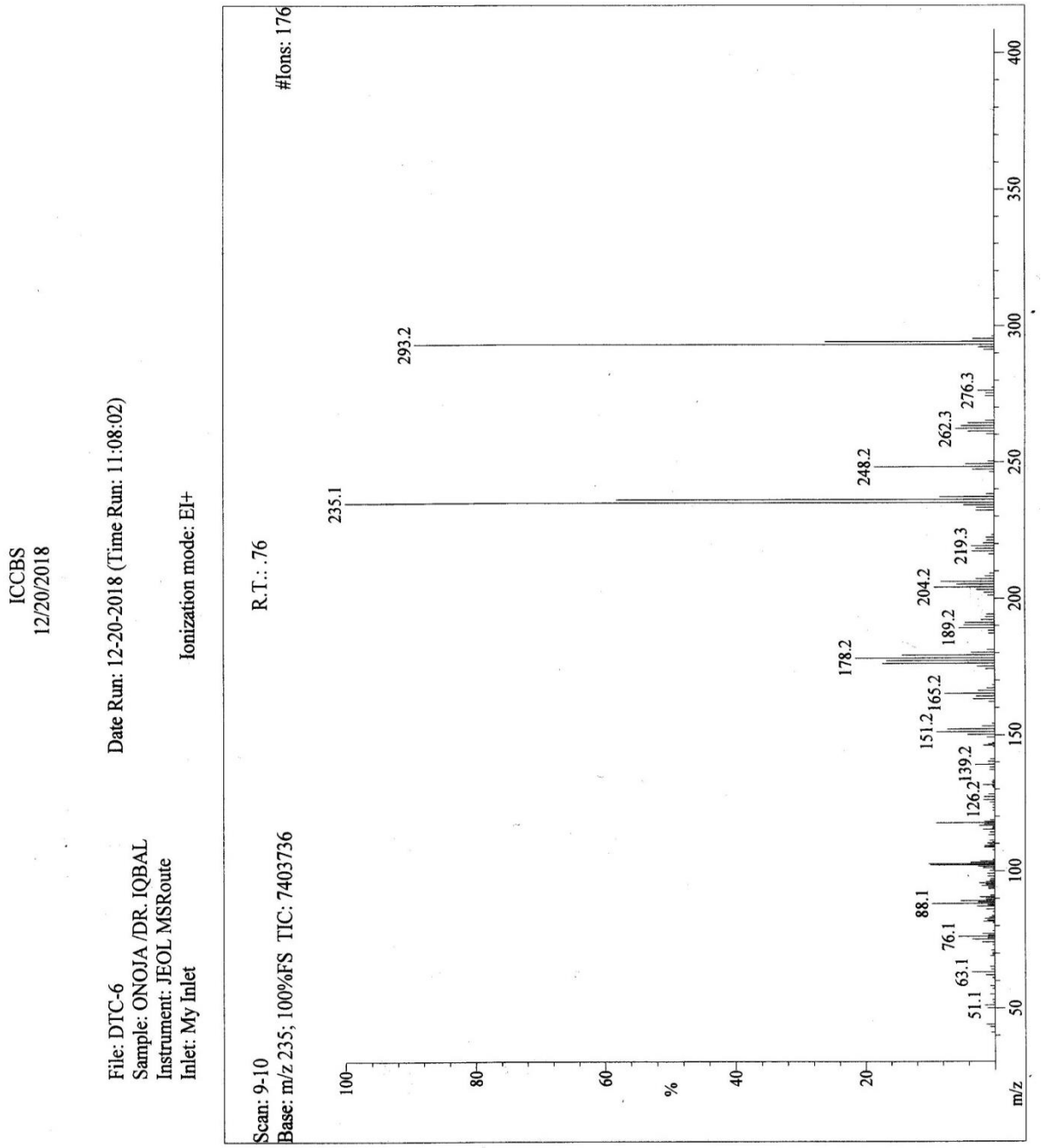

EI-MS spectra of N-formylanonaine

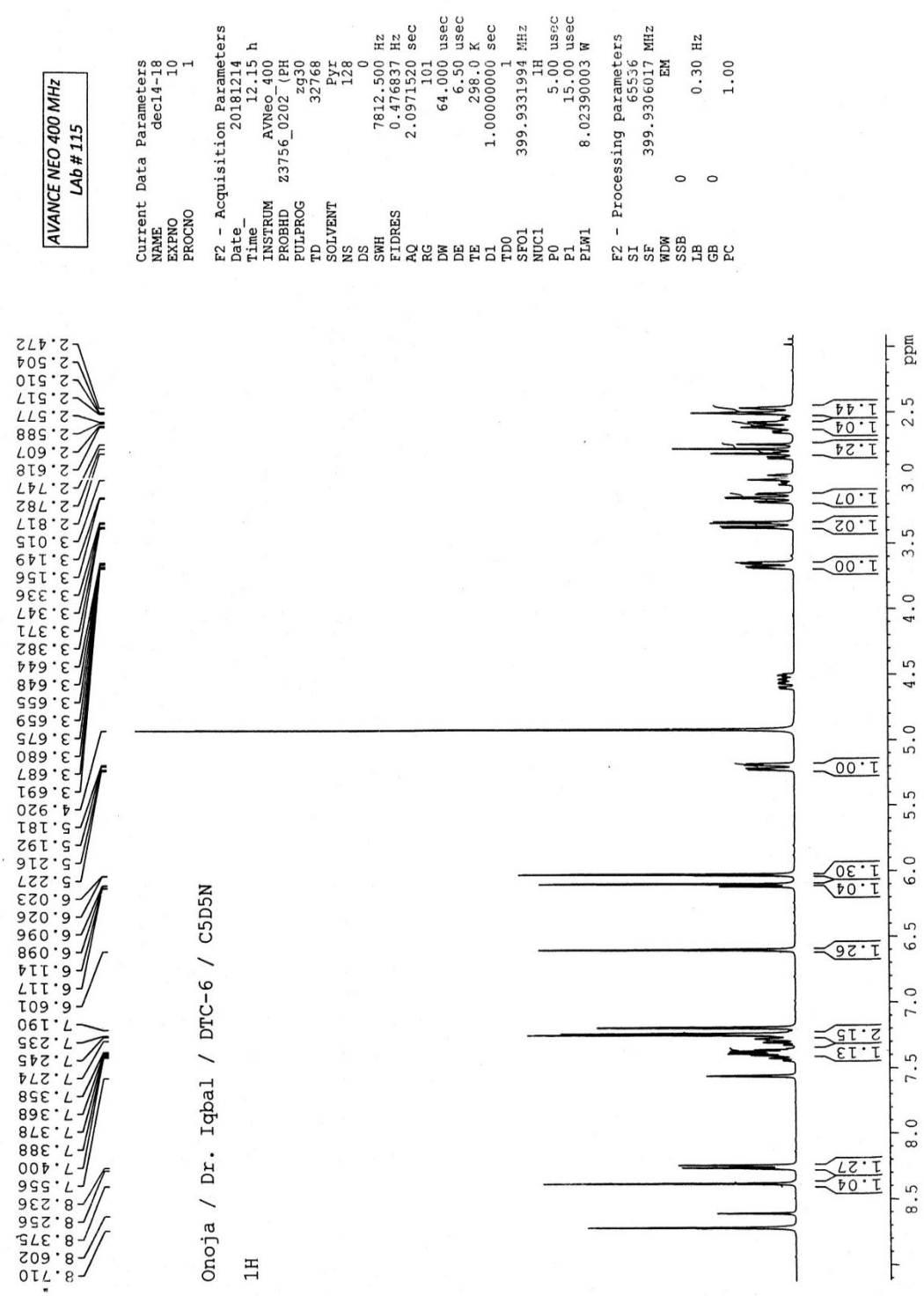

^{1}H-NMR spectra of N-formylanonaine

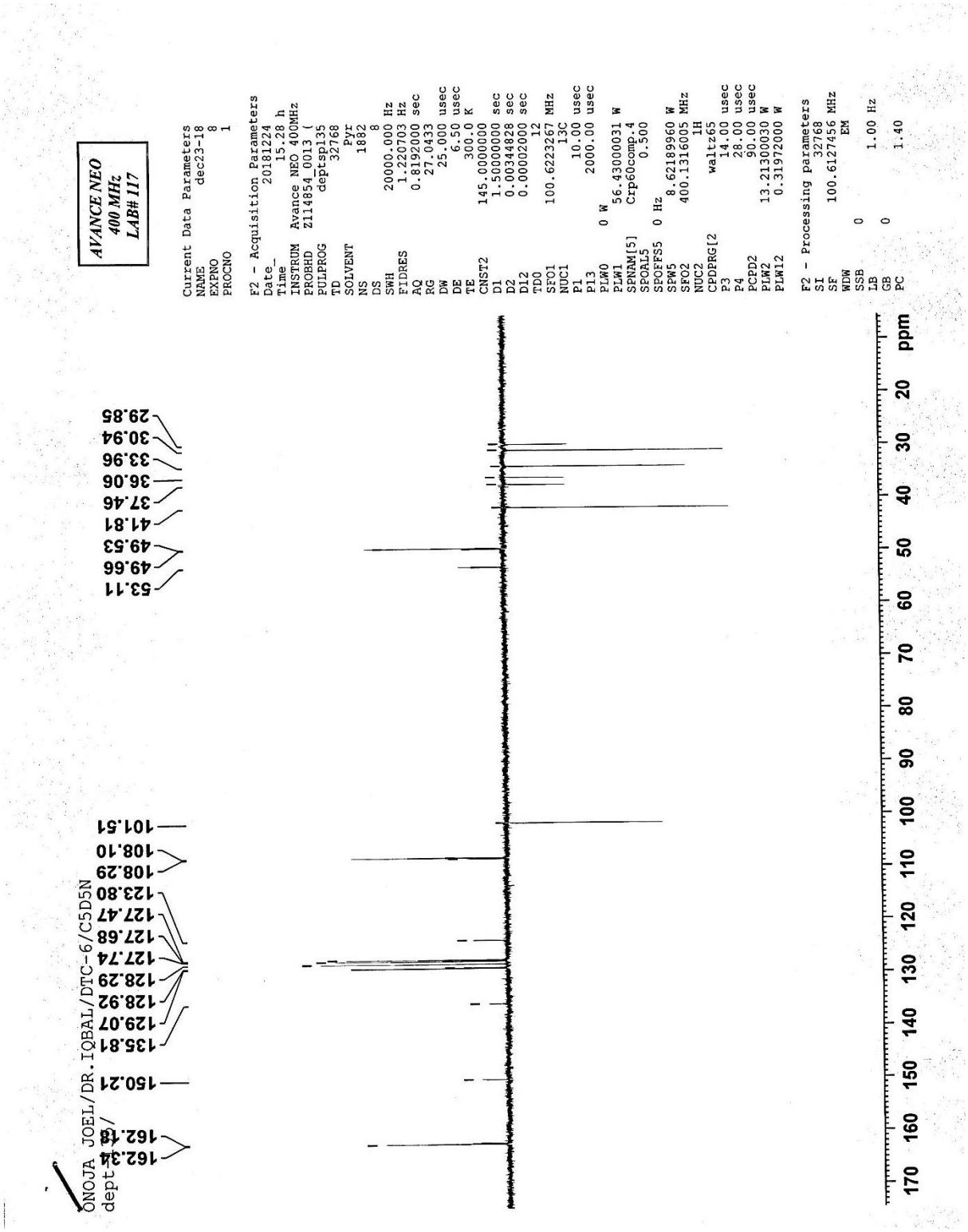

DEPT 135 spectra of N-formylanonaine

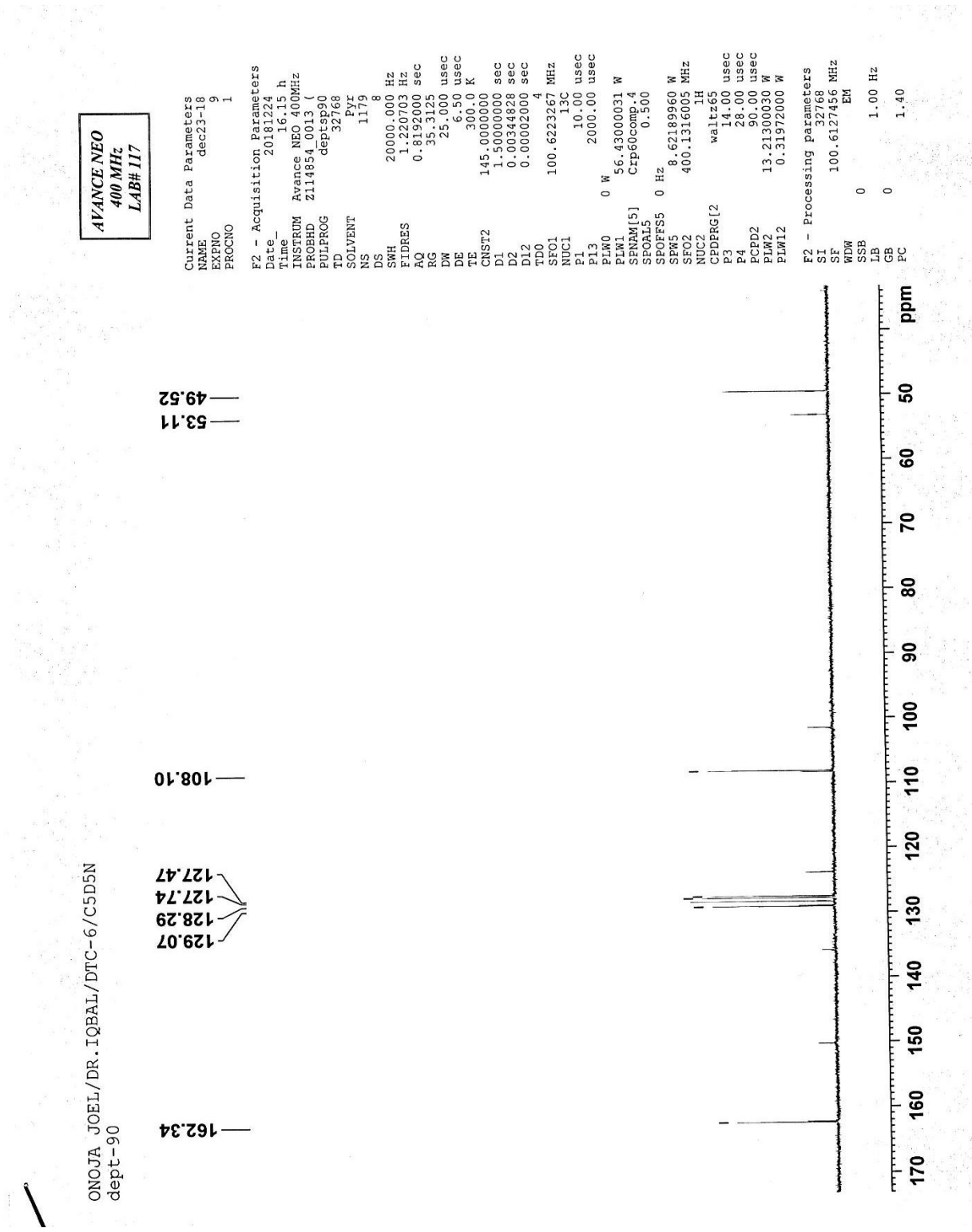

DEPT 90 spectra of N-formylanonaine

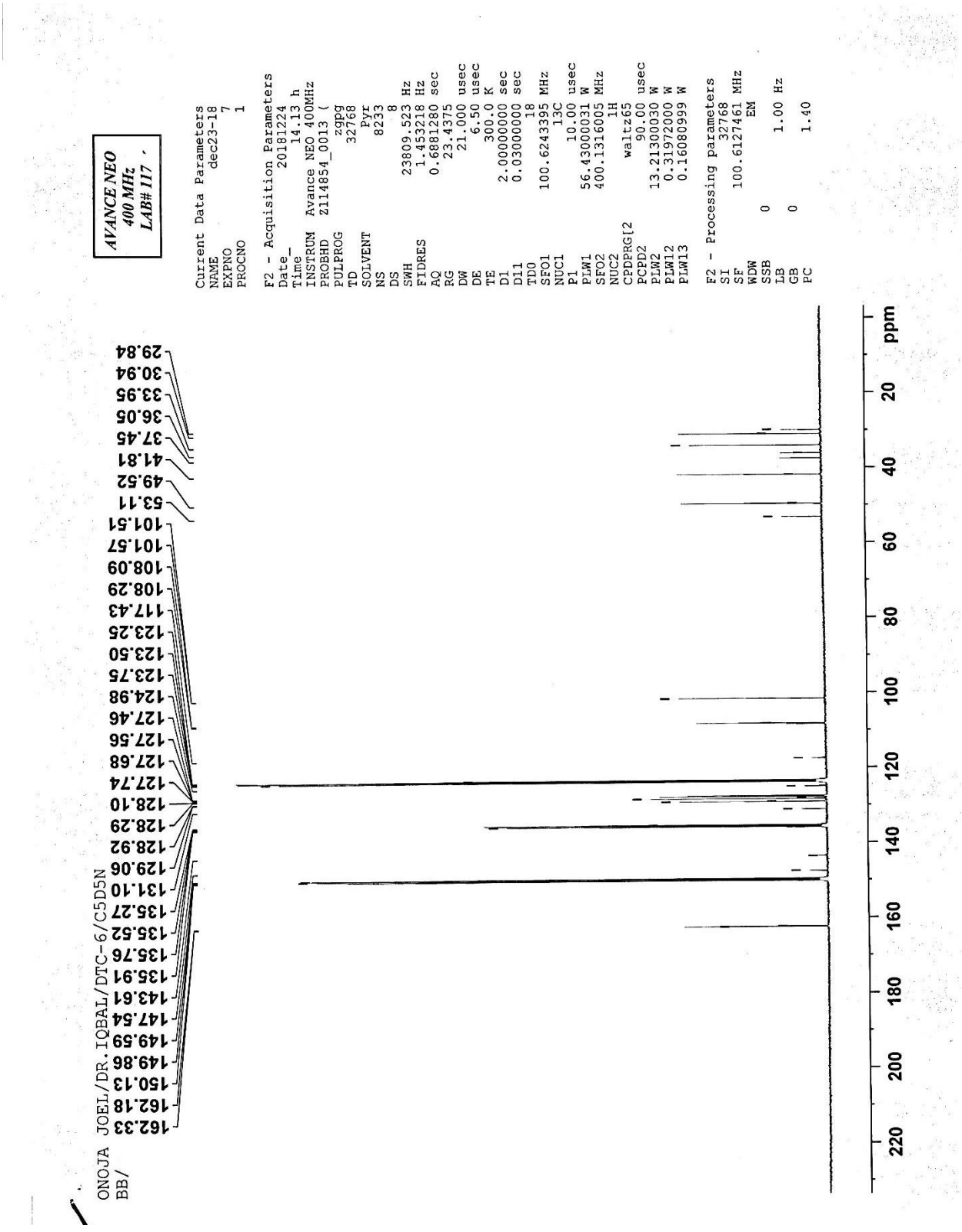

BB spectra of N-formylanonaine

Appendix 6: Spectroscopic analysis of Columbin

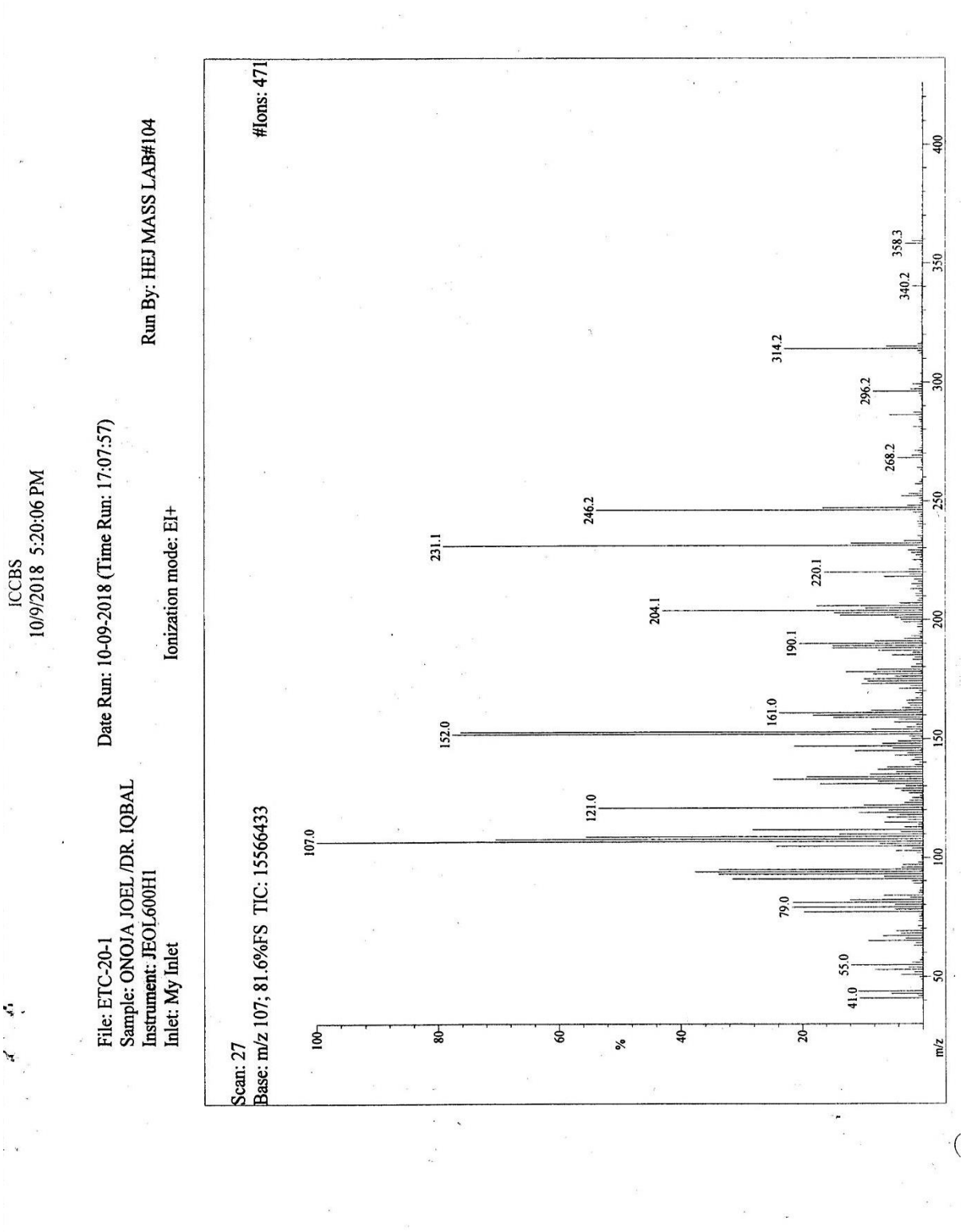

EI-MS spectra of Columbin

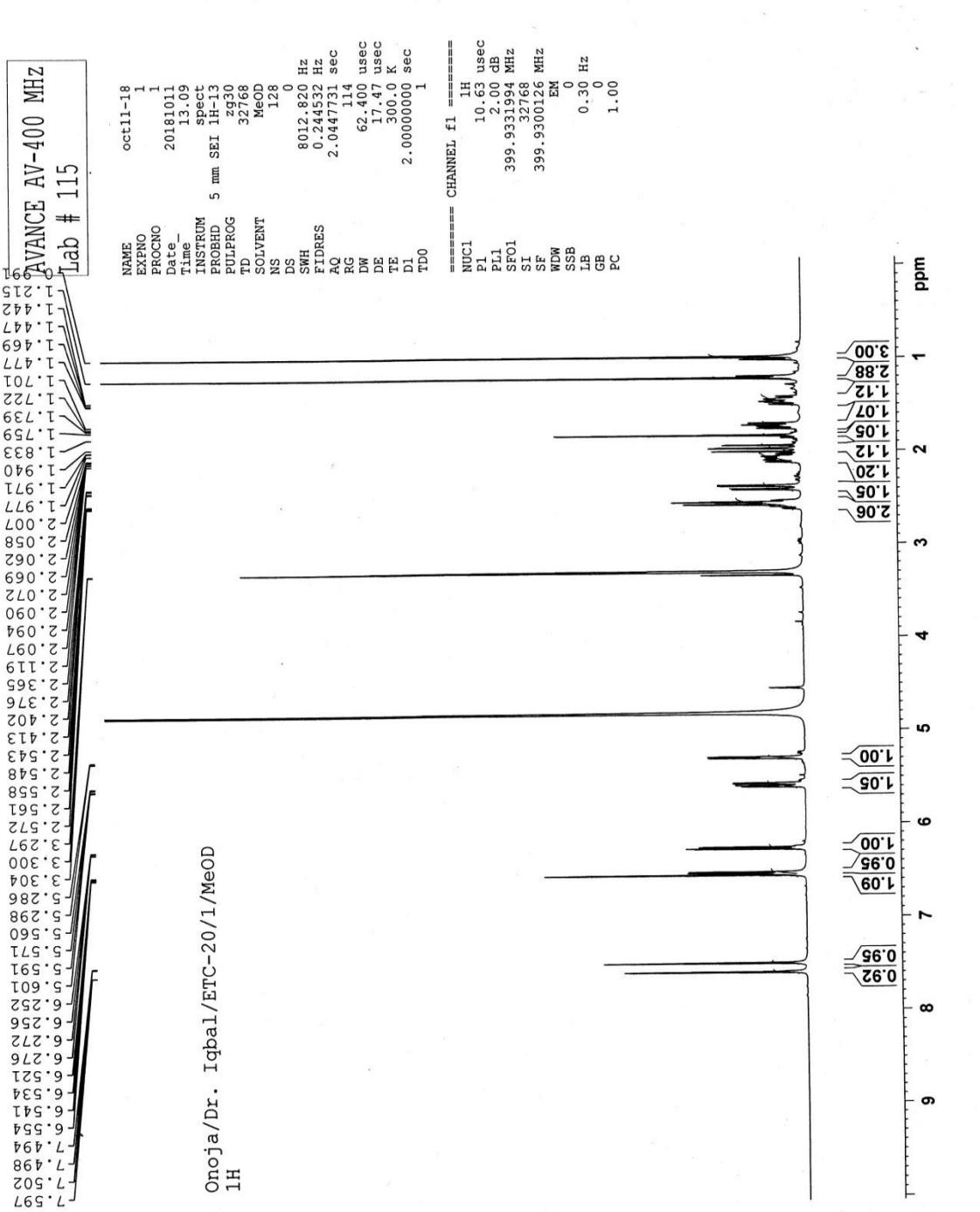

[1]H-NMR spectra of Columbin

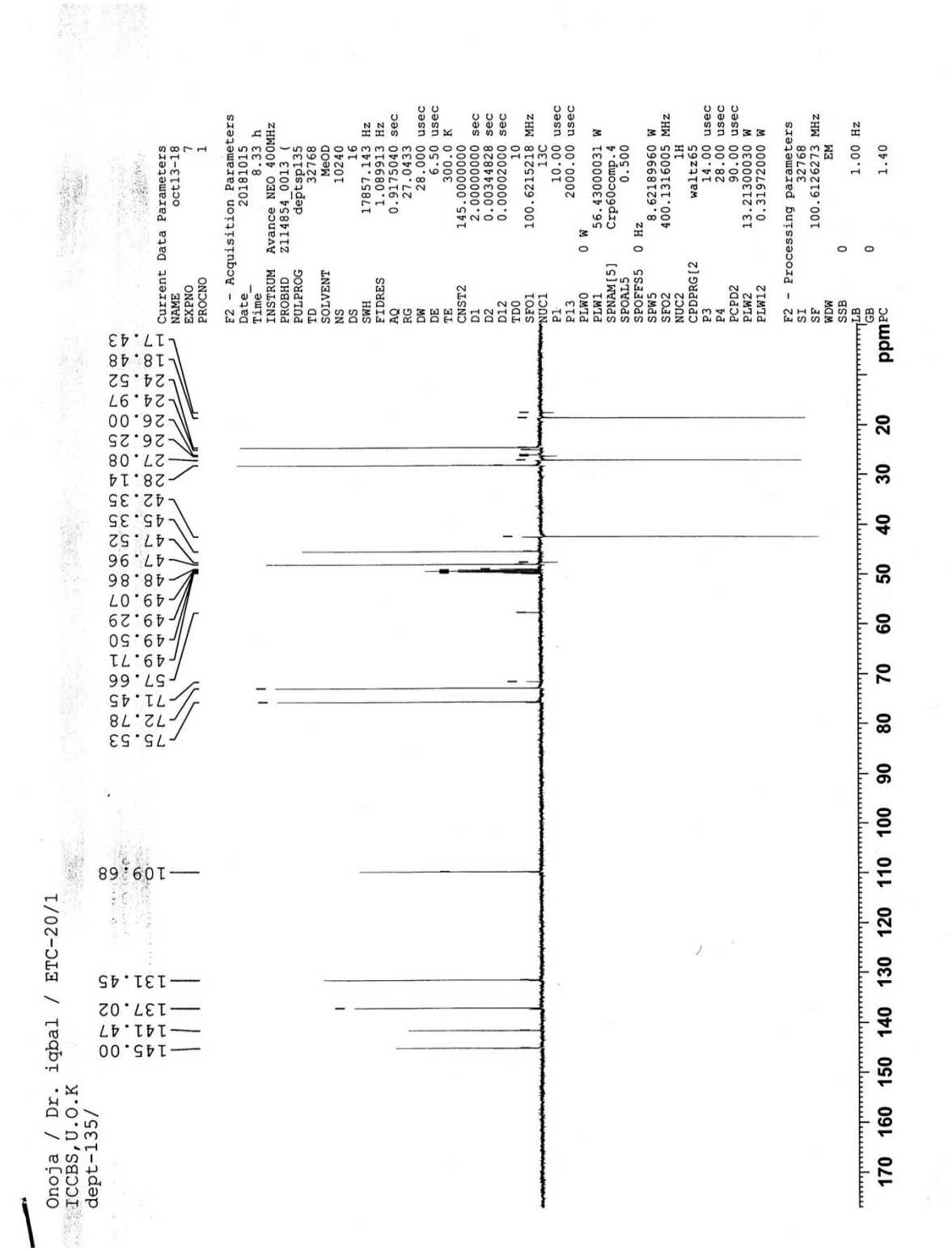

DEPT 135 spectra of Columbin

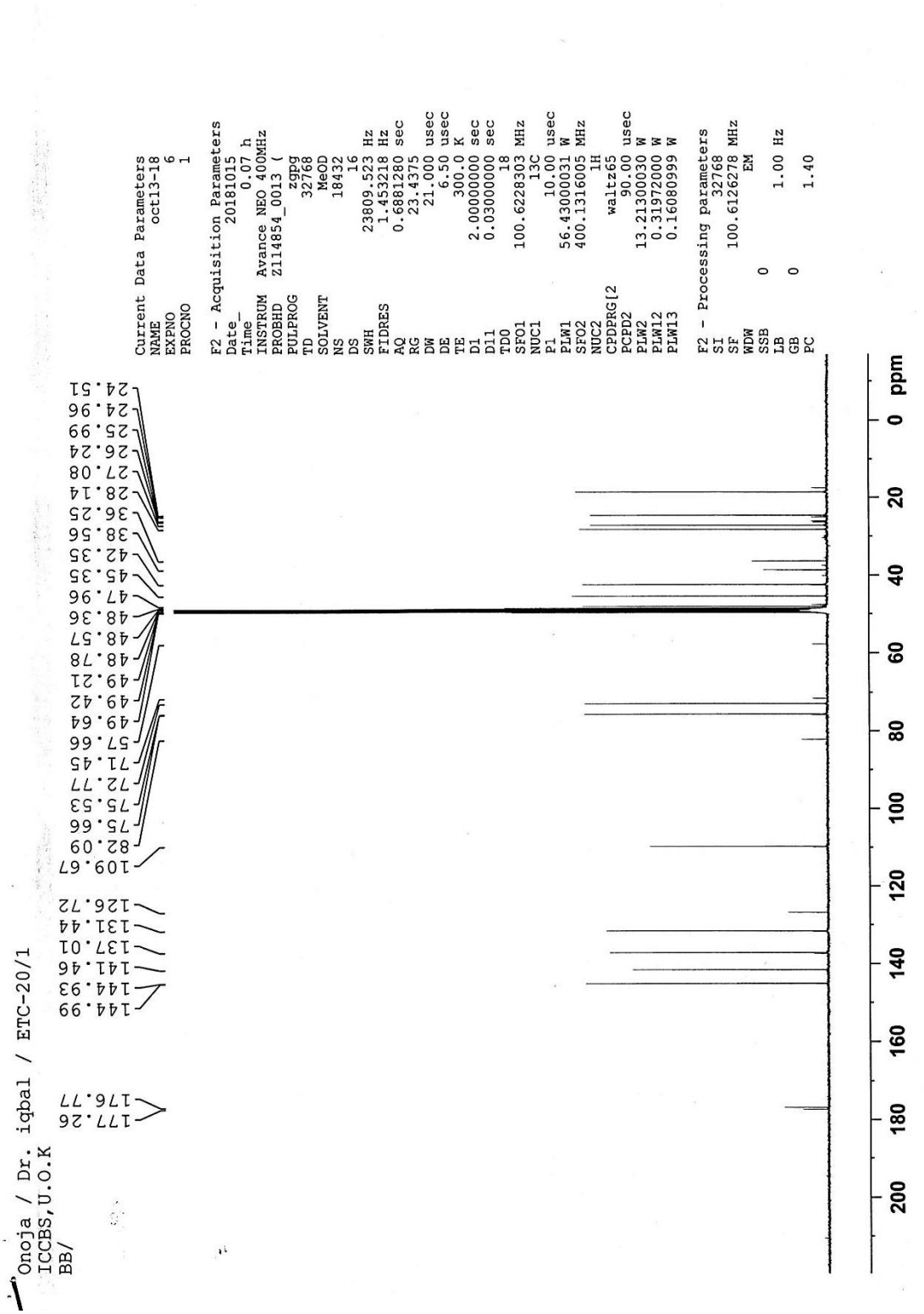

BB spectra of Columbin

Appendix 7: Spectroscopic analysis of 8-hydroxycolumbin

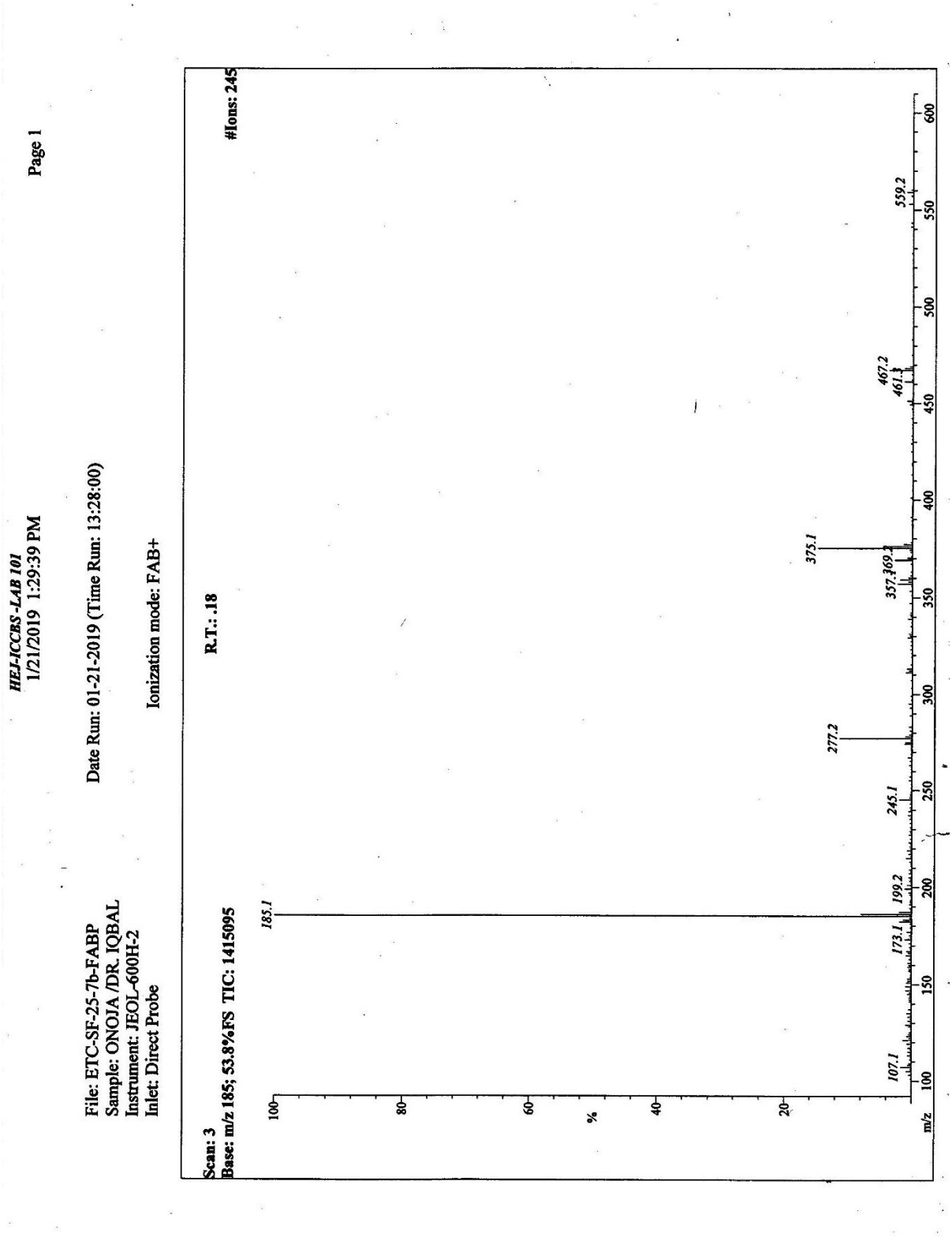

FABP spectra of 8-hydroxycolumbin

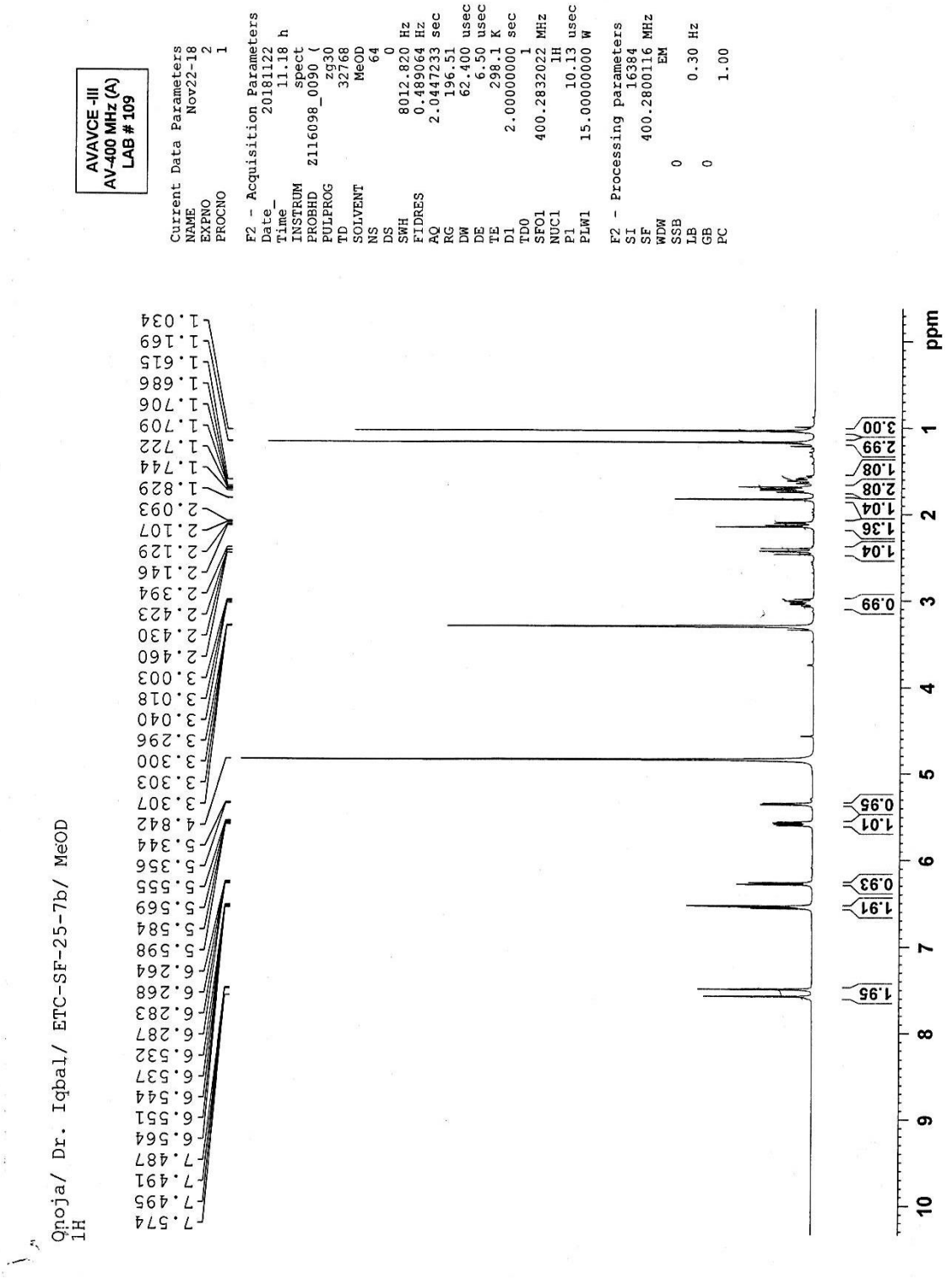

[1]H-NMR spectra of 8-hydroxycolumbin

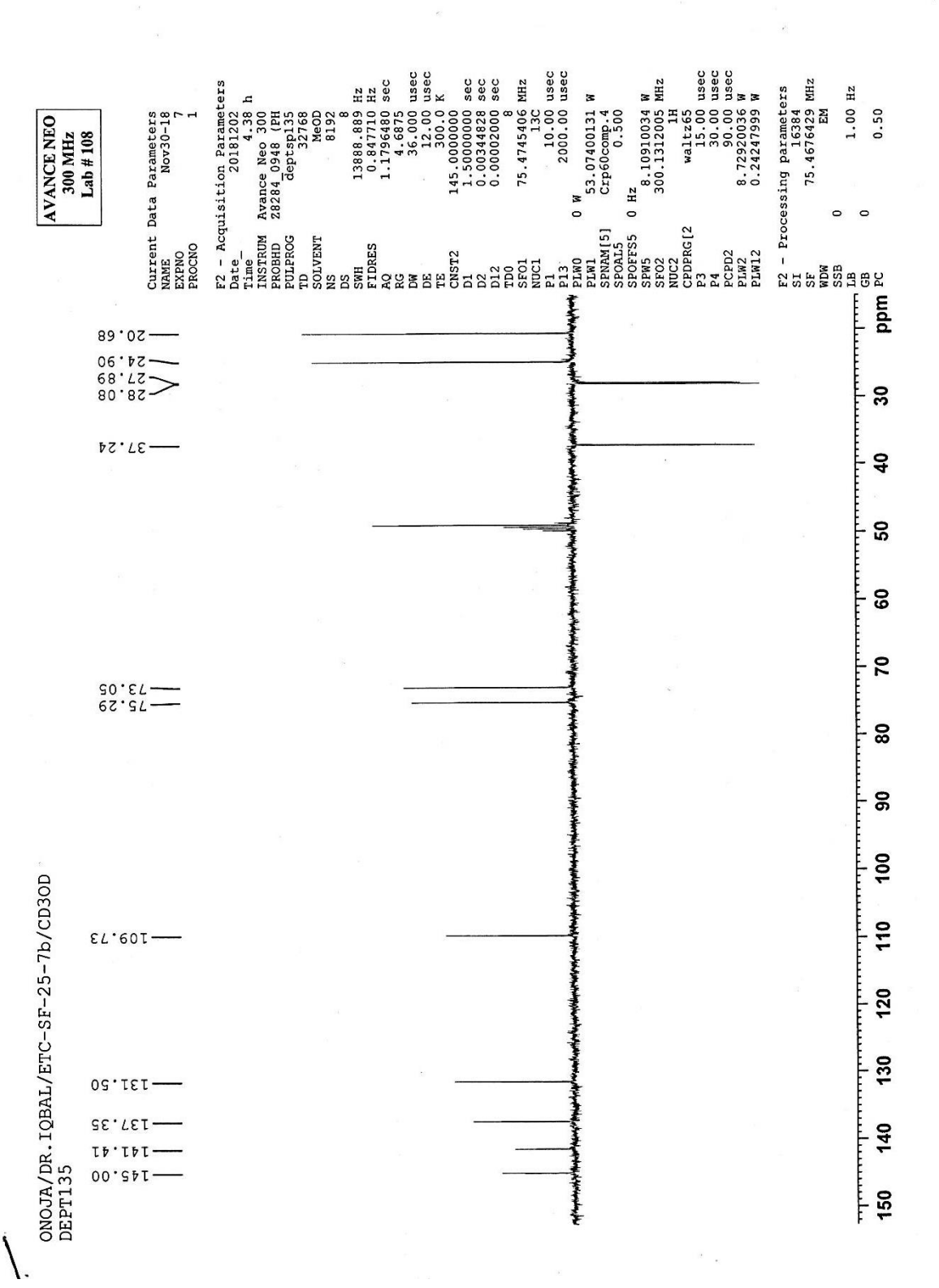

DEPT 135 spectra of 8-hydroxycolumbin

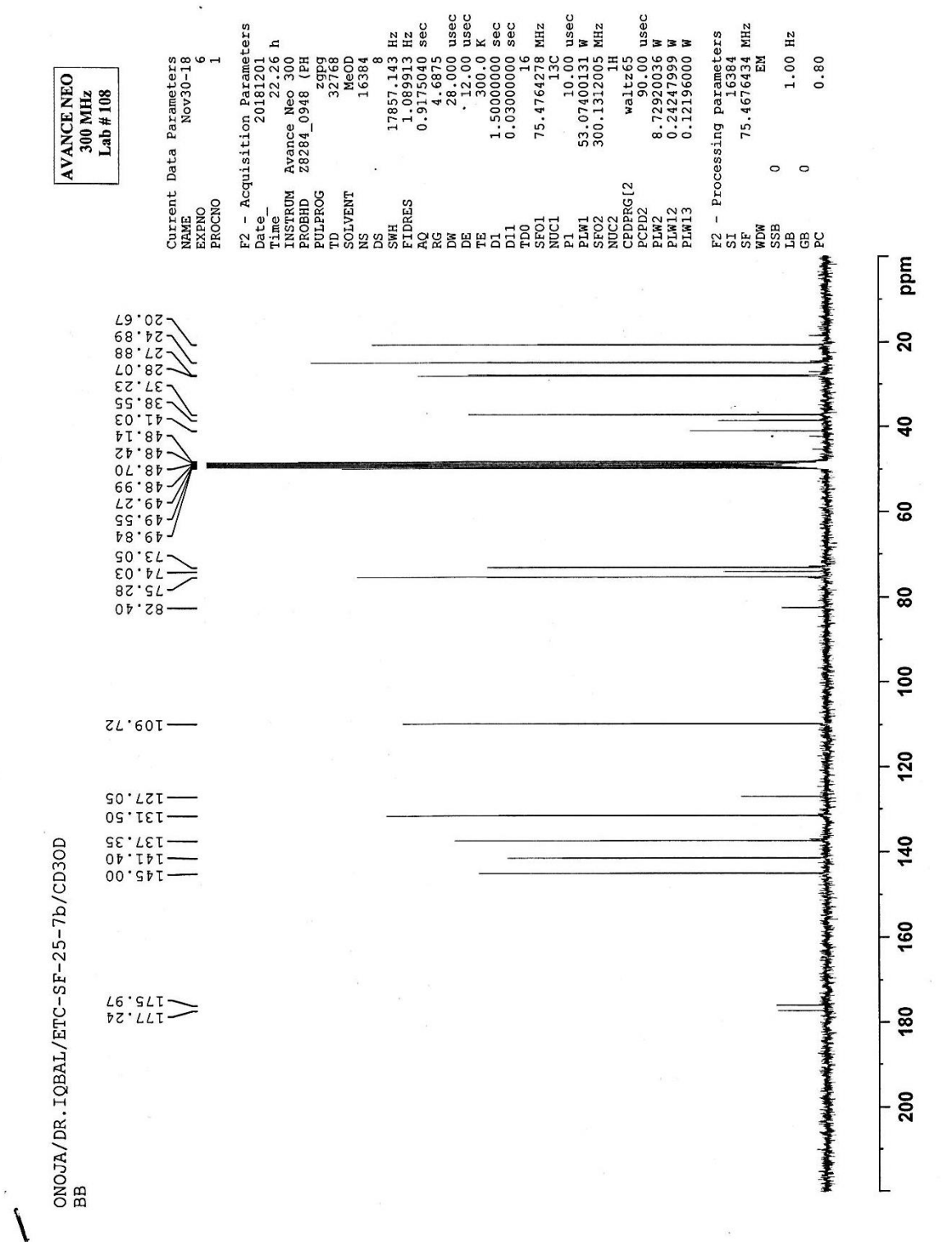

BB spectra of 8-hydroxycolumbin

Appendix 8: Spectroscopic analysis of Tinosporide

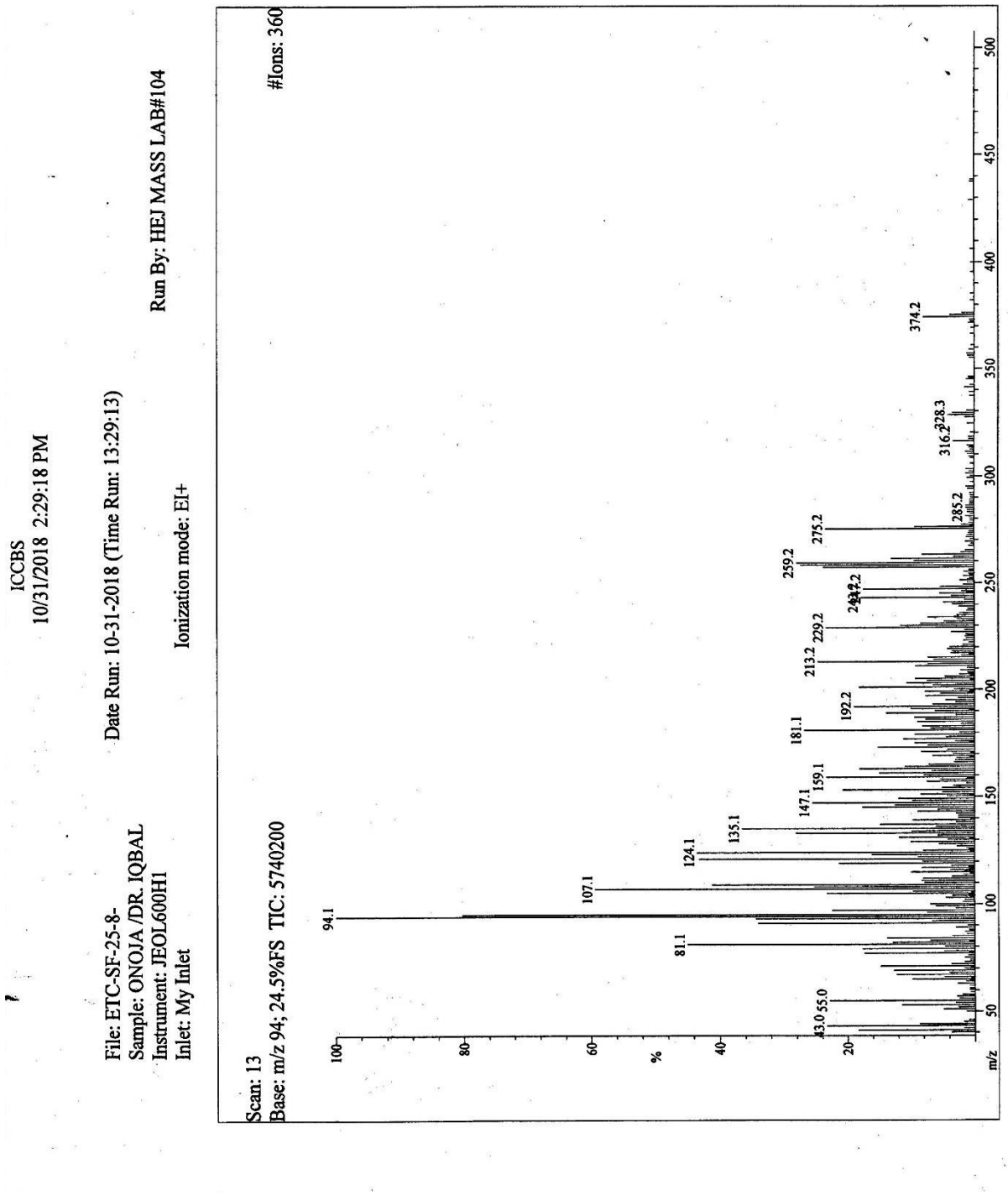

EI-MS spectra of Tinosporide

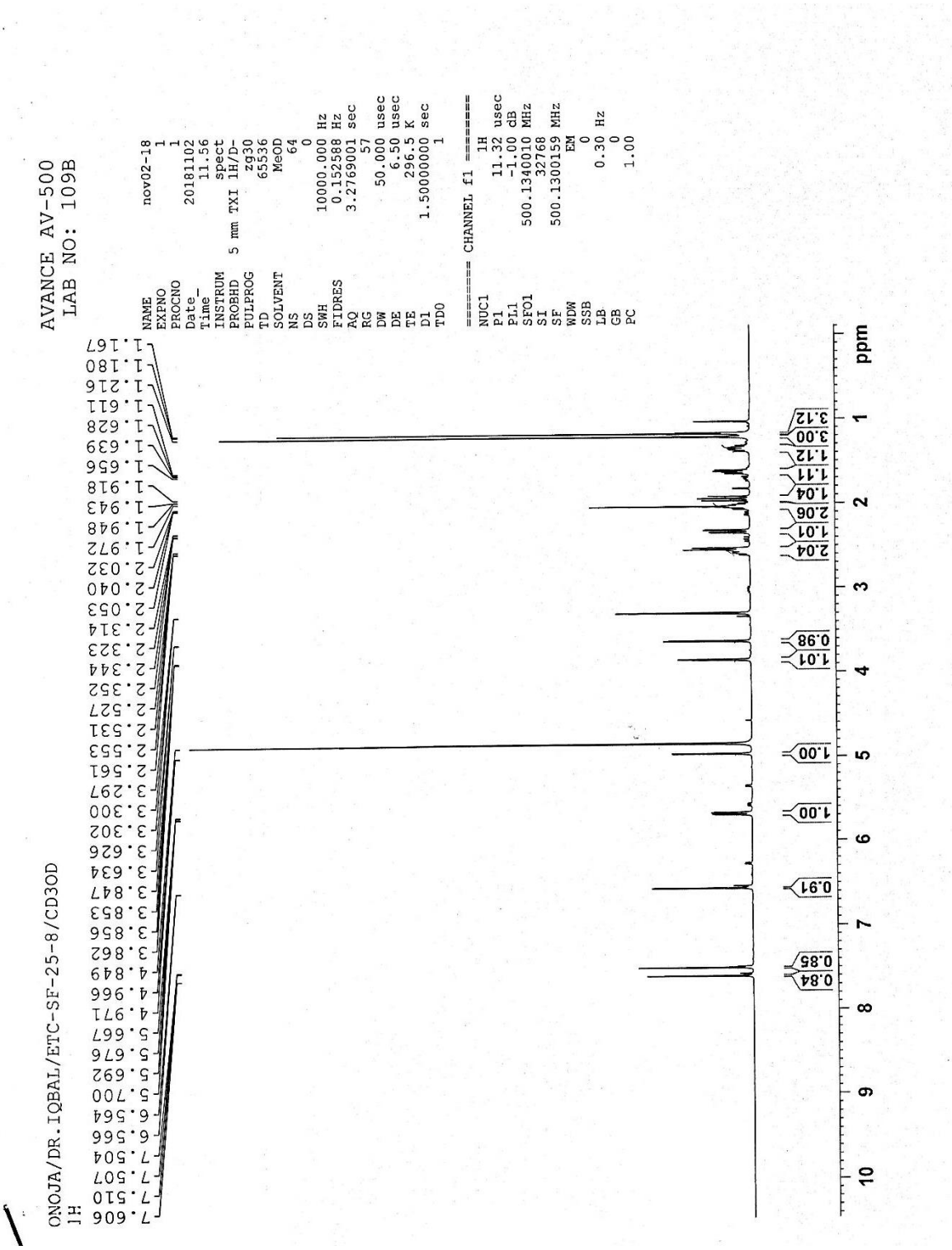

[1]H-NMR spectra of Tinosporide

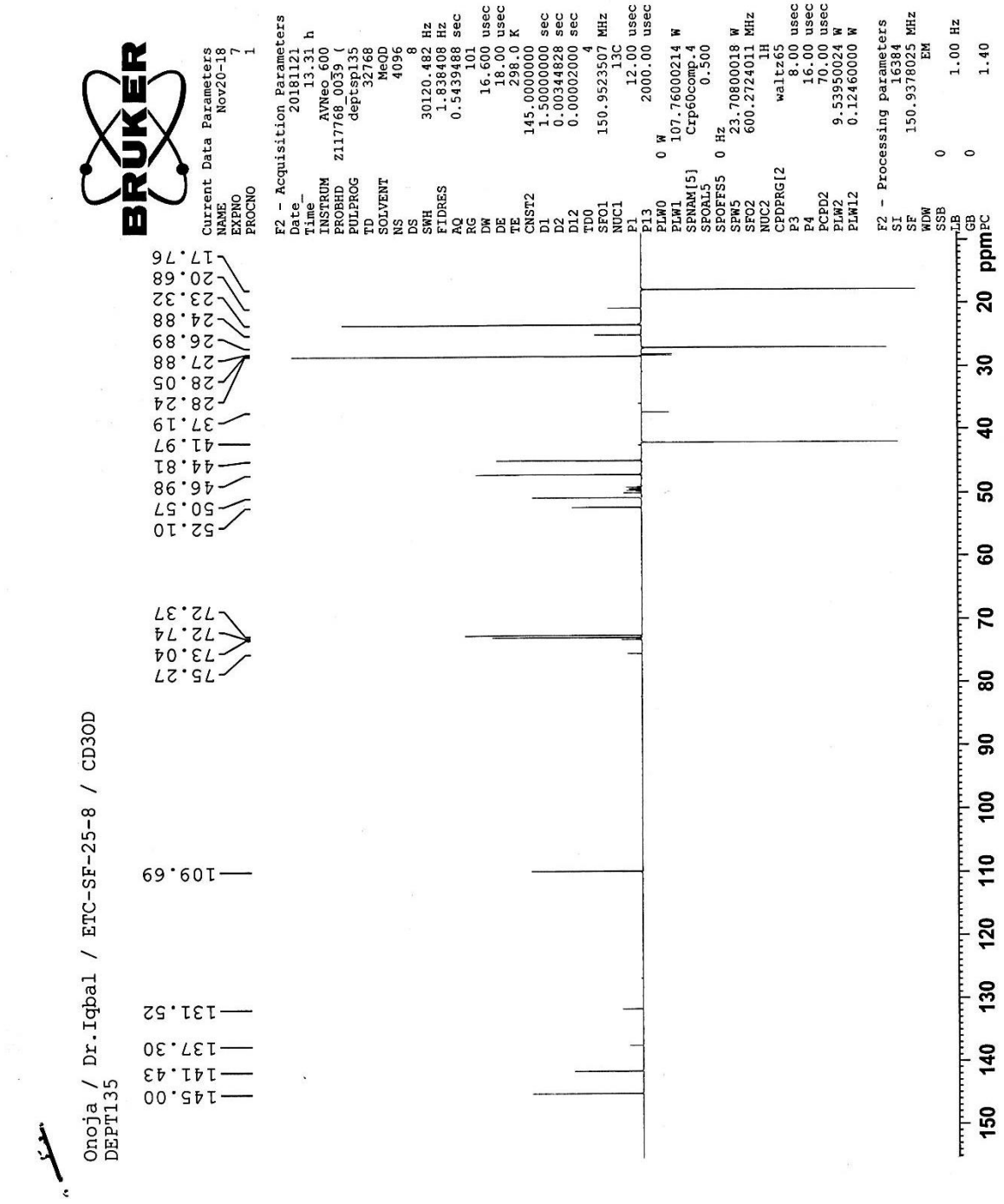

DEPT 135 spectra of Tinosporide

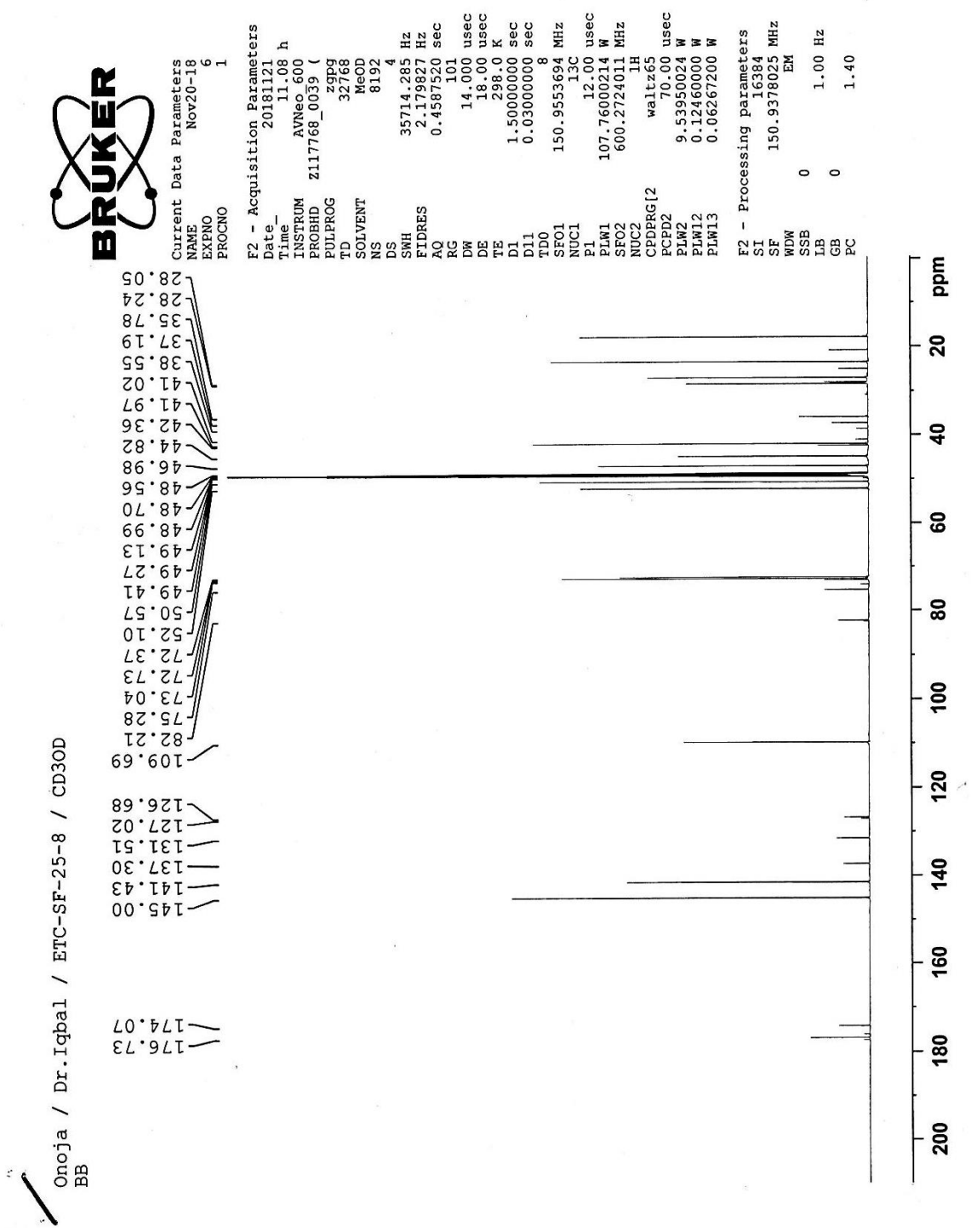

BB spectra of Tinosporide

Appendix 9: Spectroscopic analysis of Tinosporicide

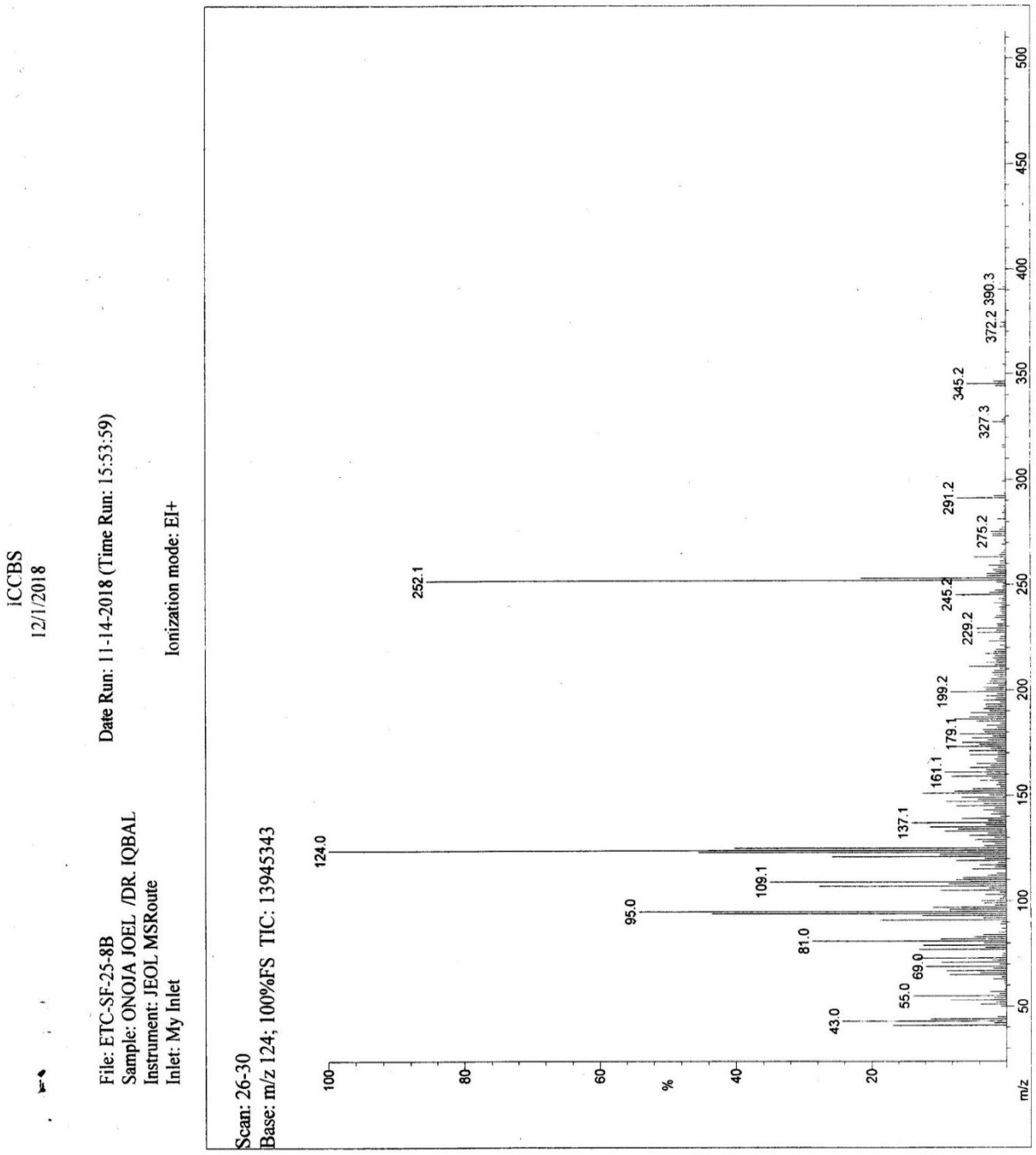

EI-MS spectra of Tinosporicide

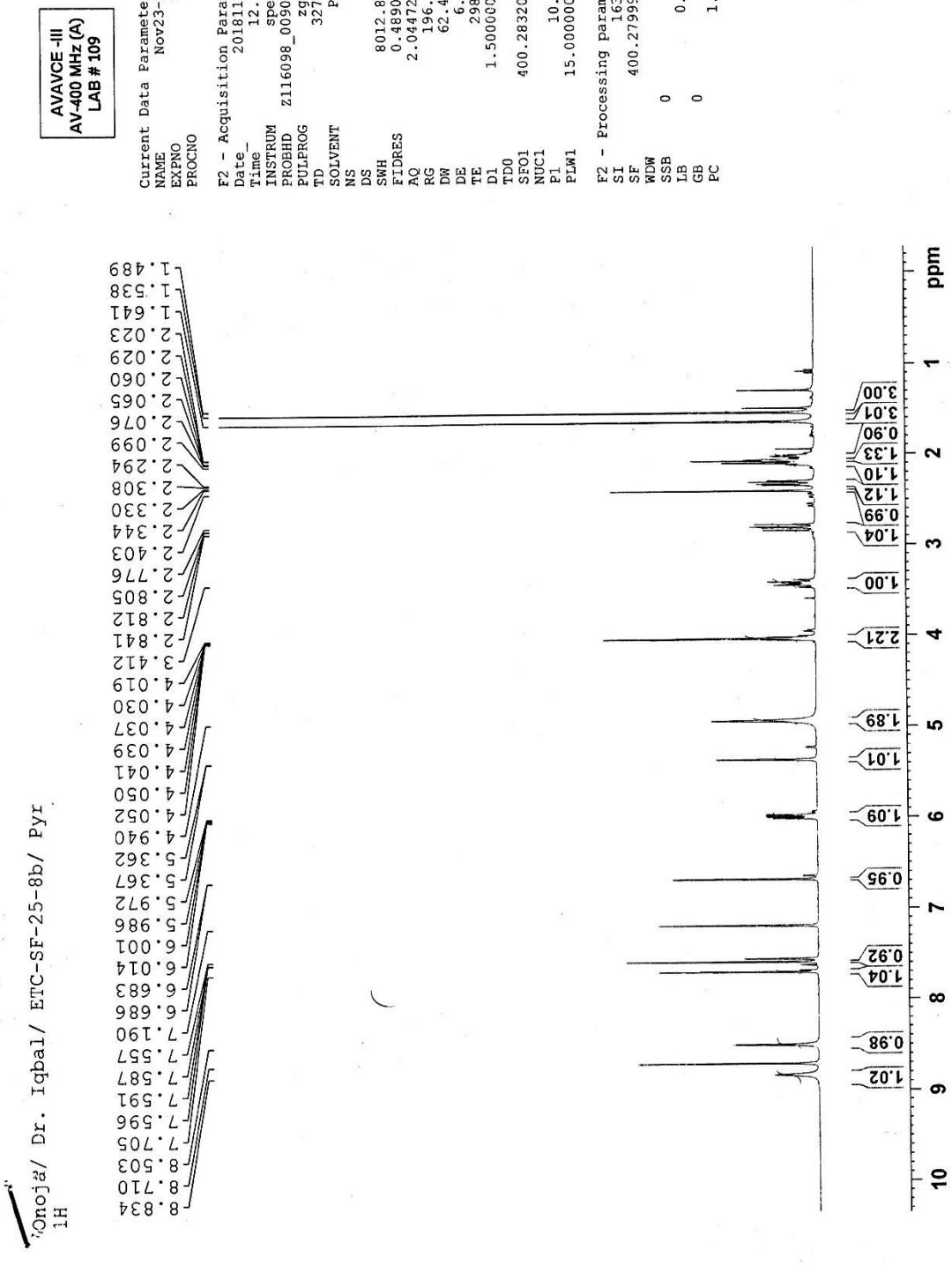

^{1}H-NMR spectra of Tinosporicide

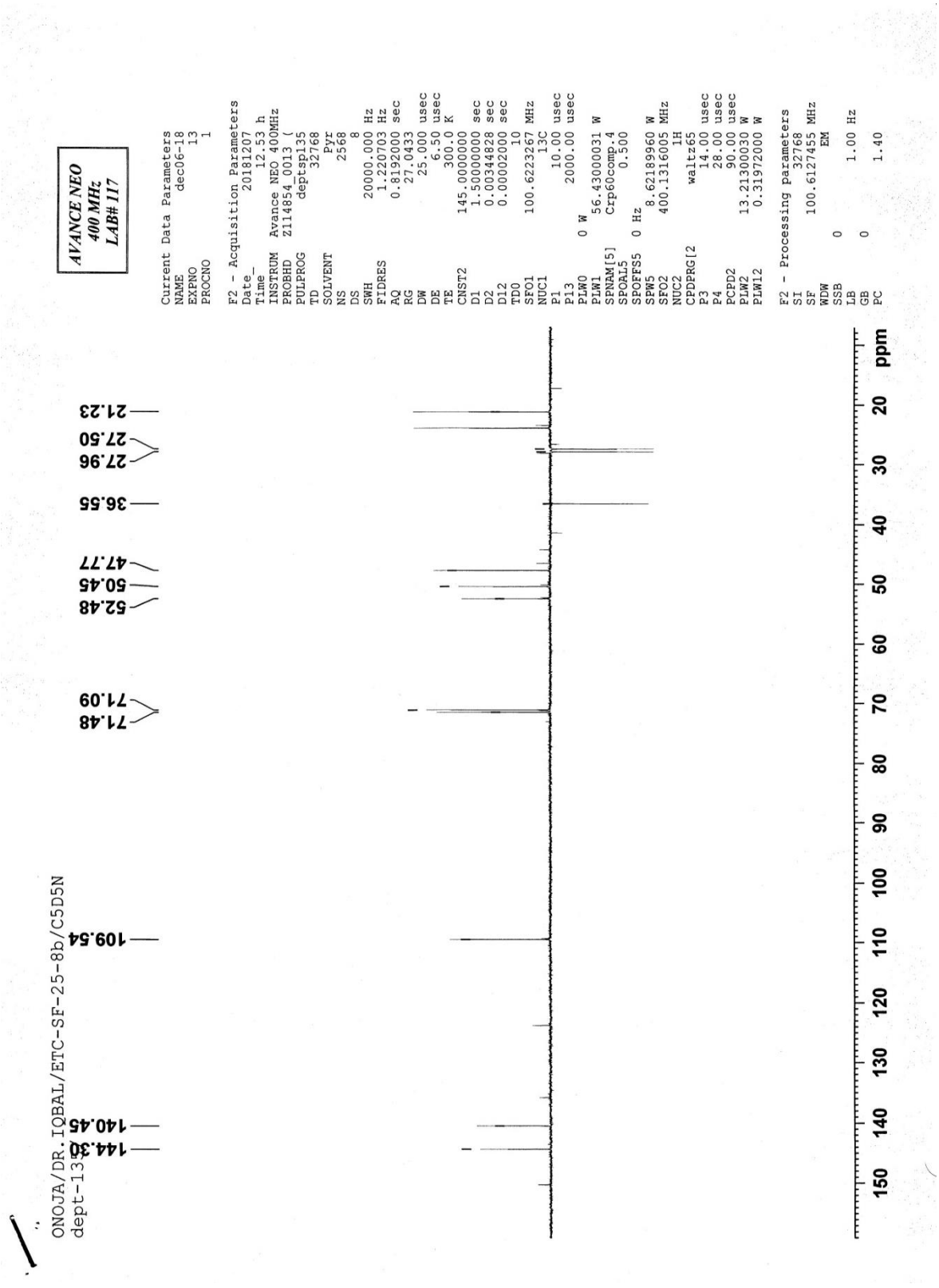

DEPT 135 spectra of Tinosporicide

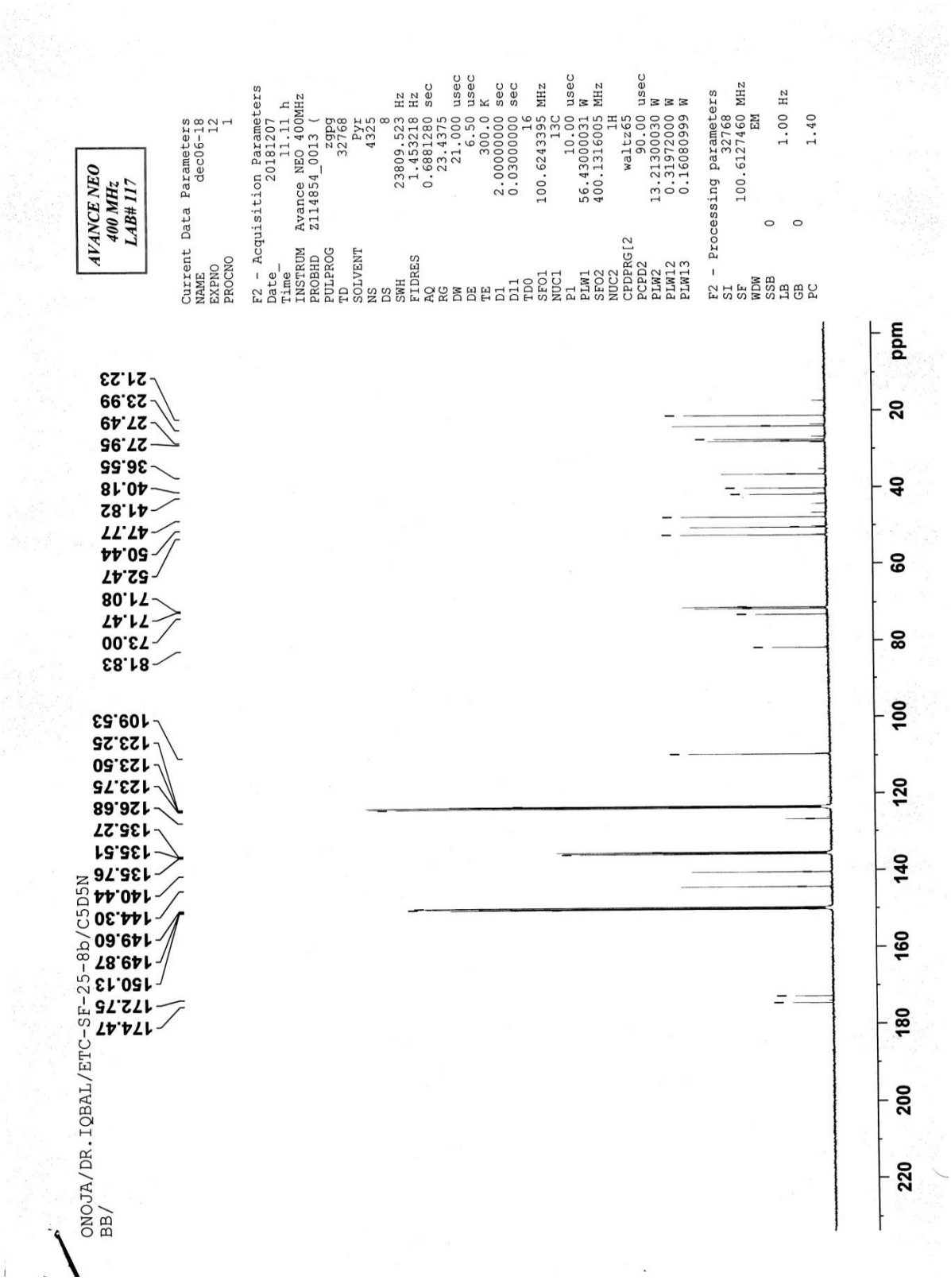

BB spectra of Tinosporicide

Appendix 10: Spectroscopic analysis of Corydine

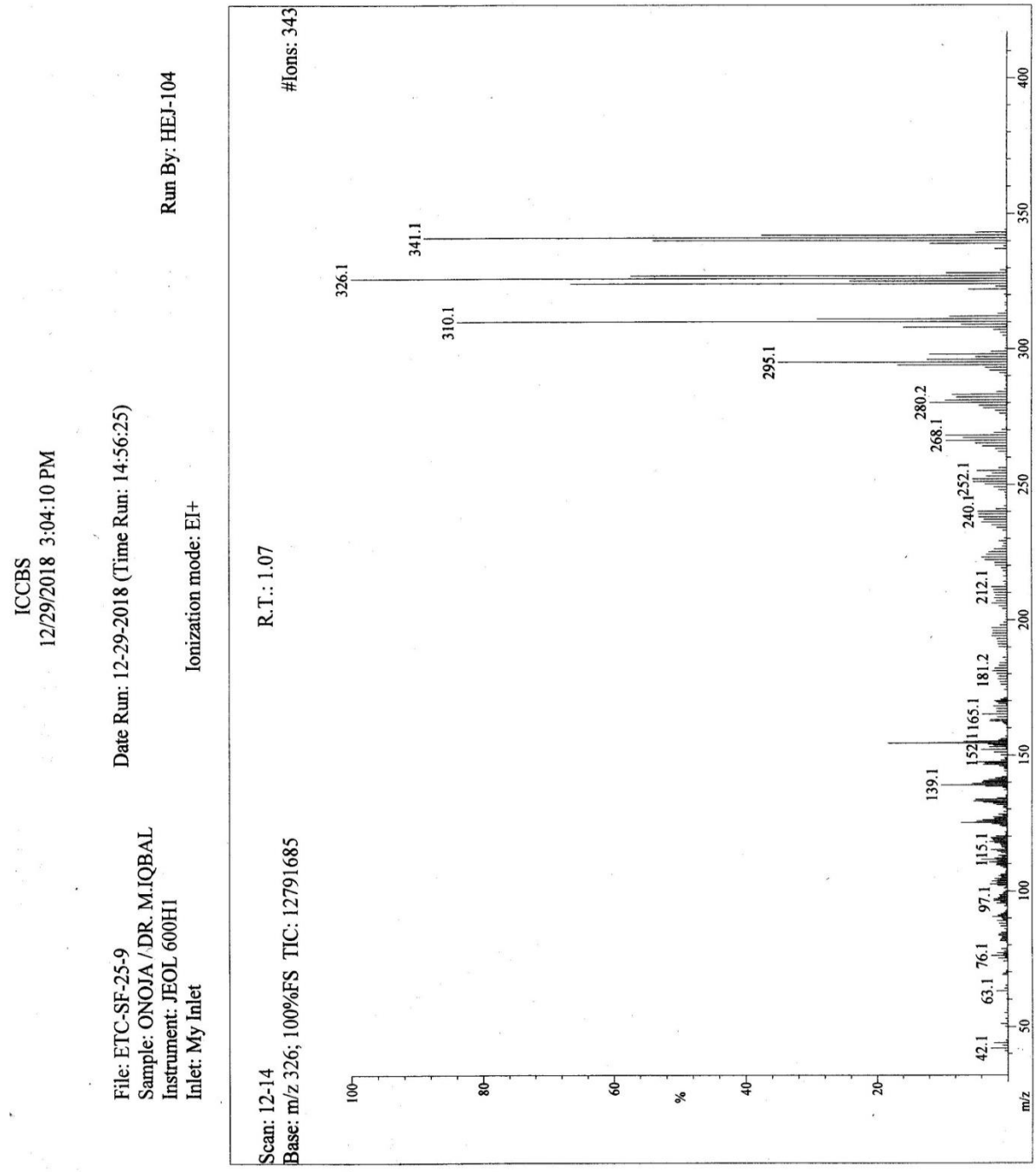

EI-MS spectra of Corydine

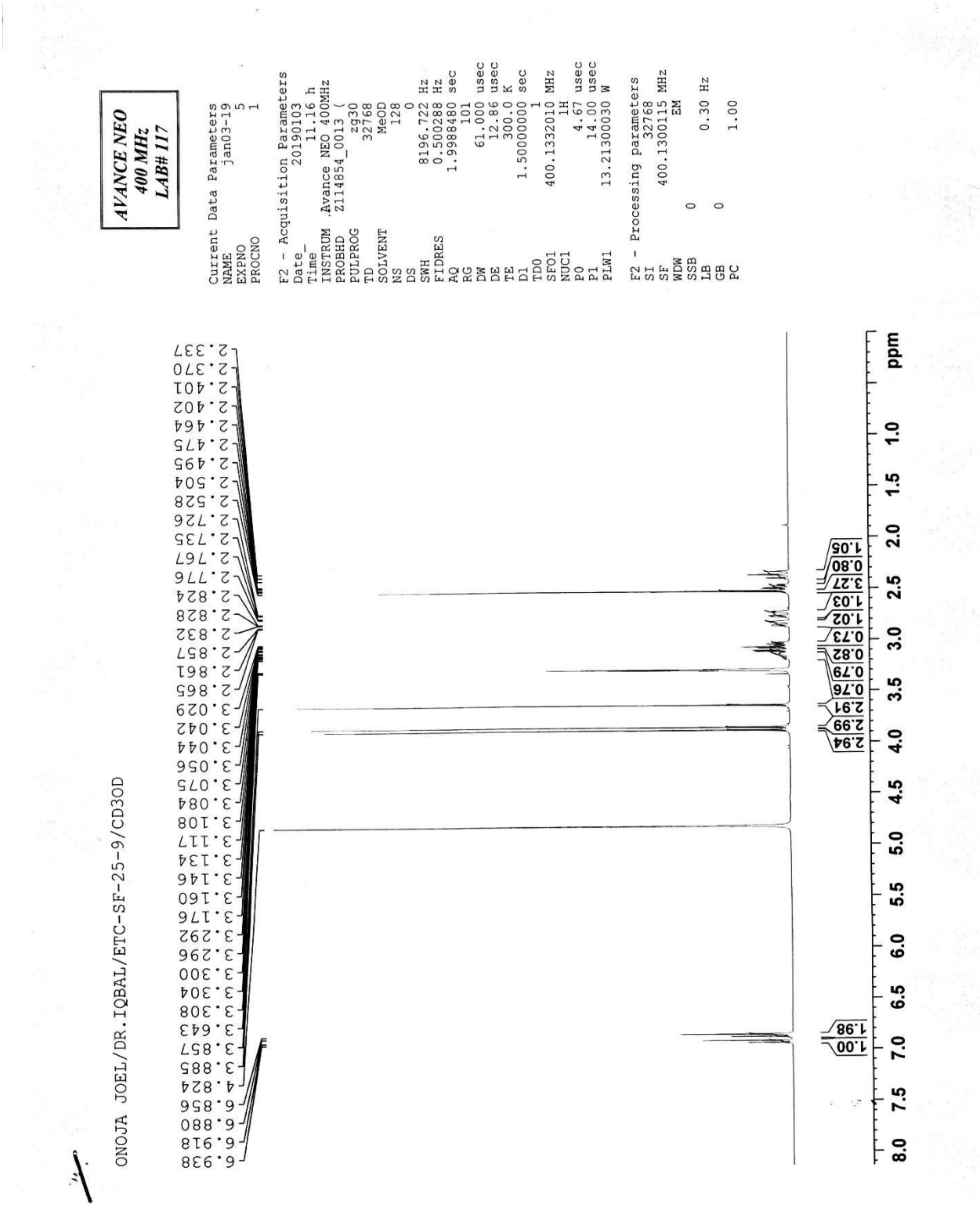

[1]H-NMR spectra of Corydine

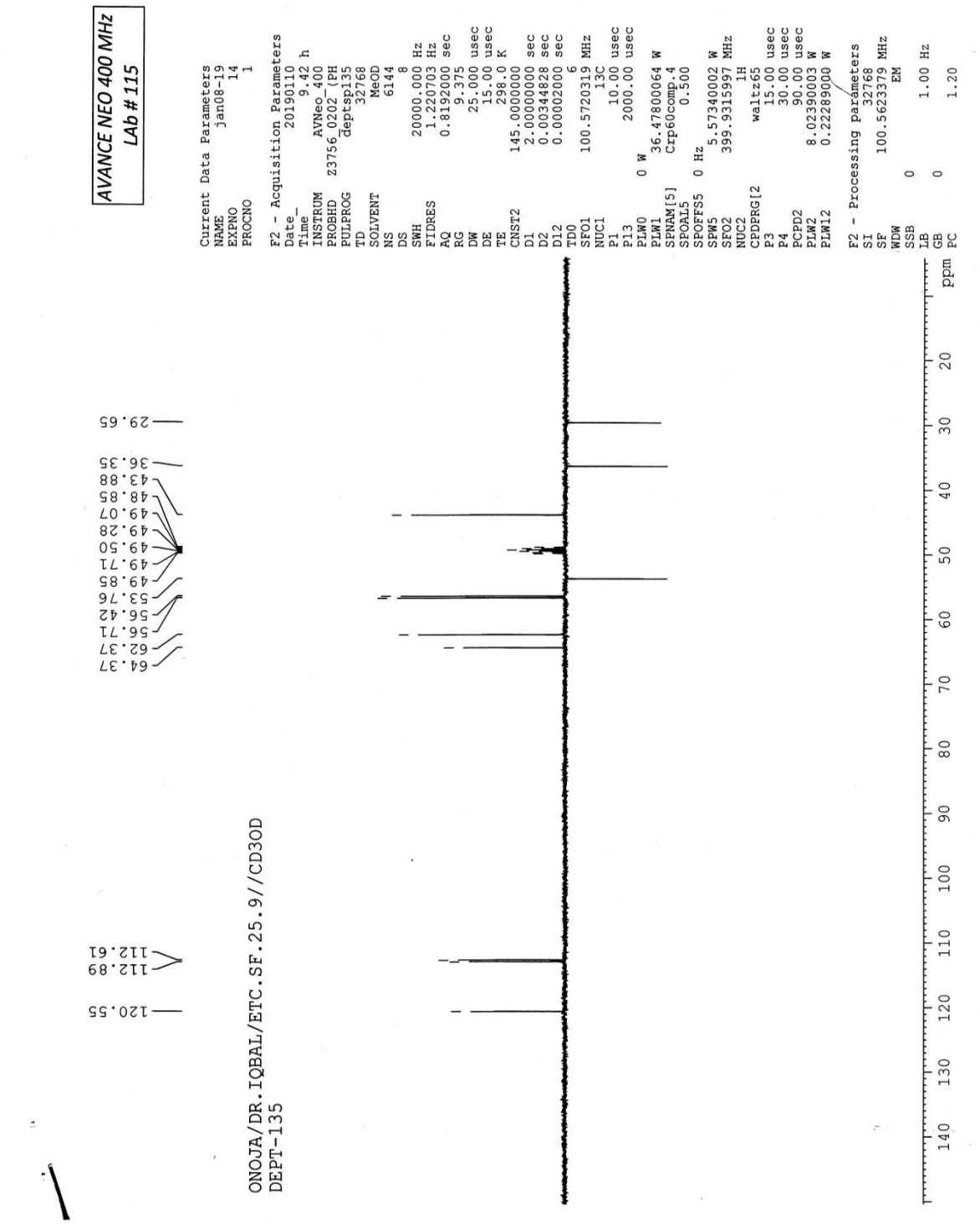

DEPT 135 spectra of Corydine

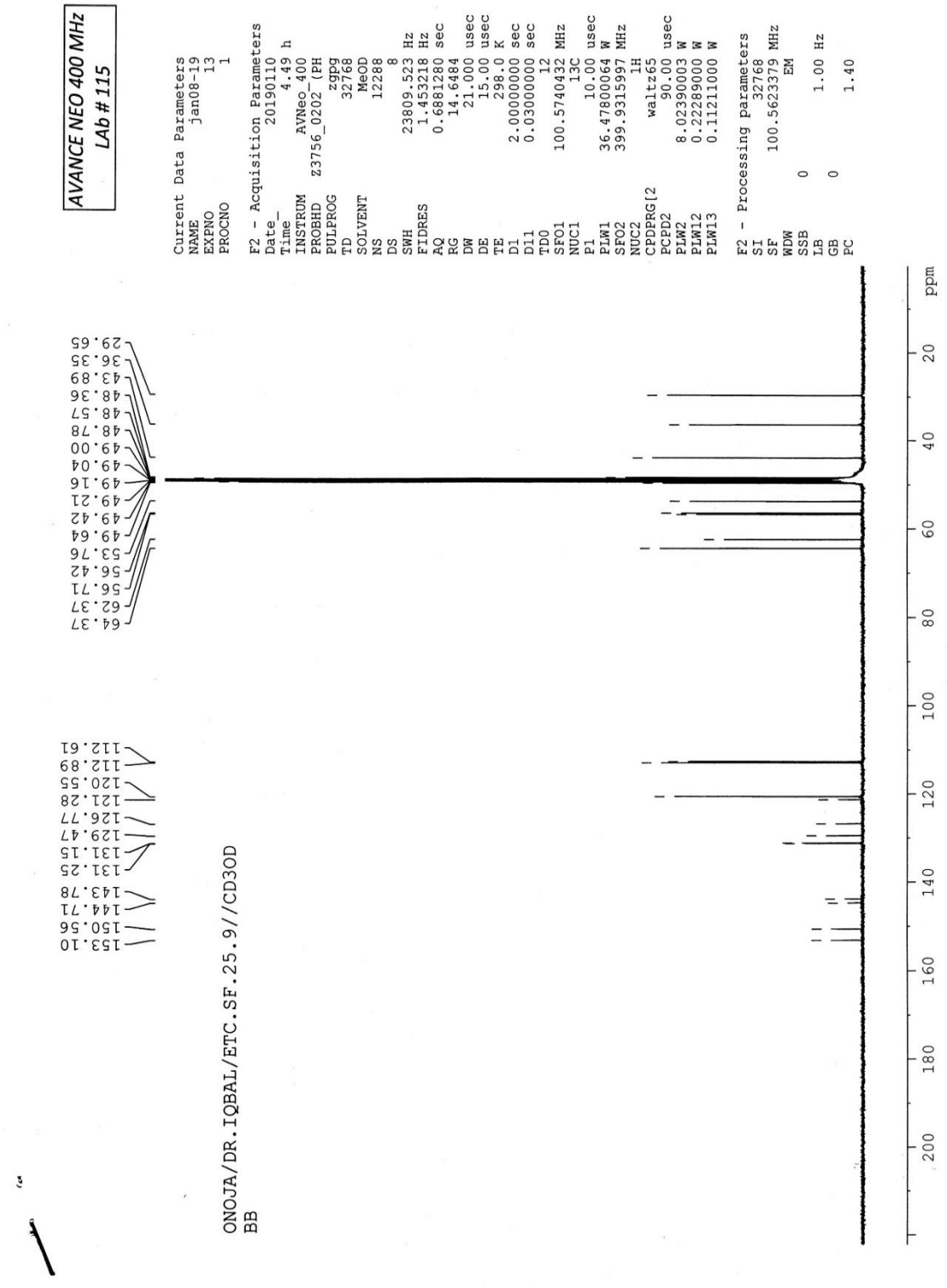

BB spectra of Corydine

Appendix 11: Spectroscopic analysis of Oxoglaucine

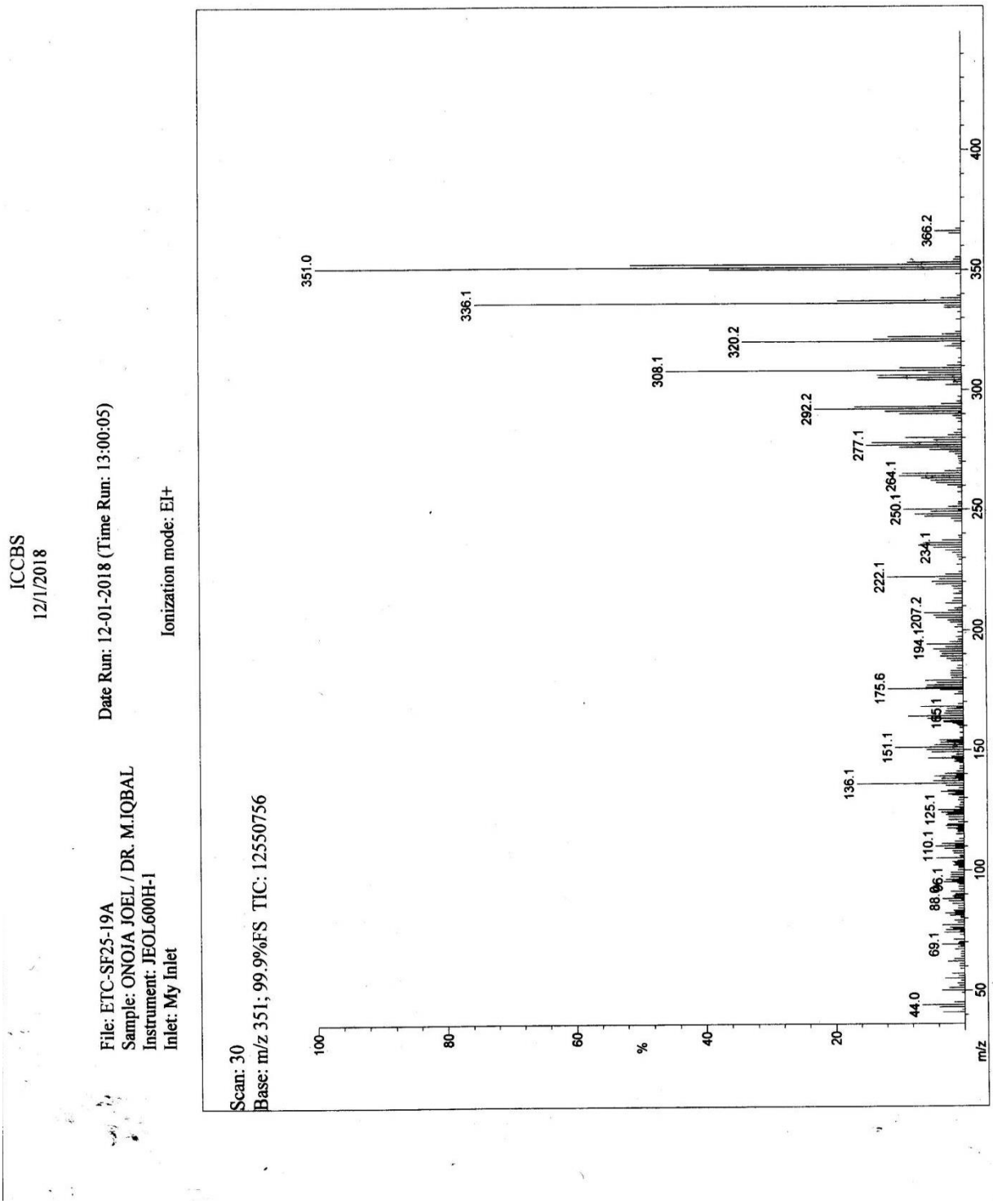

EI-MS spectra of Oxoglaucine

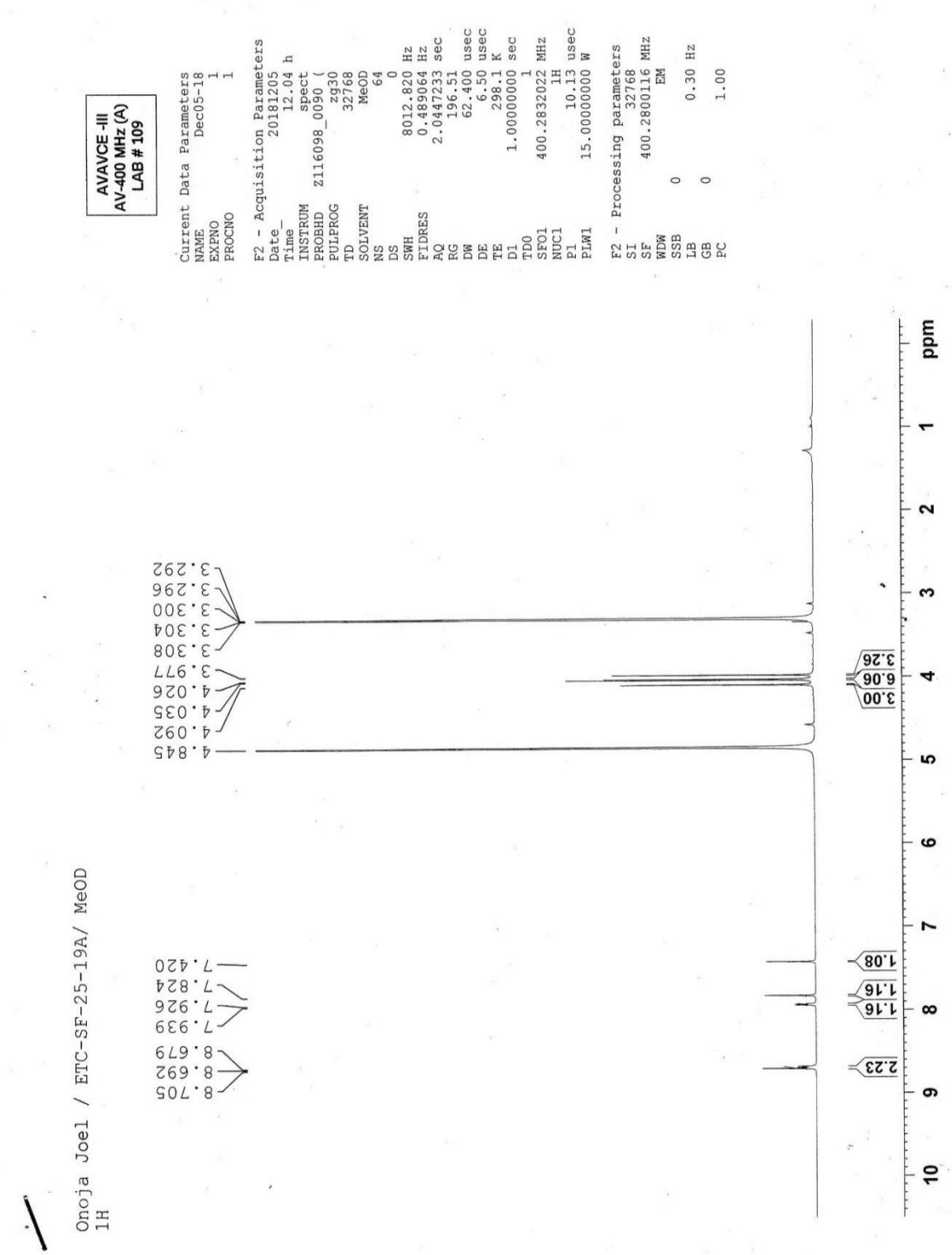

[1]H-NMR spectra of Oxoglaucine

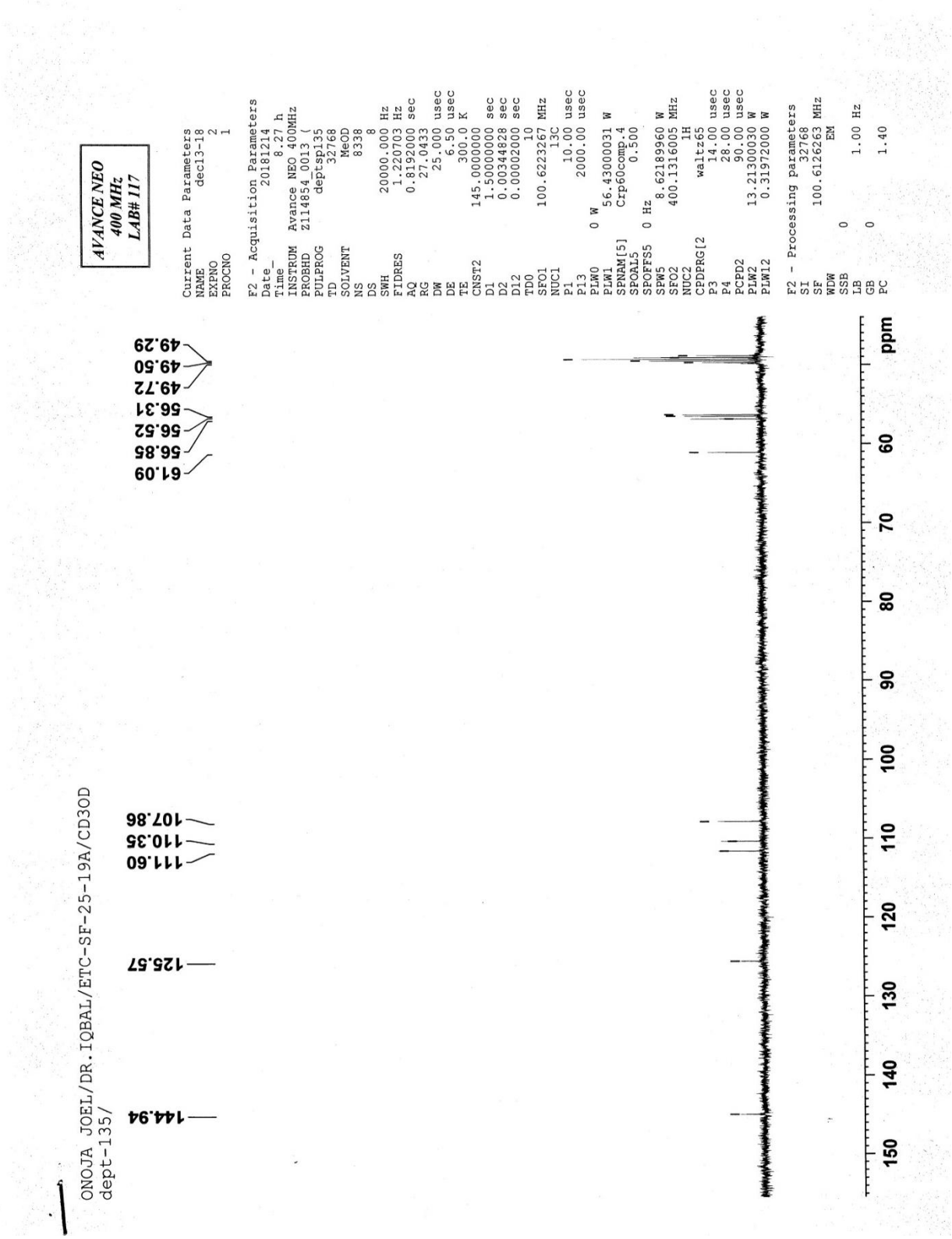

DEPT 135 spectra of Oxoglaucine

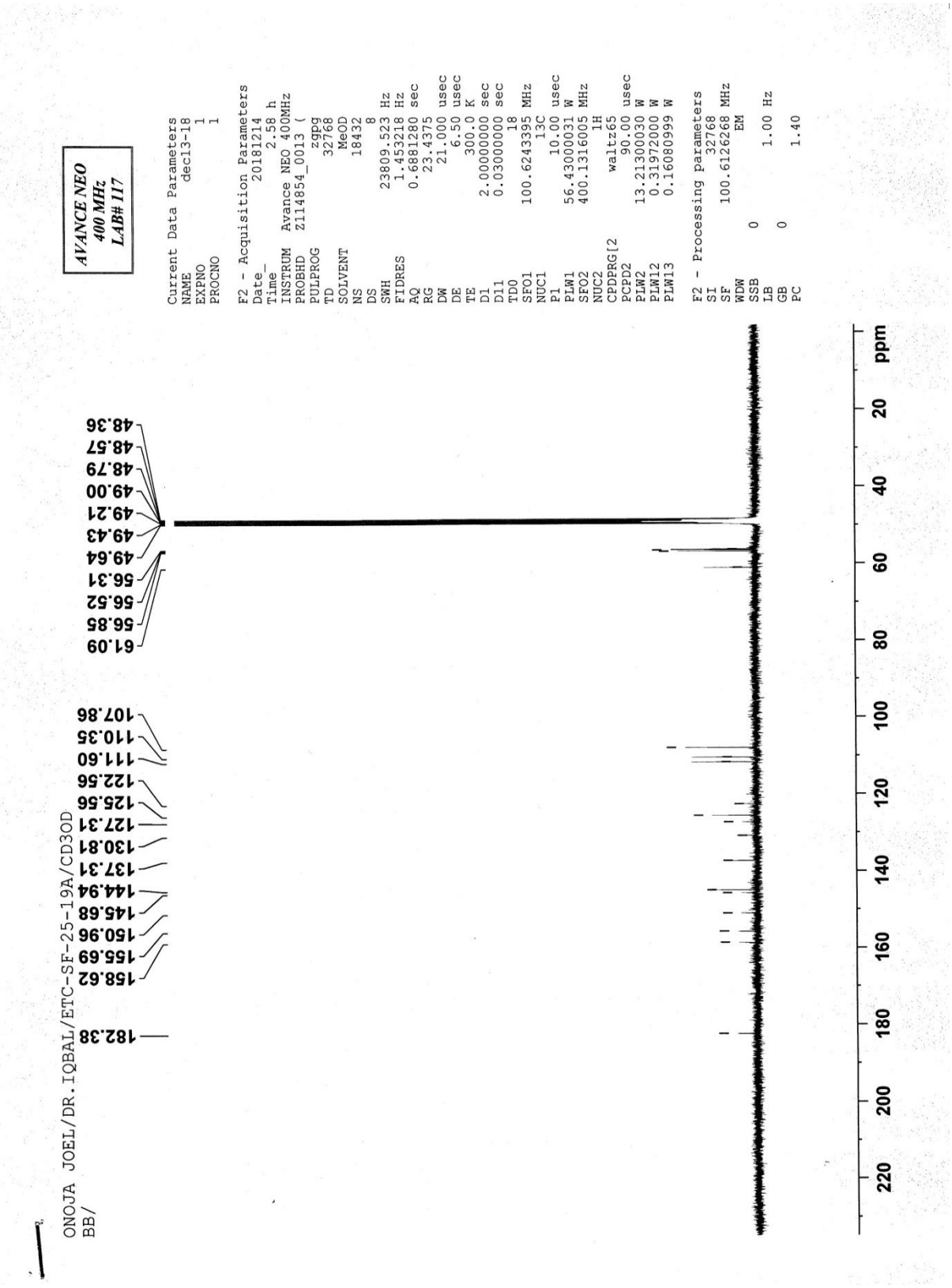

BB spectra of Oxoglaucine

Appendix 12: Spectroscopic analysis of re l - (2 S , 3 S , 4R, 1 6E) - 2 - [(2 ’R) - 2 ’ - h y d ro x y nonadecanoylamino]-heneicosadec-16-ene-1,3,4-triol

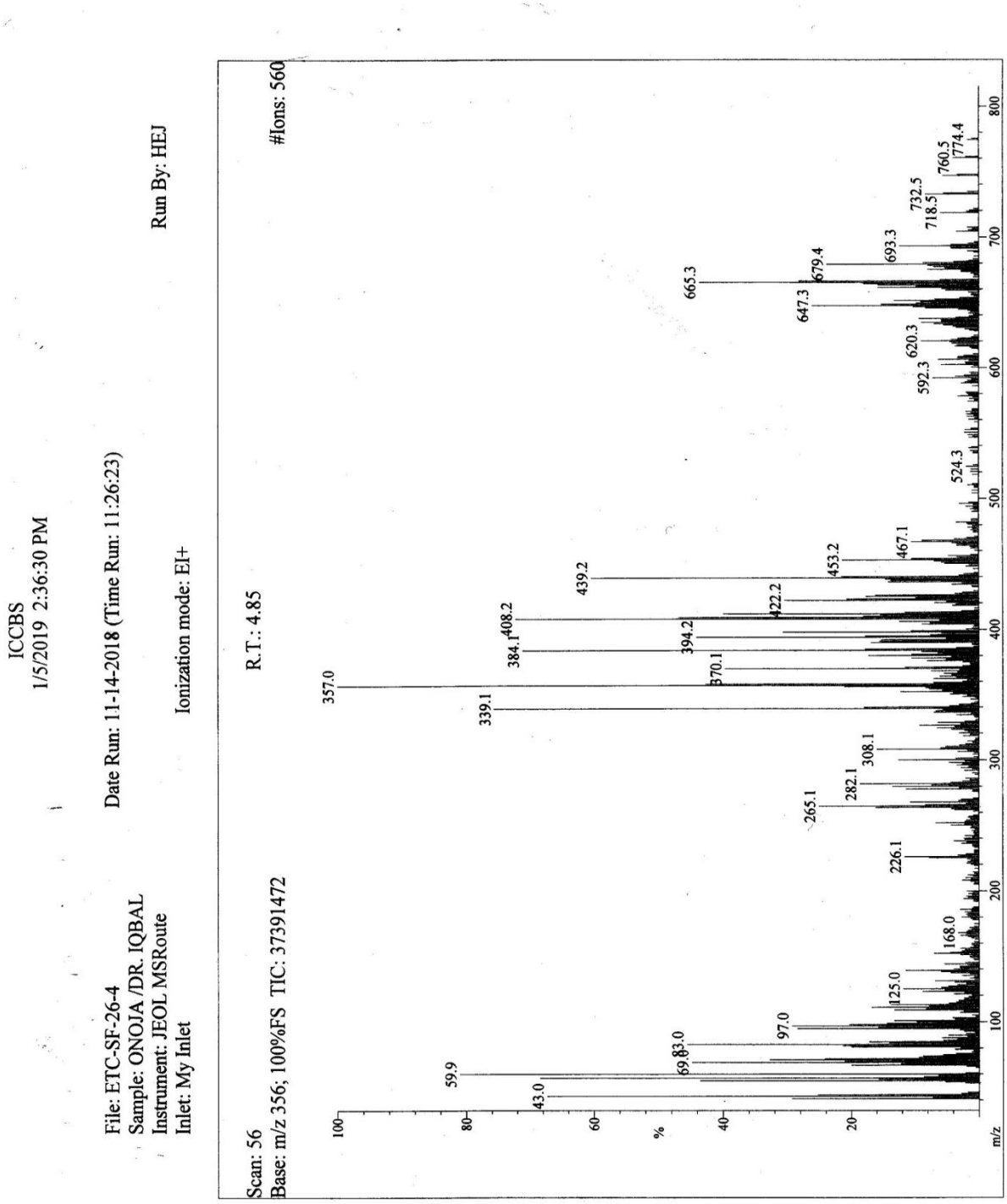

EI-MS spectra of rel-(2s,3s,4r,16e)-2-[(2'r)-2'-hydroxynonadecanoylamino]-heneicosadec-16-ene-1,3,4-triol

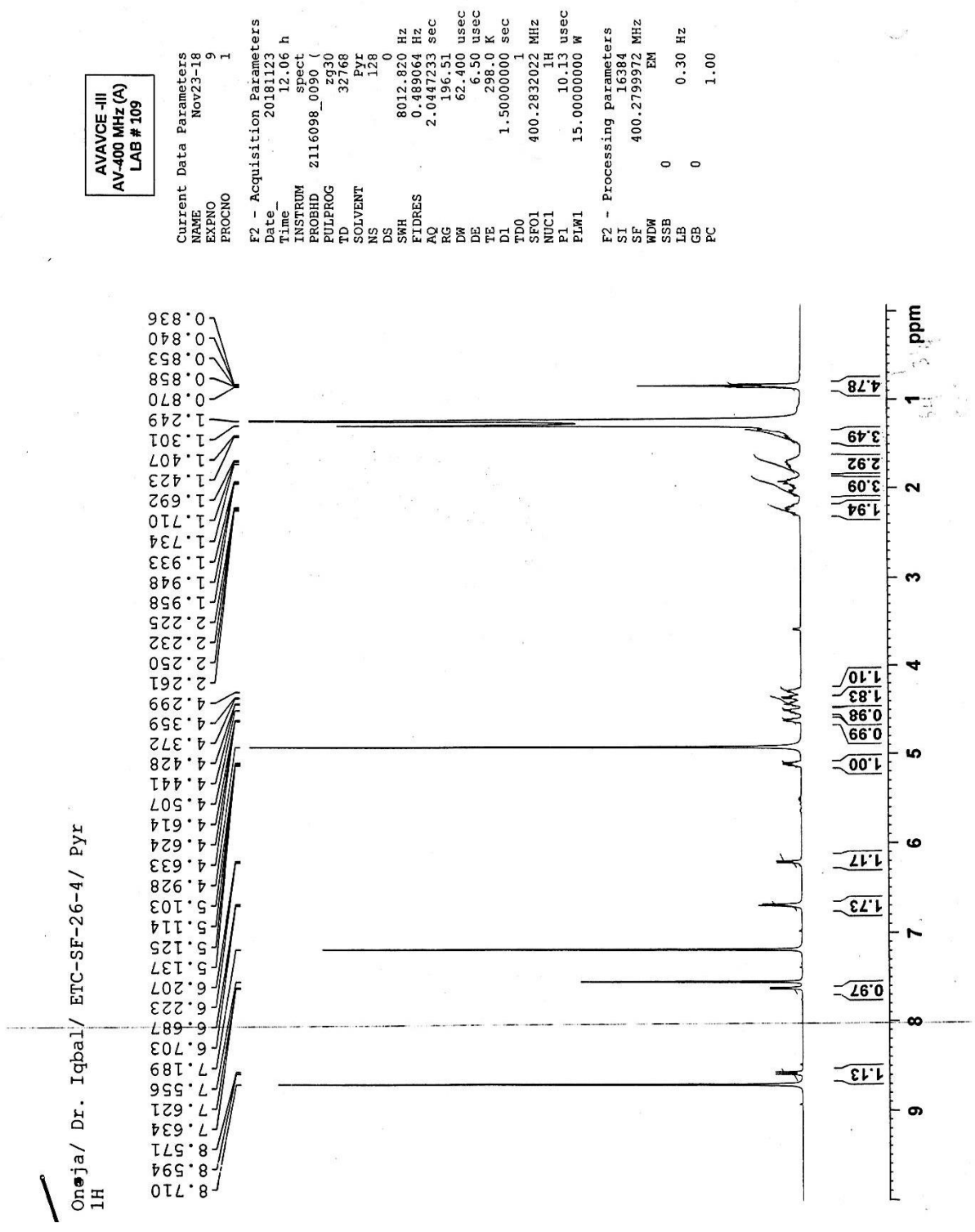

[1]H-NMR spectra of rel-(2s,3s,4r,16e)-2-[(2'r)-2'-hydroxynonadecanoylamino]-heneicosadec-16-ene-1,3,4-triol

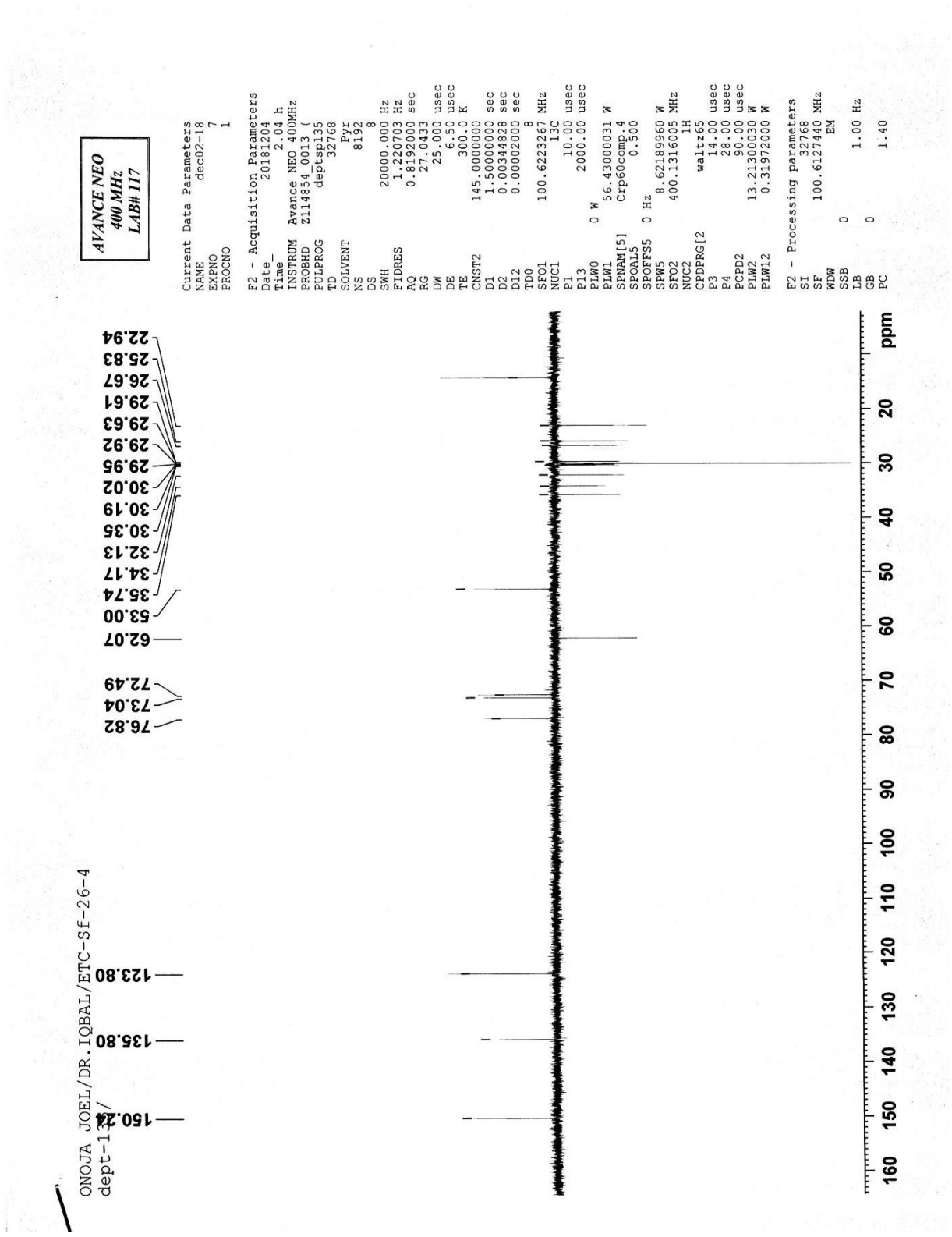

DEPT 135 spectra of rel-(2s,3s,4r,16e)-2-[(2'r)-2'-hydroxynonadecanoylamino]-heneicosadec-16-ene-1,3,4-triol

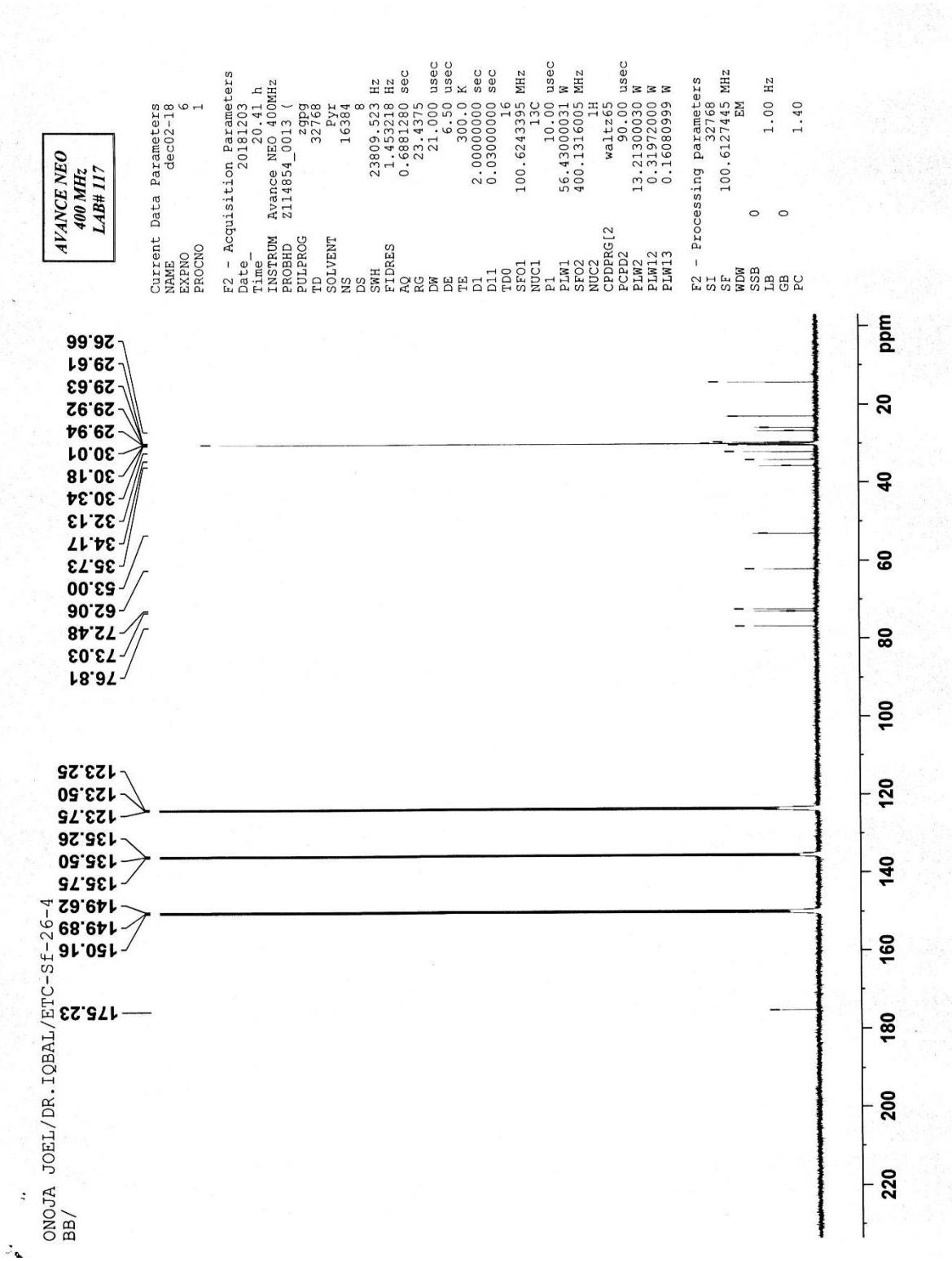

BB spectra of rel-(2s,3s,4r,16e)-2-[(2'r)-2'-hydroxynonadecanoylamino]-heneicosadec-16-ene-1,3,4-triol

Appendix 13: Spectroscopic analysis of Palmatine

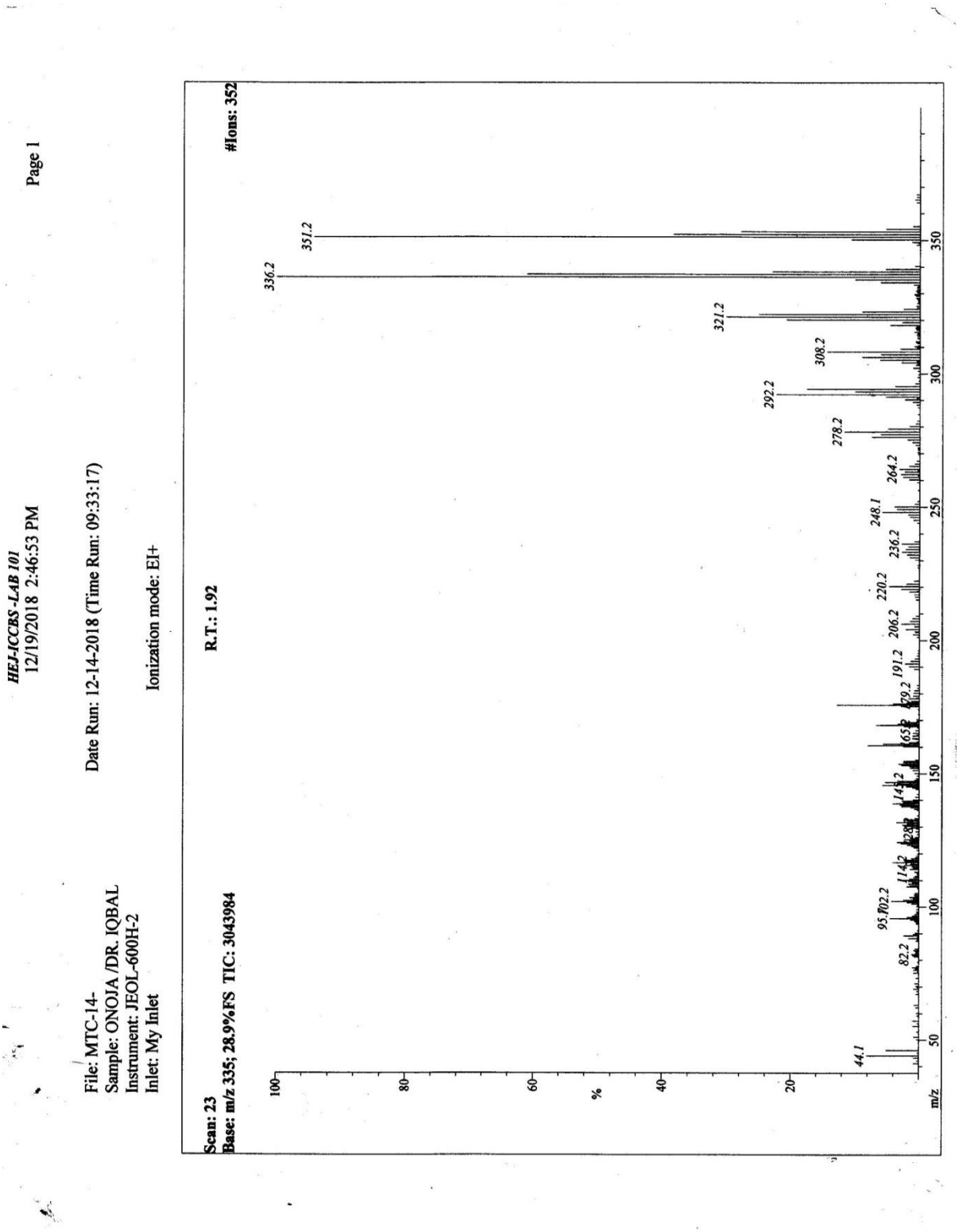

EI-MS spectra of Palmatine

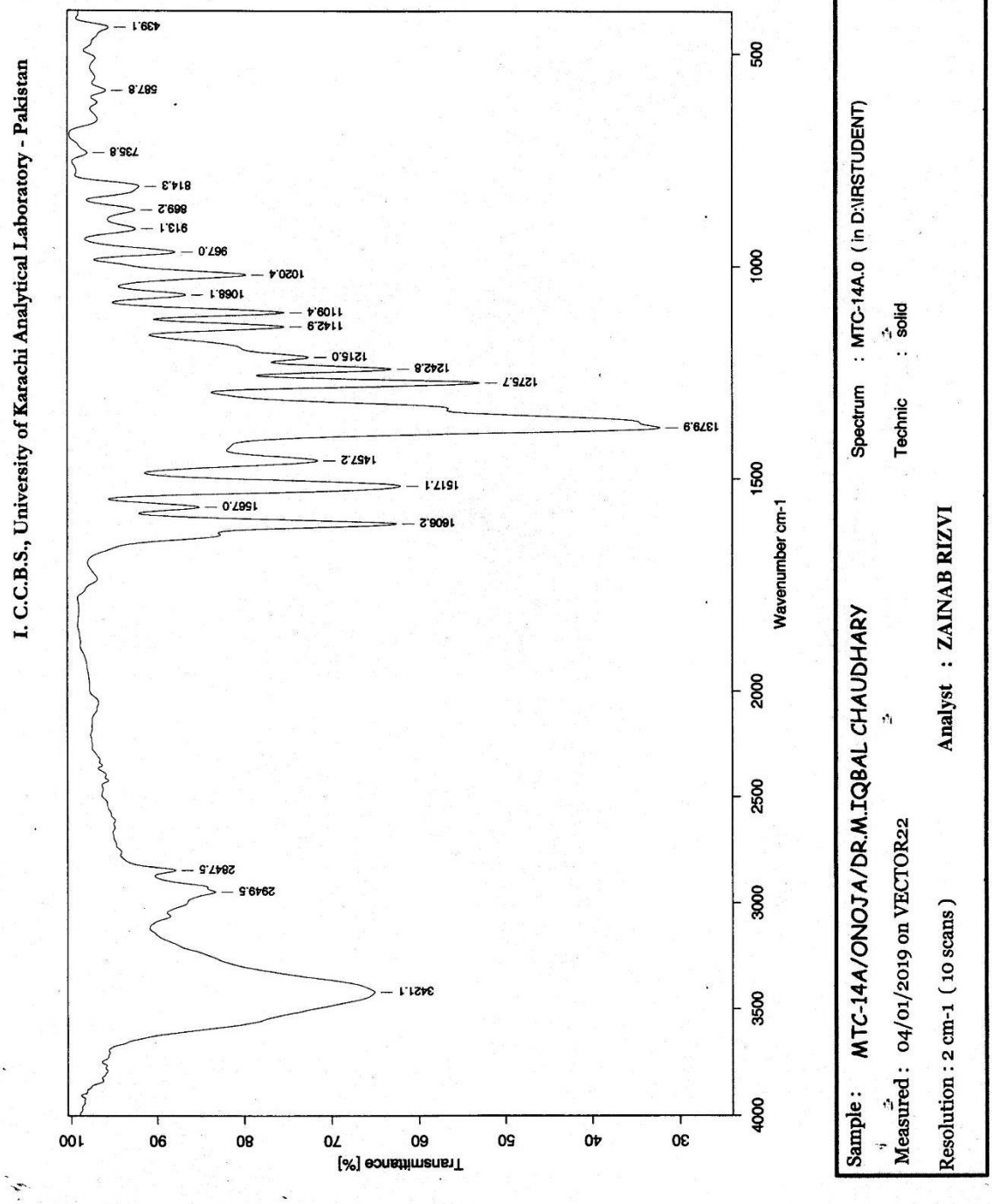

FT-IR spectra of Palmatine

THERMO ELECTRON ~ VISIONpro SOFTWARE V4.10

Operator Name	ZAINAB RIZVI	Date of Report	1/4/2019
Department	Analytical Lab.LEJ Nanotech. Center	Time of Report	11:17:28AM
Organization	ICCBS. University of Karachi		
Information	MTC-14A/ONOJA/DR.M.IQBAL CHAUDHARY		

Scan Graph

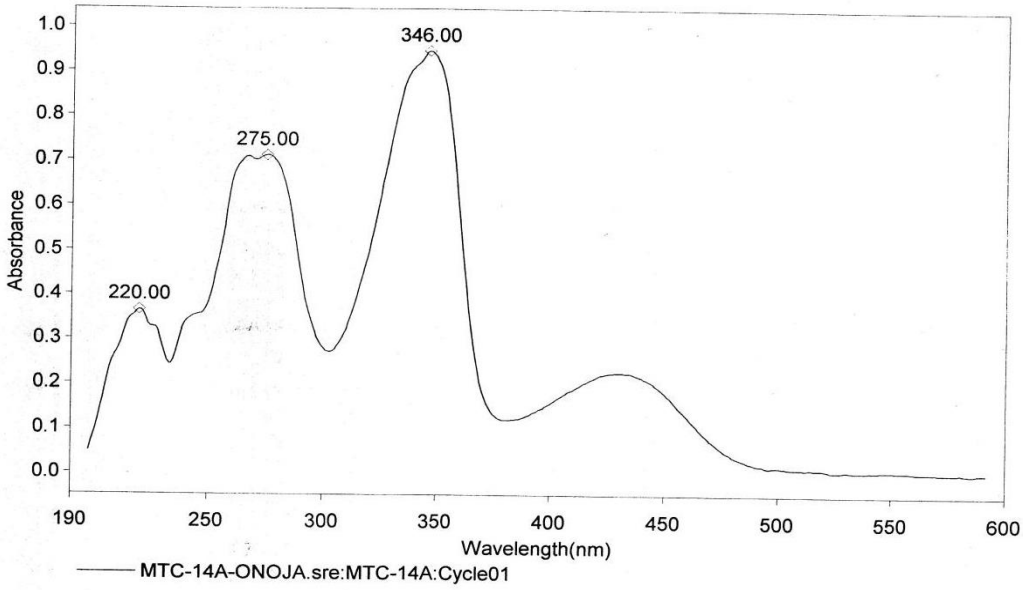

Results Table - MTC-14A-ONOJA.sre,MTC-14A,Cycle01

nm	A	**Peak Pick Method**
220.00	0.365	Find 8 Peaks Above -3.0000 A
275.00	0.712	Start Wavelength 190.00 nm
346.00	0.947	Stop Wavelength 600.00 nm
		Sort By Wavelength
Sensitivity	Auto	

Page 1, Scan Graph

UV spectra of Palmatine

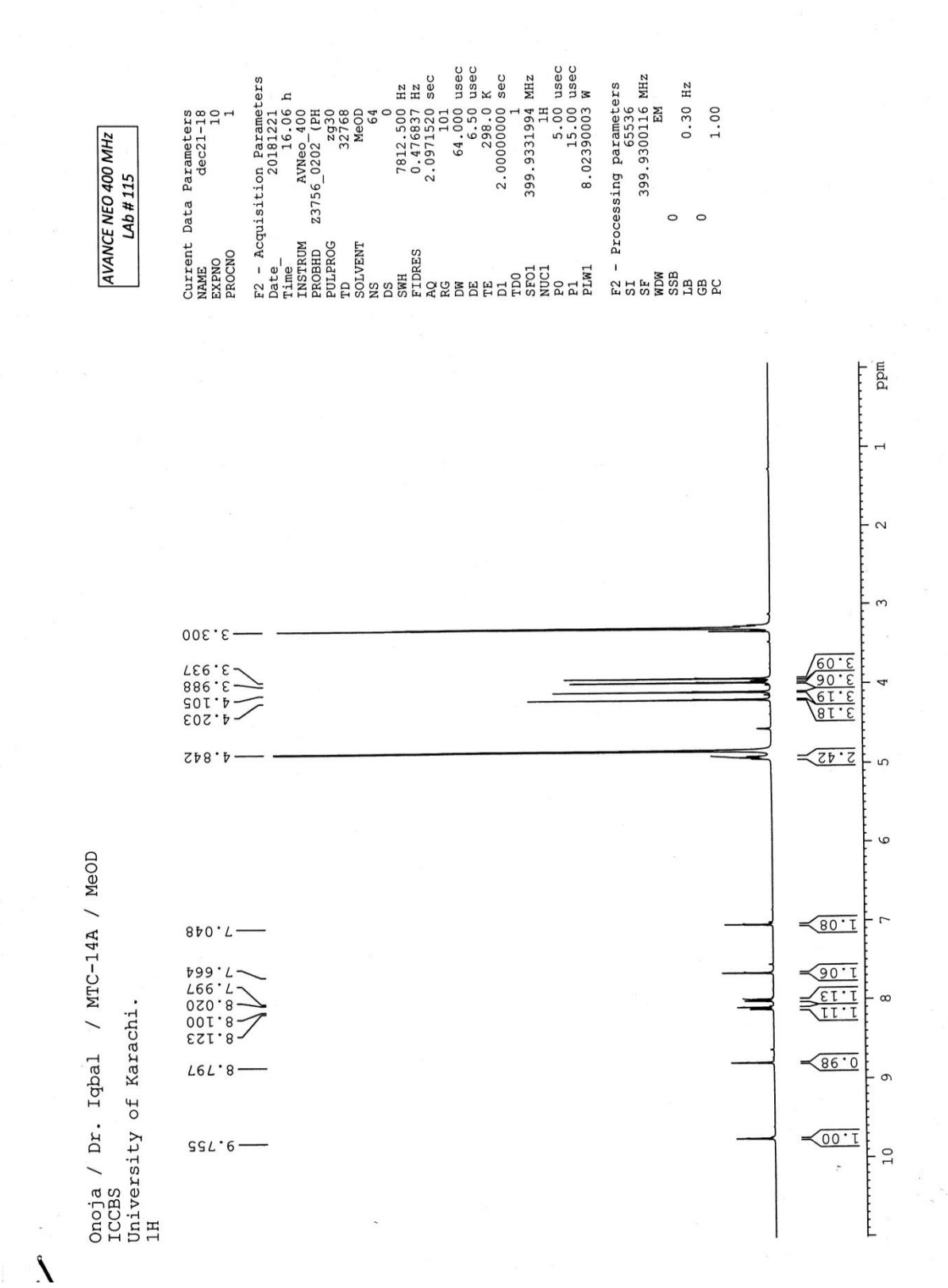

[1]H-NMR spectra of Palmatine

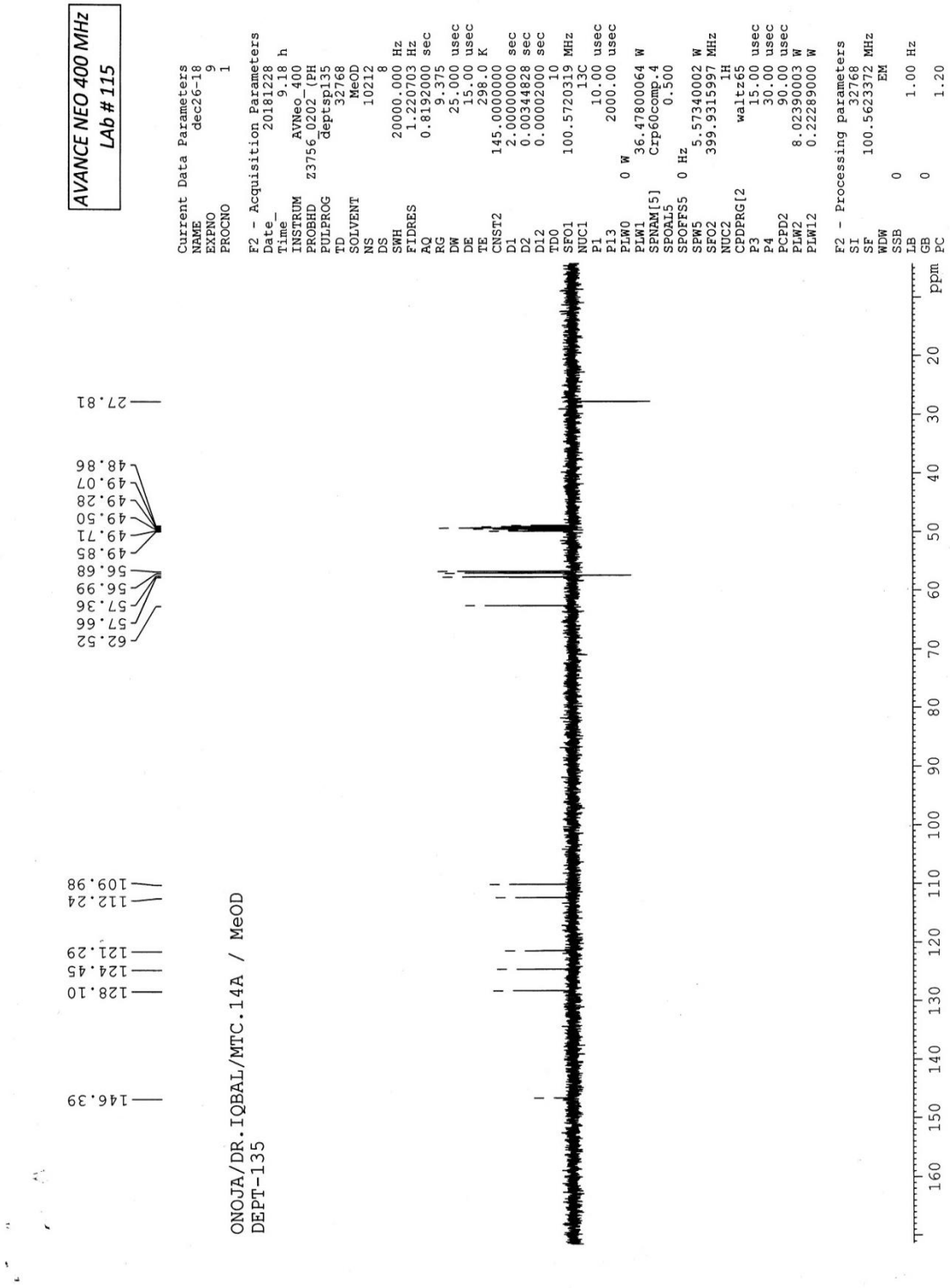

DEPT 135 spectra of Palmatine

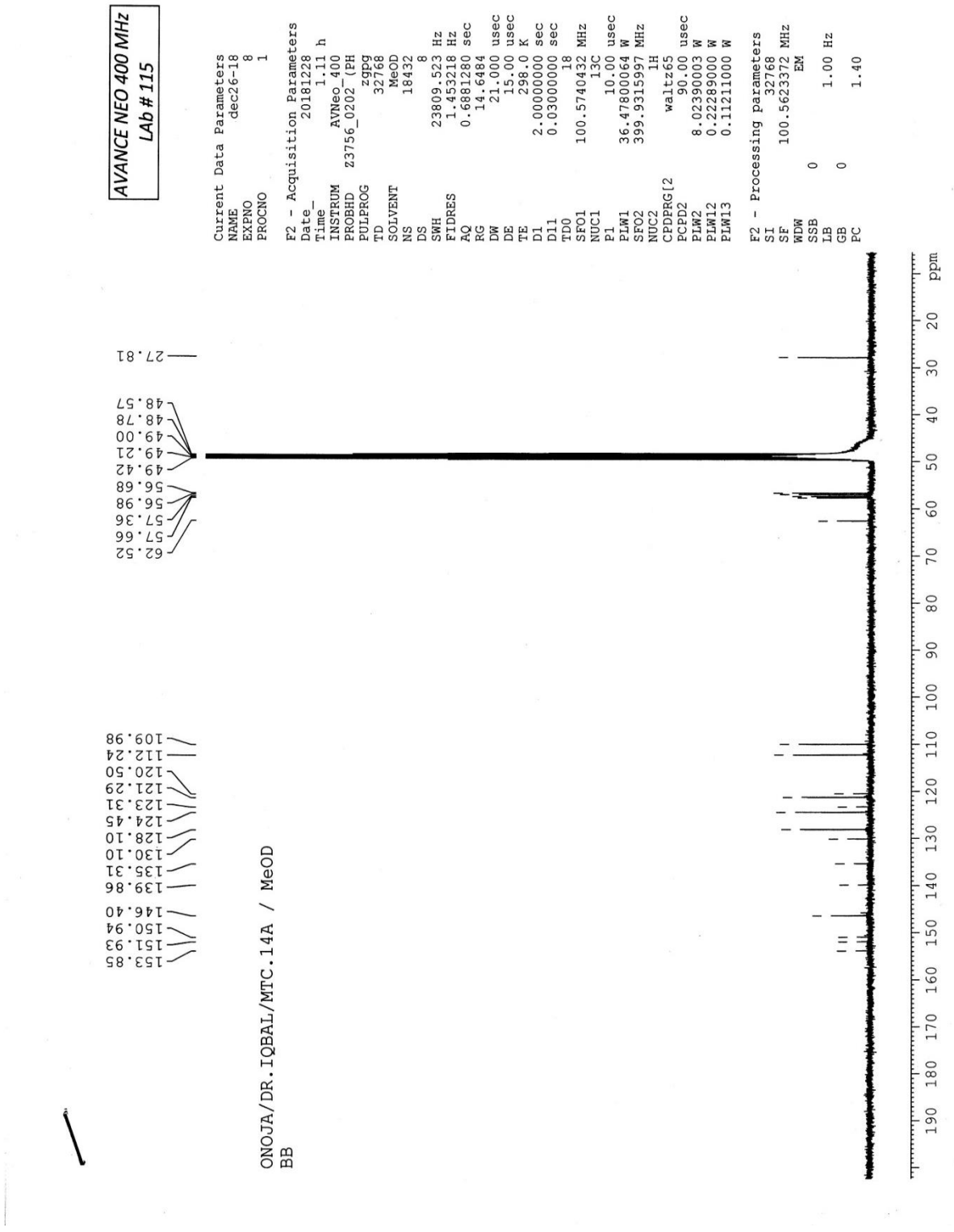

BB spectra of Palmatine

Appendix 14: Spectroscopic analysis of Liriodenine

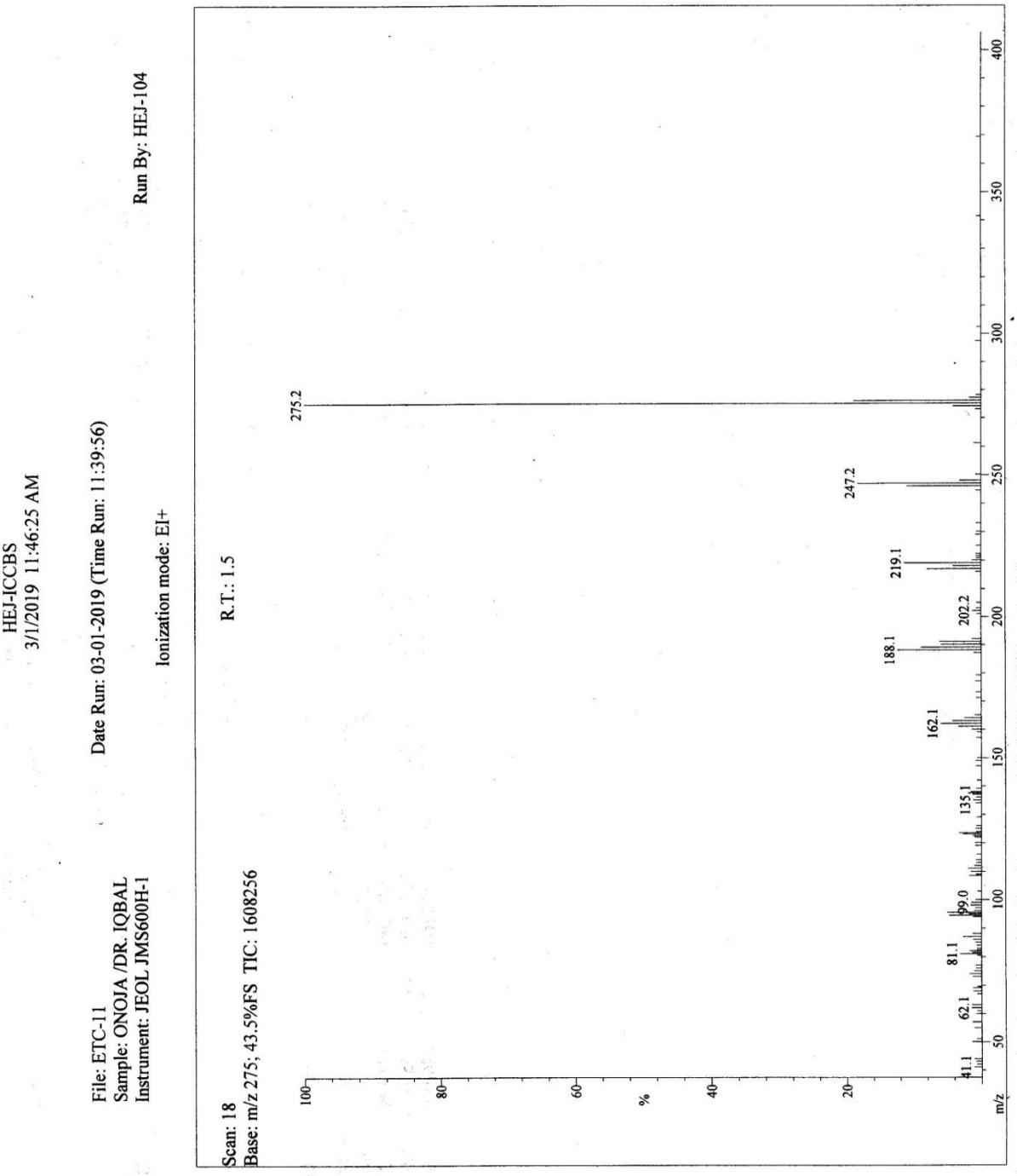

EI-MS spectra of Liriodenine

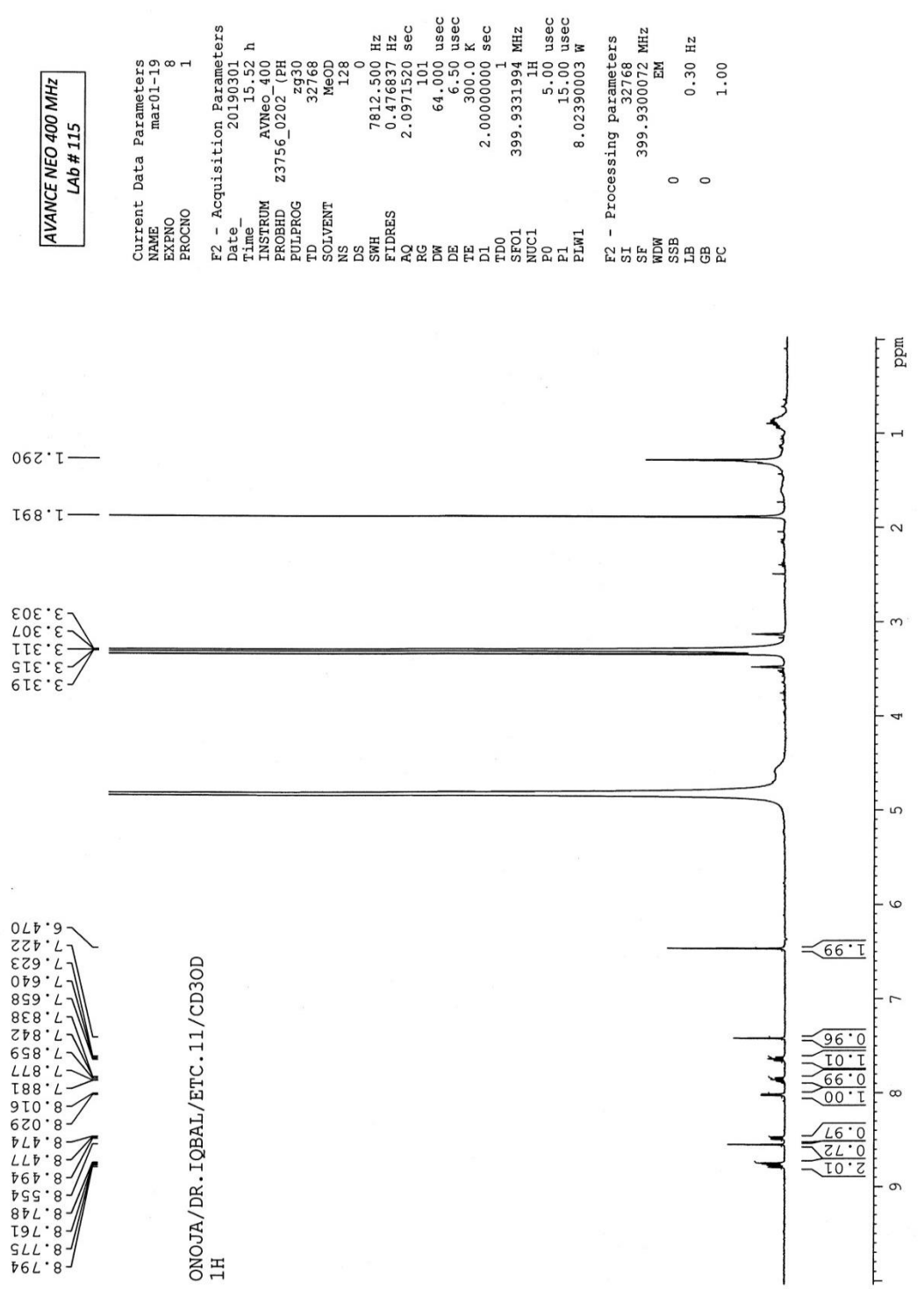

[1]H-NMR spectra of Liriodenine

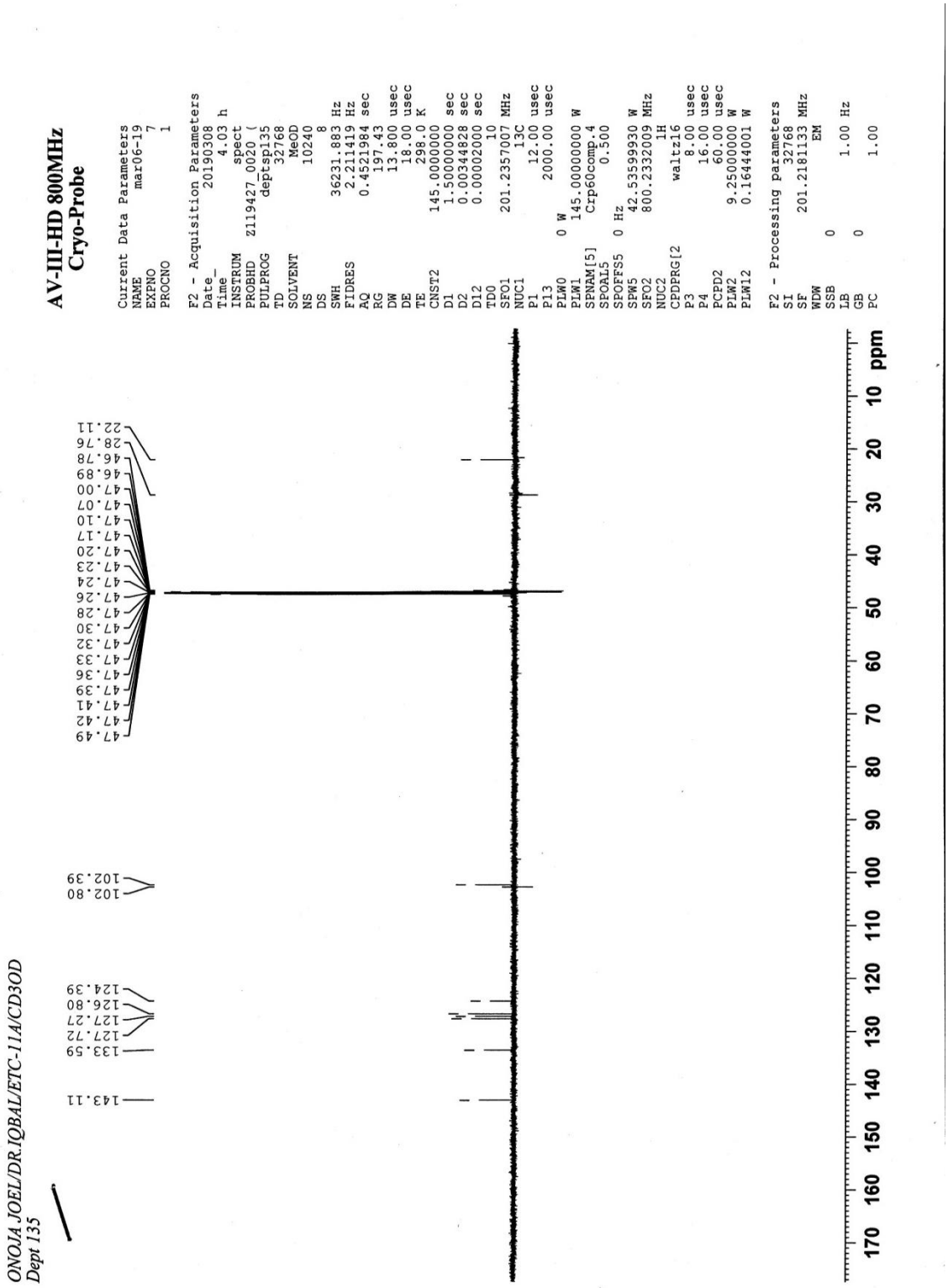

DEPT 135 spectra of Liriodenine

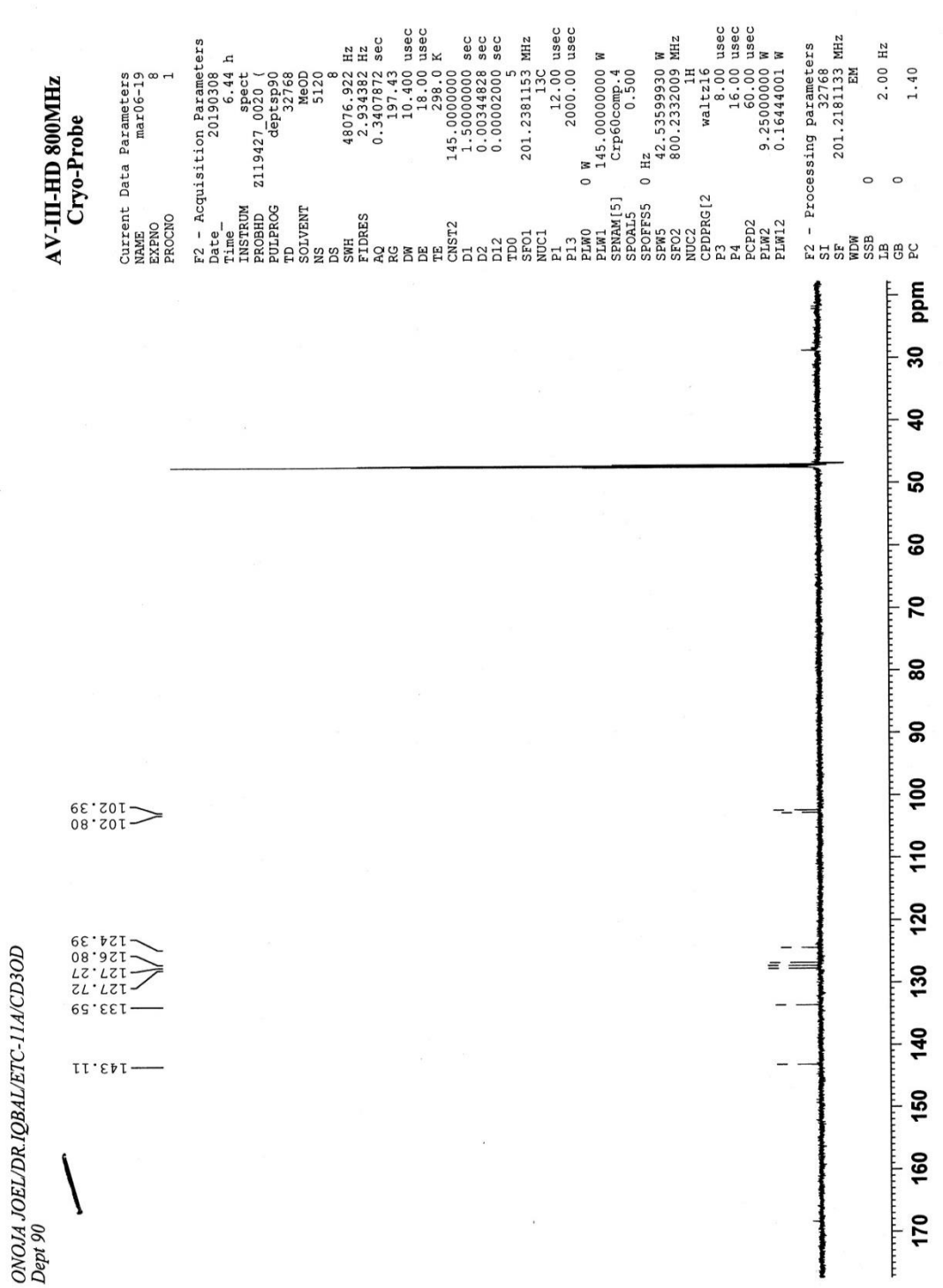

DEPT 90 spectra of Liriodenine

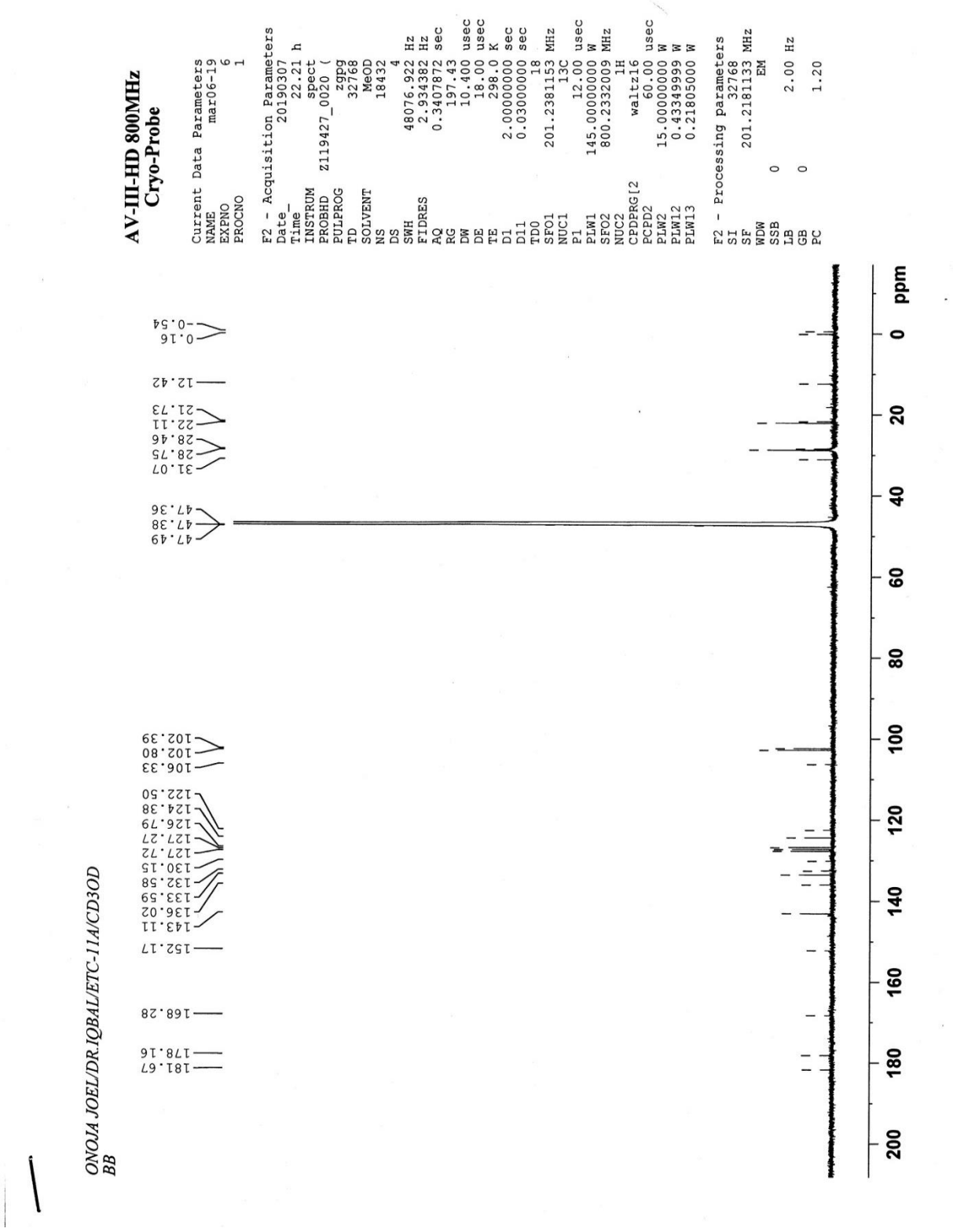

BB spectra of Liriodenine

Appendix 15: Spectroscopic analysis of 5-Hydroxymethylfurfural

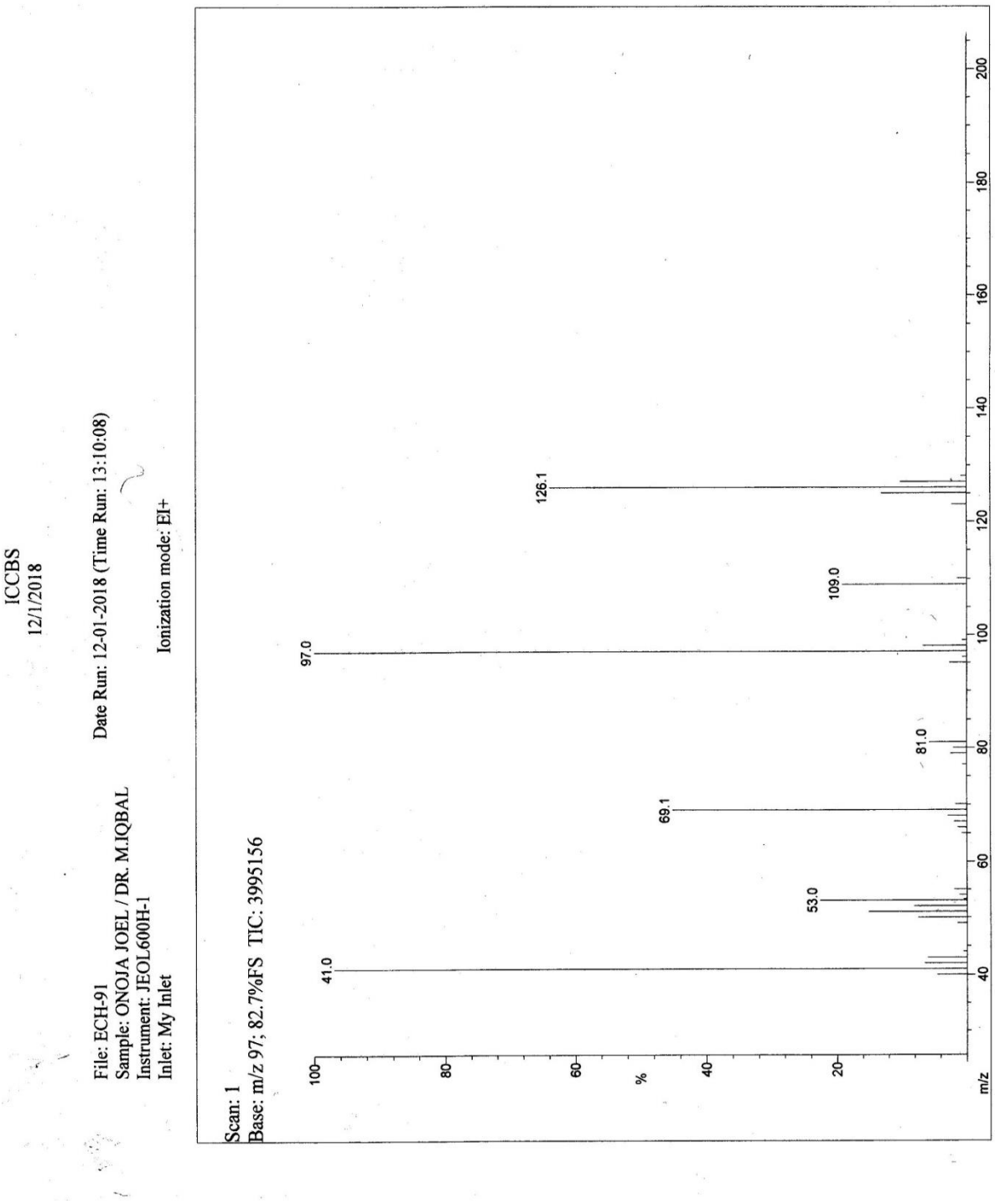

EI-MS spectra of 5-hydroxymethylfurfural

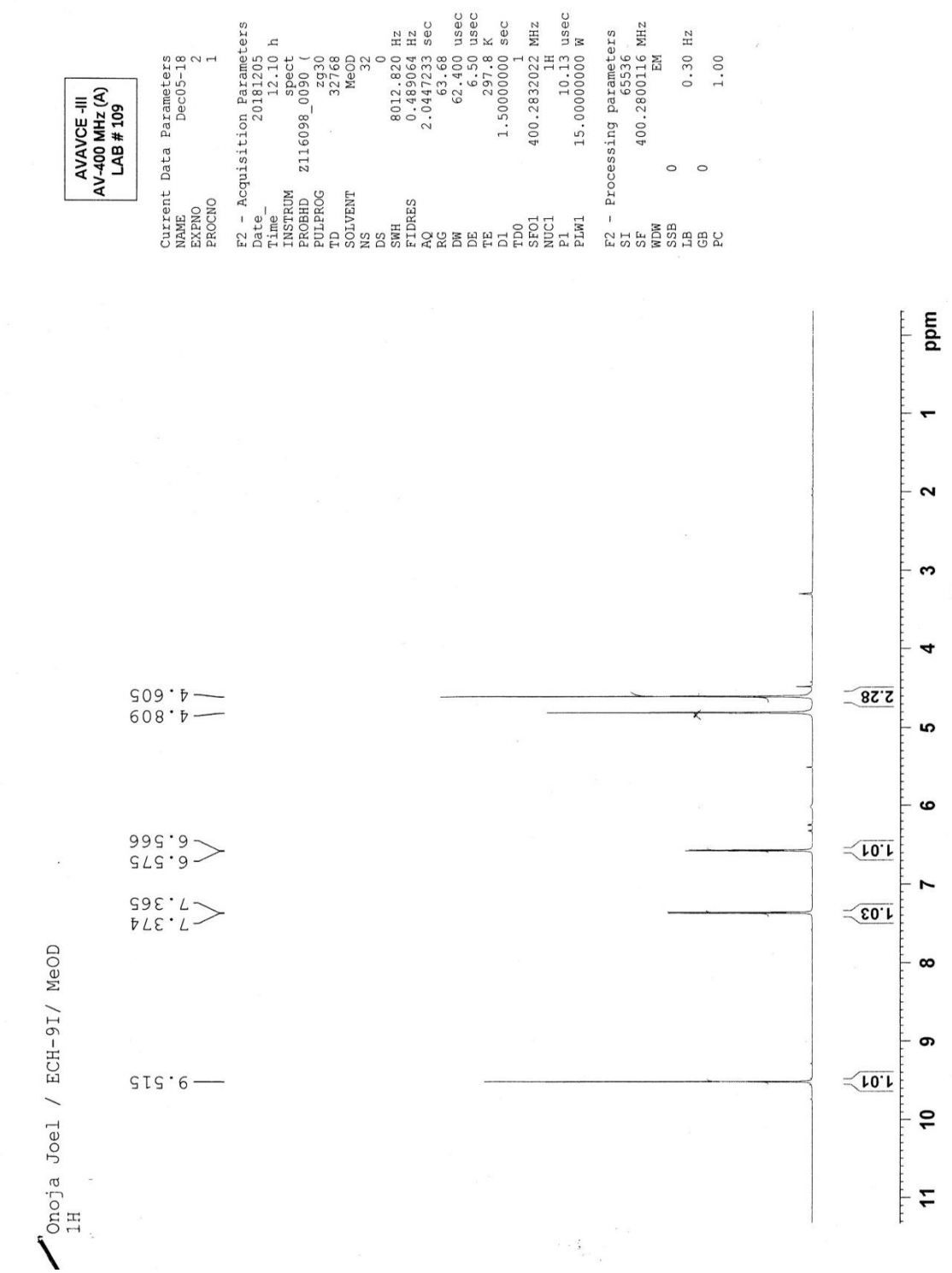

[1]H-NMR spectra of 5-hydroxymethylfurfural

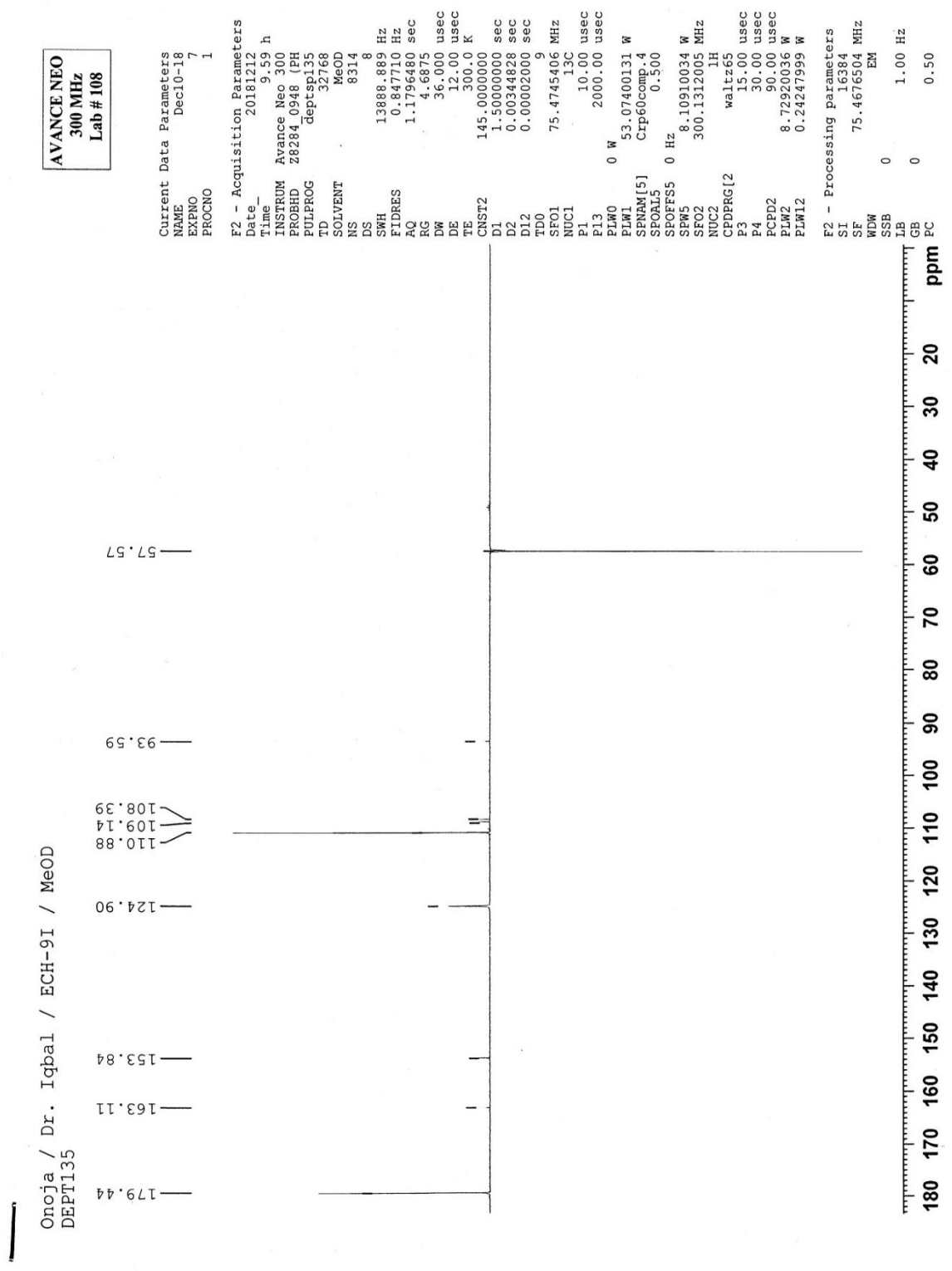

DEPT 135 spectra of 5-hydroxymethylfurfural

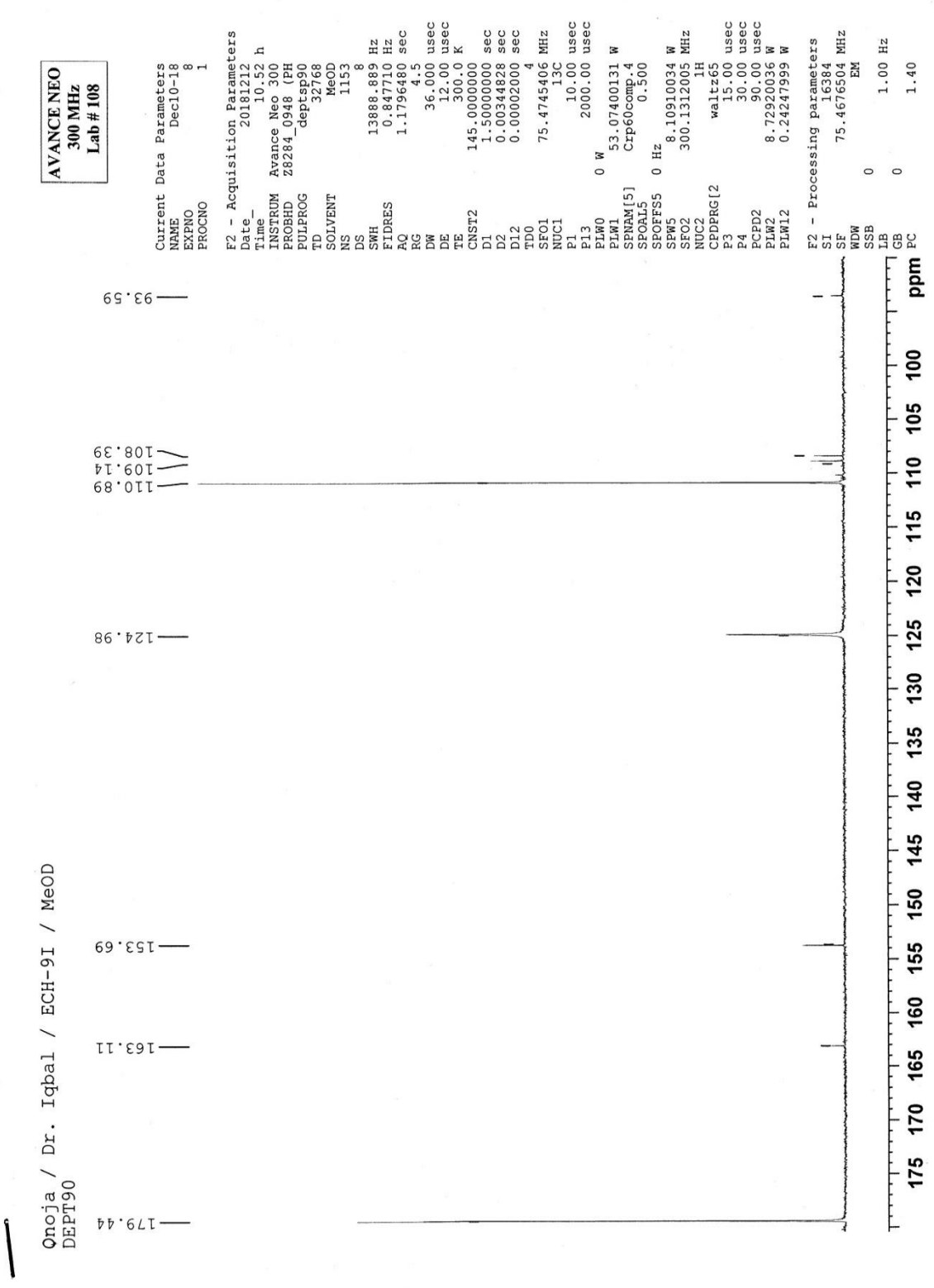

DEPT 90 spectra of 5-hydroxymethylfurfural

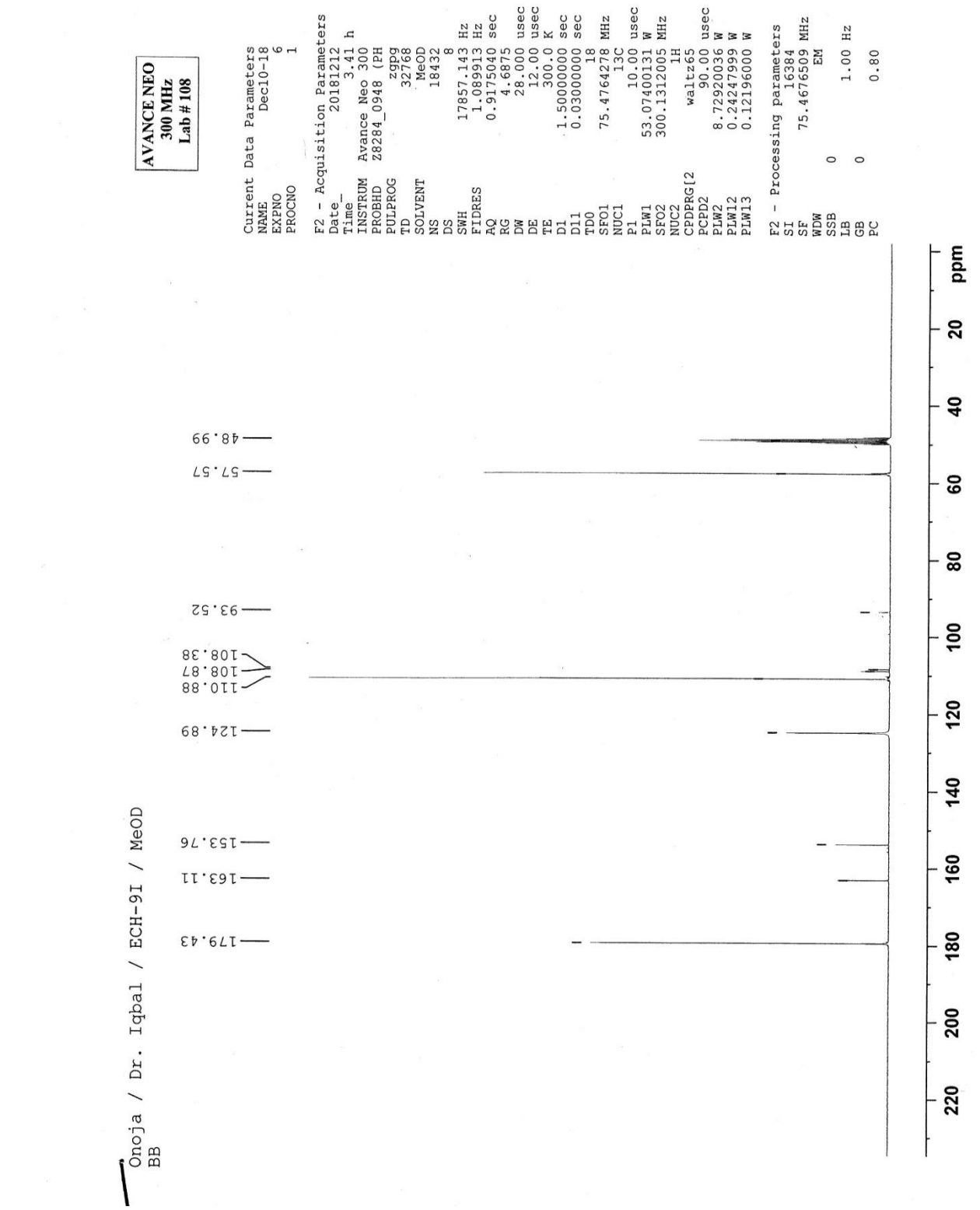

BB spectra of 5-hydroxymethylfurfural

Appendix 16: Spectroscopic analysis of 2-hydroxyquinoline-4-carboxylic acid

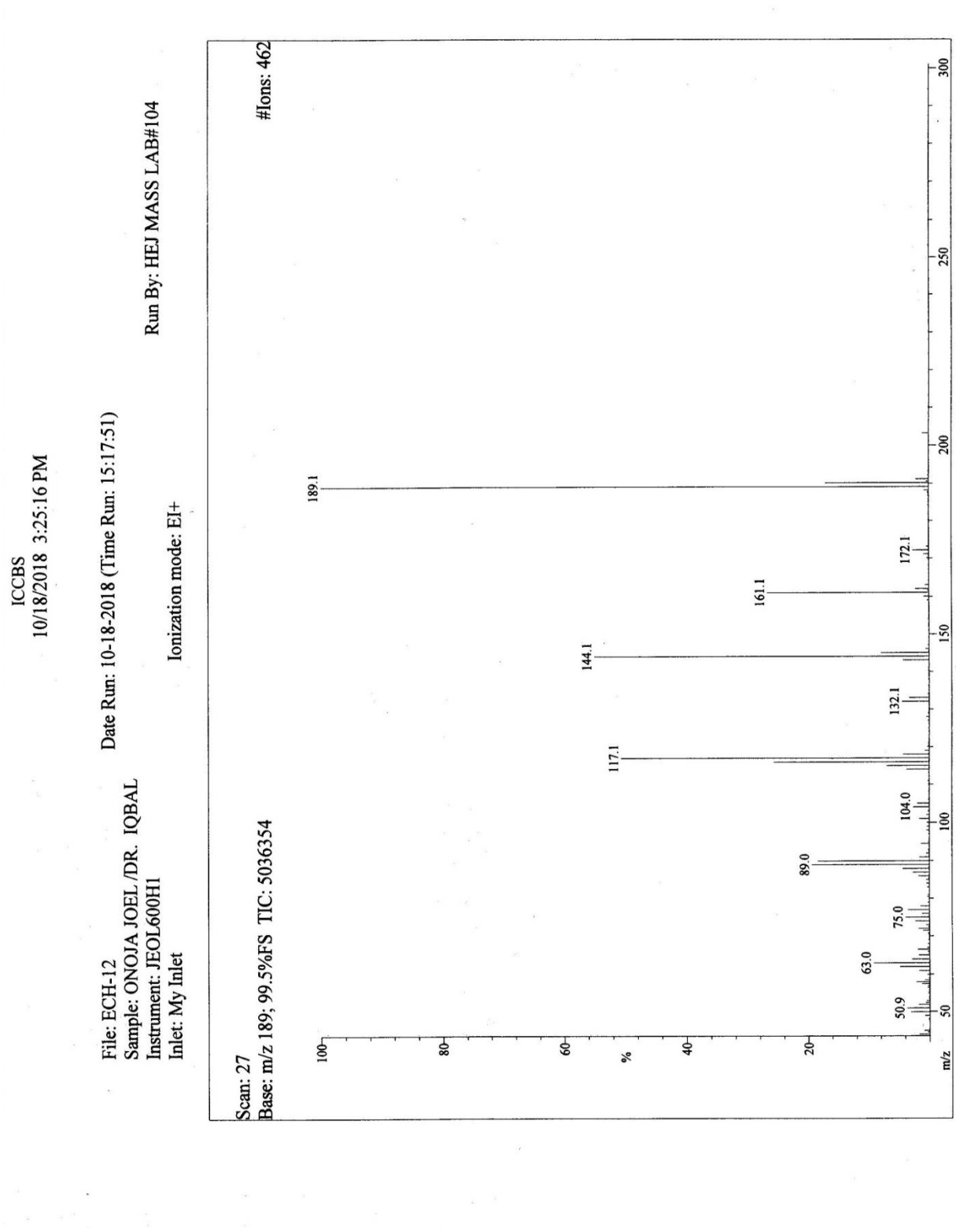

EI-MS of 2-hydroxyquinoline-4-carboxylic acid

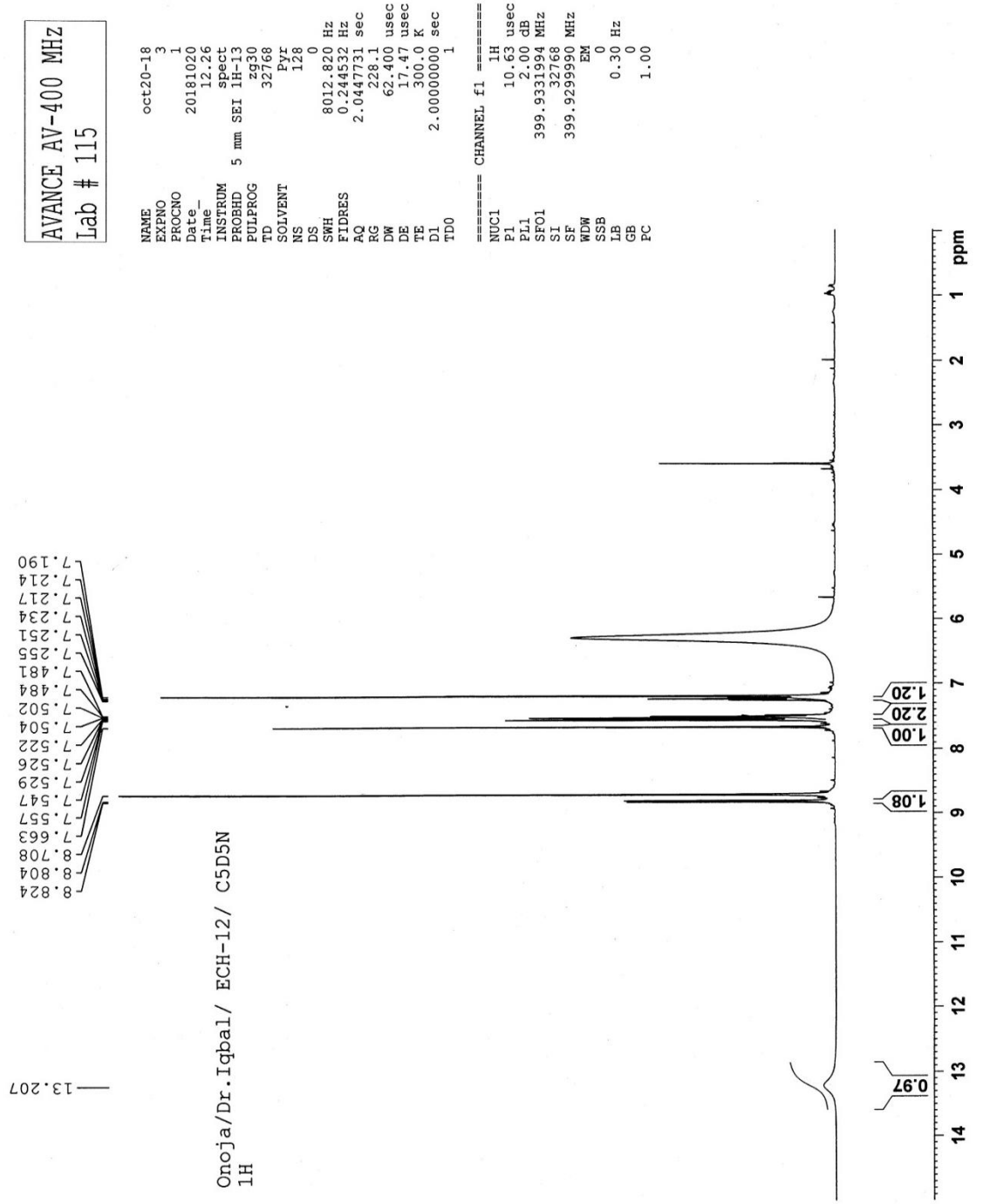

[1]H-NMR spectra of 2-hydroxyquinoline-4-carboxylic acid

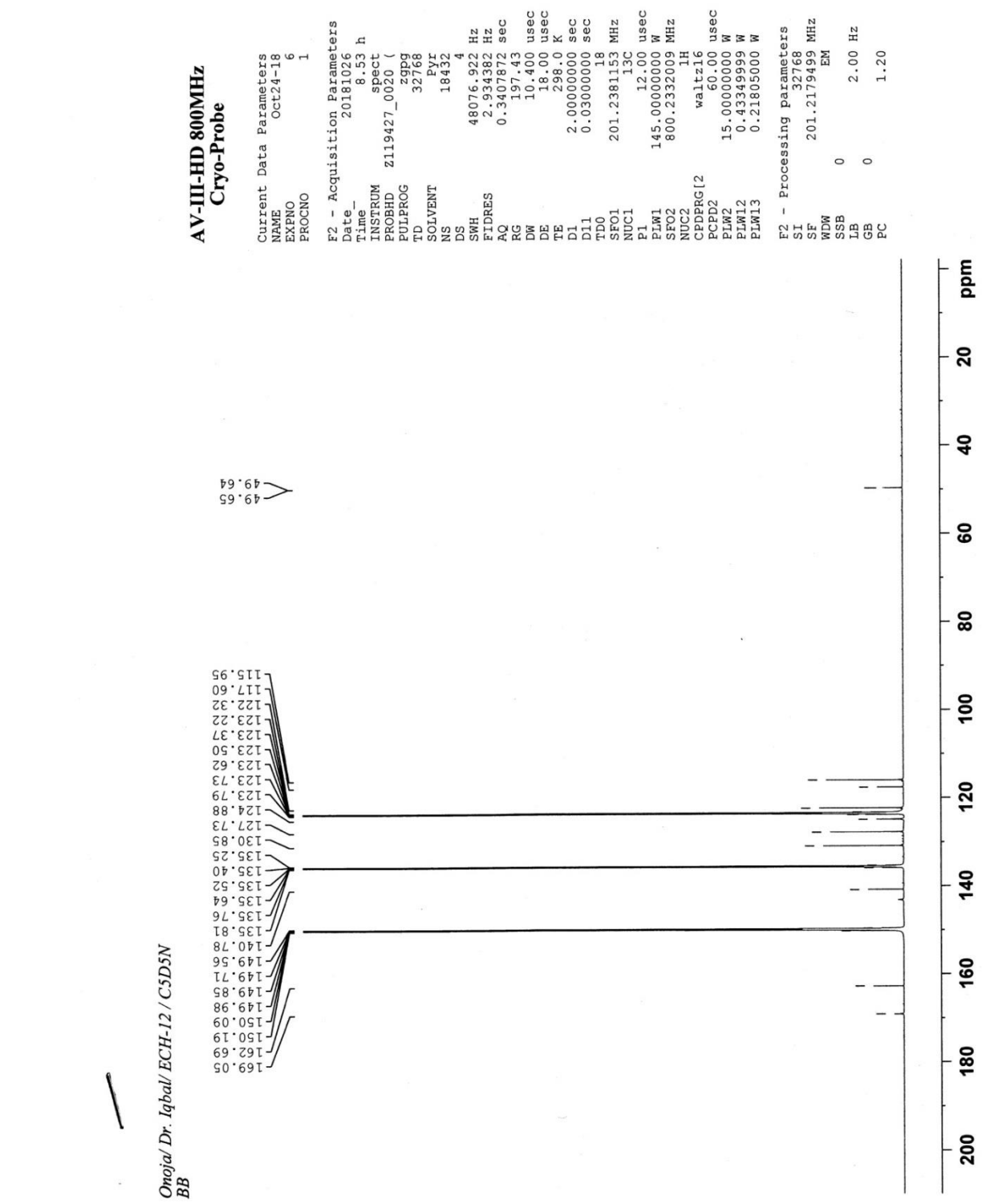

BB spectra of 2-hydroxyquinoline-4-carboxylic acid

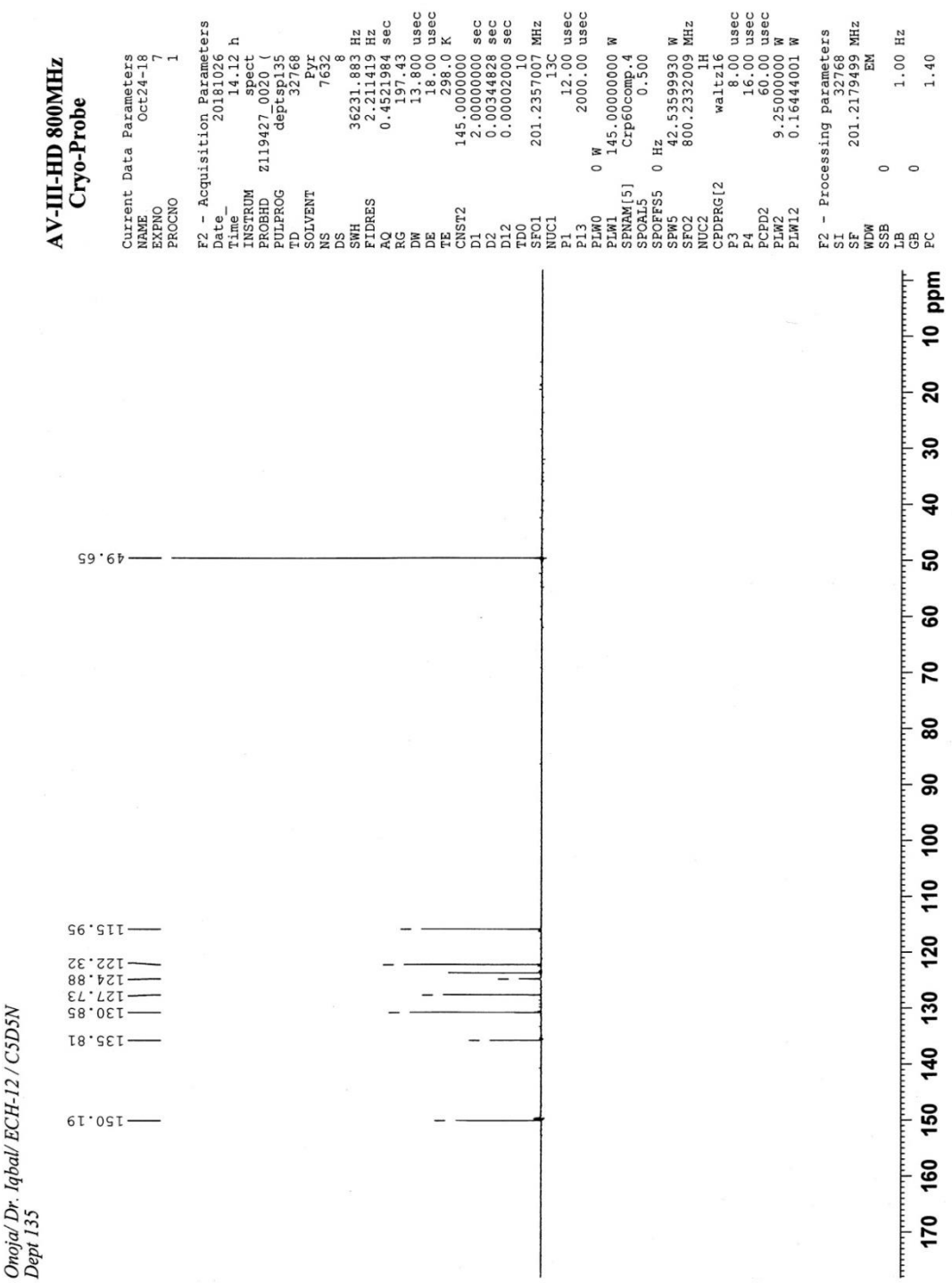

DEPT 135 spectra of 2-hydroxyquinoline-4-carboxylic acid

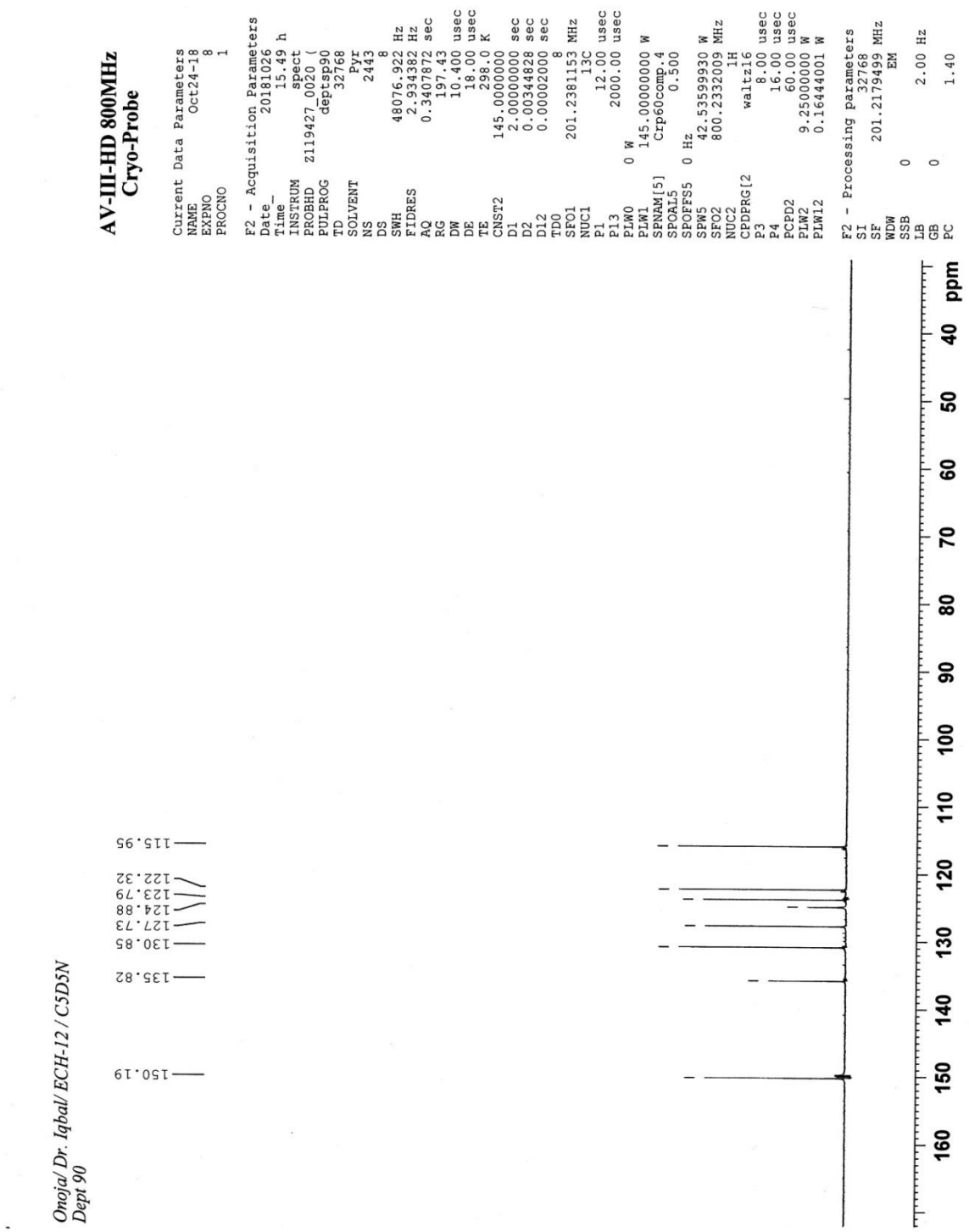

DEPT 90 spectra of 2-hydroxyquinoline-4-carboxylic acid

Appendix 17: One-way ANOVA followed by Dunnett's Multiple Comparisons analysis at $\alpha_{0.05}$ of acetylcholinesterase inhibitory activity of isolated compounds as compared to eserine

AChE inhibitory activity of Compounds

ANOVA table	SS	DF	MS	F (DFn, DFd)	P value
Treatment (between columns)	5.059	13	0.3892	F (13, 28) = 6.483	P<0.0001
Residual (within columns)	1.681	28	0.06003		
Total	6.74	41			

Alpha	0.05				
Dunnett's multiple comparisons test	**Mean Diff.**	**95.00% CI of diff.**	**Significant?**	**Summary**	**Adjusted P Value**
eserine vs. stigmasterol	-0.5868	-1.185 to 0.01088	No	ns	0.0564
eserine vs. 8-hydroxycolumbin	-0.8047	-1.402 to -0.207	Yes	**	0.0041
eserine vs. palmatine	-0.3057	-0.9034 to 0.292	No	ns	0.6533
eserine vs. corydine	-1.294	-1.892 to -0.6968	Yes	****	0.0001
eserine vs. oxoglaucine	-0.2715	-0.8692 to 0.3262	No	ns	0.7724
eserine vs. tinosporide	-0.9422	-1.54 to -0.3445	Yes	***	0.0007
eserine vs. liriodenine	-0.2758	-0.8735 to 0.3219	No	ns	0.7580
eserine vs. columbin	-0.7675	-1.365 to -0.1698	Yes	**	0.0065
eserine vs. 1-Octacosanol	-0.4694	-1.067 to 0.1283	No	ns	0.1878
eserine vs. β-sitosterol	-0.7191	-1.317 to -0.1214	Yes	*	0.0120
eserine vs. N-formylanonaine	-0.2872	-0.8849 to 0.3105	No	ns	0.7190
eserine vs. 5-hydroxymethylfurfural	-1.074	-1.672 to -0.4763	Yes	***	0.0001
eserine vs. 2-hydroxyquinoline-4-carboxylic acid	-0.5382	-1.136 to 0.05953	No	ns	0.0951

Appendix 18: One-way ANOVA followed by Dunnett's Multiple Comparisons analysis at $\alpha_{0.05}$ of metal chelating activity of isolated compounds as compared to EDTA

ANOVA table	SS	DF	MS	F (DFn, DFd)	P value
Treatment (between columns)	15.07	13	1.159	F (13, 28) = 260.1	P<0.0001
Residual (within columns)	0.1248	28	0.004457		
Total	15.2	41			

Alpha	0.05				
Dunnett's multiple comparisons test	**Mean Diff.**	**95.00% CI of diff.**	**Significant?**	**Summary**	**Adjusted P Value**
EDTA vs. stigmasterol	-0.2382	-0.4011 to -0.07535	Yes	**	0.0017
EDTA vs. 8-hydroxycolumbin	-0.5222	-0.6851 to -0.3594	Yes	****	0.0001
EDTA vs. palmatine	-1.591	-1.754 to -1.428	Yes	****	0.0001
EDTA vs. corydine	-0.5972	-0.7601 to -0.4343	Yes	****	0.0001
EDTA vs. oxoglaucine	-0.1715	-0.3343 to -0.00862	Yes	*	0.0349
EDTA vs. tinosporide	-0.6314	-0.7943 to -0.4685	Yes	****	0.0001
EDTA vs. liriodenine	-1.92	-2.083 to -1.757	Yes	****	0.0001
EDTA vs. columbin	-1.768	-1.931 to -1.605	Yes	****	0.0001
EDTA vs. 1-Octacosanol	-0.5617	-0.7246 to -0.3989	Yes	****	0.0001
EDTA vs. β-sitosterol	-0.2897	-0.4526 to -0.1269	Yes	***	0.0002
EDTA vs. N-formylanonaine	-0.3311	-0.494 to -0.1683	Yes	****	0.0001
EDTA vs. 5-hydroxymethylfurfural	-0.2502	-0.4131 to -0.08735	Yes	***	0.0009
EDTA vs. 2-hydroxyquinoline-4-carboxylic acid	-0.9156	-1.079 to -0.7528	Yes	****	0.0001